DISSERTATION

AQUEOUS PHASE SULFATE PRODUCTION IN CLOUDS AT MT. TAI IN EASTERN CHINA

Submitted by

Xinhua Shen

Department of Atmospheric Science

In partial fulfillment of the requirements

For the Degree of Doctor of Philosophy

Colorado State University

Fort Collins, Colorado

Spring 2011

Doctoral Committee:

Advisor: Jeffrey L. Collett

Sonia M. Kreidenweis
Steven A. Rutledge
Stephen J. Reynolds

ABSTRACT

AQUEOUS PHASE SULFATE PRODUCTION IN CLOUDS AT MT. TAI IN EASTERN CHINA

Clouds play an important role in the oxidation of sulfur dioxide to sulfate, since aqueous phase sulfur dioxide oxidation is typically much faster than oxidation in the gas phase. Important aqueous phase oxidants include hydrogen peroxide, ozone and oxygen (catalyzed by trace metals). Because quantities of emitted sulfur dioxide in China are so large, however, it is possible that they exceed the capacity of regional clouds for sulfate production, leading to enhanced long-range transport of emitted SO_2 and its oxidation product, sulfate.

In order to assess the ability of regional clouds to support aqueous sulfur oxidation, four field campaigns were conducted in 2007 and 2008 at Mt. Tai in eastern China. Single and 2-stage Caltech Active Strand Cloudwater Collectors were used to collect bulk and drop size-resolved cloudwater samples, respectively. Key species that determine aqueous phase sulfur oxidation were analyzed, including cloudwater pH, S(IV), H_2O_2, Fe, and Mn. Gas phase SO_2, O_3, and H_2O_2 were also measured continuously during the campaigns. Other species in cloudwater, including inorganic ions, total organic carbon (TOC), formaldehyde, and organic acids were also analyzed to provide a fuller view of cloud chemistry in the region.

Numerous periods of cloud interception/fog occurred during the four Mt. Tai field campaigns; more than 500 cloudwater samples were collected in total. A wide range of cloud pH values was observed, from 2.6 to 7.6. SO_4^{2-}, NO_3^-, and NH_4^+ were the major inorganic species for all four campaigns. TOC concentrations were also very high in some samples (up to 200 ppmC), especially when clouds were impacted by emissions from agricultural biomass burning. Back-trajectory analysis also indicated influence by dust transport from northern China in a few spring cloud events. Differences between the compositions of small and large cloud droplets were observed, but generally found to be modest for major solute species and pH. Mt. Tai clouds were found to interact strongly with $PM_{2.5}$ sulfate, nitrate, and ammonium with average scavenging efficiencies of 80%, 75%, and 78%, respectively, across 7 events studied. Scavenging efficiencies for total sulfur ($PM_{2.5}$ sulfate plus gaseous sulfur dioxide), however, averaged only 43%, indicating the majority of gaseous sulfur dioxide remained unprocessed in these cloud events.

H_2O_2 was found to be the most important oxidant for aqueous sulfate production 68% of the time. High concentrations of residual H_2O_2 were measured in some samples, especially during summertime, implying a substantial capacity for additional sulfur oxidation. The importance of ozone as a S(IV) oxidant increased substantially as cloud pH climbed above pH 5 to 5.3. Overall, ozone was found to be the most important aqueous S(IV) oxidant in 21% of the sampling periods. Trace metal-catalyzed S(IV) autooxidation was determined to be the fastest aqueous sulfate production pathway in the remaining 11% of the cases. Complexation with formaldehyde was also found to be a potentially important fate for aqueous S(IV) and should be examined in more detail in

future studies. Observed chemical heterogeneity among cloud drop populations was predicted to enhance rates of S(IV) oxidation by ozone and enhance or slow metal-catalyzed S(IV) autooxidation rates in some periods. These effects were found to be only of minor importance, however, as H_2O_2 was the dominant S(IV) oxidant most of the time.

ACKNOWLEDGEMENTS

I would like to first acknowledge my advisor, Professor Jeffrey L. Collett, for his guidance and assistance throughout the course of this project. I am also very grateful to my other committee members, Professor Sonia M. Kreidenweis, Professor Steven A. Rutledge, and Professor Stephen J. Reynolds for their insightful comments and recommendations for this work. I thank Professor Tao Wang (The Hong Kong Polytechnic University) for his consistent support for this study. I am grateful to Mr. Tingli Sun (Shandong University) for considerable logistical assistance in the field campaigns.

I would like to thank Dr. Taehyoung Lee, Jia Guo, Xinfeng Wang, Wei Nie and Rui Gao for their extensive contributions to the field campaigns and the subsequent sample analysis. Further support was given by Yi Li during sample analysis. The advice and help from various colleagues, including Katie Beem, Mandy Holden, Angela Rowe, Leigh A. Munchak, and the rest of the Collett and Kreidenweis groups, is also greatly appreciated. I thank my family and friends for their invaluable support and encouragement.

This work was supported by the US National Science Foundation (ATM-0711102) and by the National Basic Research Program of China (973 Program) (2005CB422203).

TABLE OF CONTENTS

LIST OF FIGURES

LIST OF ACRONYMS AND SYMBOLS

CASCC	Caltech Active Strand Cloudwater Collector
CCN	cloud condensation nuclei
CDTA	trans-1,2-Cylohexylenedinitrilo-tetraacetic acid
DDL	3,5-diacetyl-1,4-dihydrolutidine
DI	deionized
DMS	dimethyl sulfide
GFAAS	Graphite Furnace Atomic Absorption Spectrophotometer
HMS	hydroxymethanesulfonate
HYSPLIT	HYbrid Single-Particle Lagrangian Integrated Trajectory
IC	ion chromatography
LWC	liquid water content
MDL	method detection limit
OM	organic matter
$PM_{2.5}$	particulate matter with an aerodynamic diameter of less than 2.5 μm
POPHA	*p*-hydroxyphenyl acetic acid
PRA	pararosaniline
PVM	Particulate Volume Monitor
QA	quality assurance
RSD	relative standard deviation

S(IV)	sulfur in the +4 oxidation state
S(VI)	sulfur in the +6 oxidation state
sf-CASCC	size-fractionating Caltech Active Strand Cloudwater Collector
SOP	standard operating procedure
TOC	total organic carbon
TN	total nitrogen
TSP	total suspended particles
URG	University Research Glassware
VOCs	volatile organic compounds

CHAPTER 1 INTRODUCTION

1.1. PROJECT MOTIVATIONS

With the world's social and economic development, the demand for energy is increasing dramatically, which brings a huge amount of pollutant emissions. Sulfur dioxide (SO_2) is one of the major pollutants of energy production. Atmospheric SO_2 comes from both natural and anthropogenic sources. Anthropogenic sources of SO_2 mainly arise from fossil fuel combustion. Sulfur contained within fossil fuels is released to the atmosphere in the form of SO_2 during the combustion process. Natural sources of SO_2 include volcanic eruption and atmospheric oxidation of dimethyl sulfide (DMS) emitted by marine phytoplankton and hydrogen sulfide (H_2S) emitted by volcanic eruption and decay processes. Anthropogenic SO_2 emissions are increasing quickly and have already surpassed emissions by natural sources (Smith et al., 2001; Lu et al., 2010).

SO_2 emission is of concern because SO_2 and its oxidation product, sulfate, can cause severe environmental problems. After SO_2 is released into the atmosphere, it can be oxidized to sulfate via gas phase oxidation and aqueous phase oxidation; the majority of SO_2 oxidation occurs in the aqueous phase (Lelieveld and Heintzenberg, 1992). Atmospheric sulfate can increase atmospheric acidity and contribute to acid deposition.

Acidity is quantified based on the pH level. The pH level of unpolluted rain is around 5.0 to 5.6, which is slightly acidic compared to the neutral pH of 7.0 due to the dissolution of carbon dioxide and contributions by other naturally occurring acids (Likens et al., 1979).

Acid deposition was a major environmental problem in Europe and the USA in several decades of the last century; now it is a major environmental problem in China because of rapid growth and increasing amounts of pollution. Figure 1-1 shows the scheme of acid deposition formation.

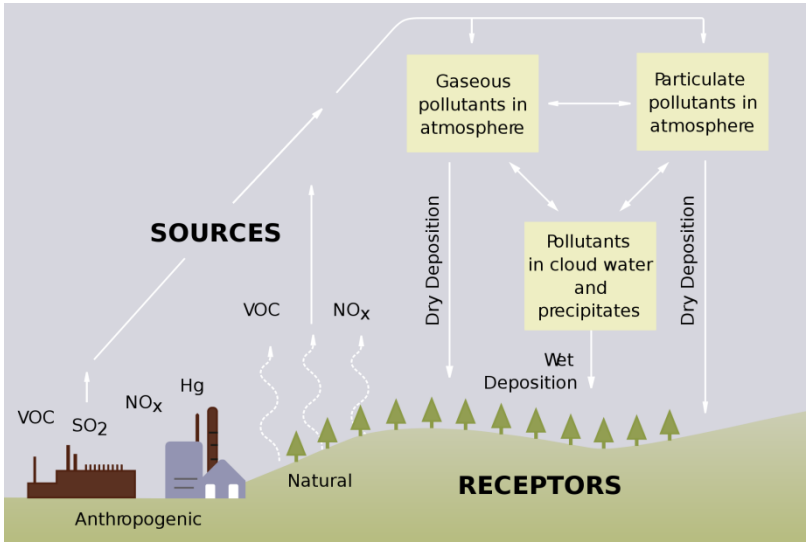

Figure 1-1. Scheme of acid deposition formation (from http://www.epa.gov/acidrain).

Numerous studies have been conducted world-wide on acid deposition formation and its effects since the 1970s (Likens and Bormann, 1974; Carter, 1979; Abelson, 1983; Singer, 1984; Abelson, 1985; Abelson, 1987; Fay and Golomb, 1989; Likens et al., 1996). Acid deposition has adverse impacts on the environment; it can increase the soil acidity and

reduce soil fertility by leaching away nutrient cations and increasing toxic heavy metals availability, thereby affecting the productivity of vegetation.

Acidification of water bodies will cause negative impact on aquatic ecosystem. Acid deposition can damage building materials and can also have indirect effects on human health (Bravo et al., 2006; Menon et al., 2007; Singh and Agrawal, 2008). Sulfate aerosol can also perturb the Earth's radiation budget directly through the backscattering of sunlight and indirectly by changing cloud microphysical properties (Charlson et al., 1992; Lelieveld and Heintzenberg, 1992; Kiehl and Briegleb, 1993; Fischer-Bruns et al., 2009).

Anthropogenic SO_2 emissions in Europe and North America have decreased in the last two decades, but they have increased in Asia due to economic growth (Manktelow et al., 2007). Anthropogenic SO_2 emissions in China have ranked highest in the word in recent years; the total anthropogenic emitted SO_2 changed dramatically during the last two decades. From the late 1980s, total SO_2 emissions in China kept increasing rapidly until 1995. After 1995 the increase in emission rate slowed down and even decreased due to a more restrictive Chinese policy on SO_2 emission. Beginning in 2002, Chinese SO2 emissions began to rapidly increase again along with economic development; emissions increased by 53% from 2000 to 2006 (Lu et al., 2010). After 2006, SO_2 emissions again decreased as desulfurization equipment was widely adopted in China (Zhang et al., 2009). Figure 1-2 shows a timeline of anthropogenic SO_2 emissions in China.

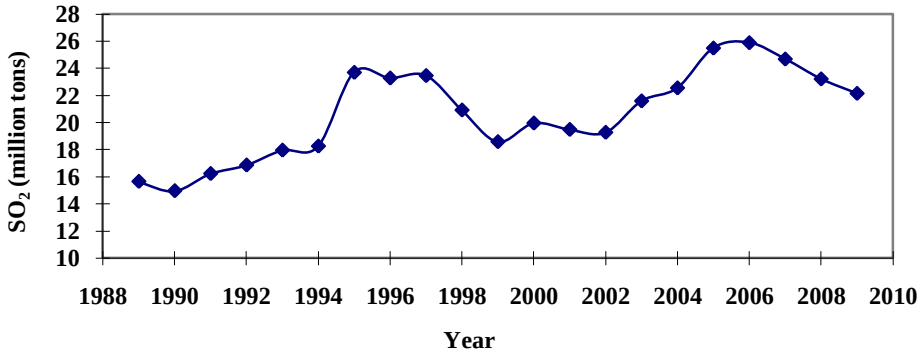

Figure 1-2. Annual anthropogenic SO_2 emissions in China 1989-2009 (Data from State Environmental Statistic Report).

The regional distribution of SO_2 emissions in China is uneven due to various economic development situations in different provinces. Table 1-1 gives the SO_2 emissions in China by province in 2006. As shown in Table 1-1, power plants are the main source of SO_2 emissions in China, accounting for more than half of the total anthropogenic SO_2 emissions. Consistent with the uneven distribution of emissions, the atmospheric SO_2 concentration is also unevenly distributed across the country, as shown in Figure 1-3.

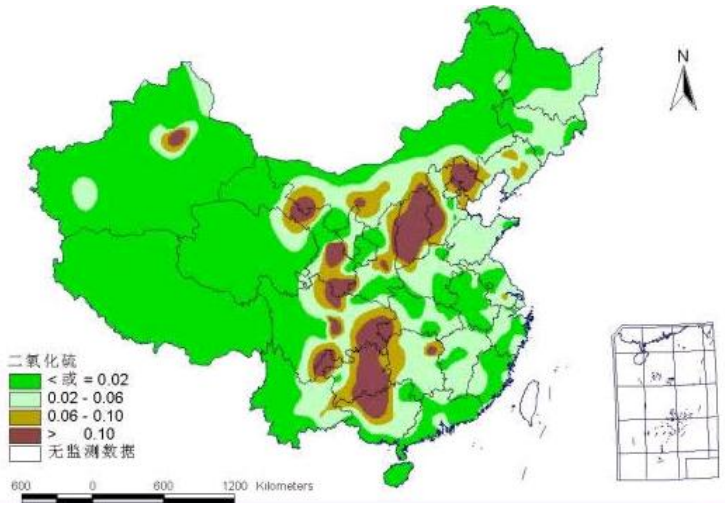

Figure 1-3. The regional distribution of atmospheric SO_2 concentrations in 2001. Concentrations are shown in units of mg/m^3. (Figure from 2001 State Environmental Statistic Report).

Table 1-1. SO_2 emissions in China by province and source category in 2006 (Unit: Gg/year, data from http://mic.greenresource.cn/static/tables/intex-b_v12/summary-2006-SO2.html).

Province	Power	Industry	Residential	Transportation	Total
Anhui	337.3	280.9	69.5	5.1	692.8
Beijing	118.0	62.0	62.7	4.9	247.6
Chongqing	588.9	447.1	173.8	1.4	1211.2
Fujian	263.0	172.3	22.2	2.9	460.4
Gansu	230.7	68.5	37.0	1.4	337.6
Guangdong	813.2	323.8	24.9	12.8	1174.6
Guangxi	344.0	507.3	26.0	2.9	880.2
Guizhou	1153.5	413.2	383.6	1.4	1951.7
Hainan	43.1	29.6	2.9	0.7	76.3
Hebei	1438.9	609.1	224.4	8.9	2281.2
Heilongjiang	194.0	34.0	10.3	3.2	241.5
Henan	1298.8	184.7	99.3	8.5	1591.3
Hong Kong	104.4	11.9	1.6	0.2	118.0
Hubei	713.6	1259.4	222.9	3.8	2199.6
Hunan	466.7	367.3	78.0	3.2	915.3
Jiangsu	1180.9	476.9	32.0	7.5	1697.3
Jiangxi	357.1	141.7	31.8	2.1	532.6
Jilin	204.3	96.1	54.2	2.7	357.3
Liaoning	672.4	268.1	81.7	4.5	1026.8
Nei Mongol	715.5	259.4	193.5	3.1	1171.5
Ningxia	295.4	63.6	20.0	0.8	379.7
Qinghai	4.1	9.2	4.6	0.6	18.5
Shannxi	684.1	167.9	52.3	2.8	907.1
Shandong	2053.7	907.7	129.3	11.5	3102.2
Shanghai	464.9	121.9	28.5	2.8	618.1
Shanxi	1273.7	339.4	187.6	3.9	1804.5
Sichuan	1001.0	1124.8	424.5	5.0	2555.3
Tianjin	214.3	87.6	32.4	1.8	336.1
Xinjiang	126.4	38.1	43.0	2.2	209.6
Xizang	0.0	0.0	0.0	0.3	0.3
Yunnan	329.6	91.9	64.0	3.8	489.3
Zhejiang	648.4	759.7	19.3	6.7	1434.1
China Total	18333.4	9725.1	2837.7	123.3	31019.5

Both wet and dry deposition of sulfur are major concerns in China. Larssen et al.(2006) report annual sulfur deposition rates at several locations in China ranging from ~2 to 16 g-S/m^2, similar to or higher than peak deposition fluxes in Europe three decades ago.

The precipitation pH value distribution in China is quite different from the SO_2 concentration distribution. Figure 1-4 shows the 2001 precipitation pH value distribution

in China. Historically, acid precipitation has been most problematic in southern China. Higher precipitation pH values in Beijing and other northern parts of China, however, do not typically reflect an absence of substantial sulfate input; rather, sufficient acid neutralizing capacity is generally present, from alkaline dust particles and gaseous ammonia, to prevent significant acidification (Wai et al., 2005). As SO_2 emissions continue to increase, however, acidic precipitation is spreading more widely across China.

Figure 1-5 shows the 2001 regional distribution of particle concentrations in China. Large concentrations of airborne soil dust contribute to high particle concentrations in China, especially in the north which is closer to primary dust source regions. Soil dust in the atmosphere may alleviate the acid deposition situation in the north by neutralizing part of the acidity contributed to precipitation by sulfuric and nitric acids. Increasing sulfur emissions are expected to also result in more acid deposition in the northern part (Zhao and Hou, 2010).

The neutralization ability of atmospheric dust particles is seasonally variable. Mt. Tai, the location of the study to be described in this dissertation, is located within the warm temperate continental monsoon climate zone; in winter, due to the cold high pressure from Mongolia, prevailing winds blow from the north; in summer, the prevailing winds blow from the Western Pacific to the continent driven by the subtropical high pressure from the southeast. Generally there is more natural dust in spring than in summer, which

can cause seasonally variable neutralization ability. This may affect the pH value and the sulfur chemistry in cloudwater.

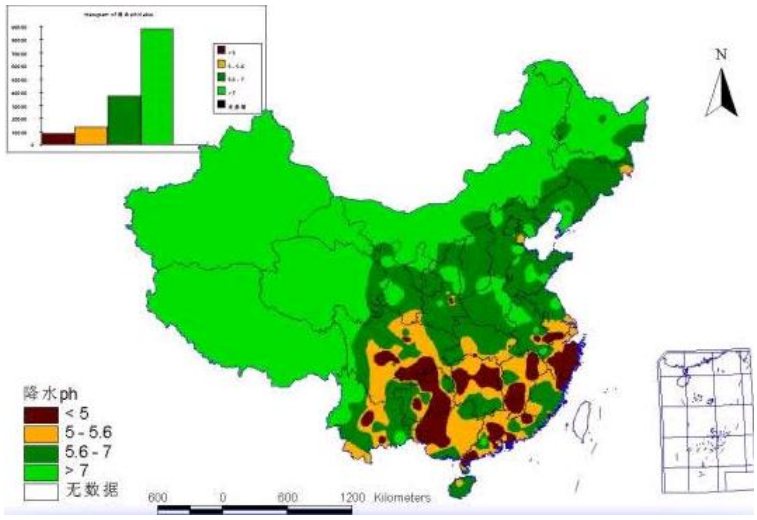

Figure 1-4. The precipitation pH value distribution in 2001. (Figure from 2001 State Environmental Statistic Report).

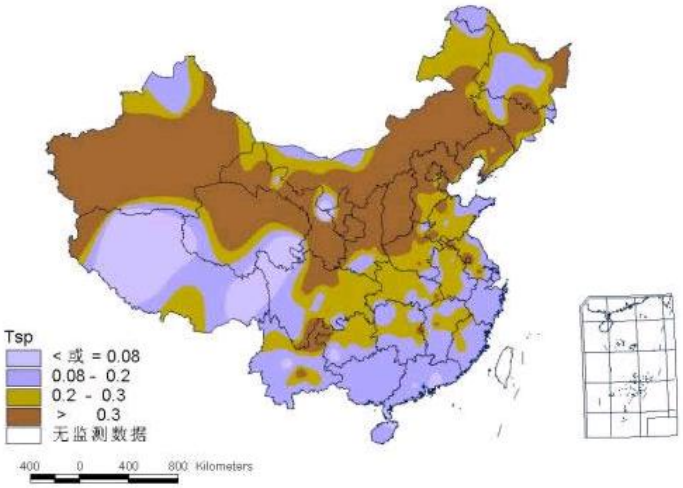

Figure 1-5. The regional distribution of Total Suspended Particles (TSP) concentrations in 2001. Concentrations are shown in units of mg/m^3. (Figure from 2001 State Environmental Statistic Report).

The sulfate that contributes to China's acid rain and deposition problems is also of interest internationally. Because quantities of emitted sulfur dioxide in China are so large (total SO_2 emission in 2009 was 22.1 million tons (China-MEP, 2010)) it is possible that they exceed the capacity of regional clouds for rapid aqueous phase sulfate production, leading to enhanced long-range transport of emitted SO_2 and its oxidation product, sulfate. Tu et al. (2004) reported that long-range transport of SO_2 from East Asia to the central North Pacific troposphere was observed on transit flights during the NASA TRACE-P mission in March and April 2001. The SO_2 emitted from East Asian sources was generally transported to the central Pacific in 3~4 days. Studies by Brock et al. (2004) indicated that following long-range transport of sulfur dioxide, particles were formed over the mid-Pacific. Fiedler et al. (2009) also found that SO_2 from East Asian sources was detected over Europe after traveling across the North Pacific, North America and the North Atlantic. High fine particle sulfate concentrations are routinely experienced in nations immediately downwind. Kim et al. (2009), for example, document impacts on S. Korea. Sulfate transport across the Pacific and into the U.S. is also a concern. Park et al. (2004) estimate that concentrations of sulfate transported across the Pacific to the United States slightly exceed the average concentration (0.12 $\mu g/m^3$) suggested by the U.S Environmental Protection Agency for estimating natural visibility conditions in the western U.S.

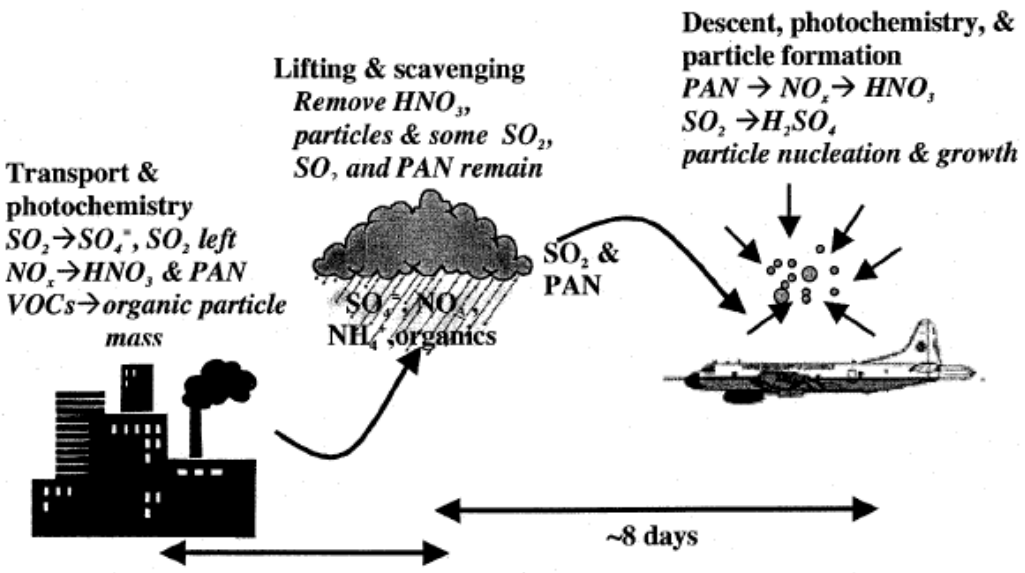

Figure 1-6. Schematic of the emission, transformation and transportation of pollutants (from Brock et al., 2004).

Figure 1-6 depicts schematically the emission, transformation and transportation of pollutants. The range of influence of emitted sulfur depends on its atmospheric lifetime. Conversion of gaseous sulfur dioxide to fine particle sulfate can enhance the lifetime of emitted sulfur. SO_2 in the atmosphere can be converted to gaseous sulfuric acid (H_2SO_4) through gas phase oxidation.

$$SO_2 + OH\cdot + M \rightarrow H_2SO_4 + M \qquad \text{Reaction 1-1}$$

Due to its low vapor pressure, H_2SO_4 partitions strongly to the particle phase.

Globally, sulfur dioxide oxidation is thought to occur mostly in clouds (Lelieveld and Heintzenberg, 1992). Depending on environmental conditions, various aqueous phase oxidation pathways can be important. These include oxidation by hydrogen peroxide, oxidation by ozone, and oxidation by oxygen, catalyzed by certain trace metals (Ervens et

al., 2003; Seinfeld and Pandis, 2006). At low to moderate pH (typically pH ~2-5), oxidation is generally expected to favor the H_2O_2 pathway. Fast S(IV) oxidation by H_2O_2 can, of course, be maintained only as long as H_2O_2 is available. If SO_2 concentrations significantly exceed H_2O_2 concentrations, this pathway may be effective in converting only a portion of the SO_2 to sulfate. Aqueous H_2O_2 can come from gas to droplet partitioning or be formed *in situ* by aqueous photochemistry (Faust et al., 1993; Anastasio et al., 1994; Zuo and Deng, 1999). At pH values above 5, oxidation by ozone and trace metal catalyzed autooxidation often increase in importance. At these higher pH values, sulfate production may also be affected by competition with S(IV) complexation by carbonyls, including formaldehyde (Munger et al., 1984; Munger et al., 1986; Olson and Hoffmann, 1989; Rao and Collett, 1995).

In model simulations of atmospheric sulfate production, Barth et al. (2000) point out the dominant role that aqueous phase chemistry plays, especially in the lower troposphere and in mid-latitude regions of the northern hemisphere. They note that, globally, the column burden of sulfate produced by aqueous phase chemistry is greatest over east Asia and point out the important roles that cloud pH, H_2O_2 concentrations, and depletion of H_2O_2 (by reactions in cloud) play in influencing sulfate production. Barth and Church (1999) simulate changes in atmospheric sulfate burdens resulting from a doubling of SO_2 emissions in SE China. Their simulations suggest a nonlinear response for this situation, in part because increased SO_2 emissions overwhelm available H_2O_2 concentrations, making gas phase sulfate production relatively more important. Because sulfate produced in the gas phase is less susceptible to rapid wet deposition than sulfate produced in-cloud,

the net effect is that a doubling of SO_2 concentrations produces more than a doubling of SE China's contribution to the global tropospheric sulfate burden.

The sulfur lifetime is also closely related to the precipitation frequency. Sulfate produced by oxidation in precipitating clouds can be rapidly removed by wet deposition. Less precipitating cloud or slower in-cloud oxidation mean fewer sulfur dioxide emissions are deposited to the surface regionally and more emissions stay in the atmosphere and are transported farther downwind (Barth and Church, 1999).

Many studies have been conducted on acid rain in China (Jernelov, 1983; Zhao and Sun, 1986; Galloway et al., 1987; Shen et al., 1996; Wang and Wang, 1996; Larssen et al., 2006), but not many studies have been devoted to cloud/fog chemistry. Cloud/fog chemistry research in China started in the 1980s (Wang and Xu, 2009; Niu et al., 2010) and most observations were conducted in areas with severe acid deposition concerns, such as Chongqing (Peng et al., 1992; Li and Peng, 1994), Nanjing (Li et al., 2008), Shanghai (Li et al., 1999), Mt. Lu (Ding et al., 1991), et al. Cloud chemistry research in China has been generally limited to routine analysis of ions.

Because aqueous phase oxidation processes are so critical to sulfate production, it is imperative to understand factors influencing cloud chemistry in China, especially the cloudwater chemical composition and key species that determine the aqueous phase sulfur chemistry.

1.2. AQUEOUS PHASE SULFUR REACTIONS IN CLOUDWATER

The total aqueous sulfur in the +4 oxidation state (S(IV)) includes hydrated SO_2, the bisulfite ion, the sulfite ion, and hydroxymethanesulfonate (HMS):

$$[S(IV)] = [SO_2 \cdot H_2O] + [HSO_3^-] + [SO_3^{2-}] + [HMS] \qquad \text{Equation 1-1}$$

Fig. 1-7 shows the mole fractions of the three S(IV) forms of dissolved sulfur dioxide, $SO_2 \cdot H_2O$, HSO_3^- and SO_3^{2-}, as a function of pH. As the pH value increases, the speciation of S(IV) shifts from $SO_2 \cdot H_2O$ toward HSO_3^- and SO_3^{2-}. The crossover points between species correspond to the pKa of the more protonated form.

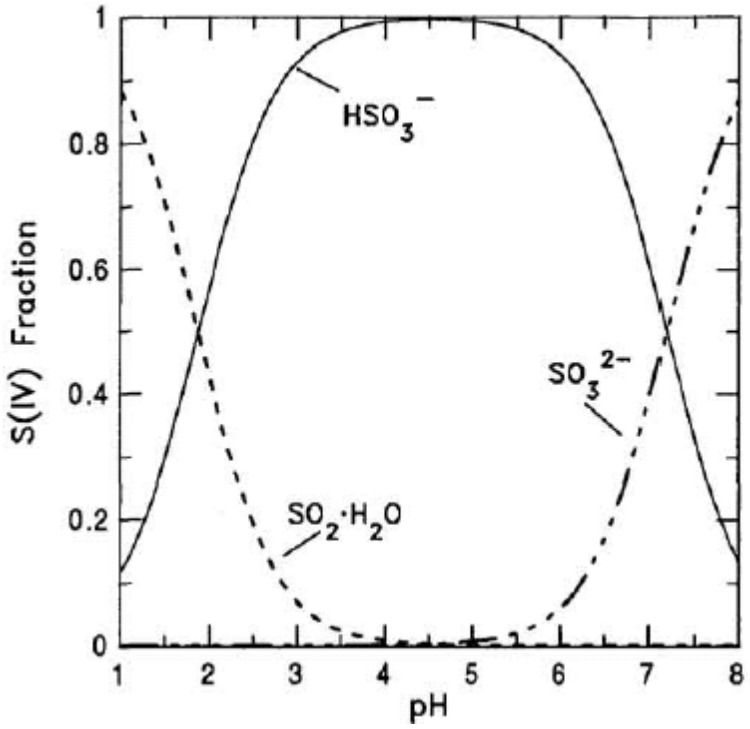

Figure 1-7. Mole fractions of S(IV) species concentrations as a function of pH (from Seinfeld and Pandis, 2006).

Important aqueous phase oxidants of dissolved sulfur dioxide include hydrogen peroxide (H_2O_2), ozone (O_3) and oxygen (O_2) (catalyzed by trace metals). The speed of aqueous phase oxidation depends on pH, oxidant availability, and liquid water content (LWC) (Liang and Jacobson, 1999).

1.2.1. S(IV) oxidation by ozone

In the three main aqueous phase oxidation pathways, aqueous phase S(IV) oxidation by O_3 tends to be most rapid at high pH. Tropospheric ozone predominantly forms through photochemical and chemical reactions of nitrogen oxides (NO_x) and volatile organic compounds (VOCs). The reaction that produces ozone can be expressed as:

$$O + O_2 + M \rightarrow O_3 + M \qquad \text{Reaction 1-2}$$

NO_x is one of the key species for the photochemical production of tropospheric ozone.

$$NO_2 + h\nu \rightarrow NO + O \qquad \text{Reaction 1-3}$$

$$NO + O_3 \rightarrow NO_2 + O_2 \qquad \text{Reaction 1-4}$$

This O_3-NO-NO_2 cycle has no net effect on O_3, but in the presence of peroxy radicals, the cycle is perturbed and ozone production is enhanced. Peroxy radicals, formed by photochemical oxidation of VOCs, oxidize NO to NO_2 and lead to accumulation of ozone.

Aqueous S(IV) oxidation by O_3 is represented as

$$S(IV) + O_3 \rightarrow S(VI) + O_2 \qquad \text{Reaction 1-5}$$

The reaction rate can be expressed as follows (Hoffmann and Calvert, 1985; Hoffmann, 1986; Seinfeld and Pandis, 2006):

$$-\frac{d[S(IV)]}{dt} = (k_0\alpha_0 + k_1\alpha_1 + k_2\alpha_2)[S(IV)][O_3] \qquad \text{Equation 1-2}$$

The characteristic time for S(IV) depletion through oxidation by O_3

$$\tau_{O_3} = 1/((k_0\alpha_0 + k_1\alpha_1 + k_2\alpha_2)[O_3]) \qquad \text{Equation 1-3}$$

α_0, α_1, and α_2 represent the fractions of total free S(IV) present as $SO_2 \cdot H_2O$, HSO_3^- and SO_3^{2-} respectively, where at 298K, $k_0 = 2.4\times10^4\,M^{-1}s^{-1}$, $k_1 = 3.7\times10^5\,M^{-1}s^{-1}$, and $k_2 = 1.5\times10^9\,M^{-1}s^{-1}$.

As shown in Fig. 1-7, when the pH value increases, the speciation of S(IV) shifts from $SO_2 \cdot H_2O$ toward HSO_3^- and SO_3^{2-}. This draws more SO_2 into the droplet (to maintain the Henry's Law equilibrium with the SO_2 partial pressure in the gas phase) and shifts the S(IV) to forms that are more rapidly oxidized by O_3 (Hoffmann, 1986). $SO_2 \cdot H_2O$, HSO_3^- and SO_3^{2-} have different reactivities, as show in equation 1-2. The rate constant of $SO_2 \cdot H_2O$-O_3 is lower than those of HSO_3^--O_3 and SO_3^{2-}-O_3. The rate constant of SO_3^{2-}-O_3 is much higher than those of the other two forms. As cloud pH increases the increase in total S(IV) concentration and the change in speciation both contribute to a rapid rise in the overall S(IV) oxidation rate by ozone.

In a chemical reaction, the species with fewer moles is the limiting reactant. The ambient mixing ratio of O_3 is generally higher than that of SO_2, so normally O_3 will not be completely depleted by the aqueous oxidation process.

1.2.2. S(IV) oxidation by hydrogen peroxide

S(IV) oxidation by hydrogen peroxide is generally expected to be most important when pH is below ~5. Atmospheric hydrogen peroxide is generated mainly through self-reaction of the HO_2 radical.

$$HO_2 \cdot + HO_2 \cdot \rightarrow H_2O_2 + O_2 \qquad \text{Reaction 1-6}$$

The HO_2 radical is mainly generated through reaction of the OH radical with CO and other VOCs. Aqueous H_2O_2 comes from gas-to-droplet partitioning and can also be produced in clouds by aqueous photochemistry (Faust et al., 1993; Anastasio et al., 1994; Zuo and Deng, 1999). H_2O_2 is moderately water soluble and the oxidation of S(IV) by H_2O_2 is very fast in clouds. The reaction and rate can be expressed as follows (Seinfeld and Pandis, 2006).

$$HSO_3^- + H_2O_2 \leftrightarrow SO_2OOH^- + H_2O \qquad \text{Reaction 1-7}$$

$$SO_2OOH^- + H^+ \rightarrow H_2SO_4 \qquad \text{Reaction 1-8}$$

$$-\frac{d[S(IV)]}{dt} = \frac{k[H^+][H_2O_2][S(IV)]\alpha_1}{1 + K[H^+]} \qquad \text{Equation 1-4}$$

The characteristic time for S(IV) depletion through oxidation by H_2O_2:

$$\tau_{H_2O_2} = (1 + K[H^+])/(k[H^+][H_2O_2]\alpha_1) \qquad \text{Equation 1-5}$$

where $k = 7.45 \times 10^7 M^{-2}s^{-1}$ and $K = 13M^{-1}$ at 298K.

As shown in Fig. 1-7, in the pH range 3-6, almost all S(IV) exists as HSO_3^-. Over a broad range of pH, the H_2O_2 oxidation pathway exhibits essentially no pH dependence. Although the total S(IV) in solution increases as pH rises (as discussed above), this is offset by a decrease in the H^+ concentration which slows reaction 1-8, which is the rate limiting step.

The ambient mixing ratio of H_2O_2 is normally much lower than that of O_3. If the mixing ratio of H_2O_2 is lower than the ambient SO_2 mixing ratio, the H_2O_2 can be consumed completely by the aqueous S(IV) oxidation process. If the SO_2 mixing ratio is lower, the ambient SO_2 can be rapidly exhausted by the reaction. In order to understand the relative importance of both the O_3 and H_2O_2 sulfur oxidation pathways, it is necessary to investigate the ambient concentrations of SO_2, O_3 and H_2O_2 as well as the cloud pH.

1.2.3. S(IV) oxidation by oxygen (catalyzed by Fe(III) and Mn(II))

Uncatalyzed S(IV) oxidation by oxygen is very slow and can be neglected. Oxidation of S(IV) to sulfate by oxygen, catalyzed by the ferric ion, Fe(III), and the manganese ion, Mn(II), is considered a possibly important contributor to the total oxidation rate of S(IV), especially in situations of reduced photochemical activity (producing less O_3 and H_2O_2)

and higher Fe(III) and Mn(II) concentrations (Ibusuki and Takeuchi, 1987). Many studies have investigated the kinetics for this oxidation pathway (Jacob and Hoffmann, 1983; Ibusuki and Takeuchi, 1987; Martin and Good, 1991; Grgic et al., 1992). Fe and Mn in the atmosphere come from both anthropogenic and natural sources. The anthropogenic source of coal combustion (Luo et al., 2008) can have an important influence on the regional concentrations of Fe and Mn in the atmosphere. Natural sources of Fe and Mn are mainly from mineral dust. Chuang et al. (2005) reported that the origin of soluble iron in the Asian atmospheric outflow is dominated by anthropogenic sources and not mineral dust sources.

The ratio of the catalytically active iron form, Fe(III), to the concentration of the inactive iron form, Fe(II), is important to the accurate calculation of the sulfur oxidation rate, since only Fe(III) acts as a catalyst for S(IV) oxidation. Generally the total Fe concentration is measured, due to the extreme difficulty in accurately speciating rapidly cycling iron oxidation states in the field, and an assumption is made regarding the abundance of the two oxidation states. Siefert et al. (1998) measured the Fe and Mn oxidations states in several cloud/fog events and found that Mn(II) was the predominant oxidation states of Mn; however, it was more difficult to identify the speciation of Fe. Following the approach of Rao and Collett (1995), the Mn was assumed in this study to be completely present as catalytically active Mn(II) and 25% of the Fe was assumed to be present as catalytically active Fe(III).

S(IV) oxidation by oxygen (catalyzed by Fe(III) and Mn(II)) can be expressed as (Ibusuki and Takeuchi, 1987):

$$S(IV) + \frac{1}{2}O_2 \xrightarrow{Mn^{2+},Fe^{3+}} S(VI) \qquad \text{Reaction 1-9}$$

$pH \le 4.2$:

$$-\frac{d[S(IV)]}{dt} = k_s^{'}[H^+]^{-0.74}[Fe(III)]\cdot[Mn(II)]\cdot[S(IV)] \qquad \text{Equation 1-6}$$

$$\tau^{'}_{O_2(Mn(II)/Fe(III))} = 1/(k_s^{'}[H^+]^{-0.74}[Fe(III)]\cdot[Mn(II)]) \qquad \text{Equation 1-7}$$

where at 296.8K, third order rate constant $k_s^{'} = 3.72\times10^7\,M^{-2}s^{-1}$.

$6.5 \ge pH \ge 4.2$:

$$-\frac{d[S(IV)]}{dt} = k_s^{''}[H^+]^{0.67}[Fe(III)]\cdot[Mn(II)]\cdot[S(IV)] \qquad \text{Equation 1-8}$$

$$\tau^{''}_{O_2(Mn(II)/Fe(III))} = 1/(k_s^{''}[H^+]^{0.67}[Fe(III)]\cdot[Mn(II)]) \qquad \text{Equation 1-9}$$

where at 296.8K, third order rate constant $k_s^{''} = 2.51\times10^{13}\,M^{-2}s^{-1}$.

As shown in equation 1-6 and equation 1-8, the rate of S(IV) oxidation by oxygen (catalyzed by Fe(III) and Mn(II)) is affected by a synergy between Fe and Mn (Ibusuki and Takeuchi, 1987; Martin and Good, 1991). This oxidation rate is also pH dependent, increasing as pH rises.

1.2.4. Aqueous SO_2 complexation with formaldehyde

Aqueous S(IV) can complex with formaldehyde in cloudwater to form hydroxymethanesulfonate (HMS). The time constant of the complexation process is pH dependent; as the pH decreases the time constant increases (Warneck, 1989). At low pH, the complexation process may not reach equilibrium during a cloud event.

$$HCHO + HSO_3^- \leftrightarrow OHCH_2SO_3^- \qquad \text{Reaction 1-10}$$

$$-\frac{d[S(IV)]}{dt} = k_4[S(IV)]\alpha_1[HCHO] + k_5[S(IV)]\alpha_2[HCHO] \qquad \text{Equation 1-10}$$

$$\tau_{HCHO} = 1/([HCHO]\cdot(k_4\alpha_1 + k_5\alpha_2)) \qquad \text{Equation 1-11}$$

where at 298K, $k_4 = 7.90\times10^2\,M^{-1}s^{-1}$, and $k_5 = 2.48\times10^7\,M^{-1}s^{-1}$.

The formation of hydroxymethanesulfonate (HMS) via the complexation of HCHO and S(IV) can compete with S(IV) oxidation and thereby inhibit the production of sulfate in clouds (Munger et al., 1984; Munger et al., 1986; Rao and Collett, 1995; Reilly et al., 2001); thus, HMS can act as a reservoir pool for S(IV) (Adewuyi et al., 1984). Although HMS formation tends to dominate hydroxyalkylsulfonate formation, due to the greater abundance and aqueous solubility of HCHO, similar reactions also occur with larger carbonyls (Olson and Hoffmann, 1989).

1.2.5. Temperature dependence of equilibrium and rate constants

The temperature dependence is represented by (Seinfeld and Pandis, 2006)

$$K = K_{298}\exp\left[-\frac{\Delta H}{R}\left(\frac{1}{T} - \frac{1}{298}\right)\right] \qquad \text{Equation 1-12}$$

where R=8.314 $Jmol^{-1}K^{-1}$, K is Henry's law coefficient and the equilibrium constant at temperature T.

Table 1-2. Thermodynamic data: Henry's law coefficients and equilibrium constants.

Reaction	K ($M\ atm^{-1}$ or M^n) 278K	283K	298K	ΔH_A at 298K ($kJmol^{-1}$)
(1) $SO_2(g)+H_2O \leftrightarrow SO_2 \cdot H_2O$	2.65	2.17	1.24	-26.13
(2) $SO_2 \cdot H_2O \leftrightarrow HSO_3^- + H^+$	2.11×10^{-2}	1.87×10^{-2}	1.32×10^{-2}	-16.2
(3) $HSO_3^- \leftrightarrow SO_3^{2-} + H^+$	9.04×10^{-8}	8.26×10^{-8}	6.42×10^{-8}	-11.8
(4) $H_2O_2(g) \leftrightarrow H_2O_2(aq)$	4.11×10^{5}	2.59×10^{5}	7.08×10^{4}	-60.6
(5) $O_3(g) \leftrightarrow O_3(aq)$	1.67×10^{-2}	1.44×10^{-2}	9.4×10^{-3}	-19.86

Note: (1), (3), (4), and (5) from Hoffmann and Calvert (1985); (2) from Jacob (1986).

Table 1-3. Kinetic data of S(IV) related reactions.

Reaction	k ($M^{-n}s^{-1}$) 278K	283K	298K	Activation Energy ($kJmol^{-1}$)
(1) $SO_2 \cdot H_2O+O_3 \rightarrow SO_4^{2-}+O_2+2H^+$			2.4×10^{4}	
(2) $HSO_3^- + O_3 \rightarrow SO_4^{2-}+O_2+H^+$	9.73×10^{4}	1.38×10^{5}	3.7×10^{5}	46
(3) $SO_3^{2-}+O_3 \rightarrow SO_4^{2-}+O_2$	4.19×10^{8}	5.86×10^{8}	1.5×10^{9}	43.9
(4) $HSO_3^- + H_2O_2 + H^+ \rightarrow H_2SO_4 + H_2O$	2.37×10^{7}	3.2×10^{7}	7.45×10^{7}	39.5
(5) S(IV)+1/2O_2(Fe(III)/Mn(II))→S(VI) pH<4.2	5.45×10^{6}	9.31×10^{6}	$3.72\times10^{7*}$	70.1
(6) S(IV)+1/2O_2(Fe(III)/Mn(II))→S(VI) pH>4.2	3.68×10^{12}	6.28×10^{12}	$2.51\times10^{13*}$	
(7) HSO_3^-+HCHO→HMS	3.86×10^{2}	4.66×10^{2}	7.9×10^{2}	24.7
(8) SO_3^{2-}+HCHO→HMS	1.39×10^{7}	1.62×10^{7}	2.48×10^{7}	20

Note: (1), (2), (3) and (4) from Hoffmann and Calvert (1985); (5) from Ibusuki and Takeuchi (1987); (6) and (7) from Boyce and Hoffmann (1984). *: The rate constants were determined at 296.8K.

1.2.6. pH dependent aqueous S(IV) reaction rates

As a summary of the above discussions in section 1.2.1-1.2.3, the oxidation rates by these three pathways were calculated under a certain set of conditions. Figure 1-8 shows the rates of the three oxidation pathways rates under the following conditions: mixing ratio of

SO_2 at 20 ppbv, O_3 at 100 ppbv, H_2O_2 at 2 ppbv; aqueous concentration of Fe(III) at 10 µM and Mn(II) at 1 µM; T = 298K.

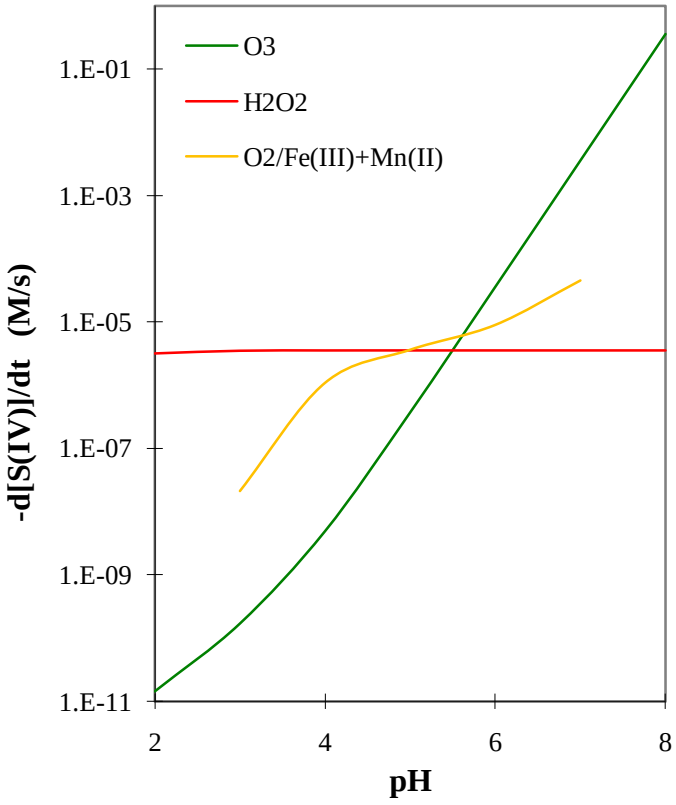

Figure 1-8. S(IV) reaction rates by different pathways, shown as a function of pH, for the conditions specified in the text.

As shown in Fig. 1-8, S(IV) oxidation by hydrogen peroxide is essentially independent of pH while S(IV) oxidation rates by ozone and by oxygen (catalyzed by Fe(III) and Mn(II)) are pH dependent. At lower pH values, S(IV) oxidation by hydrogen peroxide is much faster than the other pathways while S(IV) oxidation by ozone tends to be much faster at higher pH. The relative rates of the oxidation pathways, of course, can change with changes in the available concentrations of oxidants and catalysts.

1.3. CLOUD DROP SIZE-DEPENDENT AQUEOUS SULFUR REACTIONS

Cloudwater chemical composition can vary across the drop size spectrum for a variety of reasons, including differences in the composition of the aerosol particles on which the droplets form (Gurciullo and Pandis, 1997). Differences in drop composition as a function of size also occur due to size-dependent rates of condensational growth (dilution) and soluble gas uptake (Noone et al., 1988; Ogren and Charlson, 1992). Differences in drop composition can also give rise to differences in rates of aqueous phase chemical reactions, leading to further differentiation in droplet compositions.

Several experimental studies have demonstrated the common occurrence of cloud drop size-dependent composition (Noone et al., 1988; Rao and Collett, 1995; Bator and Collett, 1997; Gurciullo and Pandis, 1997; Rao and Collett, 1998; Hoag et al., 1999; Menon et al., 2000; Rattigan et al., 2001; Reilly et al., 2001; Ervens et al., 2003; Moore et al., 2004a; Moore et al., 2004b; Ermakov et al., 2006). It was found that since key parameters that determine aqueous phase sulfur reaction, like pH (Hoag et al., 1999; Reilly et al., 2001), Fe and Mn (Rao and Collett, 1998; Hoag et al., 1999) and aqueous HCHO (Rao and Collett, 1995), can vary with drop size, then aqueous phase SO_2 oxidation rate may also be drop size-dependent. Using the bulk (average) cloudwater composition to determine aqueous sulfate production rates may yield biased estimates. This is especially problematic because many of the S(IV) oxidation pathways discussed above exhibit a nonlinear dependence on various species concentrations, especially H^+, Fe(III), and Mn(II). The prediction of rates from an average cloudwater composition, in

such a case, is not equivalent to determining the average rate predicted from a chemically heterogeneous droplet population. Rates predicted from drop size-resolved cloud composition observations have been found to differ significantly from rates based on average cloud composition for the ozone and metal-catalyzed oxidation pathways (Gurciullo and Pandis, 1997). Because S(IV) oxidation by H_2O_2 is essentially independent of pH and little drop size dependence is expected for peroxide concentrations, this oxidation pathway has been observed to be independent of drop size (Hoag et al., 1999; Rattigan et al., 2001) and no bias in sulfate production is expected when neglecting chemical heterogeneity in cloud drop composition.

1.4. MAJOR RESEARCH OBJECTIVES

Because aqueous phase oxidation processes are so critical to sulfate production, it is imperative to understand factors influencing cloud chemistry in China in order to accurately predict effects of increasing regional SO_2 emissions on sulfate production in that part of the world and its local, regional, and intercontinental effects. While model simulations provide valuable insight into sulfur chemistry and its sensitivity to changing emissions, *in situ* observations are needed to assess actual conditions in the region. In order to more fully investigate the cloudwater chemical composition and key species that determine the aqueous phase sulfur chemistry and to assess the ability of regional clouds to support aqueous sulfur oxidation, four field campaigns were conducted in 2007 and 2008 at Mt. Tai in eastern China. Observations of cloud pH, along with key S(IV) oxidants and catalysts, are reported and used to examine the importance of various

aqueous phase sulfate production pathways. In summary, the specific research objectives include:

- Investigate the chemical composition of cloudwater in eastern China, providing a comprehensive observation data set of cloudwater chemical composition for further cloud chemistry study.

- Characterize the size-dependent chemical composition of cloudwater, especially the key species that determine sulfur chemistry in cloudwater.

- Investigate aqueous sulfur oxidation rates in sampled cloudwater and examine the capacity of the eastern China regional atmosphere to support aqueous phase sulfur oxidation by hydrogen peroxide, ozone, and oxygen (catalyzed by Fe and Mn).

- Determine the extent to which regional clouds in eastern China interact with ambient fine particles and soluble trace gases. Determine what fractions of regional nitrogen- and sulfur-containing air pollutants are actively processed in a cloud event.

- Investigate the seasonal variations of key factors that are critical to determining the chemical composition of cloudwater and sulfur oxidation chemistry. SO_2 concentrations can have seasonal variations due to residential heating that uses fossil fuel combustion in winter season and due to seasonal changes in electricity

demand. H_2O_2 and O_3 concentrations can change with season because of their origins in smog photochemistry.

CHAPTER 2 METHODOLOGY

2.1. SAMPLING TIME AND SITE LOCATION

Four cloud sampling field campaigns were conducted in spring 2007 (March 22-April 24), summer 2007 (June 16-July 20), spring 2008 (March 28-April 25) and summer 2008(June 14-July 16). Spring and summer were selected to investigate the seasonal variations of cloud chemistry. Seasonal changes might be expected due to changes in photochemical activity, prevailing transport patterns, and emissions changes including soil dust. The 2007 field campaigns were led by Shandong University and Hong Kong Polytechnic University, with technical assistance and equipment provided by CSU. CSU led the more extensive 2008 campaigns, with assistance from the other two institutions.

Field experiments were conducted at the summit of Mt. Tai (36.251 ºN, 117.101 ºE, 1534 m a.s.l.), located in eastern China (Figure 2-1). The 2007 measurements were made on the grounds of a meteorological station operated by the China Meteorological Agency. Restrictions on access to this site by CSU personnel in 2008 led to a relocation of measurements a few hundred meters away to a small hotel. Both locations were near the top of the mountain. There are several advantages to using the summit of Mt. Tai, as the sampling site. Mt. Tai is located in central Shandong province and at the eastern edge of the North China Plain, between the Bohai Economic Rim and Yangtze River Delta

Economic Zone, two of China's three major economic circles. Shandong province has the highest SO_2 emission in China, as shown in Table 1-1; the total anthropogenic SO_2 emission in 2006 was 3102.2 Gg, representing approximately 10% of total anthropogenic SO_2 emissions in China. The summit of Mt. Tai contains a number of temples and tourist facilities, but access is only by cable car or foot. No vehicles can access the summit. The elevation of Mt. Tai isolates the measurements from direct influence by large urban emission sources, providing a more representative picture of regional atmospheric composition. The summit is frequently in cloud during spring and summer and nearly half of the days each year have fog or intercepted clouds, making Mt. Tai a reliable place to sample fog and cloudwater under the influence of regional atmospheric pollution. Other investigators have also found Mt. Tai a useful site for measurement of various aerosol and gas phase pollutants (Gao et al., 2005; Wang et al., 2006; Kanaya et al., 2008; Li et al., 2008; Wang et al., 2008; Mao et al., 2009; Ren et al., 2009; Wang et al., 2009; Yamaji et al., 2010). These previous investigations of atmospheric composition at Mt. Tai have focused on study of gas and particle phase constituents, but little was known about cloud chemistry in the region prior to this study.

Figure 2-1 shows the location of Mt. Tai on a map of Asia with SO_2 emission intensities and political boundaries as background. It is obvious that Mt. Tai is surrounded by a high SO_2 emission intensity area. Sampling at Mt. Tai is an attempt to represent the atmospheric condition of the eastern coastal developed areas of China.

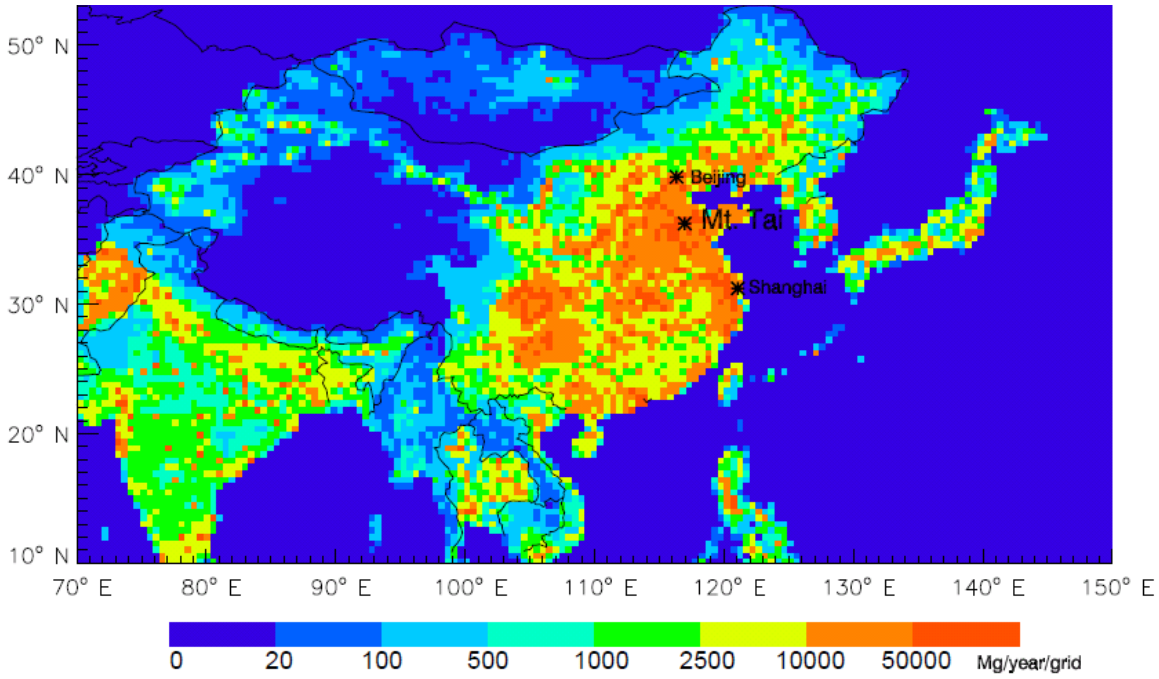

Figure 2-1. Location of the Mt. Tai sampling site and the SO_2 emission intensity distribution at 30min×30min resolution (Data from http://mic.greenresource.cn/data/intex-b).

Several previous studies at Mt. Tai have found it is influenced by transport from many directions, permitting study of possible differences in atmospheric composition and cloud chemistry under different transport patterns.

2.2. SAMPLING INSTRUMENTS

Except for a peroxide analyzer, which was operated in a second floor room, sampling instruments were set up outside to provide direct access to cloud and fog droplets as well as aerosols and trace gases. Figure 2-2 shows the setup of the sampling instruments during the 2008 campaigns.

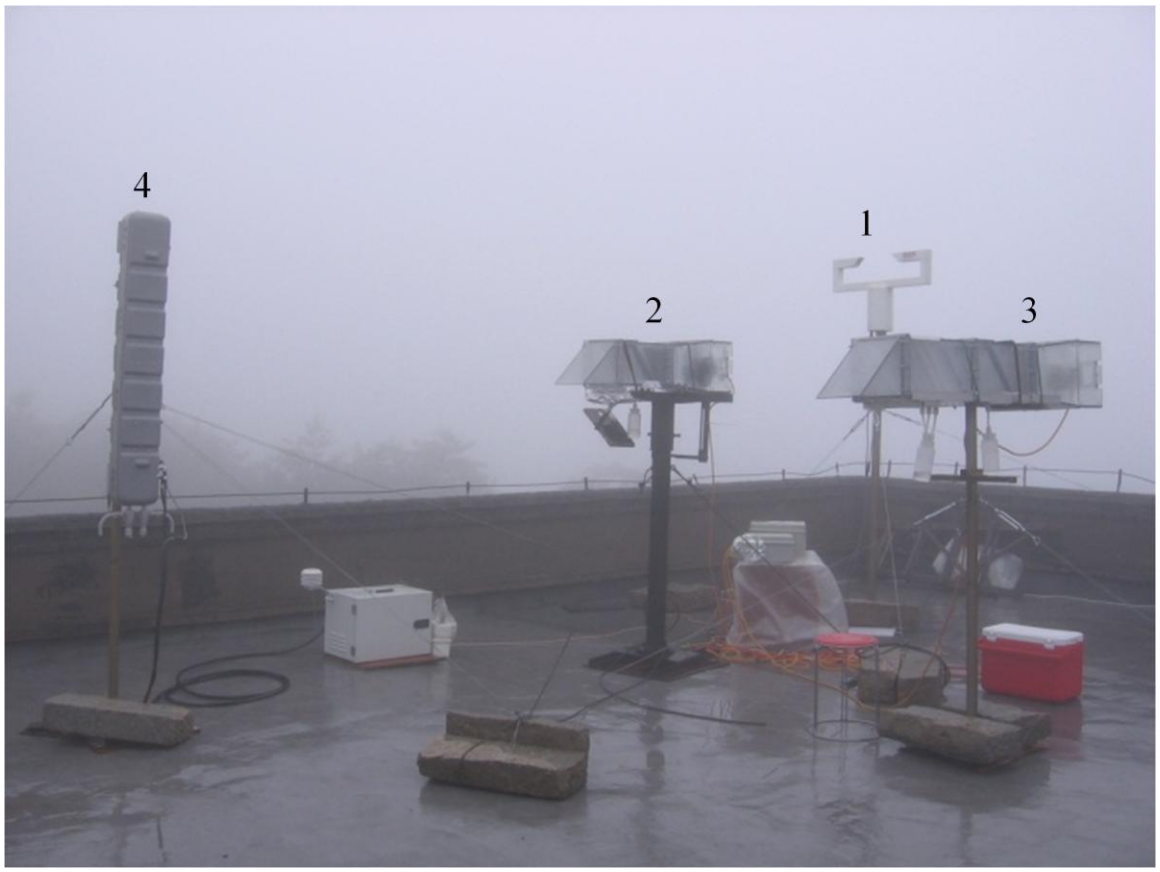

Figure 2-2. Instruments set up in 2008 campaigns. 1-PVM, 2-CASCC, 3-sf-CASCC, 4-URG.

2.2.1. Particulate Volume Monitor

In order to determine when to start and stop cloudwater collection, the cloud liquid water content (LWC) was used as an indicator of the presence of cloud. Cloud LWC was measured by a forward scattering laser spectrometer Particulate Volume Monitor (Gerber Scientific, Inc., model PVM-100). The PVM-100 can measure the volume and surface area of particles over a size range encompassing most cloud droplet sizes (Gerber, 1991). Cloud liquid water content (mg/m^3) and droplet integrated surface area (cm^2/m^3) are recorded at high frequency and averaged to one minute time resolution. The measuring

principle of the PVM-100 is based on the linear relationship between extinction and cloud liquid water content (Gerber, 1984; Gerber, 1991; Arends et al., 1992). The main components of the PVM consist of a laser, collimator optics, and receiver optics. The receiver optics include a transform lens, a light trap, a variable light transmission filter and a large-area light detector (Gerber, 1991). Figure 2-3 shows a schematic of the PVM. The PVM is calibrated by placing a manufacturer-supplied calibration disk in the light path.

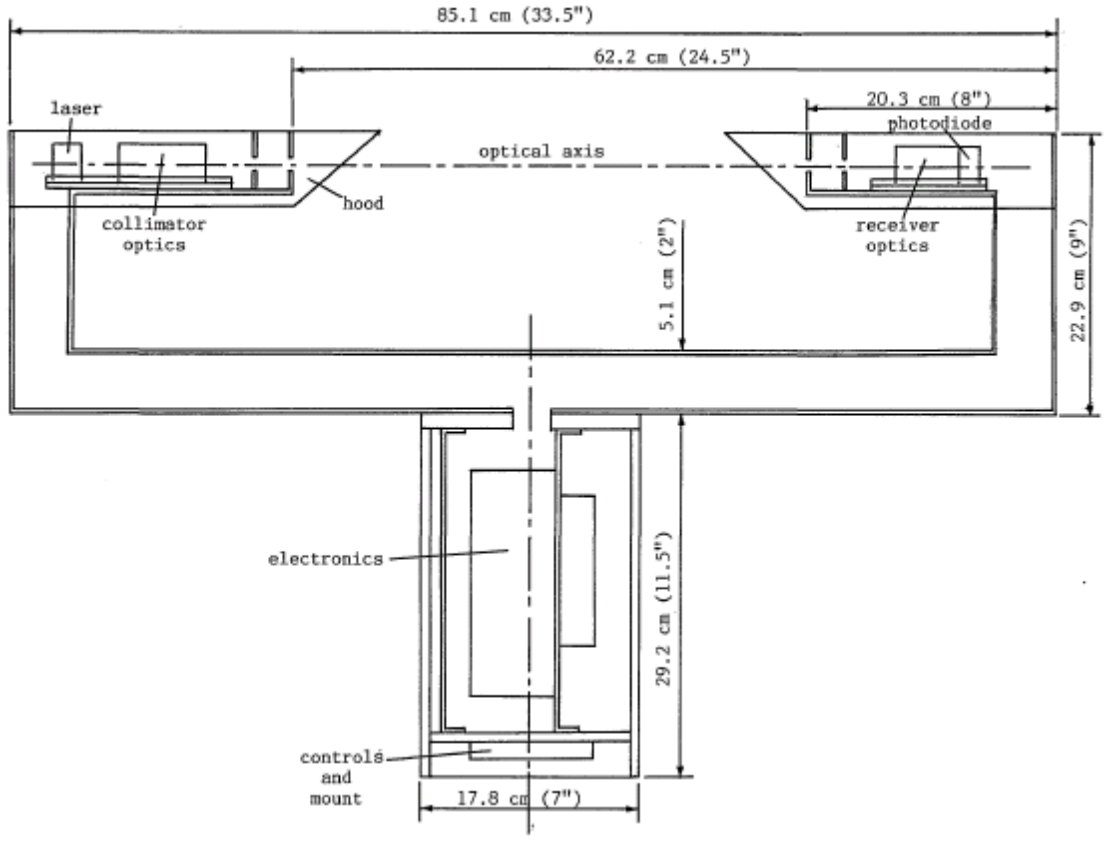

Figure 2-3. Schematic of the PVM (from Gerber 1991).

2.2.2. Cloudwater Collectors

Drop size-resolved samples of cloudwater were collected during the 2008 campaigns. Bulk (all drop sizes together) cloudwater samples were collected during both the 2007 and 2008 campaigns. Bulk cloudwater was collected using Caltech Active Strand Cloudwater Collectors (CASCC) with an air sampling rate of approximately 24 m^3/min and a 50% lower size cut of 3.5 μm diameter (Daube, 1987; Demoz et al., 1996). Figure 2-4 depicts a side view of the Caltech Active Strand Cloud Collector. Figure 2-5 depicts a front view of the Caltech Active Strand Cloud Collector.

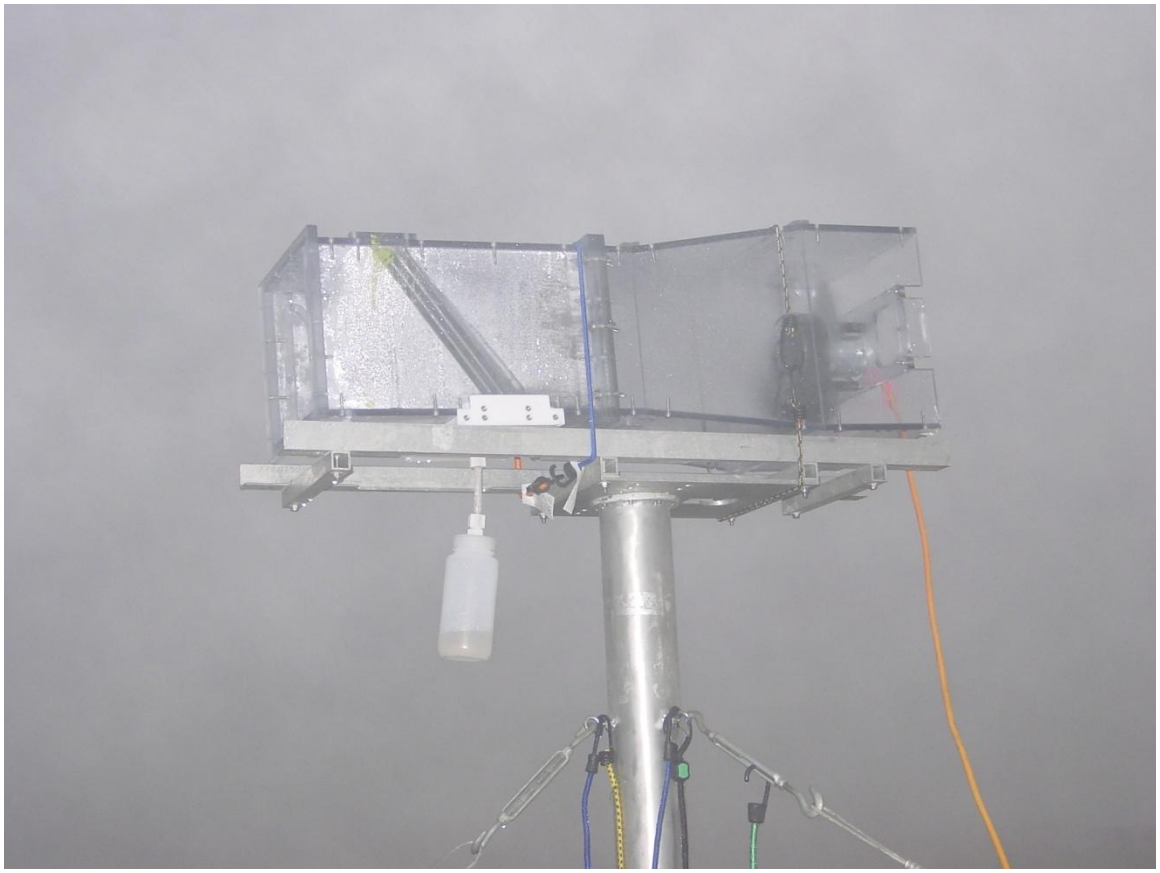

Figure 2-4. Side view of Caltech Active Strand Cloud Collector (CASCC) (picture from 2006 Fresno campaign, a rain cover was installed on the CASCC for the Mt. Tai project).

As shown in Figure 2-4, from left to right, air is drawn by a fan through the collector and across 6 rows of inclined 508 μm Teflon strands. Cloud droplets are impacted upon the Teflon strands where they coalesce and, aided by aerodynamic drag, run down the strands (as shown in Figure 2-5) and through a Teflon collection trough and Teflon tube into a polyethylene collection bottle. The CASCC was operated with a downward facing inlet (see Fig. 2-2) to exclude rain collection during periods of mixed cloud and precipitation.

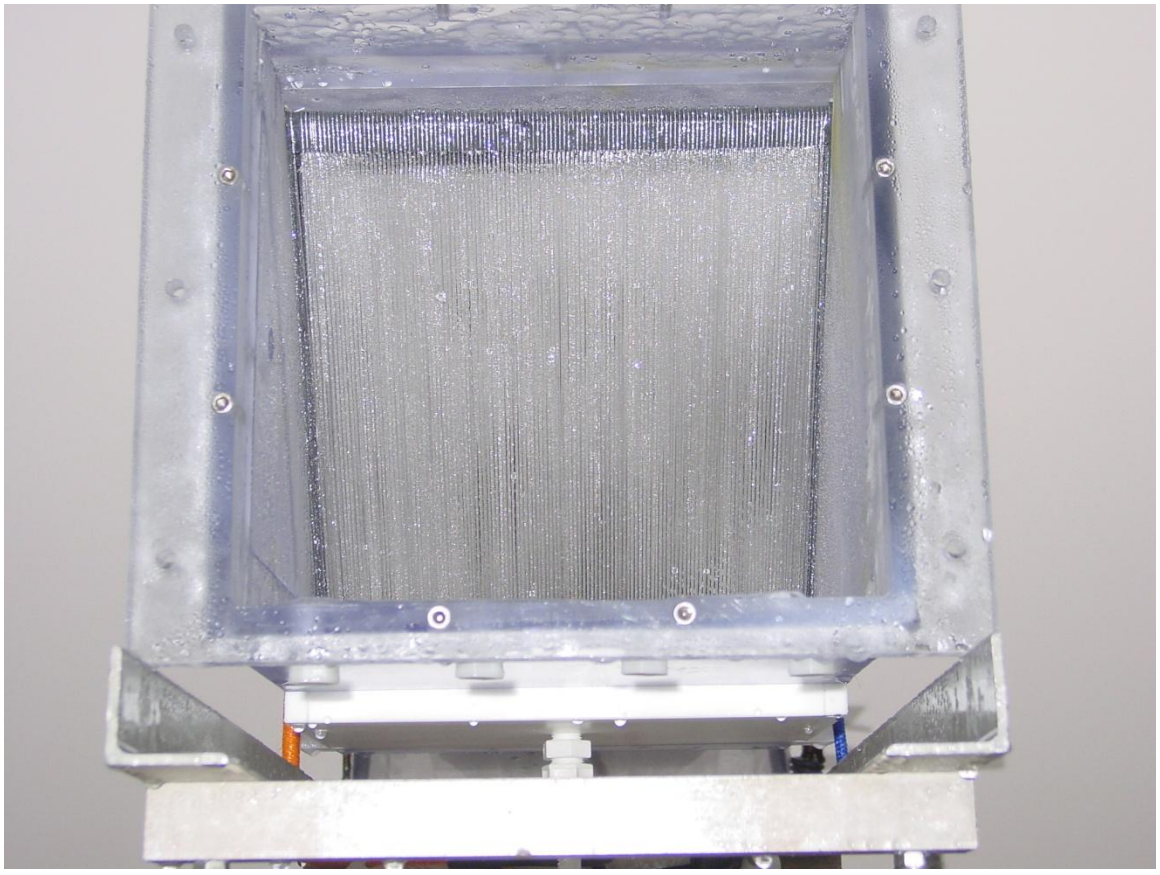

Figure 2-5. Front view of the Caltech Active Strand Cloud Collector (CASCC) without rain excluding inlet.

Drop size-resolved cloudwater samples were collected in the 2008 campaigns using a 2-stage size-fractionating Caltech Active Strand Cloudwater Collector (sf-CASCC) (Demoz

et al., 1996; Reilly et al., 2001). Large and small cloud droplets can be simultaneously collected as independent samples by the sf-CASCC. Details of the sf-CASCC cloudwater collector have been described previously (Rao and Collett, 1995; Rao and Collett, 1998; Collett et al., 1999; Hoag et al., 1999; Reilly et al., 2001). Figure 2-6 depicts a side view of the 2-stage sf-CASCC.

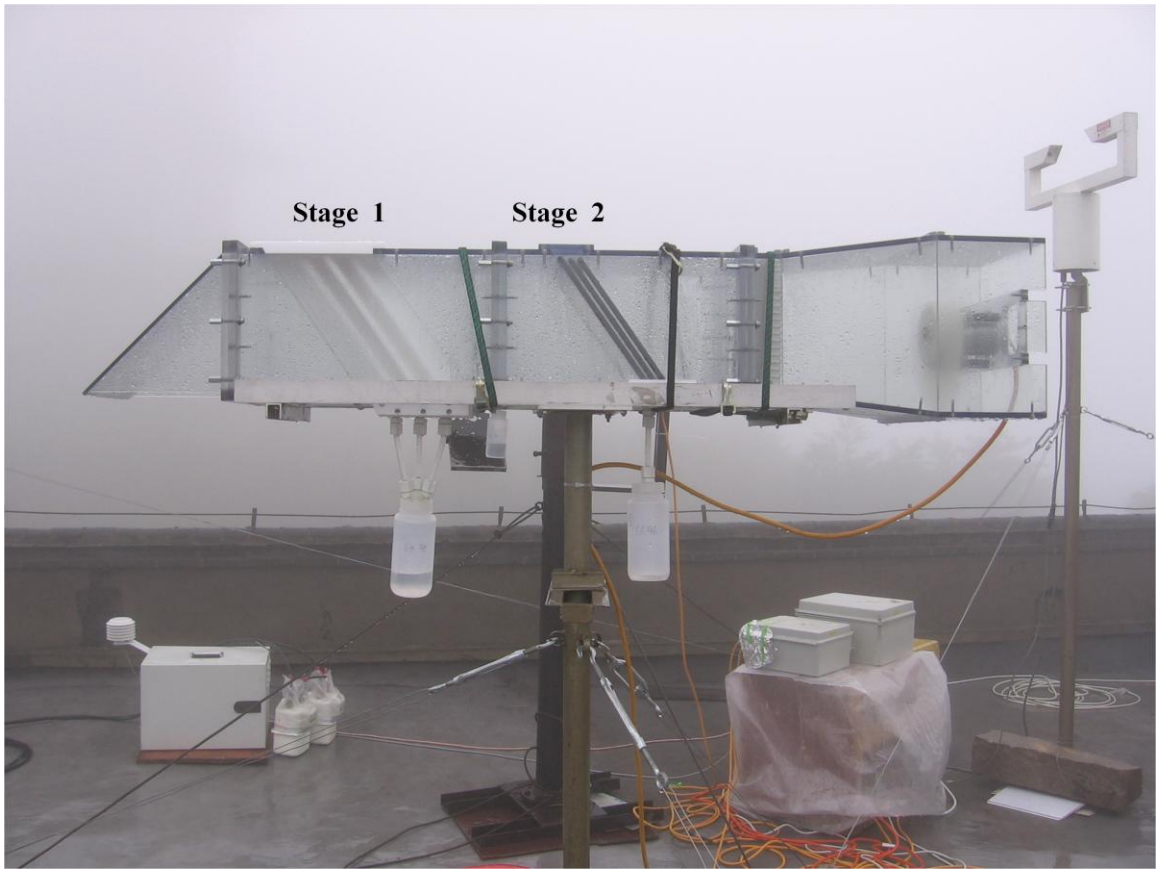

Figure 2-6. Side view of the 2-stage size-fractionating Caltech Active Strand Cloud Collector (sf-CASCC) as installed in the 2008 Mt. Tai campaigns.

As shown in Figure 2-6, from left to right, air is drawn through the first stage and the second stage by a fan located at the back of the sf-CASCC. The air sampling rate of the sf-CASCC is approximately 19 m^3/min. The first stage of the 2-stage size-fractionating

Caltech Active Strand Cloud Collector consists of 12.7 mm diameter Teflon rods, and the second stage consists of 508 μm Teflon strands identical to those of the CASCC. Larger droplets are collected on the first stage with a 50% lower size cut of approximately 16 μm. Smaller droplets are collected on the second stage with a 50% size cut of approximately 4 μm. As in the CASCC, collected droplets coalesce, run down the collection surfaces into a Teflon collection trough, and are directed through Teflon sample tubes to polyethylene sample bottles. The sf-CASCC was operated with a downward facing inlet (see Fig. 2-6) to exclude rain collection during periods of mixed cloud and precipitation.

2.2.3. URG Annular Denuder/Filter-pack System

A University Research Glassware (URG) denuder/filter pack assembly (model URG-3000C) was used in the 2008 campaigns to simultaneously collect $PM_{2.5}$ and select trace gases for chemical analysis. As shown in Figure 2-7, air was drawn in series through a cyclone (URG-2000-30EN, 10LPM, 2.5 μm aerodynamic size cut), two coated annular denuders (URG-2000-30×242-3CSS), a 37 mm Teflon® filter pack (URG-2000-22FB), and a third coated denuder.

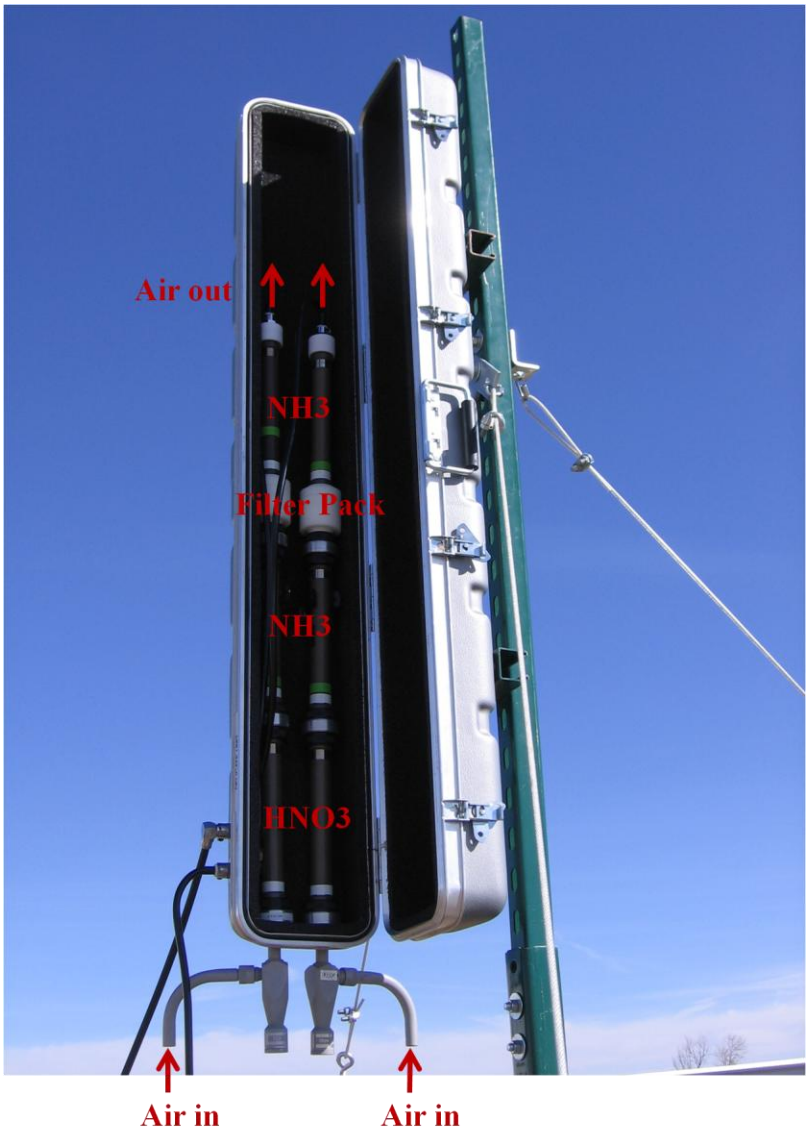

Figure 2-7. URG cyclone / annular denuder / filter pack setup.

Ambient air was drawn through the sampling train by a vacuum pump at a flow rate of 10 LPM (actual volumetric flow). The air flow initially enters the cyclone, which is used to remove coarse particles (>2.5 µm aerodynamic diameter). Air leaves the cyclone and enters the first denuder, which had the interior surfaces coated with sodium carbonate (Na_2CO_3) to react with acidic gases. Gaseous HNO_3 and SO_2 diffuse to the walls and are adsorbed from the air stream. The second denuder was coated with phosphorous acid

(H_3PO_3) to collect gaseous NH_3. As the diffusion coefficient for gases are much higher than those of particles, gases diffuse efficiently to the walls while particles continue through the denuder to be collected by filtration (Pang et al., 2002). Particulate matter is collected on a nylon filter (Nylasorb, 37 mm Pall Gelman, 1.0 μm pore size). The nylon filter also retains any nitric acid that may volatilize from collected particles (e.g., NH_4NO_3). Finally a backup denuder coated with phosphorous acid (H_3PO_3) is used to capture any gaseous NH_3 volatilized from particulate matter (e.g., NH_4NO_3) collected on the nylon filter. Downstream of the last denuder, sample stream pressure and integrated volumetric flow are measured to determine the total ambient air volume sampled.

After sampling, the annular denuders and nylon filters were extracted with high purity deionized (DI) water. The extracts were analyzed by ion chromatography (IC) at Colorado State University for concentrations of SO_4^{2-}, NO_3^-, Cl^-, NO_2^-, NH_4^+, K^+, Ca^{2+}, Na^+, and Mg^{2+}. SO_2 was converted to sulfate (SO_4^{2-}) when it was extracted from the denuders by addition of hydrogen peroxide (H_2O_2); collected nitric acid (HNO_3) was in the form of nitrate (NO_3^-); collected ammonia (NH_3) was in the form of ammonium (NH_4^+).

2.2.4. Continuous Gas Measurements

Gaseous total peroxides were measured by a custom-built continuous analyzer developed based on a fluorometric method (Lazrus et al., 1986), in which hydroperoxides react with *p*-hydroxyphenyl acetic acid (POPHA) under catalysis by horseradish peroxidase to form

a fluorescent POPHA dimer. The fluorescence intensity is proportional to the sampled peroxide concentration. The instrument is calculated by injecting a series of aqueous hydrogen peroxide standards. Details of the measurement method have been described elsewhere (Ren et al., 2009). During the 2008 spring campaign high background levels of H_2O_2 in purified water available at the site produced a high background for gas phase peroxide measurements. S(IV) was added to the water, to consume H_2O_2 as it reacts to sulfuric acid, in the summer 2008 campaign, to eliminate this problem.

Standard commercial instruments for measuring O_3 and SO_2 have been used in previous field studies and have been described in detail elsewhere (Wang et al., 2001; Wang et al., 2002; Wang et al., 2003; Wang et al., 2006). Briefly, O_3 was measured using a UV photometric O_3 analyzer (Thermo Electron Corporation, Environmental Instruments, model 49C) and SO_2 was measured by a pulsed fluorescence SO_2 analyzer (Thermo Electron Corporation, Environmental Instruments, model 43C Trace Level).

2.3. SAMPLING

When the LWC was higher than 100 mg/m^3 and the cloud appeared thick from all directions, cloud collectors were turned on and run continuously until the cloud dissipated; collecting bottles were generally changed at intervals of one or two hours.

Gas monitors were run continuously during the campaigns, although periodic zero and span checks prevented ambient measurement during some short periods.

The URG denuder/filter pack system was run daily in the 2008 campaigns from 8:00 AM to 8:00 AM local time. When cloud was present, sampling was interrupted and interstitial air (air between the cloud drops) was sampled on a second instrument channel. This approach permits investigation of $PM_{2.5}$ and trace gas composition and concentrations before cloud, during cloud and after cloud.

2.4. ON SITE PROCEDURES AND LABORATORY ANALYSIS

Aliquots were prepared on-site for each cloudwater sample for stabilization and later analysis of key species including major ions (Na^+, NH_4^+, K^+, Mg^{2+}, Ca^{2+}, Cl^-, SO_4^{2-}, and NO_3^-), S(IV), metals (Fe and Mn), HCHO, H_2O_2, organic acids, and total organic carbon (TOC). All aliquots and leftover sample portions were stored in a refrigerator on-site and were shipped and kept refrigerated until analysis. 2007 campaign samples were analyzed at Shandong University utilizing procedures recommended by CSU. 2008 campaign samples were returned to the United States for analysis at CSU. Procedures for sample measurement, including aliquot preparation and analysis, are provided below.

2.4.1. Sample weight

The sample weight was measured immediately after the cloudwater was collected.

2.4.2. Sample pH

The sample pH was measured using a portable pH meter (Orion model 290A, Thermo Electron Co., Massachusetts, USA) with a microelectrode (Microelectrodes Inc. model MI-710) calibrated with standard pH 4 and 7 buffers.

2.4.3. Major ions

Aliquots for inorganic ion analysis were prepared by pipetting 0.6 ml of cloudwater into a polyethylene autosampler vial with Teflon lined septum. The inorganic ion analysis was completed using two DIONEX DX-500 series cation and anion ion chromatography (IC) systems and standard methods of analysis. A Dionex AG14A-SC guard column, an AS14A-SC separation column, an ASRS-300 self-regenerating anion suppressor and 8mM Na_2CO_3 / 7mM $NaHCO_3$ eluent were used to quantify concentrations of major anions (Cl^-, SO_4^{2-}, and NO_3^-). A Dionex CG12A-5 µm guard column, a CS12A-5 µm separation column, a CSRS-300 self-regenerating cation suppressor and Methanesulfonic Acid 20mM eluent were used to quantify concentrations of major cations (Na^+, NH_4^+, K^+, Mg^{2+}, and Ca^{2+}). NIST-traceable accuracy check standards, DI water, and replicate samples were run every 10 samples to establish calibration accuracy, verify lack of sample carryover, and establish analytical method precision. Denuder and filter extracts were analyzed for inorganic anions and cations following these same procedures.

2.4.4. S(IV)

Aliquots for S(IV) analysis were prepared by adding a preservative solution on site. The preservative solution contains formaldehyde, trans-1,2-Cylohexylenedinitrilo-tetraacetic acid (CDTA) and sodium hydroxide, wherein S(IV) reacts with formaldehyde to form a stable compound hydroxymethanesulfonate (HMS). HMS can be decomposed to free S(IV) and formaldehyde by adding sodium hydroxide solution, and then free S(IV) and formaldehyde react with acidic pararosaniline (PRA, $C_{19}H_{19}N_3O$) to form a color product (Dasgupta et al., 1980), which can be measured by absorbance at a wavelength of 580 nm. Instrument response was calibrated through analysis of laboratory-prepared aqueous solutions of sodium sulfite.

2.4.5. Metals

Fe and Mn were stabilized by adding nitric acid and measured by a Varian SpectrAA-640Z Graphite Furnace Atomic Absorption Spectrophotometer (GFAAS) with a Varian GTA-100 graphite tube atomizer and Zeeman background correction. The GFAAS was calibrated using NIST-traceable commercial calibration solutions.

2.4.6. HCHO

Aliquots for formaldehyde analysis were prepared by adding a formaldehyde preservation solution containing bisulfite on-site to form HMS. Thereafter HMS can be decomposed to formaldehyde to be analyzed later in the lab through reaction with 2,4-pentanedione and ammonium acetate to form 3,5-diacetyl-1,4-dihydrolutidine (DDL)(Dong and

Dasgupta, 1987) which can be detected by fluorescence. 2008 analyses completed at CSU were measured on a Shimadzu model RF-1501 fluorescence spectrophotometer, calibrated with laboratory-prepared HCHO standard solutions. Excitation wavelength of 412 nm, emission wavelength of 510 nm, excitation band width of 10 nm, and emission band width of 20 nm were used for fluorescence analysis.

2.4.7. Aqueous H_2O_2

Aliquots for aqueous H_2O_2 analysis were preserved on-site by addition of a buffered solution of *p*-hydroxyphenylacetic acid (POPHA) to form a fluorescent dimer under the catalysis of horseradish peroxidase (Lazrus et al., 1985). The concentration of the dimer, which is equal to the original sample peroxide concentration, was measured by a fluorescence spectrophotometer. 2008 analyses completed at CSU were measured on a Shimadzu model RF-1501 fluorescence spectrophotometer, calibrated with H_2O_2 standard solutions. Excitation wavelength of 320 nm, emission wavelength of 400 nm, excitation band width of 10 nm, and emission band width of 10 nm were used for fluorescence analysis.

2.4.8. Organic acids

Aliquots for organic acid analysis were preserved by addition of a small amount of biocide (chloroform) and analyzed by ion chromatography. Analysis was completed on a

Dionex DX-500 IC using a Dionex AS11-HC separation column, a NaOH gradient elution, anion suppressor, and conductivity detection.

2.4.9. TOC

Total organic carbon (TOC) was measured by a TOC analyzer (Shimadzu TOC-V CSH) equipped with an automatic sample injector (ASI-V). Samples were analyzed without filtration in order to capture both dissolved and suspended particulate organic matter in the cloudwater. Instrument response was calibrated using laboratory-prepared aqueous standards of potassium hydrogen phthalate.

2.5. QUALITY ASSURANCE AND CONTROL

2.5.1. Collector cleaning and blanks

Cloud collectors were cleaned thoroughly with Triton-X100 and rinsed with deionized (DI) water prior to each field campaign. Cloud collectors were cleaned with DI water after each cloud event and field blanks were collected and aliquotted for analysis using the sample preparation procedures described above. After cleaning and drying for an appropriate time, the cloud collectors were covered by clean plastic bags to avoid contamination by dust. Samples collected during the first several minutes of each event were discarded to avoid any influence by dust or residual DI rinse water dilution.

2.5.2. Determination of uncertainties and minimum detection limits (MDL)

Duplicate aliquots were made in the field for analysis at a frequency of one out of every 10 cloud samples. Replicate analyses were also made once every 10 samples during sample analysis in the lab.

The Relative Standard Deviation (RSD), used to describe measurement precision, was calculated as follows:

$$RSD = \frac{\sqrt{\frac{\sum_{i=1}^{n}(x_{i1} - x_{i2})^2}{2n}}}{\bar{x}} \times 100\% \qquad \text{Equation 2-1}$$

Where x_{i1} and x_{i2} are one pair of duplicate results, n is the number of pairs of duplicates, $\bar{x}$ is the average of all duplicates. Measurement precision established this way includes uncertainties due to field sample processing, sample handling, and laboratory analysis. Cloud collector blanks were used to determine the minimum detection limits (MDL) by species.

In order to ensure comparable analytical results were obtained for 2007 cloud samples (analyzed by Shandong University) and 2008 cloud samples (analyzed at CSU), several 2007 samples were shared and analyzed by both laboratories for several species. Results, shown in Fig. 2-8, indicate good inter-laboratory agreement.

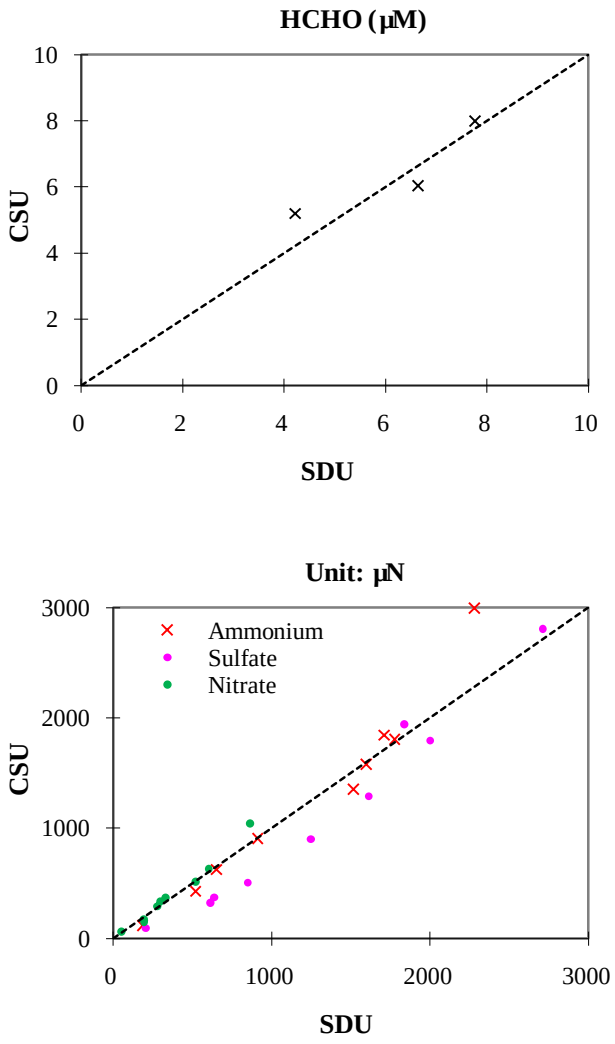

Figure 2-8. Interlaboratory comparisons for several samples collected in 2007 measured by Shandong University (SDU) and Colorado State University (CSU).

CHAPTER 3 RESULTS AND DISCUSSION

3.1. SUMMARY OF SAMPLING

Numerous periods of cloud interception/fog occurred during the four Mt. Tai field campaigns. During the spring 2007 campaign (03/22-04/22), there were 9 cloud events; a total of 36 bulk cloudwater samples were collected. During the summer 2007 campaign (06/20-07/20), there were 12 cloud events; a total of 66 bulk samples were collected. During the spring 2008 campaign (03/28-04/25), there were 4 cloud events; a total of 83 cloudwater samples (including 25 bulk samples and 58 size-fractionated samples) were collected. During the summer 2008 campaign (06/14-07/16), there were 18 cloud events; a total of 333 cloudwater samples (including 117 bulk samples and 216 size-fractionated samples) were collected.

More detailed summary data for the sampled events are provided in chapter 4, by campaign. The summaries include the number of events in each campaign, the date and time period of each sampled event, and the average (volume-weighted) cloudwater concentrations of several key species. The summaries also include estimated altitudes of cloud base for each event. Complete information about individual samples is provided in the data tables included in Appendix B and Appendix C.

Figure 3-1 shows the liquid water content (LWC) observations during the spring 2008 campaign. The four cloud interception episodes are readily apparent. Peak LWC values in the events were several hundred mg/m^3.

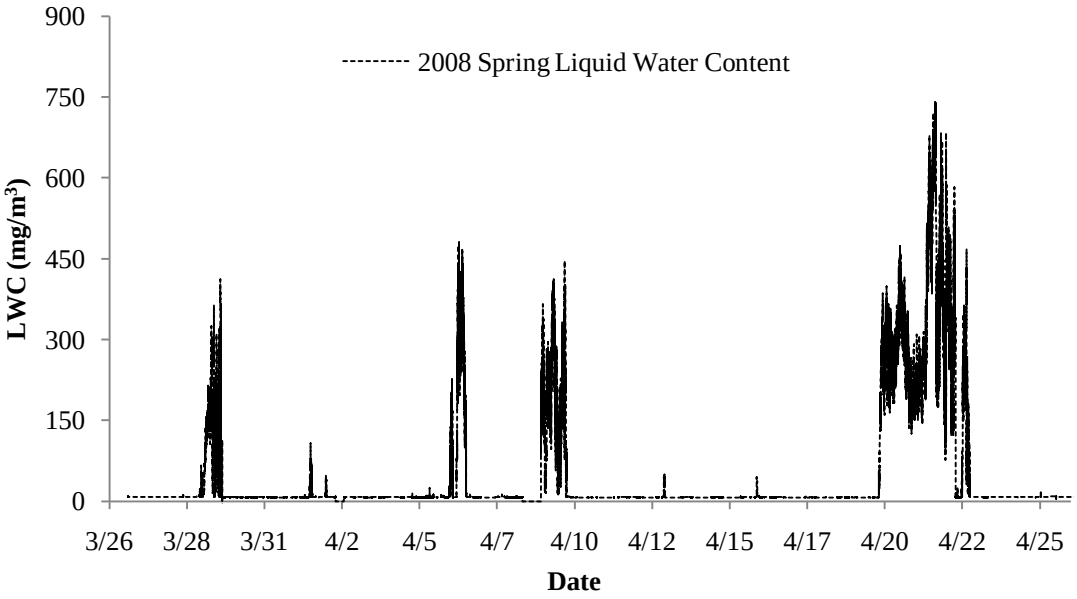

Figure 3-1. Spring 2008 Liquid Water Content.

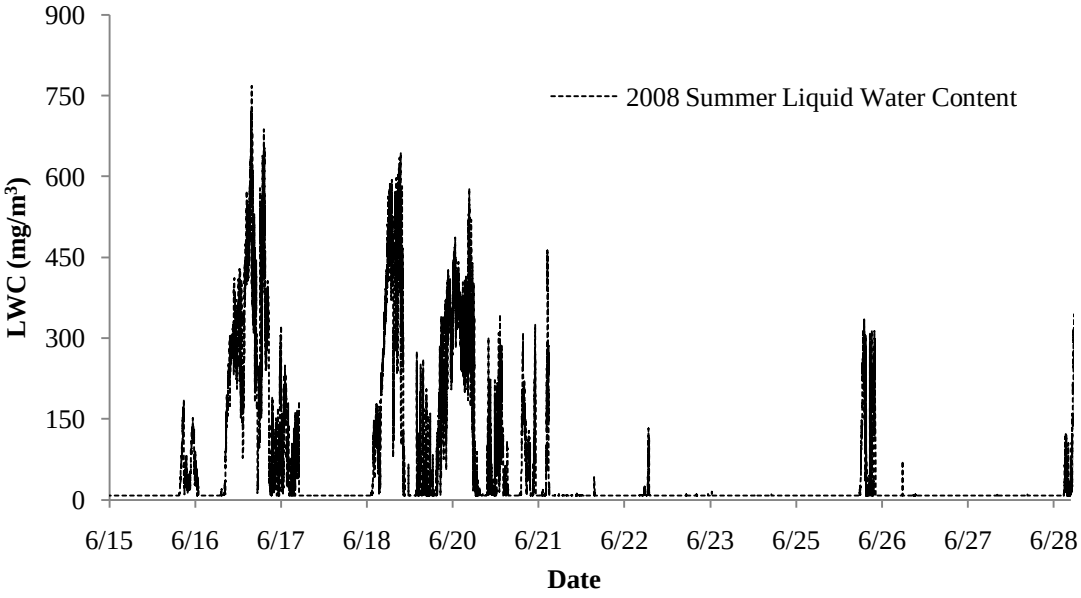

Figure 3-2. Summer 2008 Liquid Water Content.

Figure 3-2 shows the LWC observations during the summer 2008 campaign. A very active period of cloud interception is apparent between June 16 and 20. The PVM was disabled by a lightning strike midway through the summer 2008 campaign. Estimates of LWC for cloud interception periods after this time were obtained based on the cloudwater collection rate of the sf-CASCC. As discussed by Demoz et al. (1996), the rate of water collection by the CASCC family of collectors is closely related to the cloud LWC. The relationship between sf-CASCC cloudwater collection rate and PVM LWC is examined in Fig. 3-3. Here we see a strong correlation ($R^2 = 0.94$). A best-fit line to this data set is described by equation 3-1.

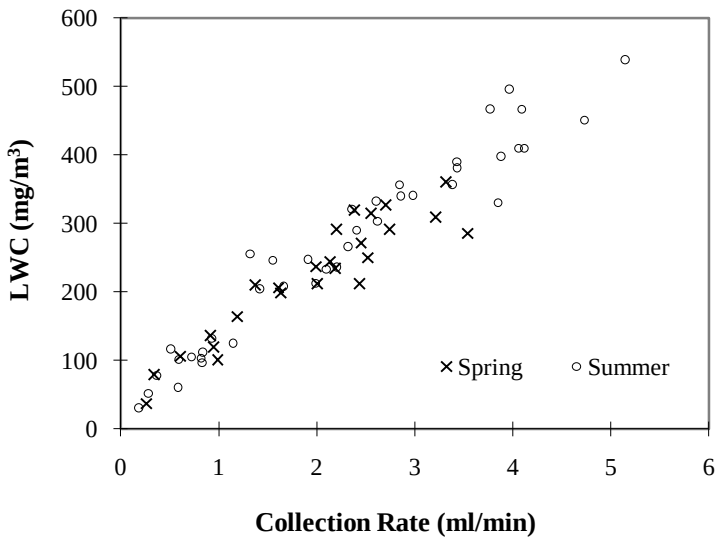

Figure 3-3. The relationship between sf-CASCC cloudwater collection rate and PVM LWC.

$$LWC = CollectionRate \times 97.3 + 44.2 \qquad \text{Equation 3-1}$$

3.2. GASEOUS SPECIES

Key gas phase species associated with aqueous sulfate production include sulfur dioxide, ozone, and hydrogen peroxide. Summaries of concentrations of these key species are provided below.

3.2.1. Gaseous H_2O_2

Ren et al. (2009) present a detailed analysis of the H_2O_2 concentrations measured at Mt. Tai in the spring and summer 2007 campaigns. H_2O_2 concentrations were generally lower in spring (2007 average mixing ratio of 0.17 ppbv) than in summer (2007 average mixing ratio of 0.55 ppbv). A similar pattern was observed in 2008, when spring H_2O_2 mixing ratios averaged 1.14 ppbv (the spring 2008 gaseous H_2O_2 data were affected by the high H_2O_2 in the analyzer system coming from the purified water bottles- the average value of 1.14 ppbv was calculated from several days that the signals were reasonable, all these days did not have cloud. An H_2O_2 mixing ratio of 0.1 ppbv was used to estimate in-cloud S(IV) oxidation rates for spring 2008). Summer 2008 H_2O_2 mixing ratios averaged 0.59 ppbv. Higher H_2O_2 concentrations are expected in summer, when more active photochemistry occurs, promoting H_2O_2 formation through both gas and aqueous phase reactions. Summertime gaseous H_2O_2 mixing ratios at Mt. Tai were observed to climb as high as 4 ppbv. Because of the fast aqueous phase reaction between H_2O_2 and dissolved SO_2, one might expect to observe an anti-correlation between gaseous H_2O_2 concentrations and the presence of clouds.

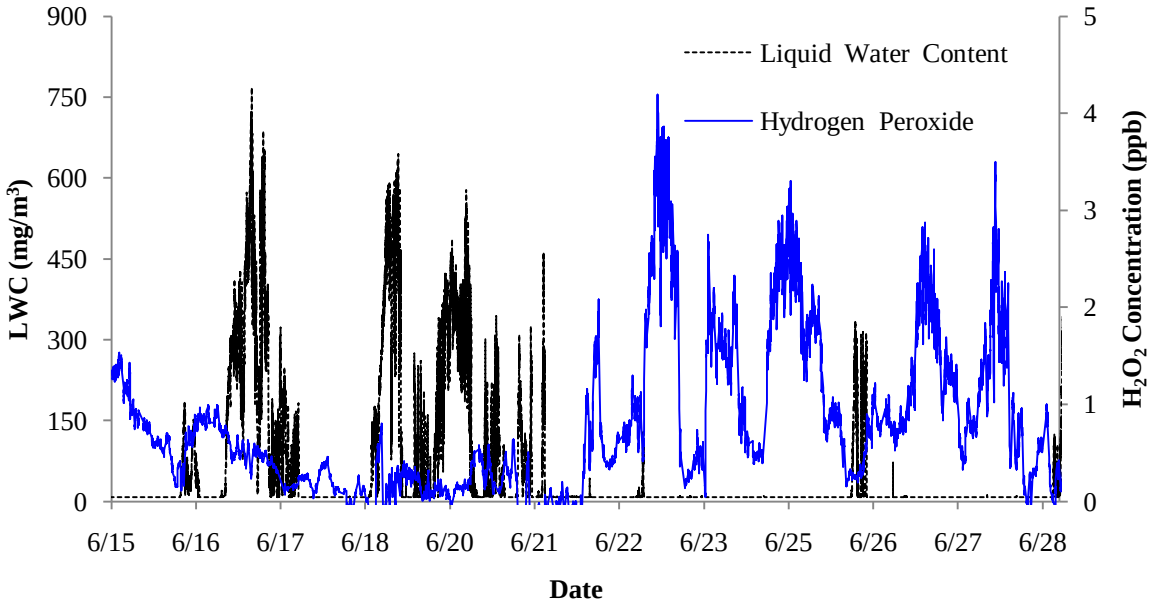

Figure 3-4. Timelines of gaseous H_2O_2 mixing ratio and cloud LWC observed at the Mt. Tai summit, 6/15-6/28/2008.

Figure 3-4 explores this relationship, plotting timelines of the gaseous H_2O_2 mixing ratio and the cloud LWC measured by the PVM for the first two weeks of the summer 2008 campaign (June 15 - June 28), before the lightning strike disabled the PVM. It is important to keep in mind that the PVM LWC only indicates the presence of clouds intercepting the Mt. Tai summit; it does not indicate whether clouds are present nearby that might also provide a medium for H_2O_2 reaction with dissolved SO_2. Nevertheless, Figure 3-4 illustrates a clear relationship between cloud interception and gas phase H_2O_2 mixing ratios. During the first half of the illustrated period, clouds were observed frequently at the summit of Mt. Tai and H_2O_2 mixing ratios generally stayed below 0.5 ppbv. During the second half of the period, cloud interception was much less common and H_2O_2 mixing ratios regularly climbed into the 2-4 ppbv range. The disappearance of

gas phase H_2O_2 during cloudy periods is consistent with its uptake by cloud droplets and consumption during aqueous phase sulfate production, a topic discussed further below.

3.2.2. O_3 and SO_2

Figures 3-5 to 3-8 give the measured mixing ratios of gaseous H_2O_2, O_3 and SO_2 during the four field campaigns. The average concentrations of SO_2 measured during the Mt. Tai spring campaigns were approximately double the summertime averages. Average mixing ratios of 15.4 ppbv and 14.5 ppbv were observed in spring 2007 and spring 2008, respectively, while average mixing ratios of 8.1 ppbv and 6.4 ppbv were observed in summer 2007 and summer 2008. Average O_3 concentrations were similar across all four campaigns, with mixing ratio averages of 62.1 ppbv and 66.0 ppbv in spring 2007 and spring 2008, respectively, and average mixing ratios of 72.1 ppbv and 68.0 ppbv in summer 2007 and 2008.

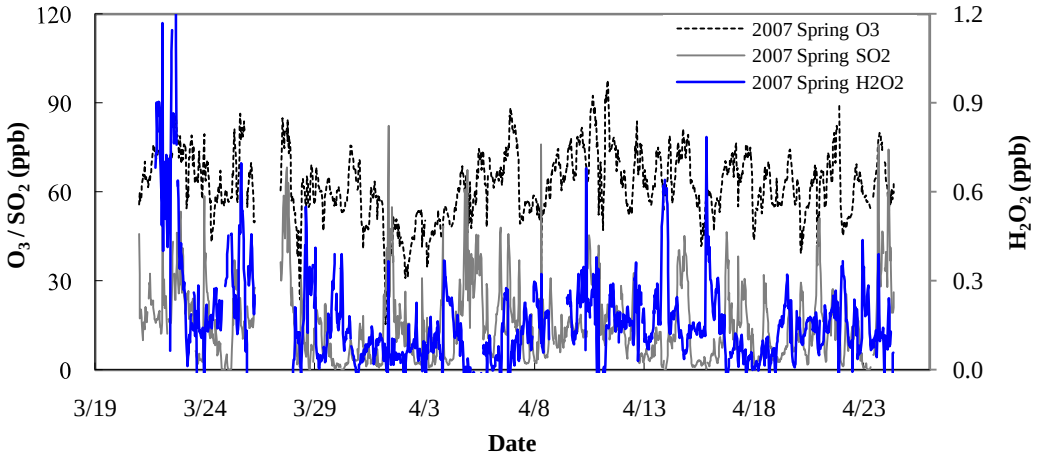

Figure 3-5. Measured mixing ratios of gaseous H_2O_2, O_3 and SO_2 during spring 2007 campaign.

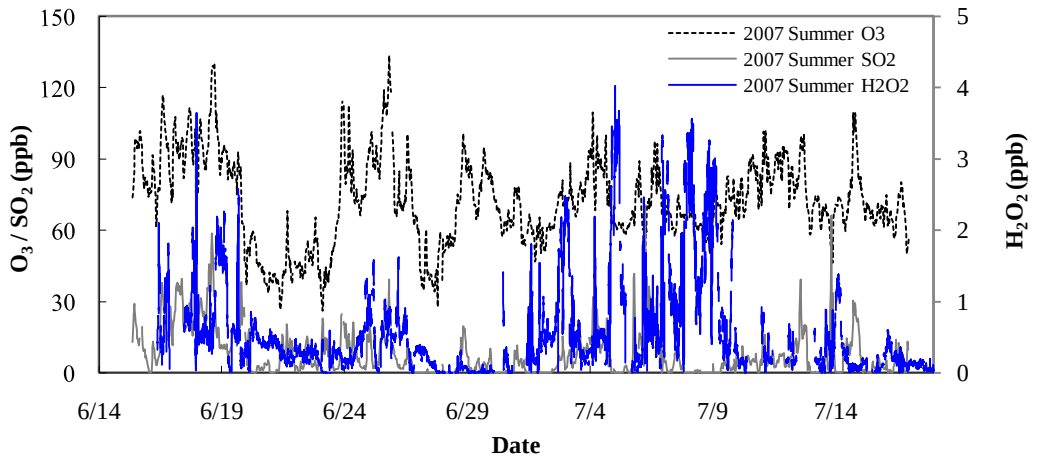

Figure 3-6. Measured mixing ratios of gaseous H_2O_2, O_3 and SO_2 during summer 2007 campaign.

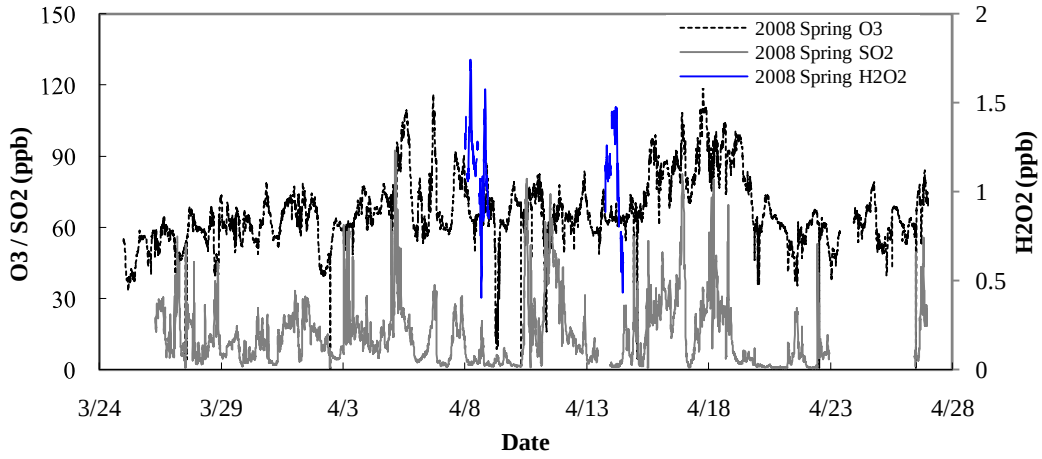

Figure 3-7. Measured mixing ratios of gaseous H_2O_2, O_3 and SO_2 during spring 2008 campaign.

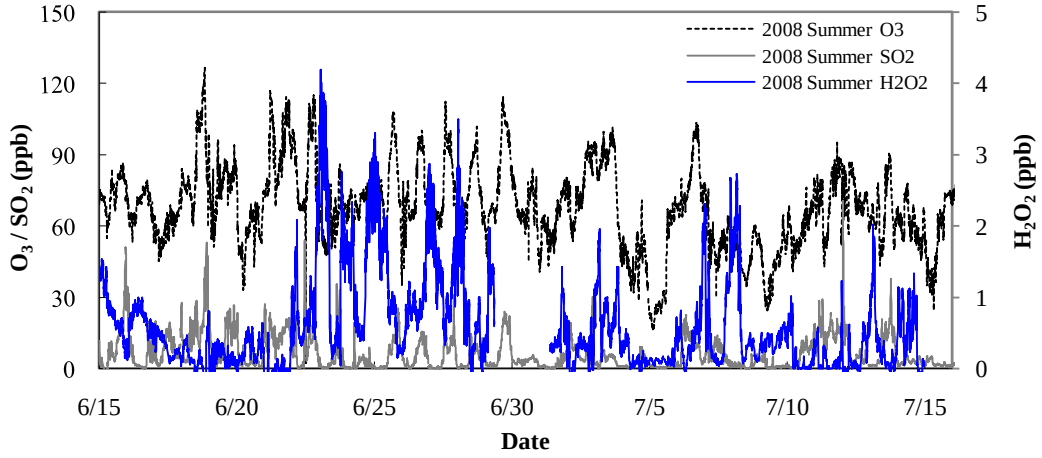

Figure 3-8. Measured mixing ratios of gaseous H_2O_2, O_3 and SO_2 during summer 2008 campaign.

3.3. BULK CLOUDWATER CHEMICAL COMPOSITION

The chemical composition of cloudwater is determined by several processes, including scavenging of aerosol particles, dissolution of soluble gases, and species consumption and production via aqueous phase chemical reactions. Assuming the cloud drops can be considered at equilibrium with gas phase sources of SO_2, O_3, and H_2O_2, the key cloud composition parameters needed to determine aqueous S(IV) oxidation rates by the pathways introduced earlier are the cloud drop pH and the cloud drop concentrations of trace metal catalysts. Concentrations of aqueous S(IV), aqueous H_2O_2, and aqueous HCHO can also aid us to better understand the availability of key reactants involved in aqueous sulfur chemistry in the region. Inorganic ions and organic matter typically make up the largest fractions of solute mass. Concentrations of all of these species are reported here for bulk cloudwater collected in both 2007 and 2008 and in section 3.4 for the drop size-resolved cloud samples collected from the sf-CASCC in 2008.

3.3.1. Cloudwater pH

A very wide range of cloud pH values was observed in bulk cloudwater samples collected at Mt. Tai. Cloudwater pH values ranged from 2.69 to 7.64 in 2007 and from 2.65 to 6.94 in 2008. These ranges are large enough that we should expect multiple S(IV) oxidation pathways to be important at various times. They also indicate strong variability in the relative contributions of acids and bases to regional cloud composition.

Frequency distributions of observed pH values in the four sampling campaigns are shown in Figure 3-9. The average pH values (determined as the volume weighted average H^+ concentrations) in spring and summer 2007 were 3.68 and 4.10, respectively. The average pH values in spring and summer 2008 were 4.34 and 3.77, respectively.

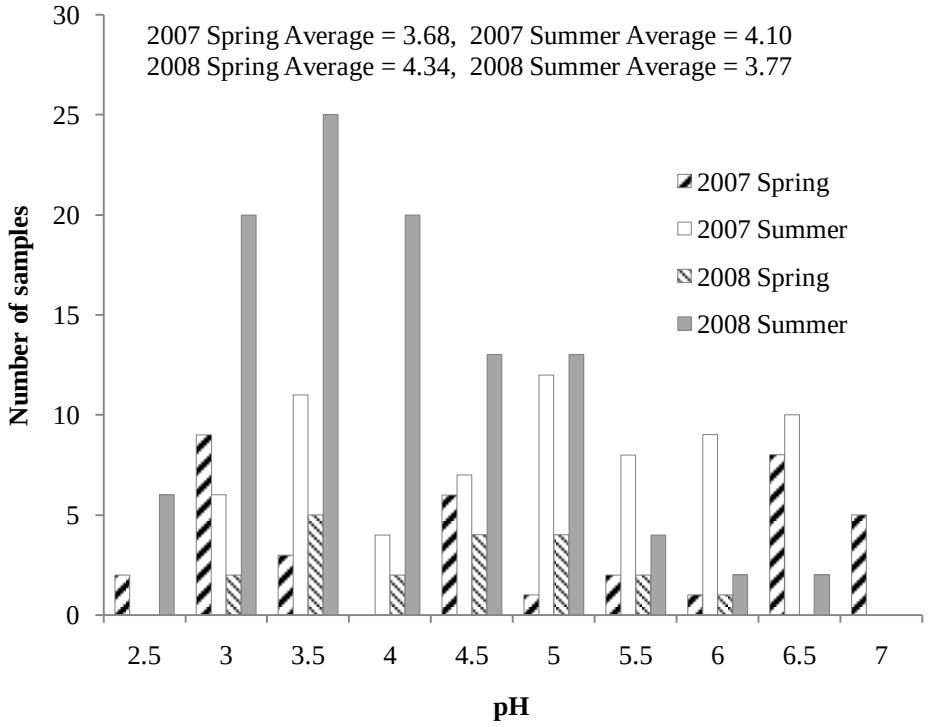

Figure 3-9. Frequency distributions of the pH values measured in bulk (CASCC) cloudwater samples collected at Mt. Tai in the four sampling campaigns.

3.3.2. TOC

Total organic carbon concentrations in cloudwater are the result both of scavenging of organic aerosol particles and uptake of soluble volatile organic compounds (VOC). Frequency distributions of bulk cloudwater TOC concentrations observed at Mt. Tai in the 2008 sampling campaigns are shown in Figure 3-10. TOC concentrations (volume-

weighted average) in spring and summer 2008 averaged 2.6 ppmC and 15.8 ppmC, respectively.

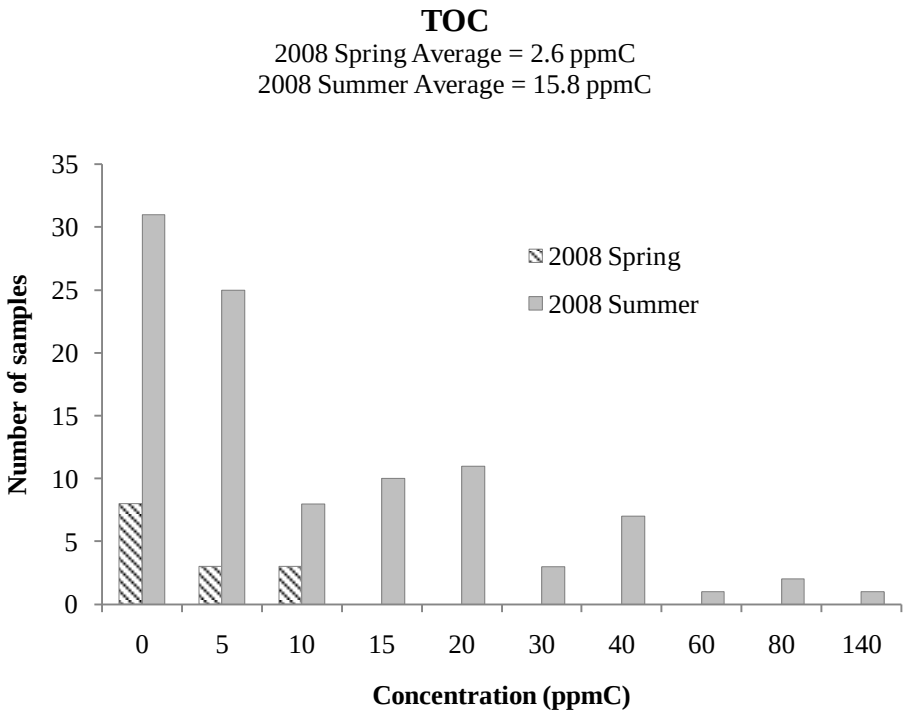

Figure 3-10. Frequency distributions of TOC concentrations measured in bulk (CASCC) cloudwater samples collected at Mt. Tai in the 2008 sampling campaigns.

These concentrations are compared in Fig. 3-11 to average TOC concentrations measured by the Collett research group in fogs and clouds sampled at several other locations. The average Mt. Tai summer cloudwater TOC concentration is second highest of all areas measured and much higher than measured in intercepted clouds at other mountain sites (the California Central Valley, Houston, and Pittsburgh studies all sampled fogwater in a shallow boundary layer).

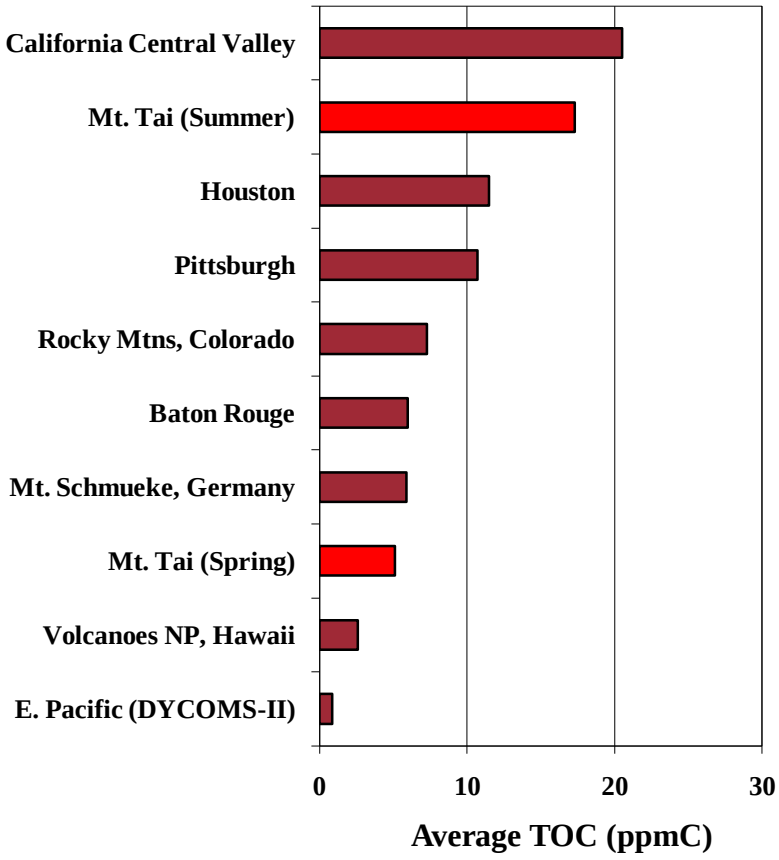

Figure 3-11. Average cloud/fog TOC concentrations measured by the Collett research group in several environments.

Concentrations of TOC are very high in some Mt. Tai cloudwater samples, reaching as much as 200 ppmC. To our knowledge, this is the highest TOC concentration measured to date in any cloud or fog worldwide. Figure 3-12 shows a photograph of several high TOC Mt. Tai cloudwater samples. A combination of elemental carbon and organic carbon likely contribute to the strong coloration of these samples. No TOC measurements were made of the 2007 samples.

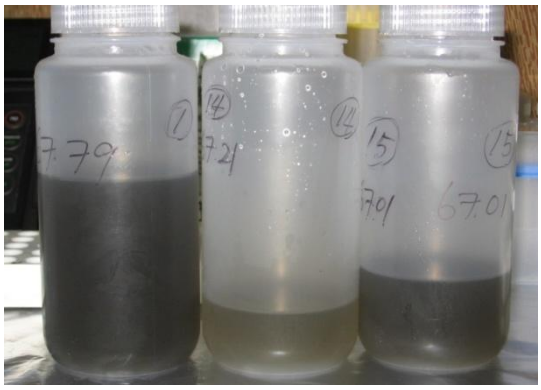

Figure 3-12. Photograph of several high TOC cloudwater samples collected on 6/18/2008 at Mt. Tai.

3.3.3. Major Ions

Figures 3-13 to 3-16 show the volume-weighted average mass compositions of the inorganic ions in Mt. Tai cloudwater samples collected during the four field campaigns. SO_4^{2-}, NO_3^-, and NH_4^+ were the major inorganic species for all of the four campaigns, accounting for approximately 39.9%, 29.9% and 15.5%, by mass, of the total measured inorganic ions, respectively, during the spring 2007 campaign; accounting for about 52.8%, 15.5% and 24.8% of the total inorganic ions, respectively during the summer 2007 campaign; accounting for about 51.2%, 20.9% and 18.6% of the total inorganic ions, respectively during the spring 2008 campaign; and accounting for about 46.6%, 25.5% and 19.2% of the total inorganic ions, respectively, during the summer 2008 campaign.

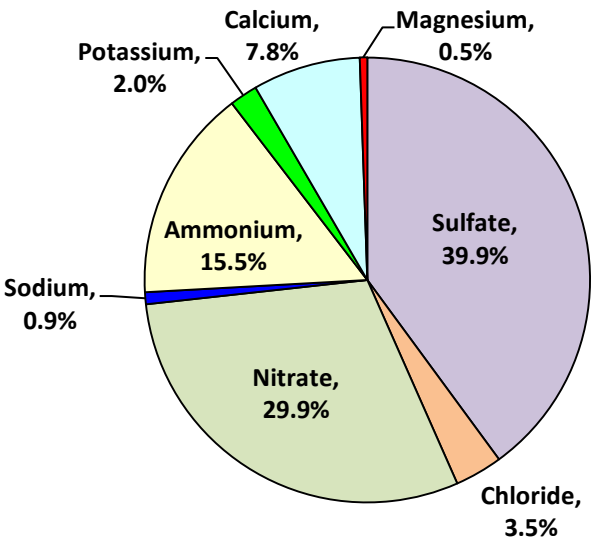

Figure 3-13. Average inorganic ion composition, by mass, of Mt. Tai cloudwater sampled during the spring 2007 campaign.

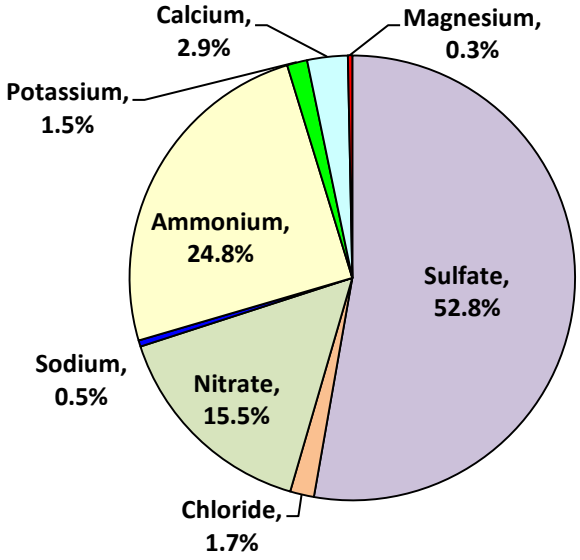

Figure 3-14. Average inorganic ion composition, by mass, of Mt. Tai cloudwater sampled during the summer 2007 campaign.

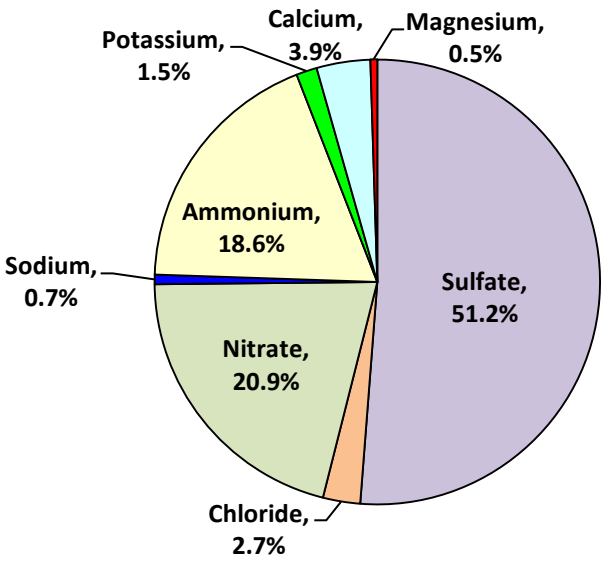

Figure 3-15. Average inorganic ion composition, by mass, of Mt. Tai cloudwater sampled during the spring 2008 campaign.

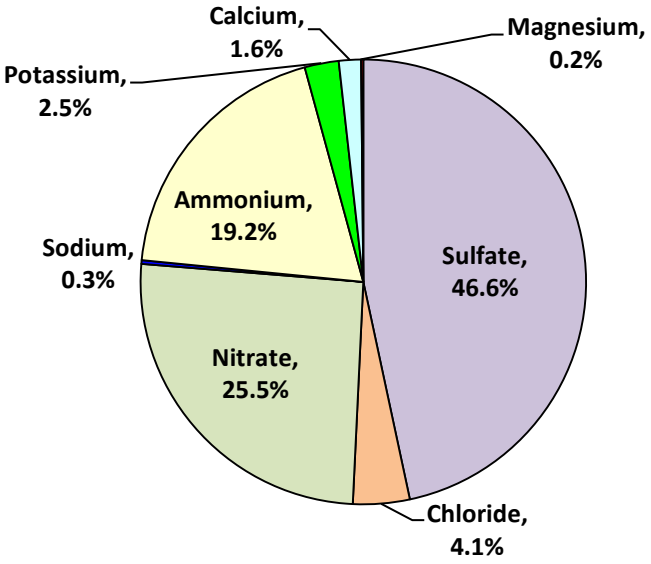

Figure 3-16. Average inorganic ion composition, by mass, of Mt. Tai cloudwater sampled during the summer 2008 campaign.

Figures 3-17 and 3-18 show the average mass compositions of the cloudwater samples, including both organic matter and inorganic ions, for the spring and summer 2008 campaigns, respectively. The mass of organic matter was estimated as 1.8 times the TOC concentration in order to account for other constituents commonly found in organic molecules (e.g., H and O). The 1.8 multiplier was chosen based on a comparison of various methods used to estimate OM/OC (Chan et al., 2010), the value 1.8 estimated by Zhang et al. (2005) from m/z ratios of the AMS mass spectra for organic aerosols measured in field experiments (Zhang et al., 2005) was adopted in this study. Given the more polar nature and high oxygen content typical of organic matter found in clouds and fogs, a ratio of 1.8 is considered a conservative estimate.

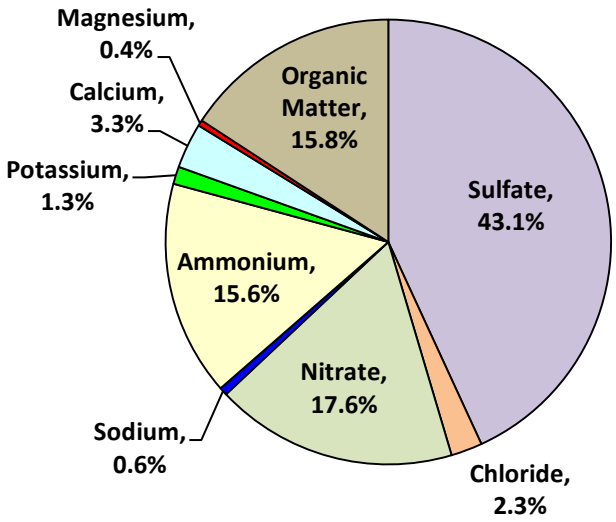

Figure 3-17. Average composition, by mass, of Mt. Tai cloudwater sampled during the spring 2008 campaign.

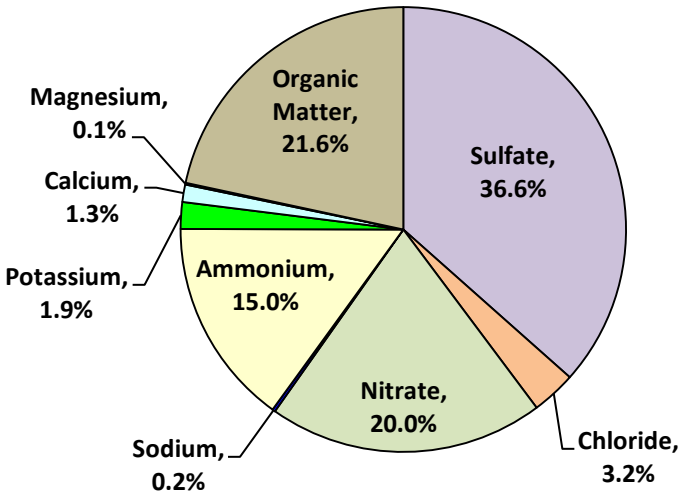

Figure 3-18. Average composition, by mass, of Mt. Tai cloudwater sampled during the summer 2008 campaign.

Frequency distributions of bulk cloudwater SO_4^{2-} concentrations observed at Mt. Tai in the four sampling campaigns are shown in Figure 3-19. The average SO_4^{2-} concentrations observed in spring and summer 2007 were 1332 μN and 1235 μN, respectively. SO_4^{2-} concentrations in spring and summer 2008 averaged 265.9 μN and 1001 μN, respectively.

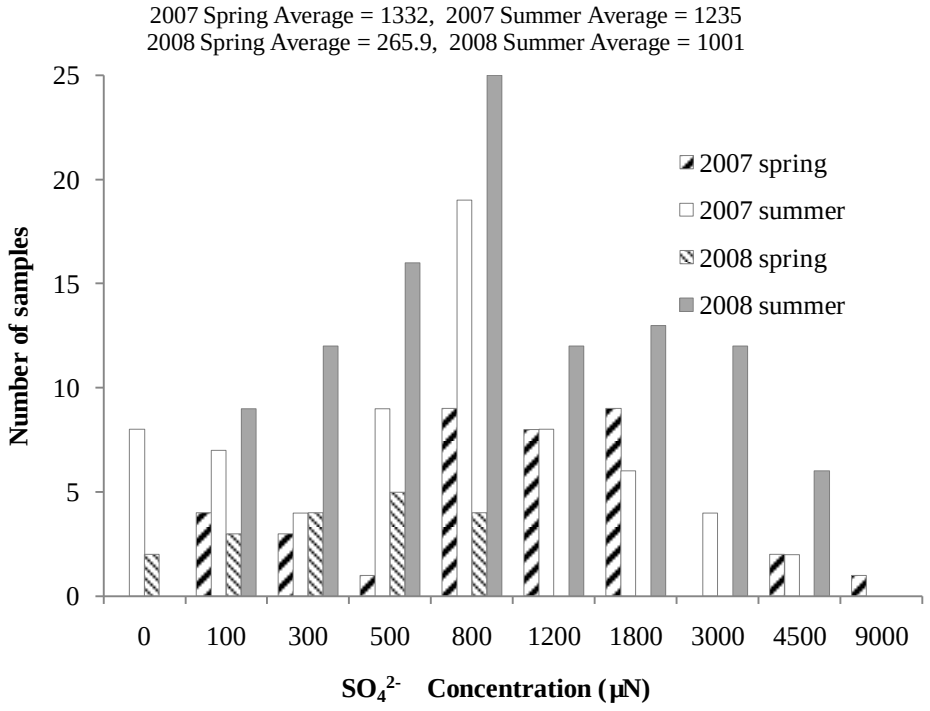

Figure 3-19. Frequency distributions of sulfate ion concentrations measured in bulk (CASCC) cloudwater samples collected at Mt. Tai in the four sampling campaigns.

Frequency distributions of bulk cloudwater NO_3^- concentrations observed at Mt. Tai in the four sampling campaigns are shown in Figure 3-20. The average NO_3^- concentrations observed in spring and summer 2007 were 772 μN and 281 μN, respectively. NO_3^- concentrations in spring and summer 2008 averaged 84.0 μN and 424.3 μN, respectively.

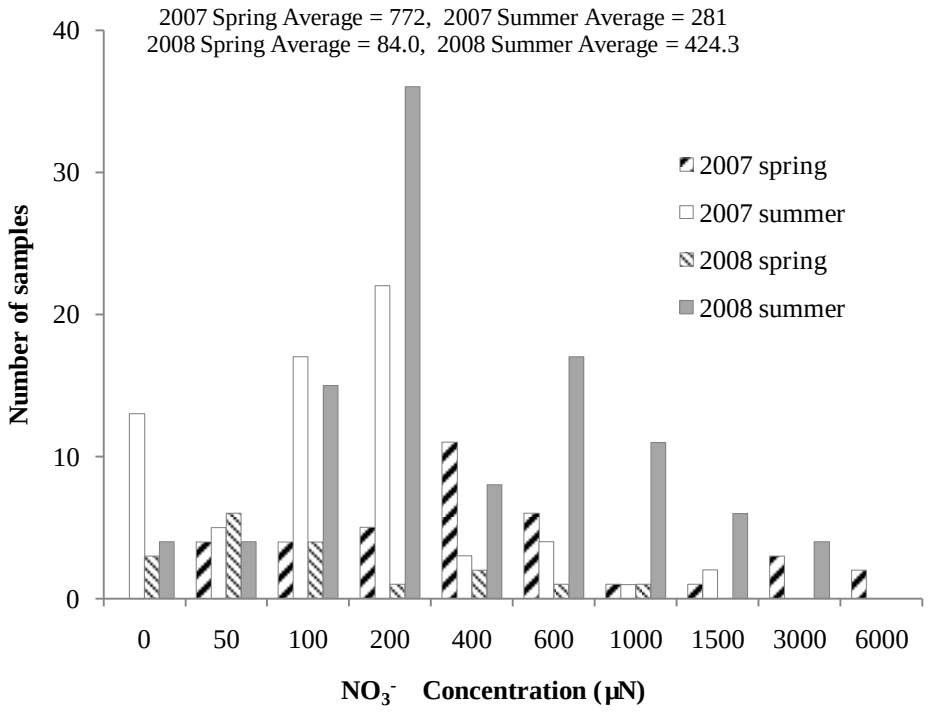

Figure 3-20. Frequency distributions of nitrate ion concentrations measured in bulk (CASCC) cloudwater samples collected at Mt. Tai in the four sampling campaigns.

Fig. 3-21 compares sulfate and nitrate concentrations measured at Mt. Tai with sulfate and nitrate concentrations measured by the Collett research group in clouds and fogs at several other locations. The average nitrate concentrations measured at Mt. Tai are similar to those measured in polluted clouds and fogs from several U.S. locations. Mt. Tai cloudwater sulfate concentrations, while high, are not higher than those measured in the 1990s at some locations in the eastern U.S.

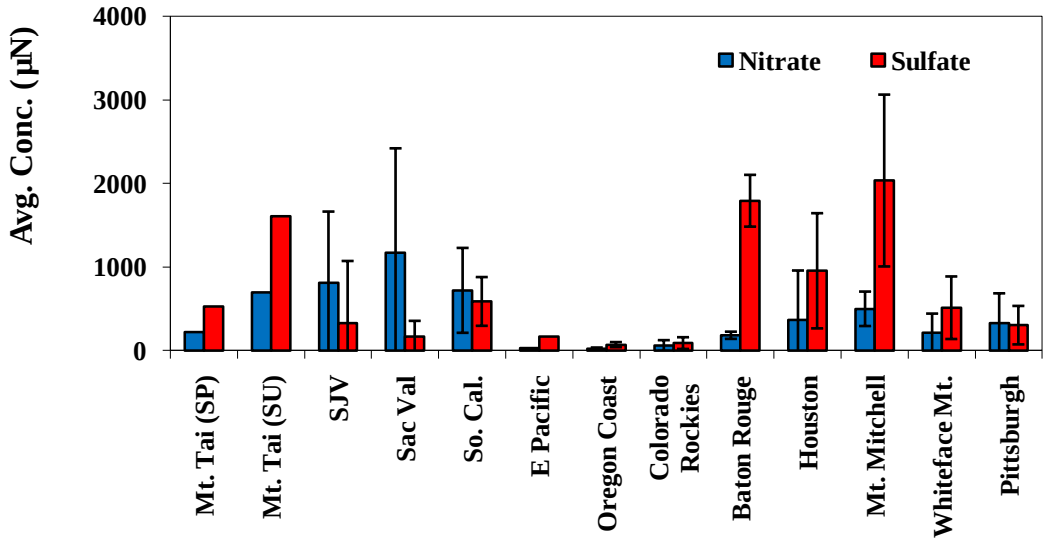

Figure 3-21. Average concentrations of sulfate and nitrate measured in 2008 spring and summer in Mt. Tai cloudwater (this study) and in clouds and fogs from several other locations (Collett et al., 2002; Raja et al., 2008; unpublished data).

Frequency distributions of bulk cloudwater Cl^- concentrations observed at Mt. Tai in the four sampling campaigns are shown in Figure 3-22. The average Cl^- concentrations observed in spring and summer 2007 were 156 μN and 55 μN, respectively. Cl^- concentrations in spring and summer 2008 averaged 19 μN and 119.4 μN, respectively.

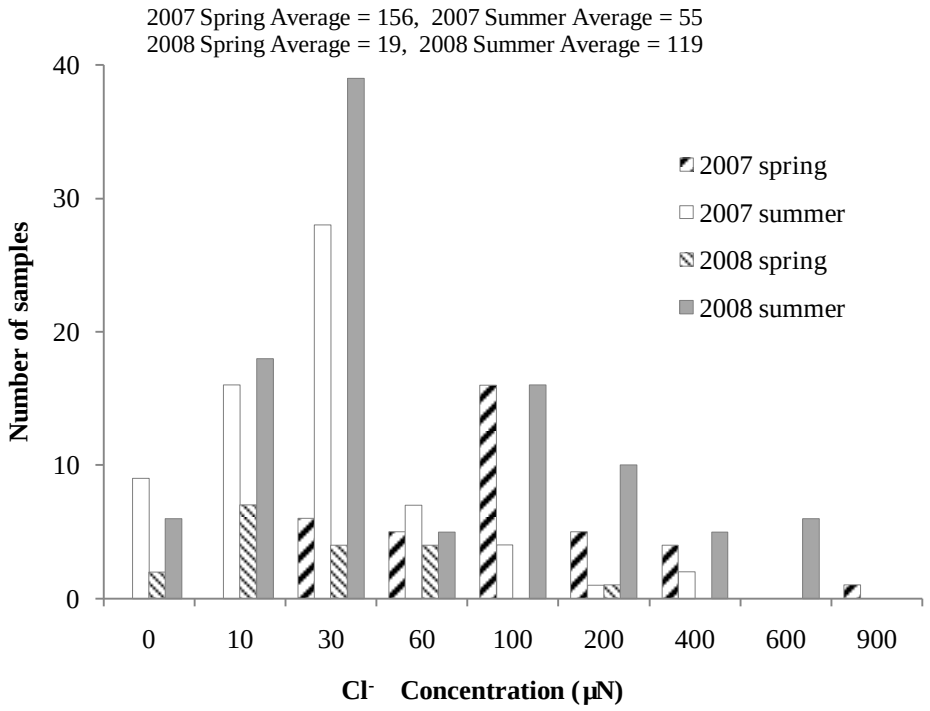

Figure 3-22. Frequency distributions of chloride ion concentrations measured in bulk (CASCC) cloudwater samples collected at Mt. Tai in the four sampling campaigns.

Frequency distributions of bulk cloudwater NH_4^+ concentrations observed at Mt. Tai in the four sampling campaigns are shown in Figure 3-23. The average NH_4^+ concentrations observed in spring and summer 2007 were 1376 μN and 1548 μN, respectively. NH_4^+ concentrations in spring and summer 2008 averaged 256.9 μN and 1098.5 μN, respectively.

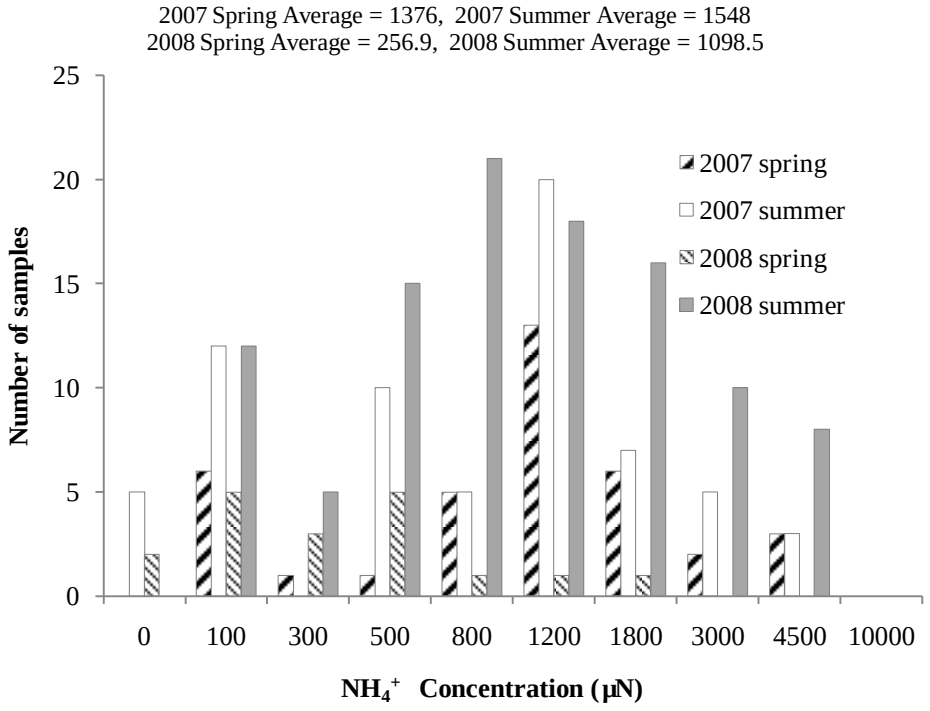

Figure 3-23. Frequency distributions of ammonium ion concentrations measured in bulk (CASCC) cloudwater samples collected at Mt. Tai in the four sampling campaigns.

Frequency distributions of bulk cloudwater Ca^{2+} concentrations observed at Mt. Tai in the four sampling campaigns are shown in Figure 3-24. The average Ca^{2+} concentrations observed in spring and summer 2007 were 626 μN and 165 μN, respectively. Ca^{2+} concentrations in spring and summer 2008 averaged 48.5 μN and 82.8 μN, respectively. The high spring 2007 campaigns are suggestive of stronger dust impacts during this campaign.

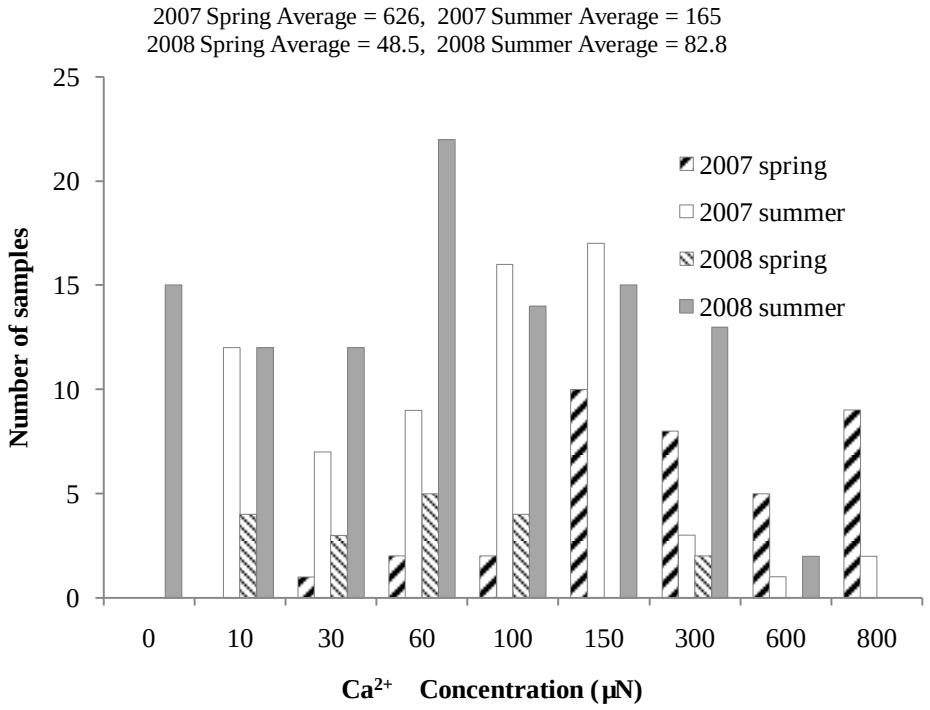

Figure 3-24. Frequency distributions of calcium ion concentrations measured in bulk (CASCC) cloudwater samples collected at Mt. Tai in the four sampling campaigns.

Frequency distributions of bulk cloudwater K^+ concentrations observed at Mt. Tai in the four sampling campaigns are shown in Figure 3-25. The average K^+ concentrations observed in spring and summer 2007 were 83.3 μN and 42.2 μN, respectively. K^+ concentrations in spring and summer 2008 averaged 9.6 μN and 65.2 μN, respectively.

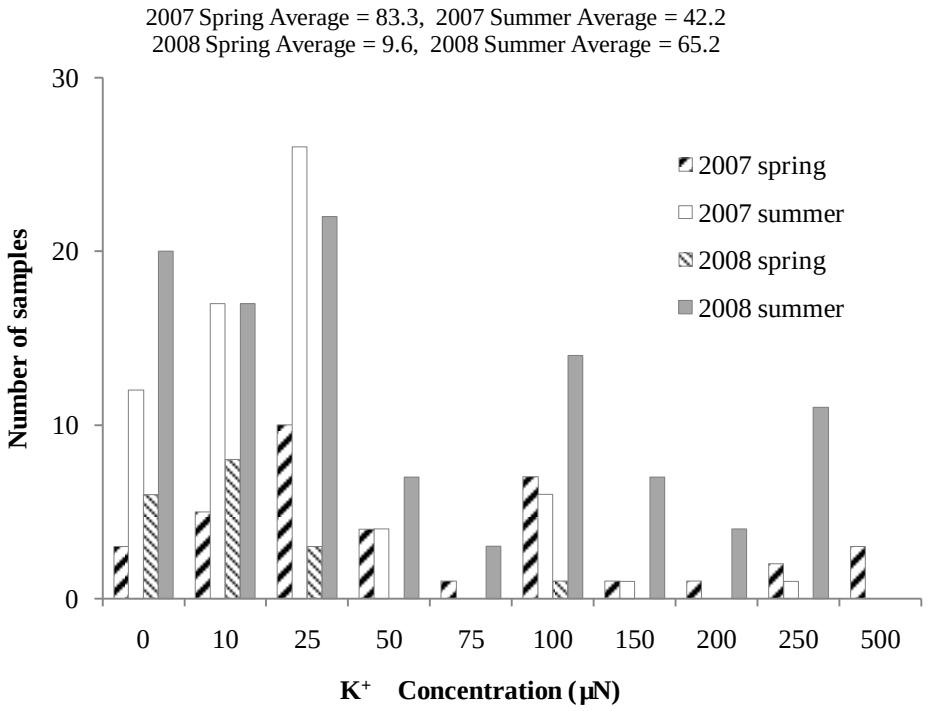

Figure 3-25. Frequency distributions of potassium ion concentrations measured in bulk (CASCC) cloudwater samples collected at Mt. Tai in the four sampling campaigns.

Frequency distributions of bulk cloudwater Na^+ concentrations observed at Mt. Tai in the four sampling campaigns are shown in Figure 3-26. The average Na^+ concentrations observed in spring and summer 2007 were 60.3 μN and 22.1 μN, respectively. Na^+ concentrations in spring and summer 2008 averaged 7.5 μN and 12 μN, respectively.

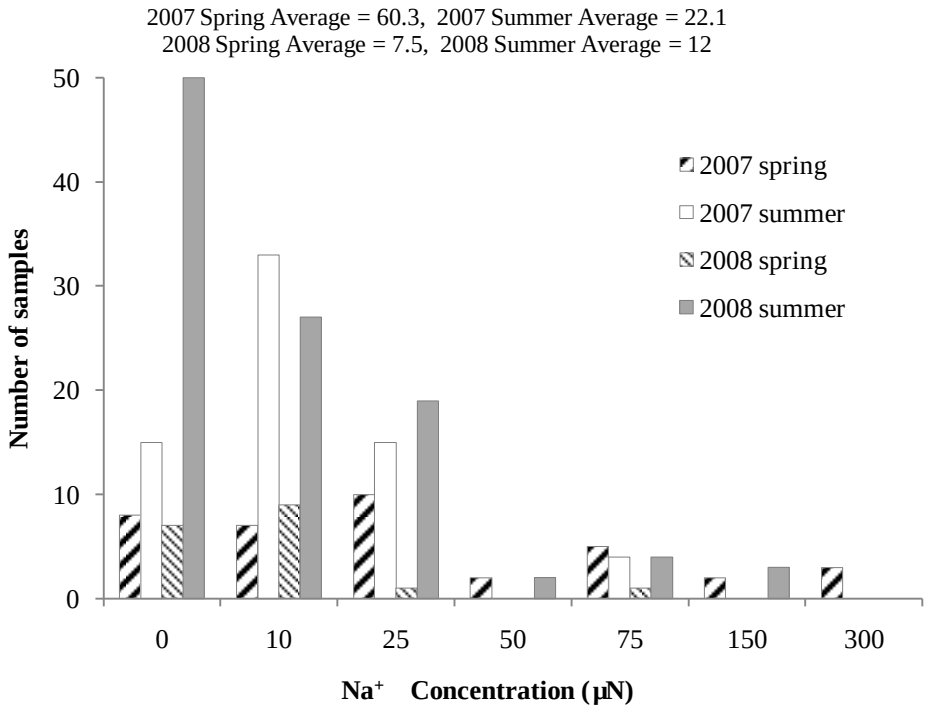

Figure 3-26. Frequency distributions of sodium ion concentrations measured in bulk (CASCC) cloudwater samples collected at Mt. Tai in the four sampling campaigns.

Frequency distributions of bulk cloudwater Mg^{2+} concentrations observed at Mt. Tai in the four sampling campaigns are shown in Figure 3-27. The average Mg^{2+} concentrations observed in spring and summer 2007 were 71.4 μN and 29.4 μN, respectively. Mg^{2+} concentrations in spring and summer 2008 averaged 10.2 μN and 13.4 μN, respectively.

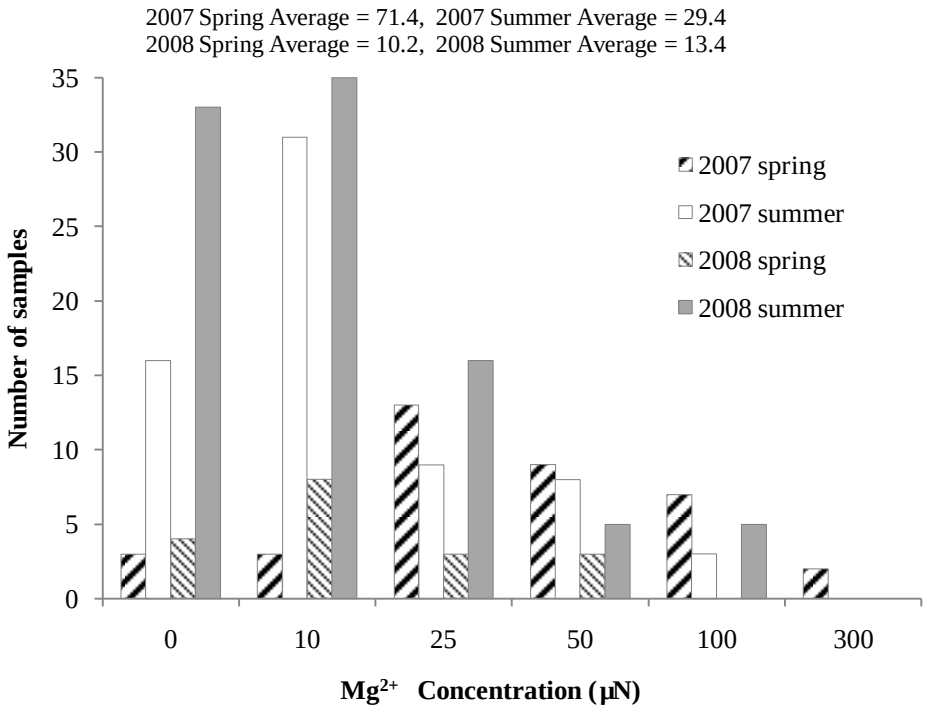

Figure 3-27. Frequency distributions of magnesium ion concentrations measured in bulk (CASCC) cloudwater samples collected at Mt. Tai in the four sampling campaigns.

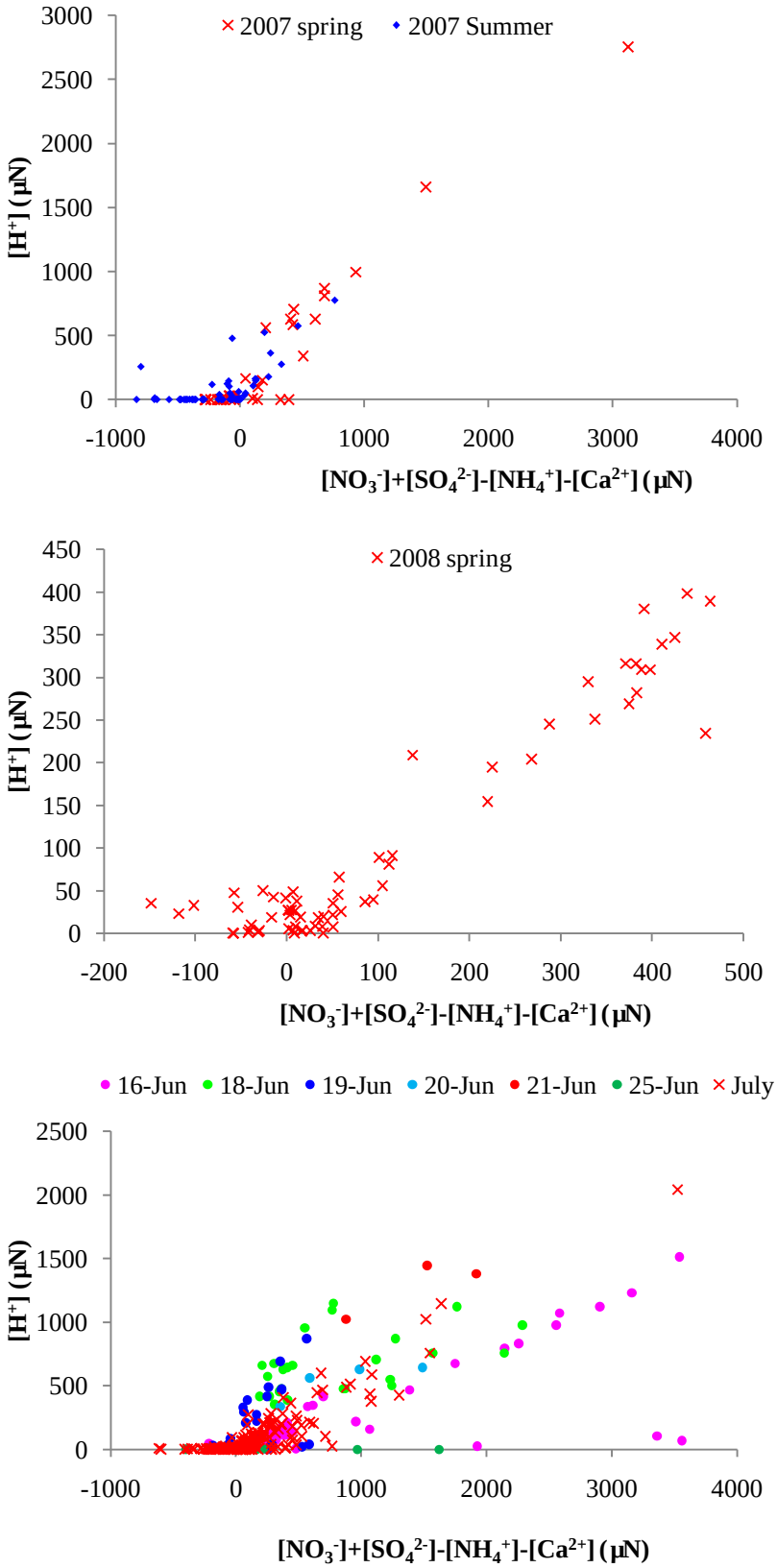

Figure 3-28. Correlations of [H+] with the concentrations of NO_3^-, SO_4^{2-}, NH_4^+, and Ca^{2+}.

3.3.4. Aqueous hydrogen peroxide and S(IV)

Frequency distributions of aqueous H_2O_2 cloudwater concentrations in the four sampling campaigns are shown in Figure 3-29. The average aqueous H_2O_2 values in spring and summer 2007 were 2.8 μM and 15 μM, respectively. The average aqueous H_2O_2 values in spring and summer 2008 were 9.2 μM and 69.1 μM, respectively. The reaction between S(IV) and H_2O_2 in aqueous solution is very fast, so that measured H_2O_2 represents "residual" H_2O_2 that was not consumed by reaction between sample collection and preservation.

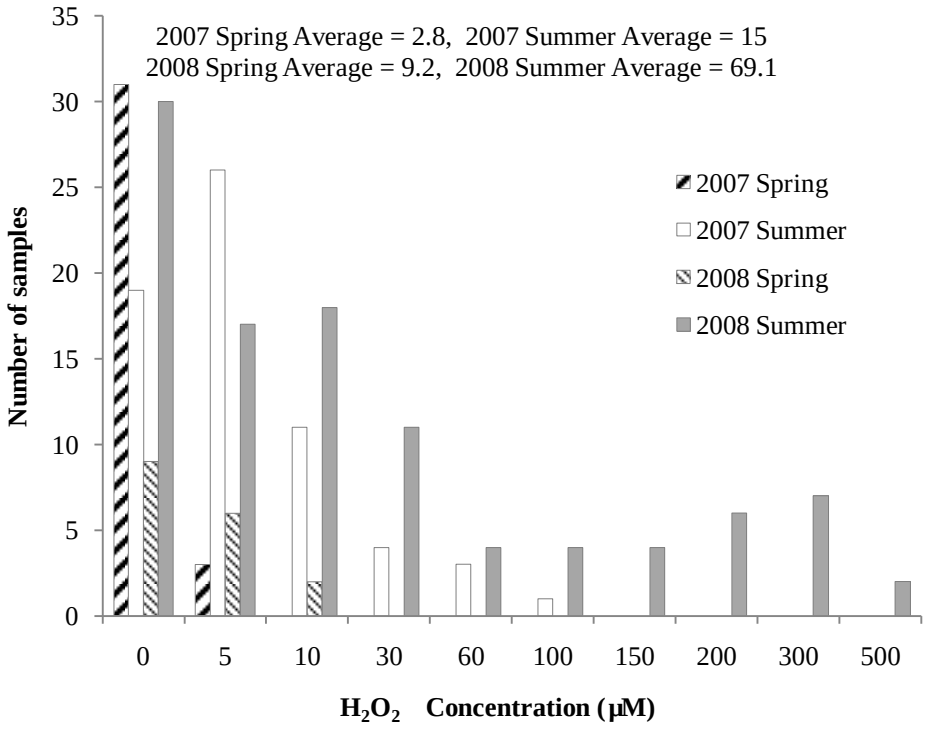

Figure 3-29. Frequency distributions of aqueous hydrogen peroxide concentrations measured in bulk (CASCC) cloudwater samples collected at Mt. Tai in the four sampling campaigns.

Frequency distributions of aqueous S(IV) cloudwater concentrations in the four sampling campaigns are shown in Figure 3-30. The average aqueous S(IV) values in spring and summer 2007 were 40.4 μM and 17.7 μM, respectively. The average aqueous S(IV) values in spring and summer 2008 were 7.7 μM and 35.6 μM, respectively. As with H_2O_2, measured S(IV) represents residual S(IV) not consumed by reaction between the times of sample collection and preservation.

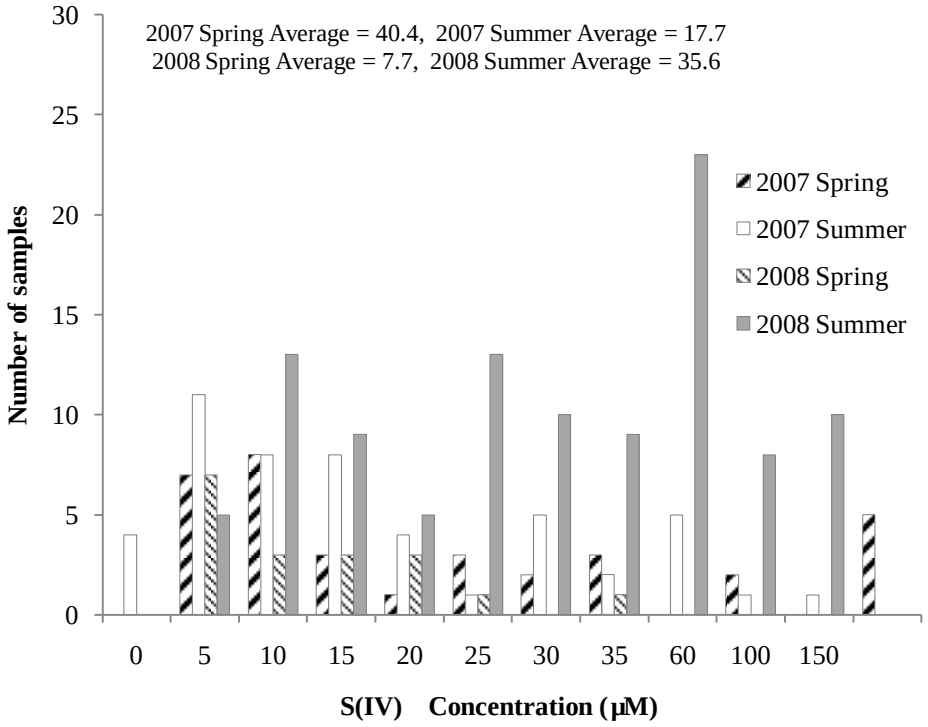

Figure 3-30. Frequency distributions of aqueous S(IV) concentrations measured in bulk (CASCC) cloudwater samples collected at Mt. Tai in the four sampling campaigns.

3.3.5. Iron and manganese

As catalysts of the S(IV) autooxidation pathway, the aqueous concentrations of Fe(III) and Mn(II) are also important to our study. Frequency distributions of bulk cloudwater Fe concentrations observed at Mt. Tai in the four sampling campaigns are shown in Figure 3-31. The average bulk cloudwater Fe concentrations measured in spring and summer 2007 were 242.5 μg/L and 44.2 μg/L, respectively. Fe concentrations measured in spring and summer 2008 averaged 241.8 μg/L and 415.7 μg/L, respectively. Higher Fe concentrations observed in 2008 might reflect changes in regional emissions (industrial activity was relocated outside Beijing in advance of the 2008 Summer Olympic Games) or diferences in metals analysis between the SDU and CSU laboratories. For comparison, total Fe was below 400 μg/L in Los Angeles basin cloudwater samples (Pehkonen et al., 1992), averaged approximately 250 μg/L in clouds sampled at Great Dun Fell, U.K. (Sedlak et al., 1997), was below 500 μg/L in clouds collected at the puy de Dome station in France (Parazols et al., 2006) and ranged up to 886 μg/L in San Joaquin Valley, California fogs (Rao and Collett, 1998).

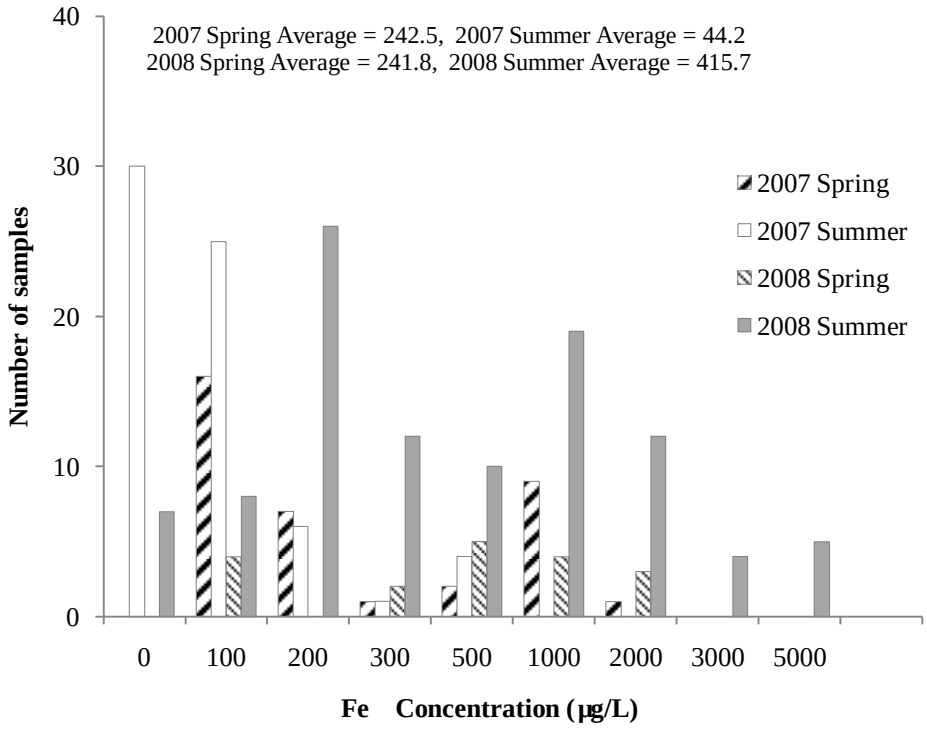

Figure 3-31. Frequency distributions of Fe concentrations measured in bulk (CASCC) cloudwater samples collected at Mt. Tai in the four sampling campaigns.

Frequency distributions of bulk cloudwater Mn concentrations observed at Mt. Tai in the four sampling campaigns are shown in Figure 3-32. The average Mn concentrations observed in spring and summer 2007 were 93.2 µg/L and 30.2 µg/L, respectively. Mn concentrations in spring and summer 2008 averaged 20.4 µg/L and 29.9 µg/L, respectively. Collett et al. (1999) reported Mn concentrations as high as 118 µg/L in San Joaquin Valley, California fogs.

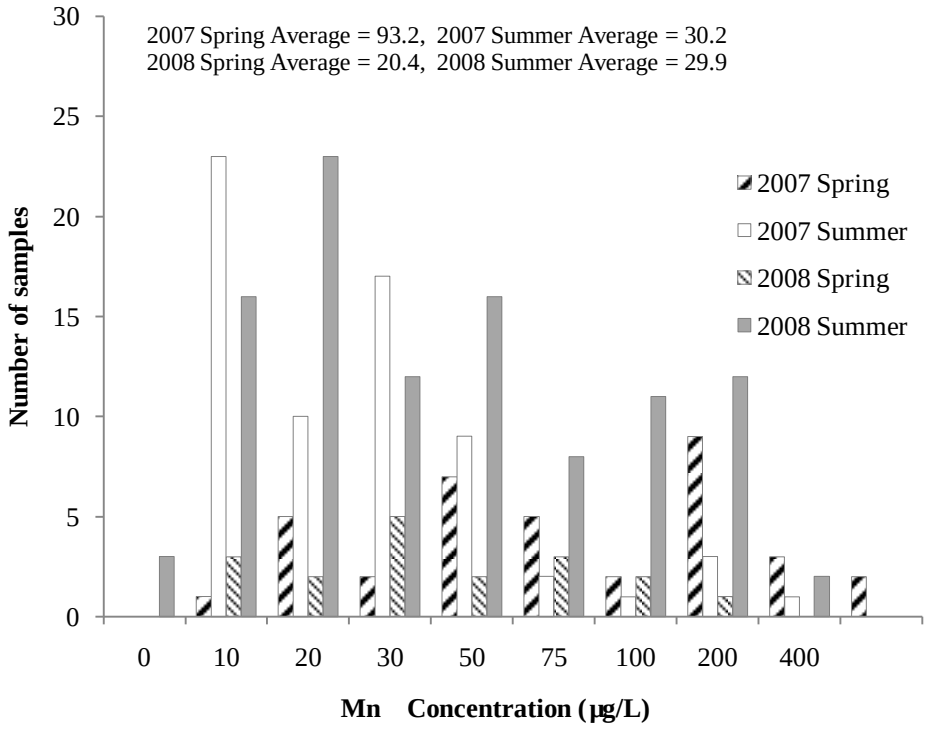

Figure 3-32. Frequency distributions of Mn concentrations measured in bulk (CASCC) cloudwater samples collected at Mt. Tai in the four sampling campaigns.

3.3.6. Formaldehyde

Formaldehyde and other carbonyl compounds can also be important players in aqueous S(IV) chemistry in clouds. The complexation of formaldehyde with dissolved S(IV), can lead to formation of hydroxymethanesulfonic acid (HMS) (Boyce and Hoffmann, 1984; Munger et al., 1984; Munger et al., 1986; Olson and Hoffmann, 1989). HMS formation tends to be important mainly at pH values above 5-6 (Rao and Collett, 1995), because the formation rate increases quickly as pH rises. Formaldehyde concentrations measured in cloudwater collected at Mt. Tai were generally fairly modest, with average concentrations of 21.3 μM and 25.4 μM, in spring and summer 2007, and average concentrations of 4.7

μM and 9.5 μM in spring and summer 2008 (Figure 3-33). Munger (1989) observed formaldehyde concentrations as high as 500 μM in San Joaquin Valley, California, fog samples. Munger et al. (1995) reported a mean cloudwater HCHO concentration of 9 μM at a rural mountain site in central Virginia.

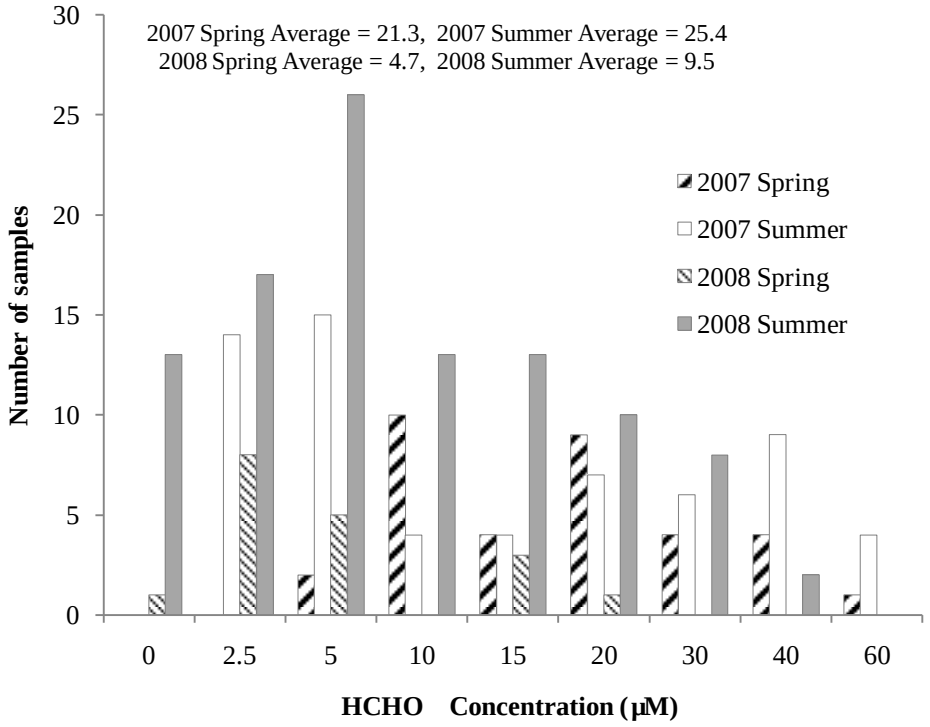

Figure 3-33. Frequency distributions of HCHO concentrations measured in bulk (CASCC) cloudwater samples collected at Mt. Tai in the four sampling campaigns.

3.4. DROP SIZE-DEPENDENT CLOUDWATER CHEMICAL COMPOSITIONS

As described in chapter 1, differences between the chemical composition of different drops within a cloud can affect the cloud chemistry, including rates of S(IV) oxidation or complexation. Here we present drop size-dependent concentrations of several major cloudwater solutes and other species of key importance to rates of S(IV) reaction. These data are taken from the two-stage size-fractionating CASCC.

3.4.1. Cloudwater pH

Figure 3-34 compares the pH values measured in small and large droplet fractions collected with the sf-CASCC during the 2008 field campaigns. While only a small pH difference is observed between the small and large drop fractions during many sample periods, fairly large pH differences of 0.5 – 1.0 pH units or greater, are observed in many other cases. The most common pattern is for large cloud drops to have a higher pH than small cloud drops, similar to the pattern first reported by Collett et al. (1994) for cloud and fog samples from a variety of environments. Differences in cloud composition as a function of drop size can arise from a variety of factors including differences in the composition of cloud condensation nuclei (CCN) that nucleate small and large cloud drops, drop size-dependent condensational growth rates, and differences in the rate of uptake of soluble gases between small and large droplets (Ogren and Charlson, 1992; Bator and Collett, 1997; Moore et al., 2004a; Moore et al., 2004b). Understanding the distribution of pH values in a population of cloud drops can be important for accurately

predicting rates of in-cloud sulfate production. Because the rates of some aqueous S(IV) oxidation pathways are nonlinear functions of the cloud drop H^+ concentration, the average H^+ concentration in a bulk cloudwater sample is not necessarily a good predictor of the average aqueous phase sulfate production rate (Seidl, 1989; Hegg and Larson, 1990; Collett et al., 1994; Gurciullo and Pandis, 1997; Hoag et al., 1999; Reilly et al., 2001).

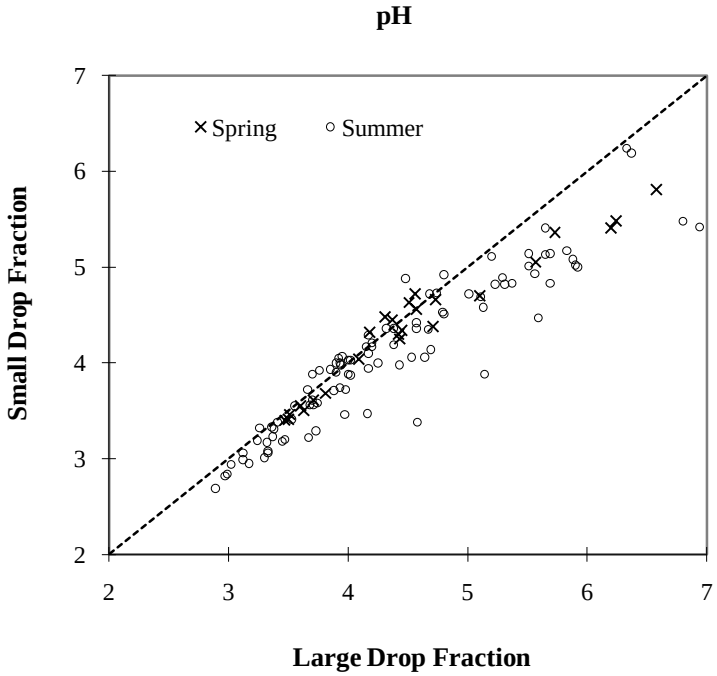

Figure 3-34. Comparison of pH values measured in small (4 < D < 16 μm) and large (D > 16 μm) cloud drop size fractions simultaneously collected with the sf-CASCC at Mt. Tai during the spring and summer 2008 field campaigns. (The diagonal dashed line is the 1:1 line).

3.4.2. Major solutes

The four panels of Figure 3-35 compare the small and large drop concentrations of four key Mt. Tai cloud solute species: TOC, sulfate, nitrate, and ammonium. Some enrichment is seen of TOC in smaller drops in some sample periods. No consistent pattern of small or large cloud drop enrichment is seen for sulfate, nitrate, or ammonium, although several individual sample pairs do show differences between small and large drop concentrations of these species. Bator and Collett (1997) previously reported these species to typically be enriched in small cloud/fog drops in several locations, although their distribution across the drop size spectrum can depend on many factors.

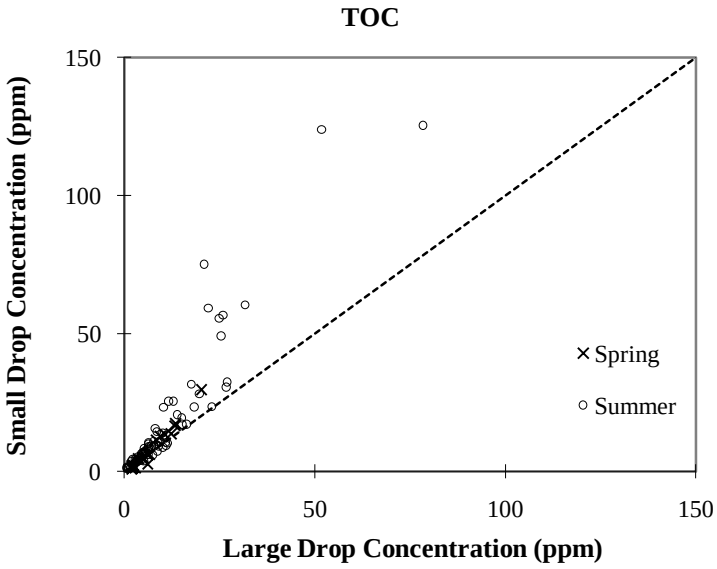

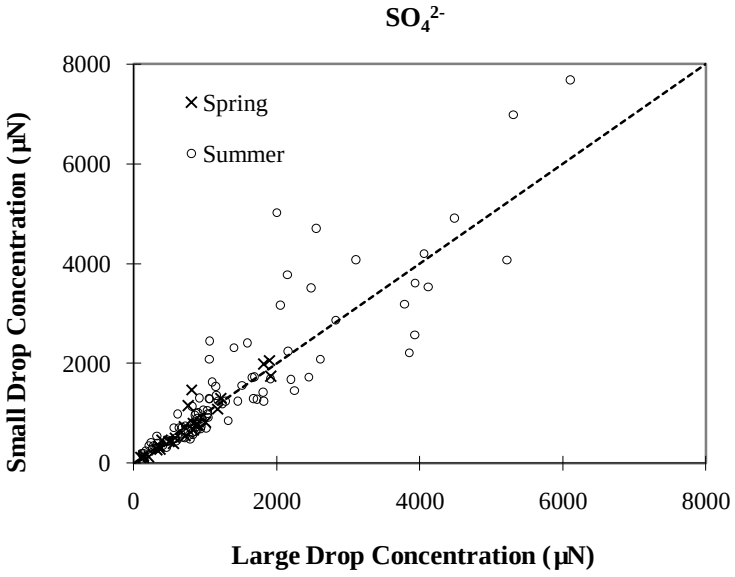
SO_4^{2-}
Spring
Summer
Small Drop Concentration (µN)
Large Drop Concentration (µN)
0
2000
4000
6000
8000

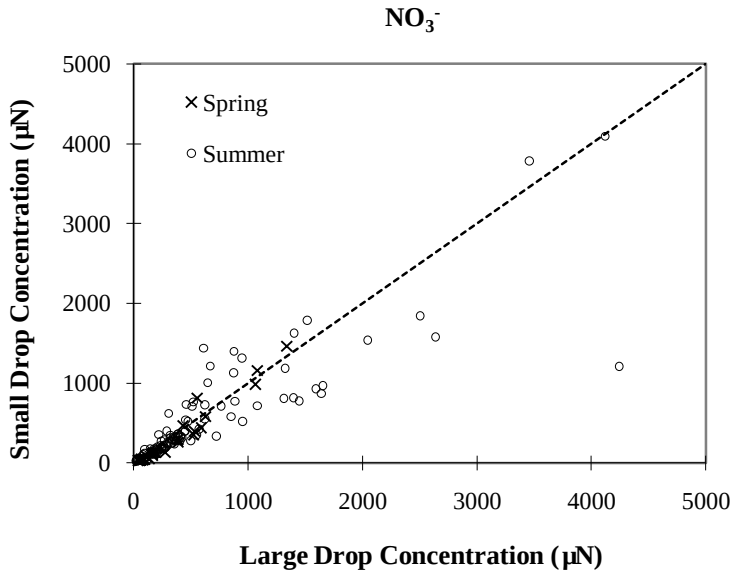
NO_3^-
Spring
Summer
Small Drop Concentration (µN)
Large Drop Concentration (µN)
0
1000
2000
3000
4000
5000

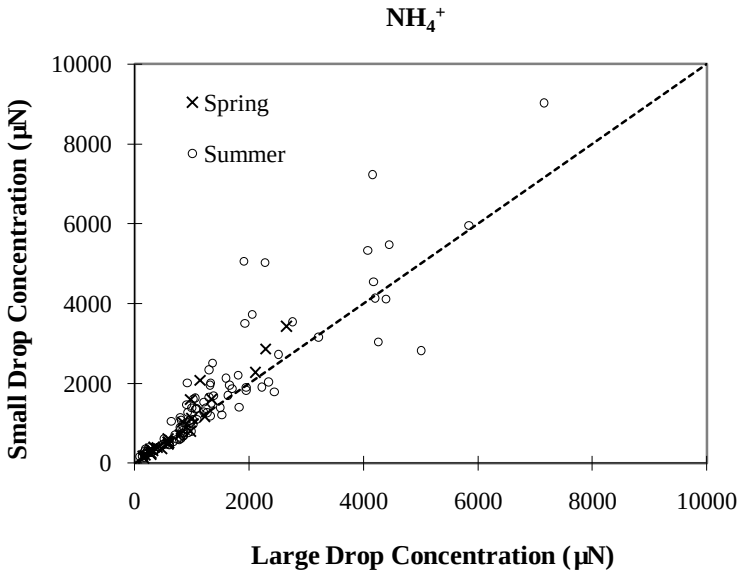

Figure 3-35. Comparisons of TOC, sulfate ion, nitrate ion and ammonium ion concentrations measured in small (4 < D < 16 µm) and large (D > 16 µm) cloud drop size fractions simultaneously collected with the sf-CASCC at Mt. Tai during the spring and summer 2008 field campaigns. (The diagonal dashed line is the 1:1 line).

In contrast to sulfate, nitrate, and ammonium, there is a more obvious difference between the Ca^{2+}, Na^{+} and Mg^{2+} concentrations of large and small cloud droplets sampled at Mt. Tai; higher concentrations of Ca^{2+}, Na^{+} and Mg^{2+} were typically found in the large drops, as shown in Figure 3-36. This pattern is similar to observations reported by Bator and Collett (1997). Ca^{2+}, Na^{+} and Mg^{2+} are typically associated with coarse mode aerosol particles (soil dust and sea salt). These larger particles, when they act as CCN, often tend to be associated with larger cloud droplets (Twohy et al., 1989; Bator and Collett, 1997). The enrichment of more alkaline, coarse mode aerosol components in larger cloud drops at Mt. Tai is likely an important contributor to the higher pH seen in these larger cloud drops.

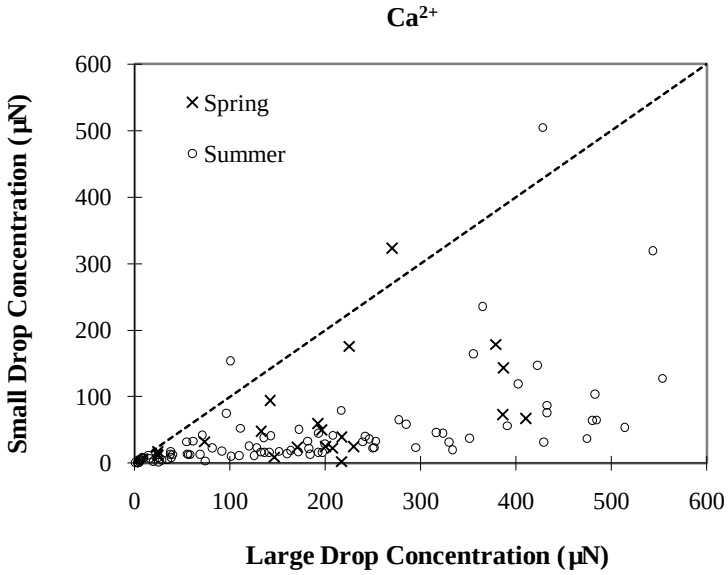
Ca2+
Spring
Summer
Small Drop Concentration (µN)
Large Drop Concentration (µN)
0
100
200
300
400
500
600

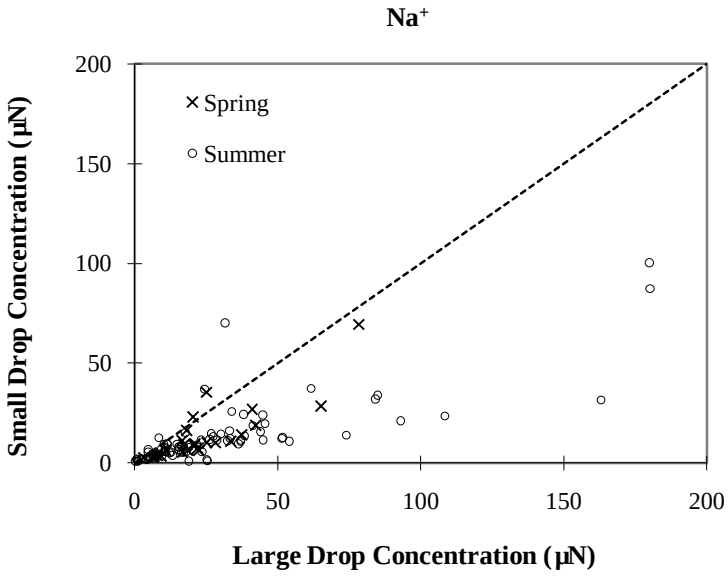
Na+
Spring
Summer
Small Drop Concentration (µN)
Large Drop Concentration (µN)
0
50
100
150
200

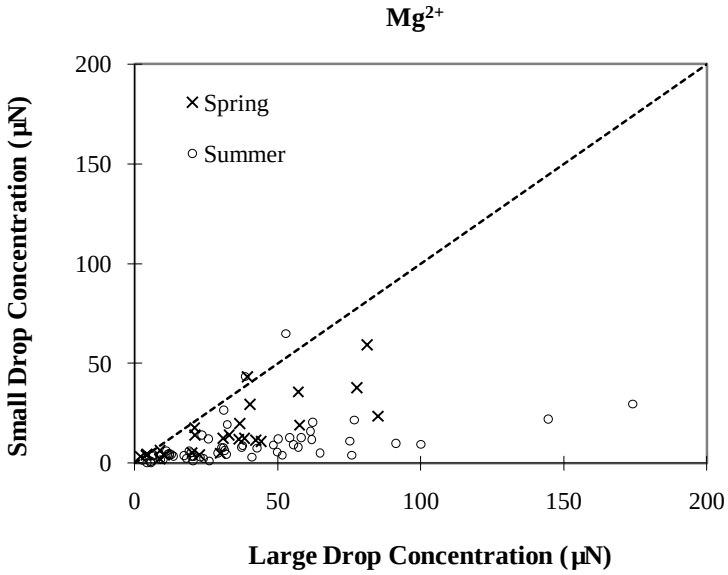

Figure 3-36. Comparisons of calcium ion, sodium ion and magnesium ion concentrations measured in small ($4 < D < 16$ μm) and large ($D > 16$ μm) cloud drop size fractions simultaneously collected with the sf-CASCC at Mt. Tai during the spring and summer 2008 field campaigns. (The diagonal dashed line is the 1:1 line).

3.4.3. Aqueous hydrogen peroxide and S(IV)

Figure 3-37 compares the aqueous H_2O_2 and S(IV) values measured in small and large droplet fractions collected with the sf-CASCC during the 2008 field campaigns. There is no obvious pattern of consistent aqueous H_2O_2 and S(IV) enrichment in either large or small cloud drops.

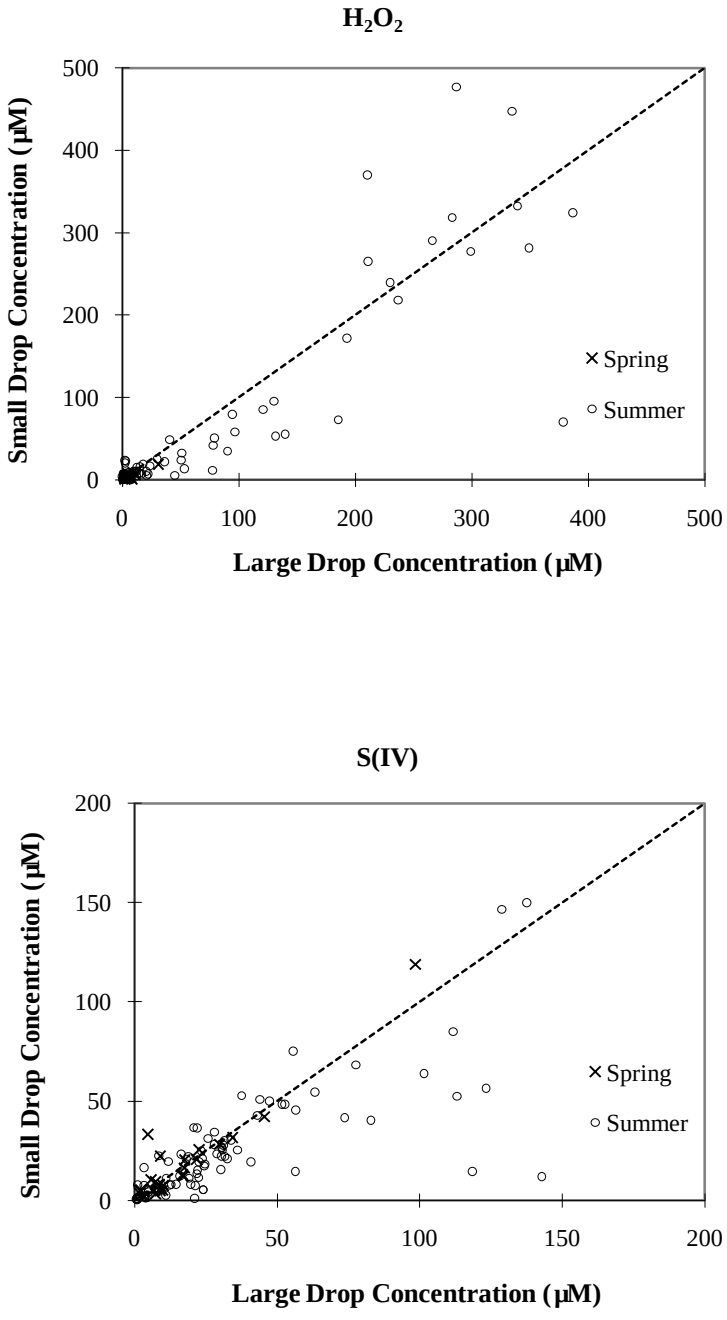

Figure 3-37. Comparisons of aqueous H_2O_2 and S(IV) concentrations measured in small (4 < D < 16 μm) and large (D > 16 μm) cloud drop size fractions simultaneously collected with the sf-CASCC at Mt. Tai during the spring and summer 2008 field campaigns. (The diagonal dashed line is the 1:1 line).

3.4.4. Iron and manganese

Comparisons of the small and large drop size fraction concentrations of Fe and Mn are illustrated in Figure 3-38, based on the spring and summer 2008 samples collected with the sf-CASCC. No clear pattern of consistent trace metal enrichment in either large or small cloud drops is observed, although considerable concentration differences are observed between the drop size fractions in many individual cases. Drop size-dependent concentrations of Fe and Mn have also previously been reported in radiation fogs and stratiform clouds from a variety of locations in the United States (Rao and Collett, 1998; Reilly et al., 2001; Moore et al., 2004a; Moore et al., 2004b). As in the case of the H^+ concentration, the non-linear dependence of the metal-catalyzed S(IV) autooxidation pathway on the metal concentrations can result in the average cloudwater metal concentration being a poor predictor of the average rate of S(IV) oxidation by this pathway (Rao and Collett, 1998), a topic that will be addressed in chapter 5.

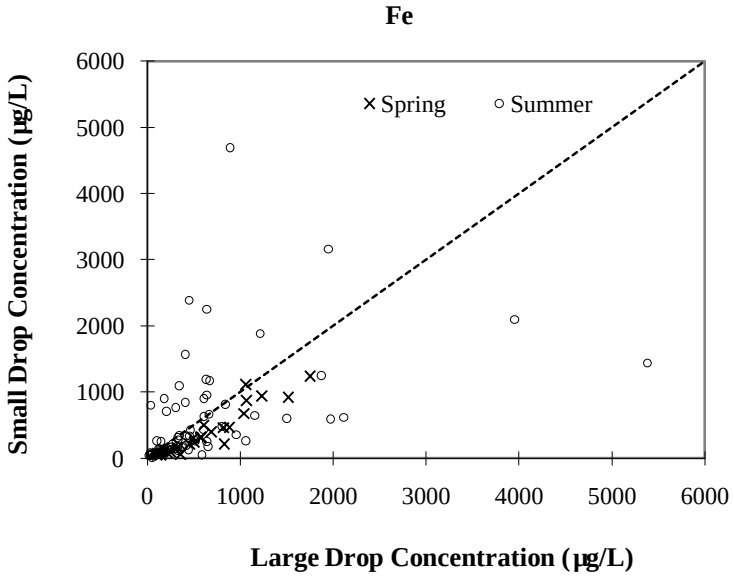

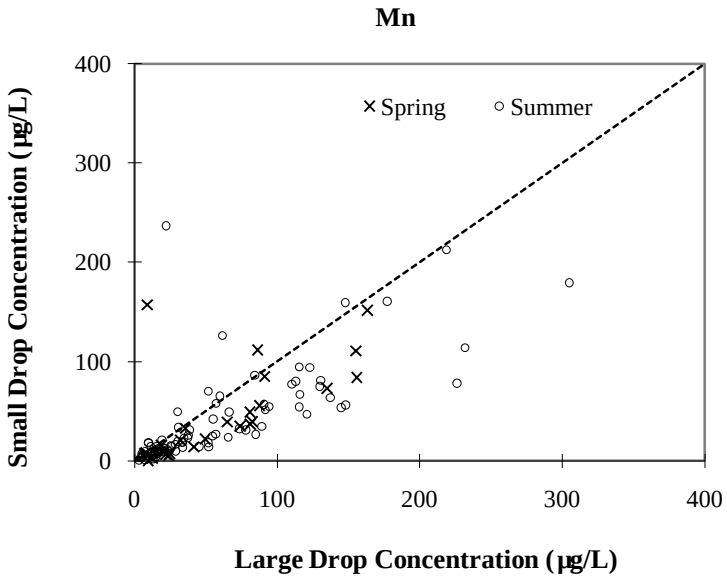

Figure 3-38. Comparisons of Fe and Mn concentrations measured in small (4 < D < 16 μm) and large (D > 16 μm) cloud drop size fractions simultaneously collected with the sf-CASCC at Mt. Tai during the spring and summer 2008 field campaigns. (The diagonal dashed line is the 1:1 line).

3.4.5. Formaldehyde

Little difference was typically observed between HCHO concentrations measured in large and small cloud drop fractions collected with the sf-CASCC (Figure 3-39), consistent with expectations of equilibrium partitioning between gas and aqueous phase HCHO across the cloud drop size spectrum.

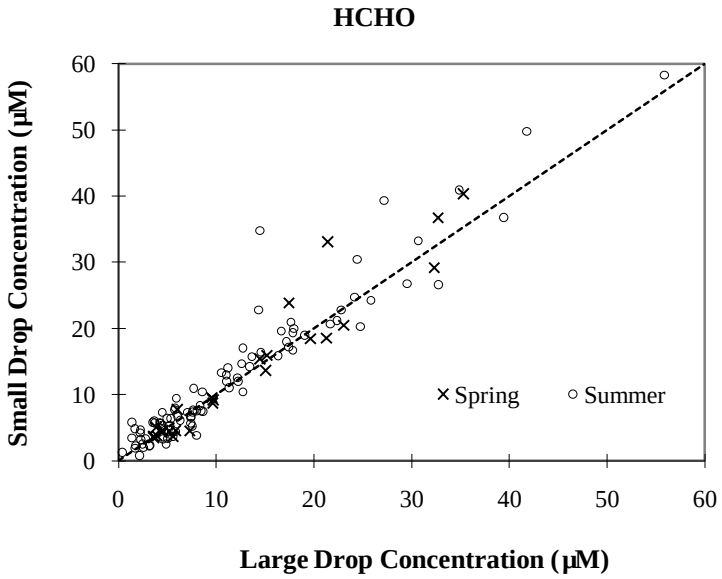

Figure 3-39. Comparison of HCHO concentrations measured in small (4 < D < 16 µm) and large (D > 16 µm) cloud drop size fractions simultaneously collected with the sf-CASCC at Mt. Tai during the spring and summer 2008 field campaigns. (The diagonal dashed line is the 1:1 line).

CHAPTER 4 CLOUD-AEROSOL INTERACTIONS

4.1. BACKWARD TRAJECTORY ANALYSIS

Backward trajectories can trace an air parcel's path before it arrives at a receptor site, the trajectory including information concerning an air parcel's origin, transport distance, and the residence time in each region during its transport. Ulman and Saxena used backward trajectories to analyze the influence of cloud-forming air mass histories on cloudwater chemical composition at Mt. Mitchell, North Carolina (Ulman and Saxena, 1997). Menon et al. reported the effect of cloud-forming air mass origin on the size-dependent cloud droplet chemical composition based on backward trajectory analysis (Menon et al., 2000). Kim et al. also used backward trajectories to investigate cloud/fog water chemical composition differences due to air masses' different transport trajectories (Kim et al., 2006).

In this study, backward trajectory analysis is used to investigate the transport history of air parcels associated with cloud interception at Mt. Tai. Then, in combination with other factors, such as atmospheric stability, precipitation, and source emission intensity, the relationship between the cloudwater chemical properties and the transport history of the precursor air parcel can be examined. Because Mt. Tai is located in a region surrounded by large urban, industrial, and agricultural activity centers, it is quite possible that

relationships between transport pattern and cloud composition may be complex and difficult to elucidate.

The National Oceanic and Atmospheric Administration (NOAA) Air Resources Laboratory's HYSPLIT (HYbrid Single-Particle Lagrangian Integrated Trajectory) model was used in this project to calculate backward trajectories. The HYSPLIT model is a useful model for computing both trajectories and dispersion/deposition simulations (Draxier and Hess, 1997; Draxier and Hess, 1998) and is widely used in numerous research studies. As described above, in order to more efficiently investigate the relationship between cloud chemical properties and the air parcel transport history, trajectories were categorized into three sectors: marine, polluted, and continental sector based on the trajectories' geographical locations and SO_2 source emission intensity distribution, as shown in Fig. 4-1.

Sector 1 represents the 'marine' region; sector 2 represents areas that the SO_2 source emission intensities are relatively higher, and is considered as a 'polluted' region; sector 3 represents areas that the SO_2 source emission intensities are somewhat lower, and is labeled as a 'continental' region. This continental sector also contains some of the large dust source regions. Note that the SO_2 emissions map shows large SO_2 emissions close to Mt. Tai in all directions. Similar patterns are seen in regional NO_x and NH_3 emissions. For these reasons, one might expect differences between the composition of clouds associated with air parcel transport from the three sectors to be less than those observed

in some of the previous studies mentioned above, where a clearer separation between source regions existed.

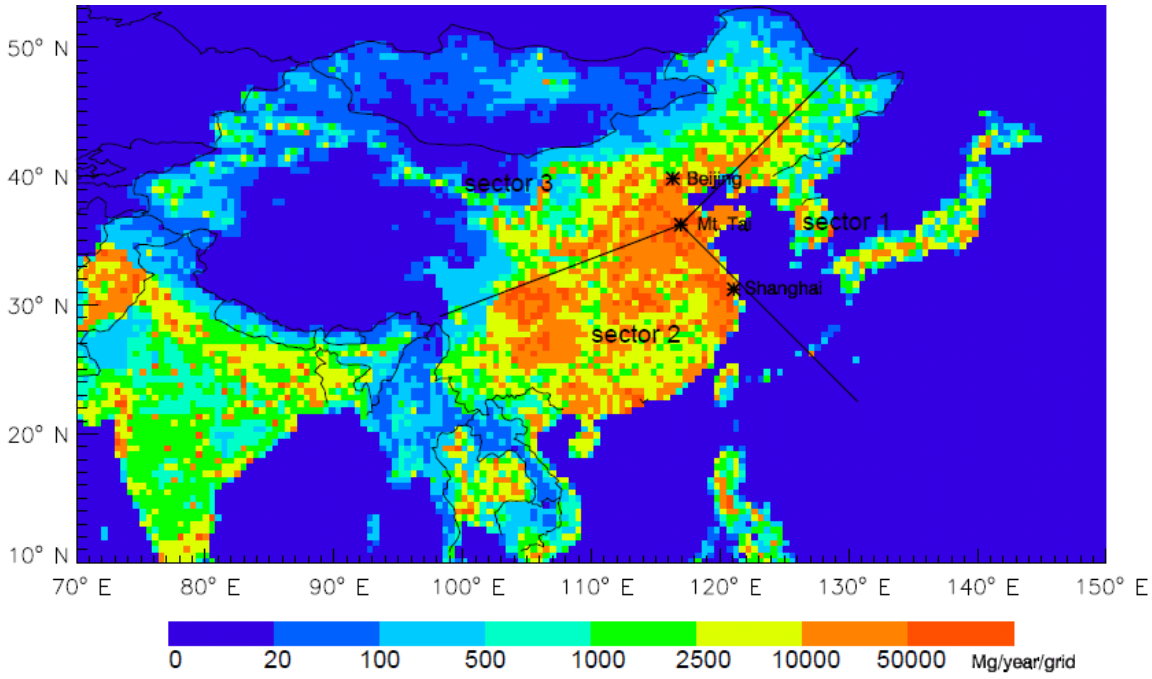

Figure 4-1. Three sectors and the SO_2 emission intensity distribution at 30min×30min resolution (Data from http://mic.greenresource.cn/data/intex-b); sector 1: marine, sector 2: polluted, sector 3: continental.

72-hour back-trajectories were calculated at one hour intervals for each cloud event, with end points at 1600 meters above mean sea-level (AMSL), representing a total of 245 individual trajectories for all the cloud events during the four field campaigns. The National Weather Service's National Centers for Environmental Prediction (NCEP) Global Data Assimilation System (GDAS) model output was used as the meteorological data set input for the back-trajectory calculations. Model vertical velocity was selected as the vertical motion calculation method.

4.1.1. Backward trajectories and cloudwater composition variations

In order to investigate the relationship between cloudwater chemical properties and the transport history of the precursor air parcel, summary data for the sampled events are provided below in tables 4-1 through 4-4, by campaign. The summaries include the number of events in each campaign, the date and time period of each sampled event, sectors that backward trajectories for each event passed through, a brief description of the air parcel's vertical motion status, and the average (volume-weighted) cloudwater concentrations of several key species. The summaries also include estimated altitudes of cloud base for each event obtained using the following equation (Ahrens, 2000):

$$H_{base} = \frac{T - T_d}{\Gamma_d - \Gamma_{dew}} = 125(T - T_d) \qquad \text{Equation 4-1}$$

Where H_{base} is the cloud base height (in meters), Γ_d is the dry adiabatic lapse rate (~9.8 ℃/km), Γ_{dew} is the dew point lapse rate (~1.8 ℃/km), T is the surface air temperature (in degrees Celsius), and T_d is the dew point temperature (in degrees Celsius). The cloud base height can be obtained from T and T_d based on equation 4-1 for most of the events. Because no meteorology data are available directly at the base of Mt. Tai, meteorological observations from Jinan (60 km to the north of Mt. Tai) were used to estimate the cloud base height, so uncertainties exist here.

Backward trajectories were represented with different colors based on the average pH value for each event to see if significant pH differences exist for different transport

trajectories. Fig. 4-2 shows the backward trajectories for cloud events during the spring 2007 campaign.

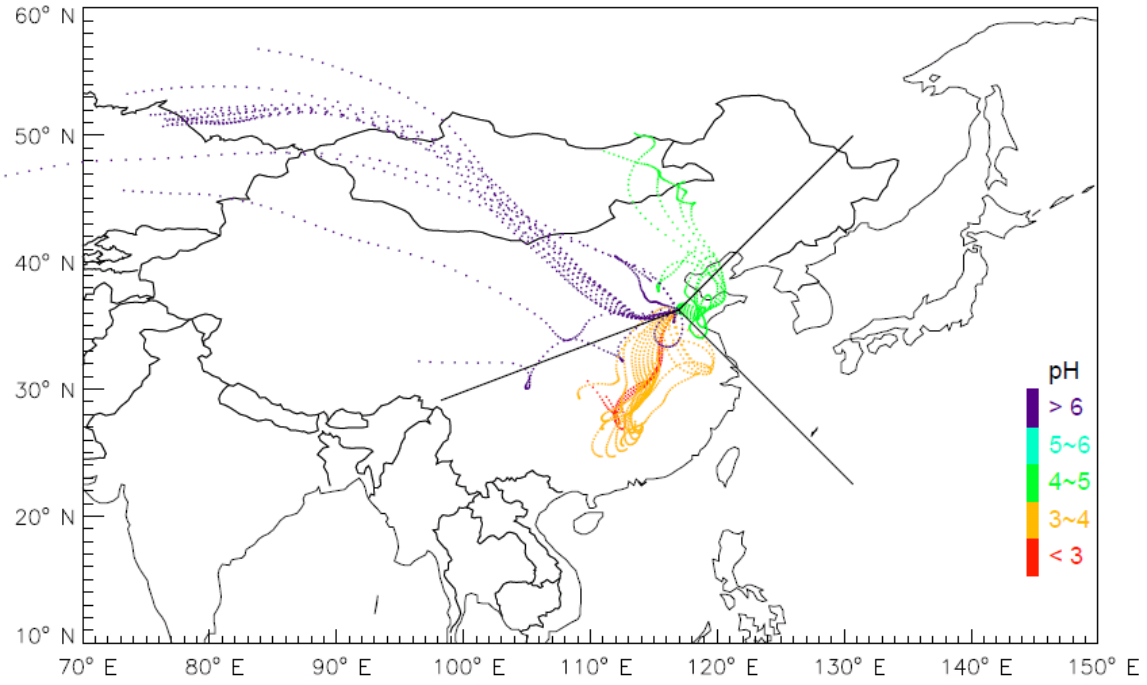

Figure 4-2. Backward trajectories for cloud events during the spring 2007 campaign.

As shown in Fig. 4-2, during the spring 2007 campaign, backward trajectories for most of the events passed through sector 2 and sector 3. There is a clear pattern that cloud events with backward trajectories passing through continental sector 3 had a higher pH than those with backward trajectories passing through the more polluted sector 2. Ren (2009) reported that two strong dust storms were observed (March 31-April 2 and April 20-21) during the spring 2007 campaign. As described in chapter 1, soil dust in the atmosphere may alleviate the acid deposition situation in the north of China by neutralizing part of the acidity contributed to precipitation by sulfuric and nitric acids. The increased dust during the spring 2007 campaign, along with lower SO_2 emissions in sector 3, are

consistent with the higher pH clouds that intercepted Mt. Tai during periods of transport from sector 3. Fig. 4-3 gives typical backward trajectories for several cloud events (4/18, 4/20 and 4/21) that were under the influence of dust storms during the spring 2007 campaign. All those trajectories have typical long transport distance, descending vertical motion and little influence from the local lower altitude air. A summary of the spring 2007 campaign is given in table 4-1.

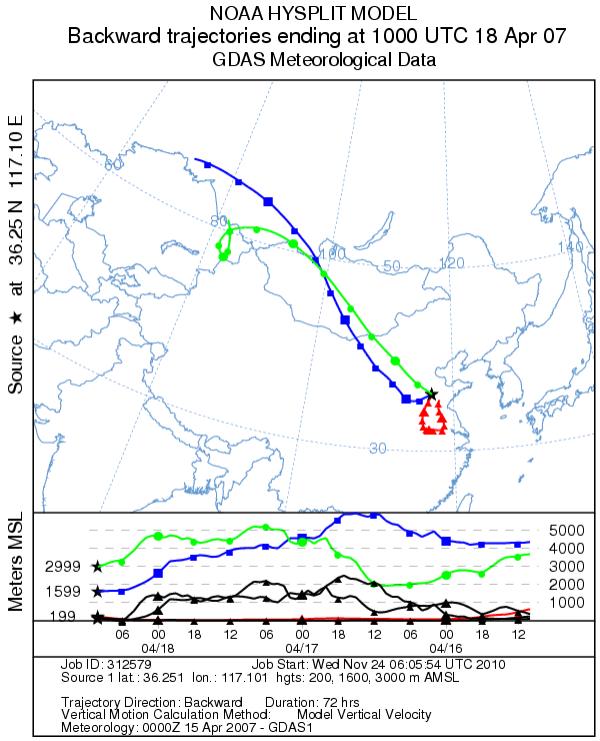

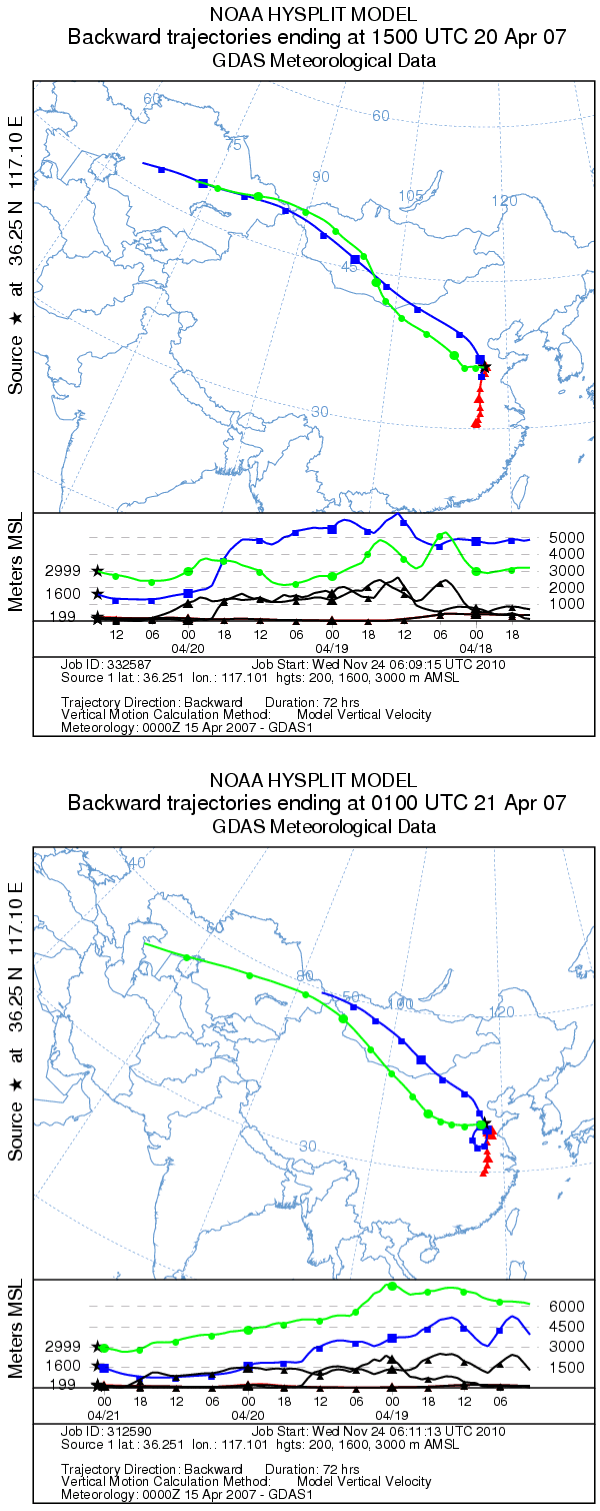

Figure 4-3. Representative backward trajectories for 3 cloud events (4/18, 4/20 and 4/21) during the spring 2007 campaign.

Table 4-1. Summary of the spring 2007 campaign.

Event	Date	Time	Sector	Vertical motion	pH	SO_4^{2-}(μN)	NO_3^-(μN)	NH_4^+(μN)	Ca^{2+}(μN)	K^+(μN)	Cl^-(μN)	Cloud Base(m)
1	3-23	04:30-07:30	2	ST	2.84	3368	4638	4392	1904	295	402	1250
2	3-23	10:50-22:40	2	ST	3.22	1571	837	1579	332	85	160	875
3	3-29	08:00-10:30	2/3(L)	LH/HL	7.32	1499	612	1424	1244	94	288	N/A
4	3-30	16:30-21:20	2	LH	3.98	1433	682	1543	452	62	155	375
5	4-15	07:53-16:00	1/3(L)	LH	4.78	331	95	279	235	13	115	250
6	4-17	23:00-08:00	3(L)	HL	7.64	1111	523	1139	625	655	99	750
7	4-18	17:30-02:30	3	HL	6.59	1349	435	1436	531	47	87	1500
8	4-20	23:00-24:00	3	HL	6.69	6439	3044	5271	3884	855	531	1750
9	4-21	09:00-10:00	3/2	HL	6.53	9734	7774	8060	9054	691	1230	1125

Note: Vertical motion status is represented as stable (ST), from high elevation to low elevation (HL), or from low elevation to high elevation (LH).

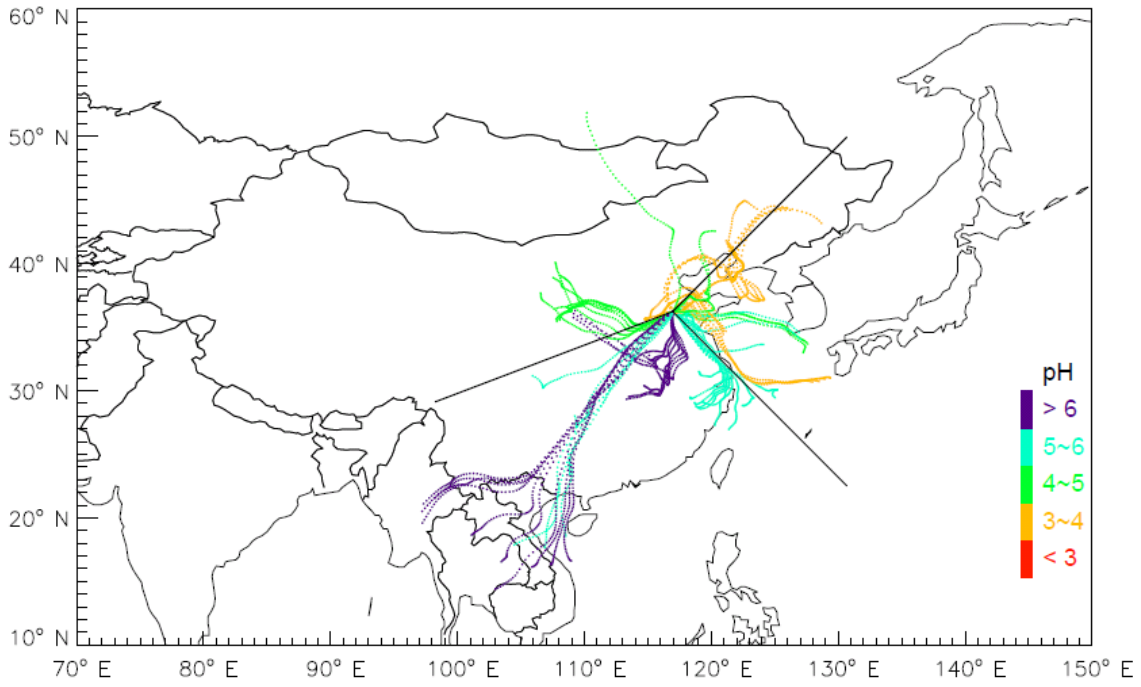

Figure 4-4. Backward trajectories for cloud events during the summer 2007 campaign.

Fig. 4-4 shows the back-trajectories for cloud events during the summer 2007 campaign. Cloud events with backward trajectories passing through sector 2 generally had relatively higher pH than those with backward trajectories passing through sectors 1 and/or 3. The trajectories for the cloud event (7/14) with the highest ion concentrations during the summer 2007 campaign passed through sectors 1 and 3 and the origins were from the area close to the Beijing megalopolis, a highly polluted region. The trajectories for the cloud event (6/20) with the lowest ion concentrations during the summer 2007 campaign passed through sectors 1 and 2 covering Shanghai city; it was raining during this event. From several events' ion concentration data, it is obvious that upwind precipitation scavenging of aerosol and trace gases has a significant impact on the cloudwater chemical composition observed at Mt. Tai.

A summary of the summer 2007 campaign is given in table 4-2.

Table 4-2. Summary of the summer 2007 campaign. Saturated: air was saturated at surface.

Event	Date	Time	Sector	Vertical Motion	pH	SO_4^{2-}(μN)	NO_3^-(μN)	NH_4^+(μN)	Ca^{2+}(μN)	K^+(μN)	Cl^-(μN)	Cloud Base(m)
1	6-19	19:00-03:00	1	ST	4.99	1197	658	1528	579	139	183	875
2	6-20	07:28-22:30	1/2	ST	5.11	93	26	109	22	7	10	Saturated
3	6-21	11:00-17:50	1	ST	3.53	490	158	364	118	22	42	Saturated
4	6-22	20:25-23:55	1	ST	3.53	734	164	664	97	17	17	Saturated
5	6-23	09:35-18:35	1	ST	3.26	2038	512	2230	194	58	175	750
6	6-26	16:25-02:55	3/2(L)	HL/ST	6.67	1639	519	2377	252	53	78	875
7	7-1	09:30-20:00	1/3	ST	3.80	726	212	797	68	23	44	Saturated
8	7-12	09:30-12:30	3	HL	4.54	1859	466	2443	264	62	70	875
9	7-14	06:15-23:15	1/3	ST	4.30	5062	1385	5847	678	149	213	1000
10	7-16	20:10-09:00	3	ST	4.23	1399	280	1826	141	38	36	625
11	7-17	13:15-00:45	2	ST	5.75	2019	353	2471	226	77	54	1125
12	7-18	06:05-18:30	2	ST/LH	6.07	987	129	1317	107	24	29	500

Note: Vertical motion status is represented as stable (ST), from high elevation to low elevation (HL), or from low elevation to high elevation (LH).

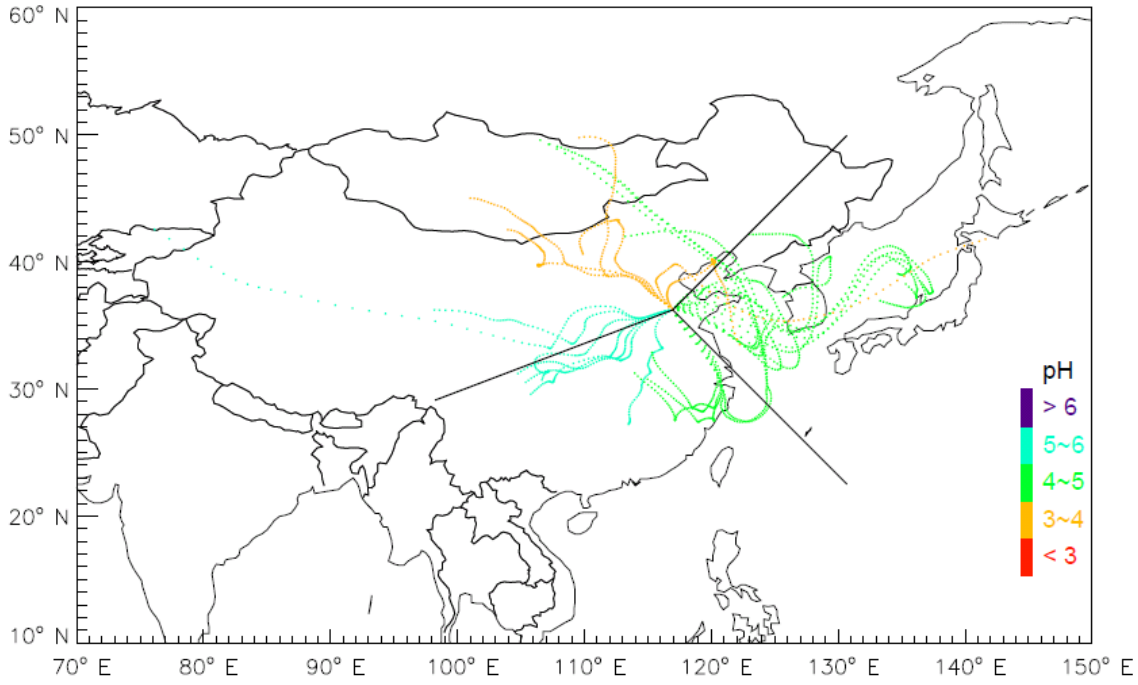

Figure 4-5. Backward trajectories for cloud events during the spring 2008 campaign.

Figure 4-5 shows the backward trajectories for cloud events during the spring 2008 campaign. It was generally windy during spring 2008 cloud interception episodes and backward trajectories for all four cloud events passed through two sectors. The April 6 cloud event had the highest ion concentrations during the spring 2008 campaign and no precipitation occurred during this event. It was drizzling/raining during two cloud events (4/8 and 4/19) and cloudwater ion concentrations during these two events decreased dramatically. The event with the most acidic cloudwater, April 22, occurred after two days raining; the cloudwater ion concentrations for this event are also lower than those for the cloud event (4/6) without precipitation. This cloud event featured transport especially from continental sector 3, contrasting with the tendency for this region to yield higher pH clouds in spring 2007.

A summary of the spring 2008 campaign is given in table 4-3.

Table 4-3. Summary of the spring 2008 campaign.

Event	Date	Time	Sector	Vertical motion	pH	TOC (ppmC)	SO_4^{2-}(μN)	NO_3^-(μN)	NH_4^+(μN)	Ca^{2+}(μN)	K^+(μN)	Cl^-(μN)	Cloud Base(m)
1[a]	4-6	01:00-12:00	2/3	ST/HL	5.85	10.9	1132	589	1526	213	58	64	750
2	4-8	22:30-17:30	3/1	HL	4.17	3.0	487	106	406	86	15	31	Saturated
3	4-19	22:00-02:00	2/1	ST	4.86	1.3	94	42	126	20	6	9	Saturated
4	4-22	13:00-18:00	1/3	ST	3.48	11.7	877	507	877	137	34	69	500

Note: Vertical motion status is represented as stable (ST), from high elevation to low elevation (HL), or from low elevation to high elevation (LH).

1[a]: cloudwater concentrations listed for this event are volume-weighted average concentrations calculated from size-fractionated cloudwater compositions data, the bulk cloudwater compositions data are not available due to the CASCC leaking during this event.

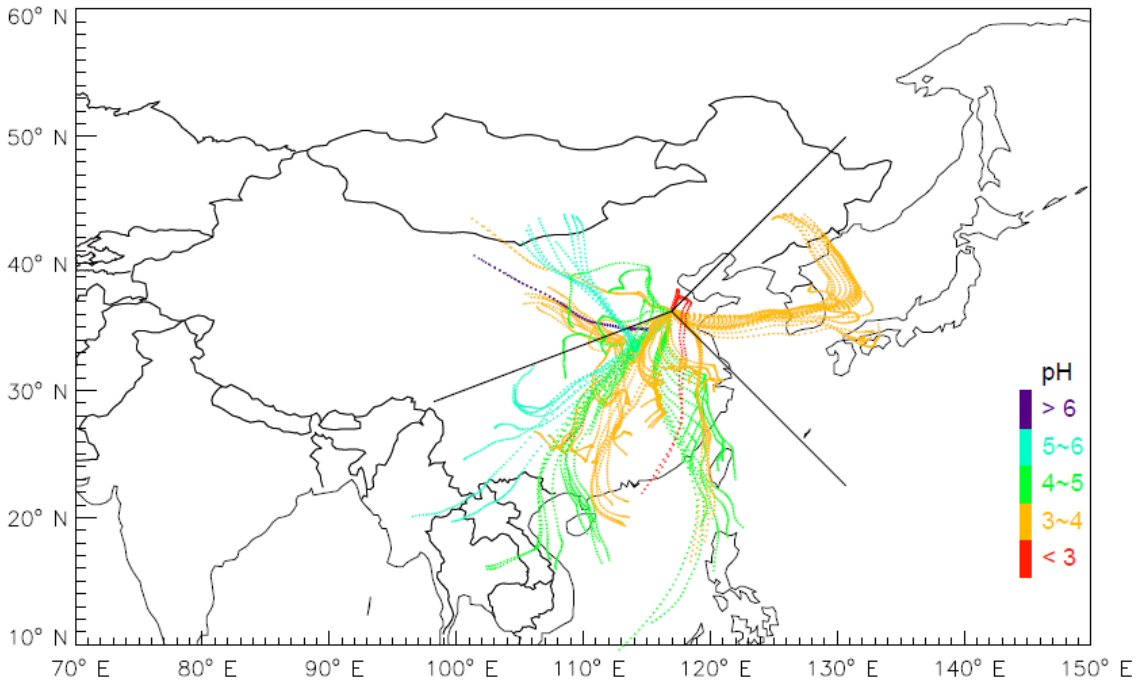

Figure 4-6. Backward trajectories for cloud events during the summer 2008 campaign.

Fig. 4-6 shows back-trajectories for summer 2008 campaign cloud events. Two-thirds of cloud events had low pH values (<4); some cloud events (6-21 and 7-11) had very acidic cloudwater with pH values even lower than 3. A summary of the summer 2008 campaign is given in table 4-4. From analysis of the backward trajectories for all the cloud events, a preliminary conclusion can be reached that transport patterns do not have obvious impact on the cloudwater chemical composition for these events. As discussed above, Mt. Tai is surrounded by regions of high pollutant emission giving the potential for polluted cloudwater regardless of the longer distance origins of air trajectories. Cloud-forming air parcels' origins and vertical motions and precipitation histories all can have a significant influence on the cloudwater composition.

Table 4-4. Summary of the summer 2008 campaign.

Event	Date	Time	Sector	Vertical motion	pH	TOC (ppmC)	SO_4^{2-}(μN)	NO_3^-(μN)	NH_4^+(μN)	Ca^{2+}(μN)	K^+(μN)	Cl^-(μN)	Cloud Base(m)
1	6-16	02:00-07:30	1	ST	3.80	22.9	3053	2217	4289	517	296	450	750
2	6-16	17:00-15:00	1	ST	3.59	6.5	719	303	513	24	31	44	Saturated
3	6-18	21:00-08:00	2/3	HL	3.15	85.6	1656	1045	1955	120	248	564	750
4	6-19	19:00-08:15	2	ST	3.62	24.0	1251	727	1663	177	164	313	875
5	6-20	16:45-19:20	2	ST	3.22	19.0	2076	552	1909	37	133	116	500
6	6-21	09:00-09:40	2	ST	2.86	45.7	3857	1269	3018	190	267	406	375
7	6-25	23:10-00:45	3	ST	6.66	20.0	4178	885	4462	467	143	127	1125
8	7-2	04:05-05:50	3	HL	3.43	17.6	3372	959	3410	367	126	155	375
9	7-3	20:00-11:40	3/2	HL/ST	5.30	14.7	1691	343	2017	152	39	47	1000
10	7-4	15:00-21:45	2	LH	4.78	6.7	992	245	1065	94	26	34	875
11	7-5	04:30-06:30	2	ST	5.50	2.1	487	56	417	21	9	11	375
12	7-5	10:00-22:15	2/3	LH/ST	4.62	1.4	219	59	223	10	5	9	Saturated
13	7-7	08:00-12:30	2	ST	3.27	15.2	2526	1325	2732	229	152	127	Saturated
14	7-7	15:30-16:30	2	ST	3.98	21.9	4281	1996	5142	418	191	122	N/A
15	7-8	14:30-05:30	2	ST	4.03	5.9	957	415	1058	83	49	42	Saturated
16	7-10	08:15-11:45	2	ST	3.87	5.3	638	262	889	16	13	37	375
17	7-11	04:15-07:40	2	ST	2.77	25.4	5042	3349	5398	414	197	257	Saturated
18	7-14	18:00-03:00	2	ST	3.85	2.3	684	221	693	38	8	31	375

Note: Vertical motion status is represented as stable (ST), from high elevation to low elevation (HL), or from low elevation to high elevation (LH).

4.1.2. Case studies on the influence of biomass burning on cloudwater composition

Aerosol particles emitted by biomass burning can contribute to high organic carbon contents in cloudwater. They can also potentially modify cloud microphysics, for example reducing cloud droplet size and enhancing cloud reflectance (Kaufman and Fraser, 1997; Andreae et al., 2004). Yamaji et al. (2010) and Suthawaree et al. (2010) observed the impact of agricultural biomass burning on air quality at Mt. Tai in June 2006 during the MTX2006 field campaign. Several cloudwater samples collected in the summer 2007 and 2008 Mt. Tai campaigns have much higher concentrations of TOC than average, indicating possible influence by regional biomass burning emissions. Extensive agricultural burning is common in this region of China in late spring/early summer. The first half of June is the wheat harvest season for North China Plain.

In order to analyze possible impacts of biomass burning on observed cloud composition, fire locations in combination with backward trajectories were used to examine periods of possible fire impact. An open source version of the Web Fire Mapper developed by the Fire Information for Resource Management System (FIRMS) is used to display the Moderate Resolution Imaging Spectroradiometer (MODIS) hotspot/fire locations (Satellite source: Aqua & Terra) during the time period of interest. The cloudwater potassium ion concentration can also be used as an indicator of biomass burning impacts. One cloud event (6/19) in summer 2007 and two cloud events (6/16, 6/18) in summer 2008 that exhibit high potassium ion concentrations with no apparent impact from dust storms are selected as case studies. Cloud cover may obscure active fire detection

(FIRMS Web Fire Mapper, 2010) so that hotspot locations during cloudy days may not be actually reflected in the fire map. Consequently, hotspot locations of dates right before the cloudy days were examined.

Fig. 4-7 shows hotspot locations during 6/11/2007-6/18/2007, before the cloud event of 6/19/2007, which featured a high cloudwater potassium ion concentration of 139 μN.

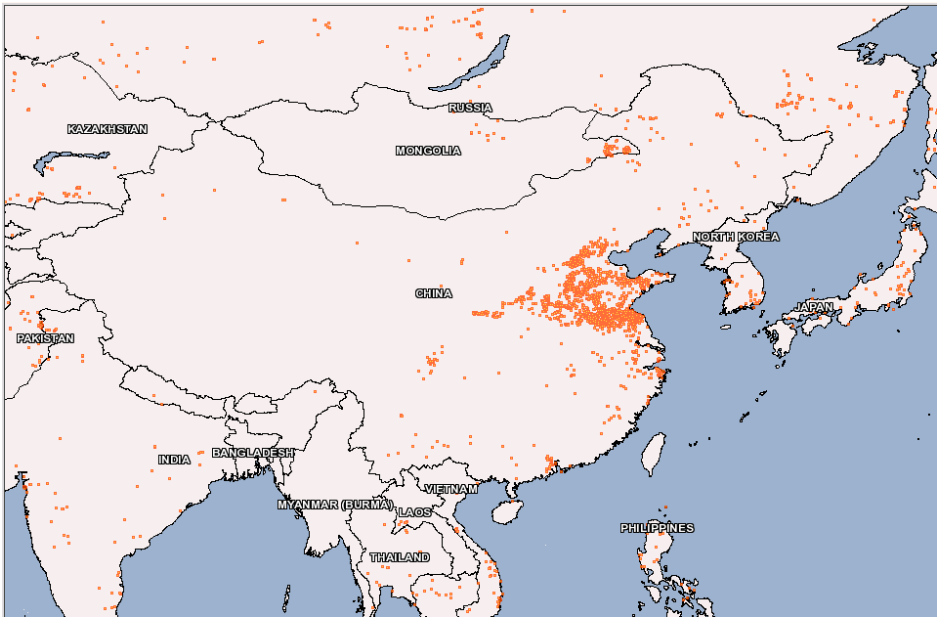

Figure 4-7. Hotspot locations during 6/11/2007-6/18/2007 (Figure from http://firefly.geog.umd.edu/firemap/).

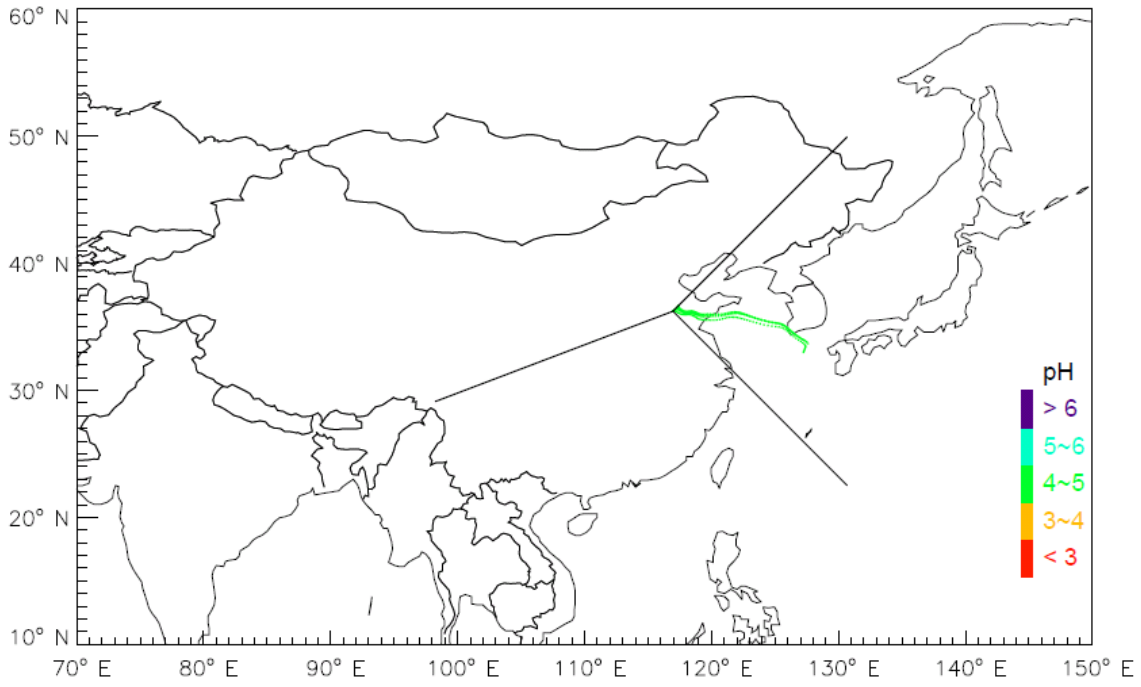

Figure 4-8. Backward trajectories of cloud-forming air parcels for event 6/19/2007.

Fig. 4-8 depicts backward trajectories of cloud-forming air parcels for the 6/19/2007 cloud event. Comparing Fig. 4-8 to Fig 4-7 and considering the high measured potassium concentrations, it appears likely that cloudwater collected on 6/19/2007 was influenced by emissions from biomass burning.

Fig. 4-9 shows hotspot locations during the period 6/12/2008-6/15/2008, before the cloud events on 6/16/2008 and 6/18/2008 which featured high potassium ion concentrations of 296 µN and 248 µN. These two episodes also featured exceptionally high Average TOC concentrations of 22.9 ppmC and 85.6 ppmC, respectively. The highest individual cloud sample TOC concentration during this period was 203 ppmC (6/19/2008 3:00 am - 4:00 am). To our knowledge this is the highest TOC concentration ever measured in cloud or fogwater anywhere in the world, including in fogs formed in urban environments where a

shallow boundary layer traps emissions near the surface. Fig. 4-10 gives back-trajectories of cloud-forming air parcels for the cloud events on 6/16/2008 (sector 1) and 6/18/2008 (sectors 2 and 3).

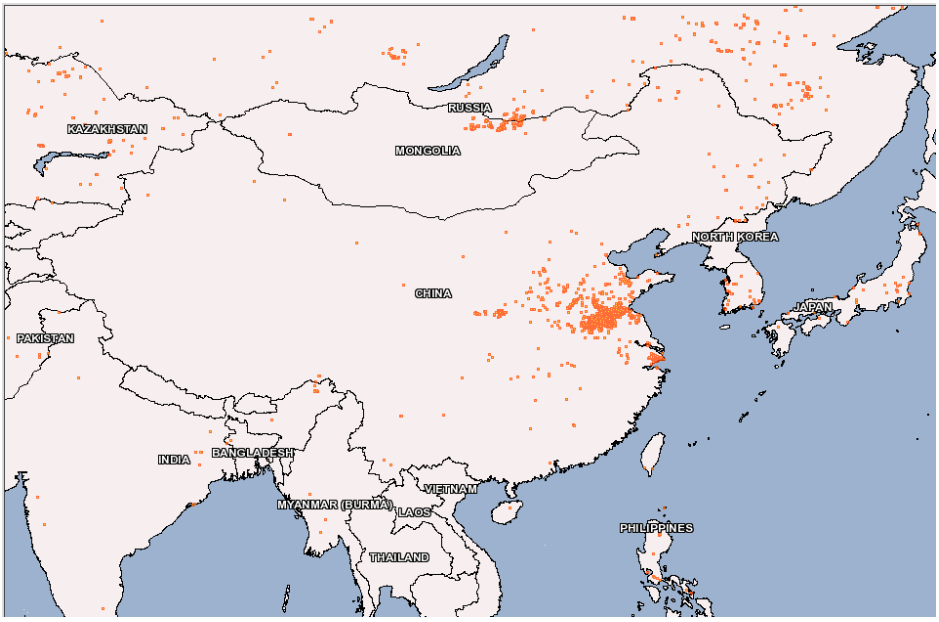

Figure 4-9. Hotspot locations during 6/12/2008-6/15/2008 (Figure from http://firefly.geog.umd.edu/firemap/).

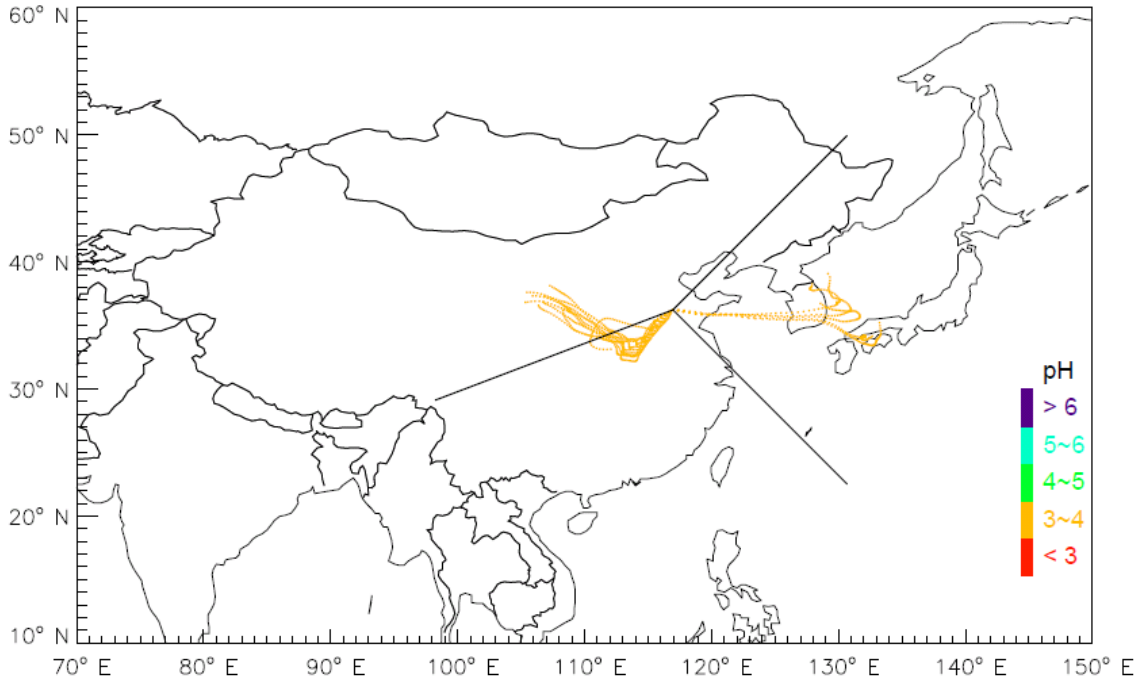

Figure 4-10. Backward trajectories of cloud-forming air parcels for events on 6/16/2008 and 6/18/2008.

The back-trajectories and fire maps suggest likely influence of biomass burning on clouds sampled during this period at Mt. Tai. The high potassium ion and TOC concentrations are confirmation of these impacts. Some cloudwater samples were also atomized and analyzed by aerosol mass spectrometer (AMS) (Yele Sun, personal communication) and it was found that the sample with highest TOC (6/19/2008 3:00 am - 4:00 am) has a large peak at mass fragment 60 ($C_2H_4O_2^+$). This fragment has been identified in the AMS community as a marker for biomass burning emissions (Lee et al., 2010) and can be produced by fragmentation of levoglucosan and other structurally similar molecules. The mass ratio of $C_2H_4O_2^+$/OM (organic matter) could reach 0.7%, much higher than the average ratio observed in cloudwater without substantial influence of biomass burning, usually below 0.2%.

4.2. AEROSOL AND GAS PROCESSING BY CLOUDS

Clouds act as important processors of ambient aerosols and soluble trace gases (Oberholzer et al., 1992; Collett et al., 1993; Oberholzer et al., 1993; Hoag et al., 1999; Collett et al., 2002; Herckes et al., 2002; Herckes et al., 2002; Collett et al., 2008; Hoose et al., 2008). Many experimental and modeling studies (Flossmann et al., 1985; Hoppel et al., 1986; Flossmann et al., 1987; Flossmann and Pruppacher, 1988; Ahr et al., 1989; Alheit et al., 1990; Gillani et al., 1995; Respondek et al., 1995; Henning et al., 2004; Roelofs et al., 2006; Hoose et al., 2008; Ivanova and Leighton, 2008) have examined cloud-aerosol interactions. During the cloud formation process, activated aerosol particles heterogeneously nucleate water vapor and grow to cloud droplets. Additional aerosol particles can be scavenged by other mechanisms, including interception, diffusion, and electrophoresis. Ambient soluble trace gases are taken up by the droplets and various aqueous phase reactions can occur in the cloudwater. Scavenged and newly formed species can be removed through occult or wet deposition processes or be released back to the ambient air as the cloud dissipates.

In order to examine the possible fates of atmospheric pollutants in the vicinity of clouds, it is useful to examine the extent (efficiency) of particle and trace gas scavenging by the clouds. Such observations are relatively rare, although some reports have been made in the literature (Dutkiewicz and Husain, 1998; Hitzenberger et al., 2000; Hitzenberger et al., 2001; Collett et al., 2008). Dutkiewicz and Husain (1998), for example, illustrate a scavenging efficiency for sulfate aerosol by clouds sampled at Whiteface Mtn, NY, that

varies with atmospheric sulfate concentration. Observed values varied between approximately 50% and 90%, with a tendency for decreased efficiencies at higher aerosol sulfate loadings. The sulfate scavenging efficiencies observed at Whiteface Mtn. were generally higher than those reported in Austria by Hitzenberger et al. (2001) for black carbon aerosol particles. Collett et al. (2008) reported a range of scavenging efficiencies for carbonaceous aerosol components in California radiation fogs, with a low efficiency for elemental carbon and high scavenging efficiencies for more polar organic molecules such as levoglucosan. Species of particular interest in the Mt. Tai study include the main nitrogen (ammonia/ammonium and nitric acid/nitrate) and sulfur-containing (sulfur dioxide and sulfate) pollutants.

In the spring and summer 2008 campaigns at Mt. Tai, a University Research Glassware (URG) denuder/filter pack assembly (model URG-3000C) was used to simultaneously collect $PM_{2.5}$ and select trace gases for chemical analysis. The URG denuder/filter pack system was run daily from 8:00 AM to 8:00 AM local time. When cloud was present, sampling was interrupted and interstitial air (containing aerosol particles and gases not scavenged by the cloud droplets) was sampled on a second instrument channel that pulled air from behind the collection strands of the cloudwater collector. Regular aerosol + gas sampling was resumed after cloud interception ceased.

4.2.1. Before / after cloud

The ambient sulfur and nitrogen compositions before cloud can be specified as follows. Sulfur includes gaseous sulfur dioxide, $SO_2(g)$, and sulfate in aerosol particles, $SO_4^{2-}(p)$. N(-III) includes gaseous ammonia, $NH_3(g)$, and ammonium in aerosol particles, $NH_4^+(p)$. N(V) includes gaseous nitric acid, $HNO_3(g)$, and nitrate in aerosol particles $NO_3^-(p)$. The ambient sulfur and nitrogen compositions after cloud can be specified the same way as before cloud.

4.2.2. During cloud

The ambient sulfur and nitrogen compositions during cloud can be specified as follows. Sulfur includes interstitial (between droplet) gaseous sulfur dioxide, $SO_2(ig)$, sulfate in interstitial aerosol particles, $SO_4^{2-}(ip)$, SO_2 in cloudwater, $SO_2(c)$, and sulfate in cloudwater, $SO_4^{2-}(c)$. N(-III) includes gaseous ammonia, $NH_3(ig)$, ammonium in interstitial aerosol particles, $NH_4^+(ip)$, and ammonium in cloudwater, $NH_4^+(c)$. N(V) includes gaseous nitric acid, $HNO_3(ig)$, nitrate in interstitial aerosol particles, $NO_3^-(ip)$, and nitrate in cloudwater, $NO_3^-(c)$.

4.2.3. Aerosol scavenging efficiency

All the species extracted from denuders and filters and measured in aqueous concentration units (μN) are converted to ambient concentration units ($\mu g/m^3$) based on measured air sample volumes (m^3) measured by a dry gas meter. All the species in cloudwater measured in aqueous concentration units (μN) are converted to ambient

loading units ($\mu g/m^3$) using the measured cloud LWC (mg/m^3). Appropriate additional unit conversion factors are included in each case.

Aerosol scavenging efficiency was initially calculated by comparing the pre-cloud and interstitial concentrations of a species using the following equation edited from previous work (Collett et al., 2008):

$$\eta_1 = 1 - \frac{X_{ip}}{{}_{beforecloud}X_p} \qquad \text{Equation 4-2}$$

Where η_1 is the scavenging efficiency of species X, X_{ip} is the ambient loading ($\mu g/m^3$) of species X existing in interstitial aerosol particles during cloud. ${}_{beforecloud}X_p$ is the ambient loading ($\mu g/m^3$) of species X existing in aerosol particles before cloud. The advantage of this approach is that it allows us to directly compare aerosol species' concentrations. The main limitation is that temporal changes in atmospheric composition between the pre-cloud and interstitial samples can confound the analysis.

An alternative way to calculate species scavenging efficiency, while avoiding the problems of temporal composition changes, is to examine species partitioning between simultaneously measured cloudwater and interstitial air phases:

$$\eta_2 = \frac{X_c}{X_{ig} + X_{ip} + X_c} \qquad \text{Equation 4-3}$$

Where η_2 is the scavenging efficiency of species X, X_c is the ambient loading ($\mu g/m^3$) of species X existing in the cloudwater droplets, X_{ig} is the ambient loading ($\mu g/m^3$) of

species X existing in gaseous phase during cloud, X_{ip} is the ambient loading ($\mu g/m^3$) of species X existing in interstitial aerosol particles during cloud. One drawback to this approach is that we can no longer directly examine aerosol or gas scavenging efficiency for those compounds where gas and particle phase counterparts yield the same species in the cloudwater. This is the case for ammonia/ammonium (both yield ammonium in the cloud sample) and for nitric acid/nitrate (both yield nitrate in cloudwater). Sulfur dioxide and sulfate can also both yield cloudwater sulfate if sufficient oxidants are available to drive aqueous phase oxidation of sulfur dioxide to sulfate (the topic of the next chapter). In these cases, however, we can still look at the overall scavenging efficiency of N(-III), N(V) and sulfur.

Table 4-5, 4-6 and 4-7 give summaries of the sulfur, N(-III), N(V) concentrations before cloud, during cloud and after cloud for several selected events during the 2008 campaigns; scavenging efficiencies of different species are also determined. The events selected for this analysis feature relatively long duration and fewer disturbances (high wind and/or rain). Figures 4-11 to 4-13 illustrate the amounts of the various species found in the various phases, before, during, and after cloud interception.

Table 4-5. Summary of the sulfur concentrations before cloud, during cloud and after cloud during select 2008 campaign events selected for scavenging analysis. Concentrations are shown in units of μgS/m^3. Scavenging efficiencies of sulfate and total sulfur are calculated.

Items	Events →	04/08	06/16A	06/16B	06/18	06/19	07/03	07/14
SO_2	Before Cloud SO_2(g)	5.79	15.92	1.31	14.36	8.79	4.71	1.92
	During Cloud SO_2(ig)	3.51	12.61	7.11	11.64	7.12	0.96	1.99
	After Cloud SO_2(g)	1.48	1.31	11.95	8.79	1.44	2.08	1.06
SO_4^{2-}	Before Cloud SO_4^{2-}(p)	1.91	4.40	1.65	14.98	7.85	6.57	11.13
	During Cloud SO_4^{2-}(ip)	0.20	1.02	0.36	2.37	2.31	2.24	0.86
	In cloudwater SO_4^{2-}(c)	1.63	2.89	3.00	12.11	5.82	5.73	7.80
	After Cloud SO_4^{2-}(p)	1.21	1.65	5.02	7.85	8.24	1.45	3.95
Sulfur	Before Cloud S(g)+S(p)	7.70	20.32	2.97	29.34	16.64	11.28	13.05
	During Cloud S(ig)+S(ip)	3.71	13.64	7.48	14.01	9.43	3.21	2.86
	In cloudwater S(c)	1.63	2.89	3.00	12.11	5.82	5.73	7.80
	After Cloud S(g)+S(p)	2.69	2.97	16.97	16.64	9.67	3.53	5.01
Ratio	SO_4^{2-}(c)/(SO_4^{2-}(ip)+SO_4^{2-}(c))	0.89	0.74	0.89	0.84	0.72	0.72	0.90
η_1	1-SO_4^{2-}(ip)/beforecloud SO_4^{2-}(p)	0.90	0.77	0.78	0.84	0.71	0.66	0.92
η_2	S(c)/(S(ig)+S(ip)+S(c))	0.31	0.17	0.29	0.46	0.38	0.64	0.73

Table 4-6. Summary of the N(-III) concentrations before cloud, during cloud and after cloud during select 2008 campaign events selected for scavenging analysis. Concentrations are shown in units of μgN/m^3. Scavenging efficiencies of ammonium and total N(-III) are calculated.

Items	Events →	04/08	06/16A	06/16B	06/18	06/19	07/03	07/14
NH_3	Before Cloud NH_3(g)	1.77	2.80	1.77	1.71	2.36	13.70	1.77
	During Cloud NH_3(ig)	1.20	1.95	0.35	0.58	0.48	4.65	1.09
	After Cloud NH_3(g)	0.71	1.77	1.27	2.36	2.72	6.09	1.03
NH_4^+	Before Cloud NH_4^+(p)	1.93	6.27	2.07	14.57	8.22	6.60	9.85
	During Cloud NH_4^+(ip)	0.26	2.21	0.40	3.50	1.96	2.14	0.57
	In cloudwater NH_4^+(c)	1.21	3.50	1.99	12.49	6.74	5.86	6.91
	After Cloud NH_4^+(p)	1.57	2.07	3.15	8.22	6.19	2.74	2.47
N(-III)	Before Cloud N(-III)(g)+N(-III)(p)	3.69	9.07	3.84	16.28	10.58	20.30	11.62
	During Cloud N(-III)(ig)+N(-III)(ip)	1.46	4.16	0.75	4.09	2.44	6.78	1.65
	In cloudwater N(-III)(c)	1.21	3.50	1.99	12.49	6.74	5.86	6.91
	After Cloud N(-III)(g)+N(-III)(p)	2.28	3.84	4.42	10.58	8.91	8.83	3.51
Ratio	NH_4^+(c)/(NH_4^+(ip)+NH_4^+(c))	0.82	0.61	0.83	0.78	0.77	0.73	0.92
η_1	1-NH_4^+(ip)/beforecloud NH_4^+(p)	0.87	0.65	0.80	0.76	0.76	0.68	0.94
η_2	N(-III)(c)/(N(-III)(ig)+N(-III)(ip)+N(-III)(c))	0.45	0.46	0.73	0.75	0.73	0.46	0.81

Table 4-7. Summary of the N(V) concentrations before cloud, during cloud and after cloud during select 2008 campaign events selected for scavenging analysis. Concentrations are shown in units of μgN/m^3. Scavenging efficiencies of nitrate and total N(V) are calculated.

Items	Events →	04/08	06/16A	06/16B	06/18	06/19	07/03	07/14
HNO_3	Before Cloud HNO_3(g)	0.14	0.18	0.17	0.39	0.23	0.26	0.66
	During Cloud HNO_3(ig)	0.08	0.24	0.12	0.43	0.30	0.17	0.12
	After Cloud HNO_3(g)	0.12	0.17	0.25	0.23	0.27	0.41	0.25
NO_3^-	Before Cloud NO_3^-(p)	0.42	1.34	0.42	2.68	1.99	1.16	1.00
	During Cloud NO_3^-(ip)	0.06	0.67	0.08	1.02	0.59	0.27	0.05
	In cloudwater NO_3^-(c)	0.33	1.79	1.12	6.52	2.96	1.01	2.15
	After Cloud NO_3^-(p)	0.31	0.42	0.60	1.99	0.90	0.26	0.08
N(V)	Before Cloud N(V)(g)+N(V)(p)	0.56	1.52	0.59	3.08	2.23	1.42	1.67
	During Cloud N(V)(ig)+N(V)(ip)	0.13	0.90	0.19	1.45	0.89	0.43	0.17
	In cloudwater N(V)(c)	0.33	1.79	1.12	6.52	2.96	1.01	2.15
	After Cloud N(V)(g)+N(V)(p)	0.44	0.59	0.85	2.23	1.17	0.67	0.32
Ratio	NO_3^-(c)/(NO_3^-(ip)+NO_3^-(c))	0.86	0.73	0.94	0.86	0.83	0.79	0.98
η_1	1-NO_3^-(ip)/beforecloud NO_3^-(p)	0.87	0.50	0.81	0.62	0.70	0.77	0.95
η_2	N(V)(c)/(N(V)(ig)+N(V)(ip)+N(V)(c))	0.71	0.67	0.85	0.82	0.77	0.70	0.93

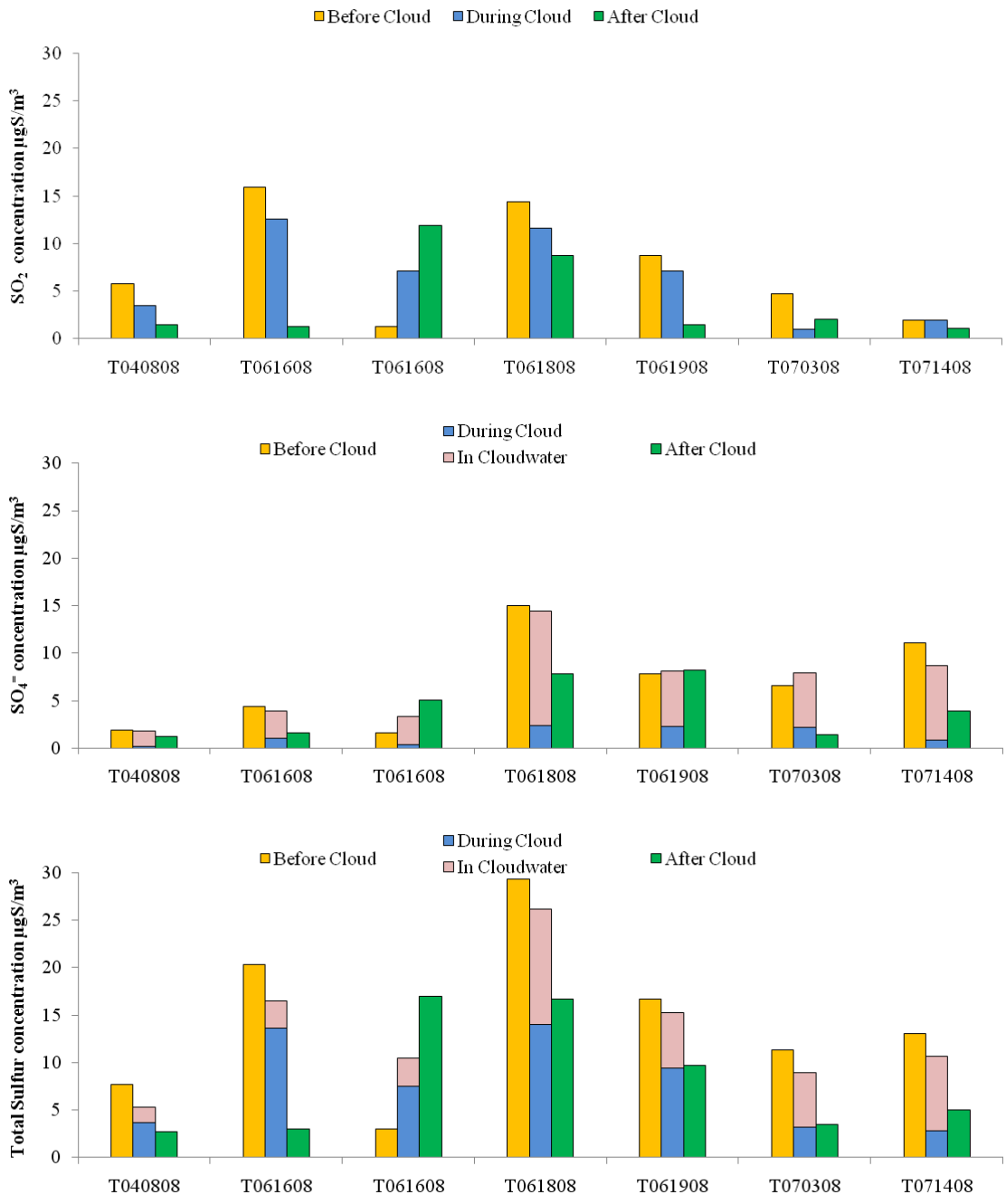

Figure 4-11. SO_2(g), SO_4^{2-}, and total sulfur concentrations before cloud, during cloud and after cloud during select 2008 campaign events.

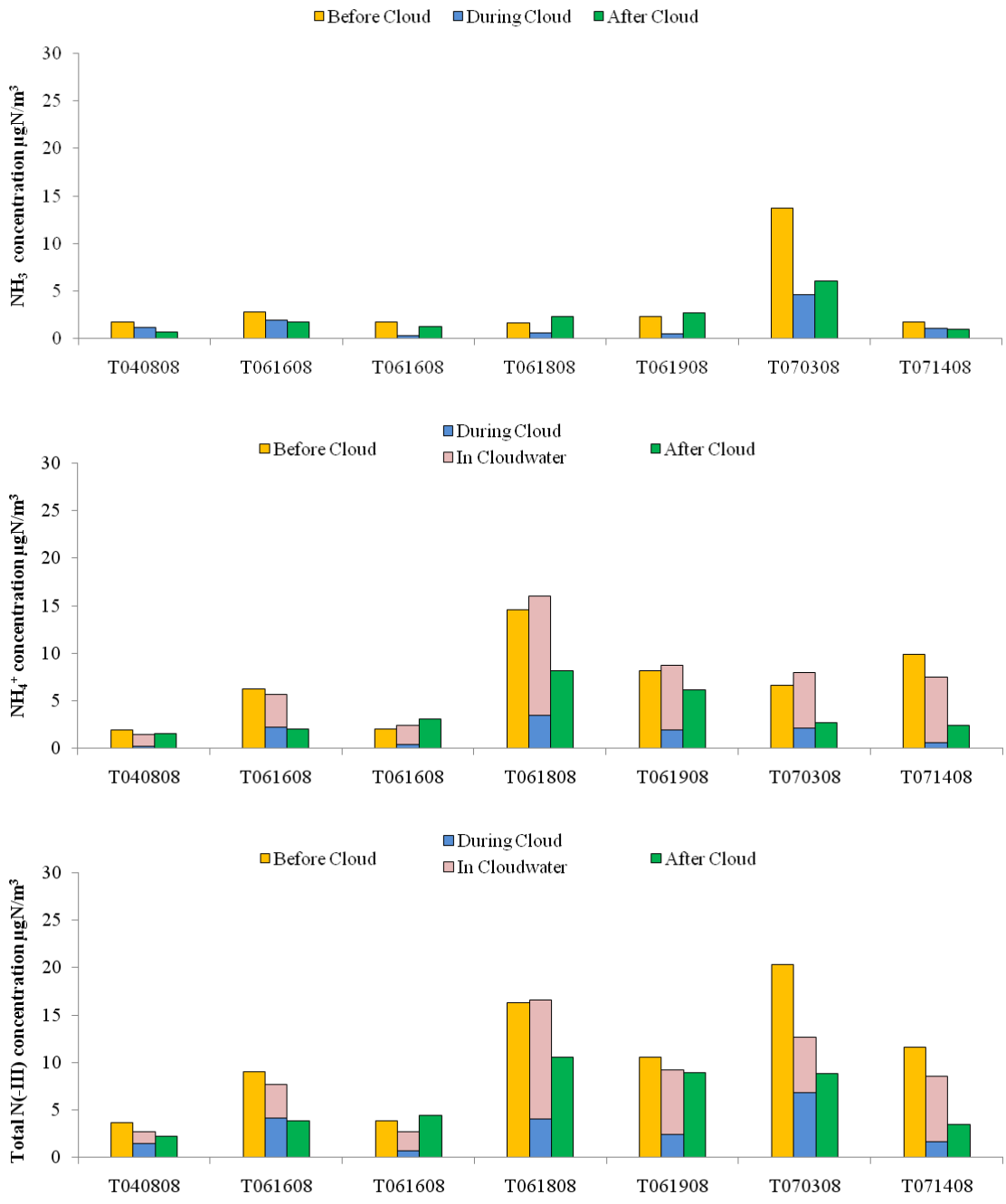

Figure 4-12. $NH_3(g)$, NH_4^+, and total N(-III) concentrations before cloud, during cloud and after cloud during select 2008 campaign events.

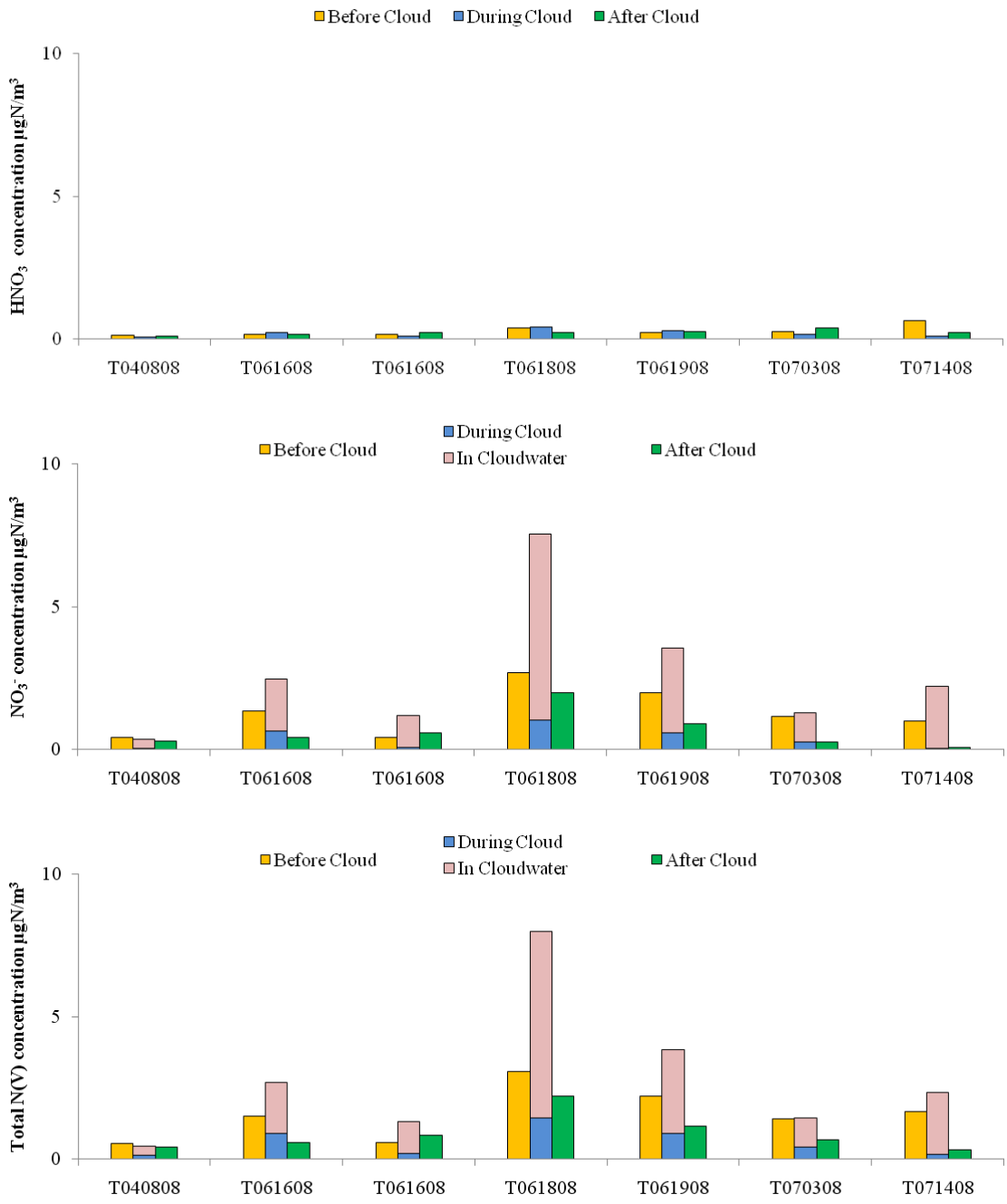

Figure 4-13. $HNO_3(g)$, NO_3^-, and total N(V) concentrations before cloud, during cloud and after cloud during select 2008 campaign events.

As given in Table 4-5 and shown in Fig. 4-11, computed scavenging efficiencies for sulfate aerosol by method 1, η_1, were fairly high, with values ranging from 66% to 92%. This is similar to the range of sulfate scavenging efficiencies reported by Dutkiewicz and Husain (1998) for intercepted clouds at Whiteface Mtn, NY. Scavenging efficiencies of total sulfur (η_2=S(c)/(S(ig)+S(ip)+S(c))) showed a much broader range, from 17% to 73%, reflecting appreciable sulfur dioxide gas that remained unscavenged during some of the events.

Studied Mt. Tai clouds also exhibited efficient scavenging of aerosol ammonium (see Table 4-6 and Fig. 4-12). Scavenging efficiencies, η_1, for ammonium particles ranged from 65% to 94%. These values are very similar to those determined for aerosol sulfate, likely reflecting the close association of ammonium and sulfate in regional aerosol particles. Scavenging efficiencies of total N(-III) (η_2=N(-III)(c)/(N(-III)(ig)+N(-III)(ip)+N(-III)(c))) ranged from 45% to 81%. These values are considerably higher than observed for sulfur, reflecting the higher solubility of gaseous ammonia vs. sulfur dioxide. As illustrated in Table 4-7 and Fig. 4-13, scavenging efficiencies, η_1, for aerosol nitrate ranged from 50% to 95%. Scavenging efficiencies of total N(V) (η_2=N(V)(c)/(N(V)(ig)+N(V)(ip)+N(V)(c))) were comparable or higher, ranging from 67% to 93%, consistent with the very high solubility of gaseous nitric acid.

Scavenging efficiencies for different species are compared, by event, in Fig. 4-14. Here we see some tendency for scavenging efficiencies of all three aerosol species to move up and down together. We also see that that scavenging efficiency for aerosol ammonium

tends to usually fall between the scavenging efficiencies for aerosol nitrate and aerosol sulfate. This pattern is expected because both aerosol nitrate and sulfate are typically found as ammonium salts in $PM_{2.5}$ aerosol in polluted environments where excess ammonia resides in the gas phase as observed at Mt. Tai (Fig. 4-12). Fig. 4-14 also illustrates the general tendency for scavenging of N(V) to be more efficient than N(-III) scavenging which is typically more efficient than scavenging of S. As discussed above, this trend follows expectations based on the solubility of the gas phase species. At the pH values observed in Mt. Tai clouds, the following solubility trend is expected: nitric acid > ammonia > sulfur dioxide.

Table 4-8 presents average scavenging efficiencies observed for each species across the seven studies events. Aerosol scavenging efficiencies for sulfate, ammonium, and nitrate were all quite similar, with average values of 80%, 78%, and 75%, respectively. The average N(V) scavenging efficiency was 78%, while average scavenging efficiencies for N(-III) and S were 63% and 43%, respectively. These observations suggest that while most of the N(V) and nearly two-thirds of the N(-III) undergoes cloud processing in a given cloud event, more than half of the sulfur remains unprocessed.

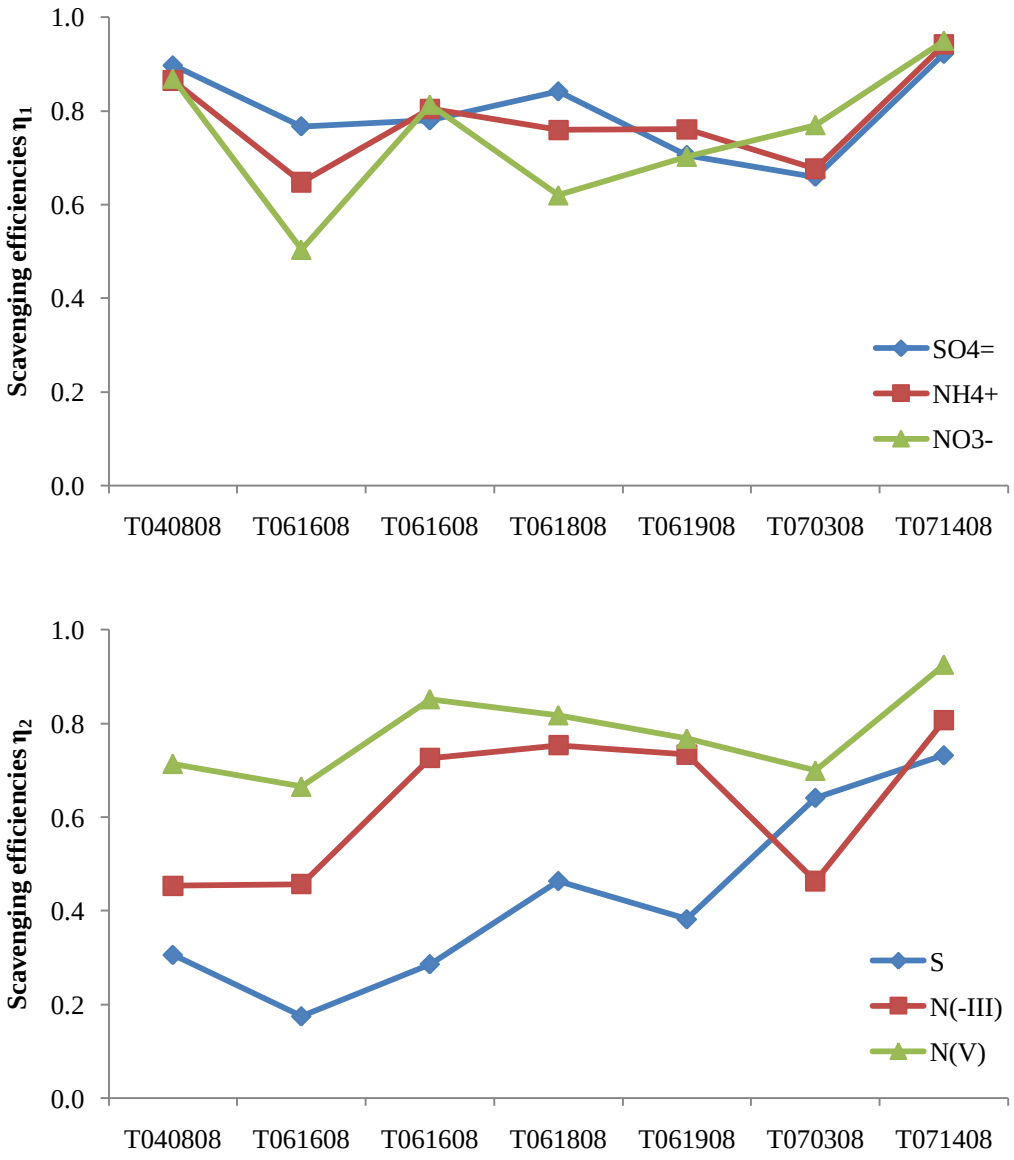

Figure 4-14. Scavenging efficiencies for different species by event.

	SO_4^{2-}	NH_4^+	NO_3^-
$\bar{\eta}_1 \pm \sigma$	0.80 ±0.10	0.78 ±0.10	0.75 ±0.15
	S	N(-III)	N(V)
$\bar{\eta}_2 \pm \sigma$	0.43 ±0.20	0.63 ±0.16	0.78 ±0.09

Table 4-8. Summary of scavenging efficiencies for different species.

CHAPTER 5 AQUEOUS PHASE SULFATE PRODUCTION

(in preparation for submission to *Atmospheric Environment*)

Utilizing the cloudwater and gas phase measurements described in previous chapters, we can compute rates of aqueous phase S(IV) oxidation by H_2O_2, by O_3, and by O_2 with trace metal (Fe(III) and Mn(II)) catalysis. Literature rate expressions (Hoffmann and Calvert, 1985; Hoffmann, 1986; Ibusuki and Takeuchi, 1987; Seinfeld and Pandis, 2006) used for these calculations are listed in Table 5-1. In completing the rate calculations, aqueous H_2O_2 and O_3 concentrations were determined assuming Henry's Law equilibrium with the measured gas phase concentrations during the period the cloud sample was collected. The measured aqueous cloudwater H_2O_2 concentration was not considered appropriate to use in these calculations because it can be rapidly consumed by reaction with S(IV) during the time (ranging from a few minutes up to 1-2 hr) between cloud drop impaction on the collector strands and retrieval and chemical stabilization of the cloud sample. The H_2O_2 concentration was assumed to be 0.1 ppbv during periods in spring 2008 when valid gas phase H_2O_2 concentrations were not available. Concentrations of H_2SO_3, HSO_3^-, and SO_3^{2-} in solution were determined from measured gaseous SO_2 concentrations and measured cloudwater pH, assuming Henry's Law and acid base equilibria. The H^+ concentration was taken from the measured cloud sample pH. Metal catalyst concentrations were taken from measured cloud sample Fe and Mn concentrations. Following the approach of Rao and Collett (1995), the Mn was assumed

to be completely present as catalytically active Mn(II) and 25% of the Fe was assumed to be present as catalytically active Fe(III). Henry's law coefficient is a function of temperature, the actual temperature at the top of Mt. Tai is used in the Henry's law coefficient calculation.

Oxidation rates calculated for each bulk cloudwater sample for each of these three oxidation pathways are depicted in Fig. 5-1. Among the three S(IV) oxidation pathways, oxidation by H_2O_2 was generally found to be the fastest pathway for pH values less than approximately 5. The importance of O_3 as an oxidant increased strongly as pH values climbed above 5 to 5.3. These general tendencies are known behaviors of these oxidation pathways, although the pH where the transition occurs depends on local conditions, including the relative abundance of H_2O_2 and O_3. Fig. 5-2 shows the total S(IV) oxidation rate for the 2007 and 2008 campaigns. At low pH the total rate is similar to the hydrogen peroxide pathway; at high pH we see the increasing rate (vs. pH) associated with the ozone pathway.

Table 5-1. Rate expressions used for S(IV) oxidation and S(IV) reaction with HCHO.

Reaction Rate (M/s)	**Characteristic Time (s)**		
$-\frac{d[\mathrm{S(IV)}]}{dt} = (k_0\alpha_0 + k_1\alpha_1 + k_2\alpha_2)[\mathrm{S(IV)}][\mathrm{O_3}]$	$\tau_{\mathrm{O_3}} = 1/((k_0\alpha_0 + k_1\alpha_1 + k_2\alpha_2)[\mathrm{O_3}])$		(Hoffmann and Calvert, 1985)
$-\frac{d[\mathrm{S(IV)}]}{dt} = \frac{k[\mathrm{H^+}][\mathrm{H_2O_2}][\mathrm{S(IV)}]\alpha_1}{1+K[\mathrm{H^+}]}$	$\tau_{\mathrm{H_2O_2}} = (1+K[\mathrm{H^+}])/(k[\mathrm{H^+}][\mathrm{H_2O_2}]\alpha_1)$		(Seinfeld and Pandis, 2006)
$-\frac{d[\mathrm{S(IV)}]}{dt} = k_s^{'}[\mathrm{H^+}]^{-0.74}[\mathrm{Fe(III)}]\cdot[\mathrm{Mn(II)}]\cdot[\mathrm{S(IV)}]$	$\tau^{'}_{\mathrm{O_2(Mn(II)/Fe(III))}} = 1/(k_s^{'}[\mathrm{H^+}]^{-0.74}[\mathrm{Fe(III)}]\cdot[\mathrm{Mn(II)}])$	$(\mathrm{pH} \le 4.2)$	(Ibusuki and Takeuchi, 1987)
$-\frac{d[\mathrm{S(IV)}]}{dt} = k_s^{''}[\mathrm{H^+}]^{0.67}[\mathrm{Fe(III)}]\cdot[\mathrm{Mn(II)}]\cdot[\mathrm{S(IV)}]$	$\tau^{''}_{\mathrm{O_2(Mn(II)/Fe(III))}} = 1/(k_s^{''}[\mathrm{H^+}]^{0.67}[\mathrm{Fe(III)}]\cdot[\mathrm{Mn(II)}])$	$(6.5 \ge \mathrm{pH} \ge 4.2)$	(Ibusuki and Takeuchi, 1987)
$-\frac{d[\mathrm{S(IV)}]}{dt} = k_4[\mathrm{S(IV)}]\alpha_1[\mathrm{HCHO}] + k_5[\mathrm{S(IV)}]\alpha_2[\mathrm{HCHO}]$	$\tau_{\mathrm{HCHO}} = 1/([\mathrm{HCHO}]\cdot(k_4\alpha_1 + k_5\alpha_2))$		(Boyce and Hoffmann, 1984)

α_0, α_1, and α_2 represent the fractions of total free S(IV) present as $SO_2 \cdot H_2O$, HSO_3^- and SO_3^{2-} respectively. $k_0 = 2.4\times10^4\,\mathrm{M^{-1}s^{-1}}$, $k_1 = 3.7\times10^5\,\mathrm{M^{-1}s^{-1}}$, $k_2 = 1.5\times10^9\,\mathrm{M^{-1}s^{-1}}$, $k = 7.45\times10^7\,\mathrm{M^{-2}s^{-1}}$, $K = 13\,\mathrm{M^{-1}}$, $k_s^{'} = 3.72\times10^7\,M^{-2}S^{-1}$, $k_s^{''} = 2.51\times10^{13}\,M^{-2}S^{-1}$, $k_4 = 7.9\times10^2\,\mathrm{M^{-1}s^{-1}}$ and $k_5 = 2.48\times10^7\,\mathrm{M^{-1}s^{-1}}$ at 298K, k_s' and k_s" were determined at 296.8K.. Equilibrium and rate constants were adjusted for ambient temperature using the thermodynamic data from Table 1-2 and 1-3.

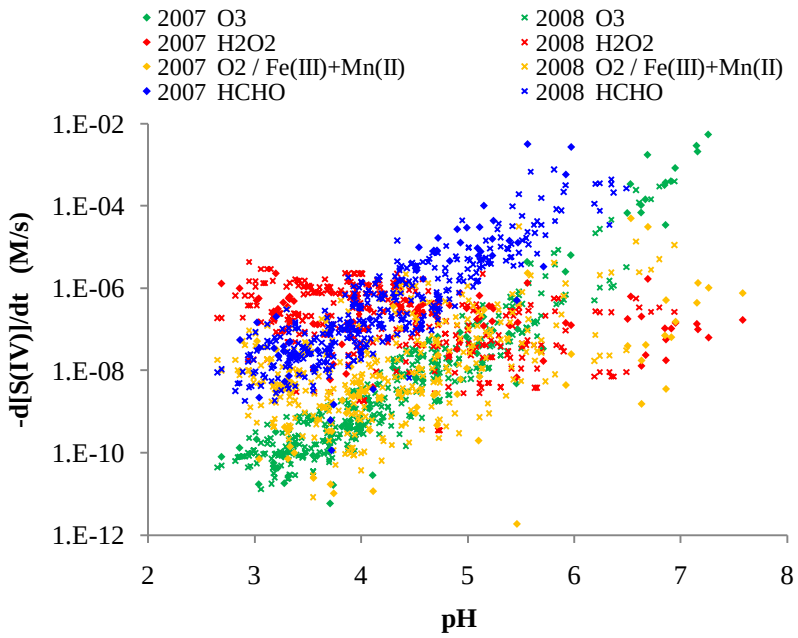

Figure 5-1. S(IV) reaction rates determined for individual cloudwater samples according to the approach outlined in the text. Rates of reaction are included for S(IV) oxidation by O_3, by H_2O_2, and by O_2 (catalyzed by Fe and Mn) and for S(IV) reaction with HCHO to form HMS.

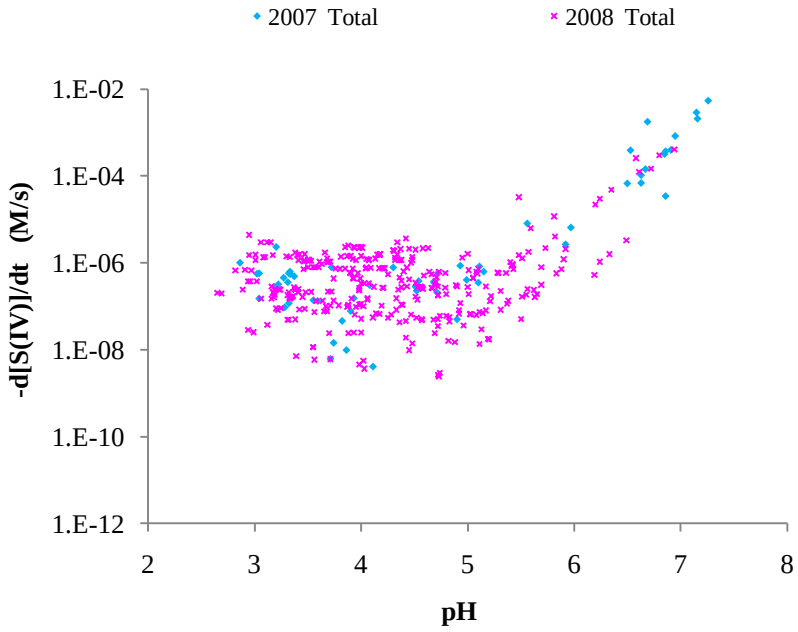

Figure 5-2. Total S(IV) oxidation rate.

As depicted in Fig. 5-3, variations in the rate of S(IV) oxidation by ozone show little overall dependence on the ozone concentration. This is because the influence of cloudwater pH is much stronger. At higher pH, partitioning of the H_2SO_3-HSO_3^--SO_3^{2-} shifts toward the deprotonated S(IV) forms; this increases the SO_2 oxidation rate because more SO_2 is drawn into solution and the S(IV) speciation shifts toward more reactive forms (SO_3^{2-}>HSO_3^->H_2SO_3).

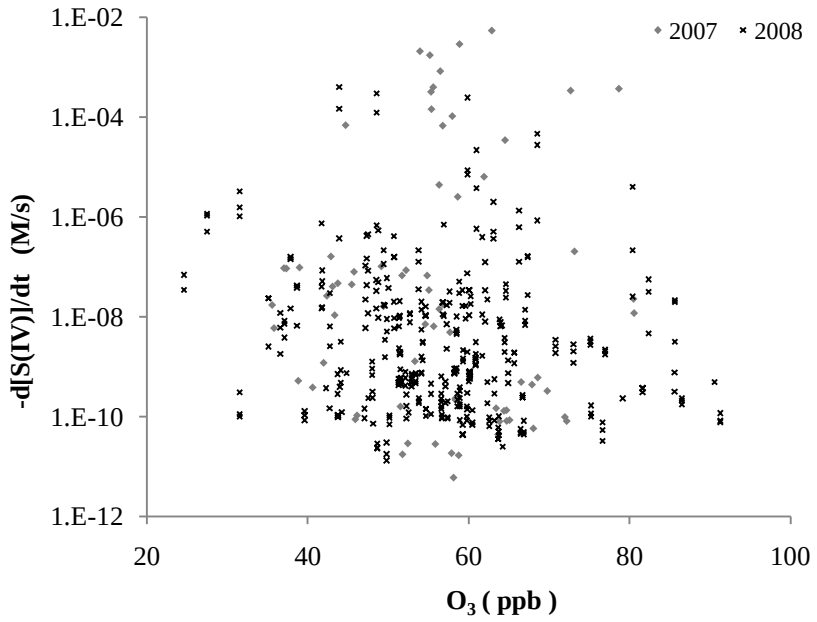

Figure 5-3. Rates of S(IV) oxidation by O_3, determined for the Mt. Tai cloud samples, plotted as a function of the ambient O_3 mixing ratio.

Computed metal-catalyzed S(IV) autooxidation rates, also shown in Fig. 5-1, are highly variable, reflecting high variability in cloudwater trace metal concentrations and the nonlinear dependence of the Ibusuki and Takeuchi (1987) rate expression on these concentrations. In general, the rate of this oxidation pathway is typically 2nd or 3rd fastest of the three computed oxidation pathways across the full observed pH range. There are a

few samples, however, where the metal-catalyzed pathway appears fast enough to make some contribution to aqueous sulfate production.

The overall oxidation rate patterns depicted in Fig. 5-2 and described above are fairly similar for the 2007 and 2008 cloud samples, suggesting that these patterns are fairly robust under a variety of emission, cloud formation, and transport patterns during the period. Note that the 2008 summer campaign period concluded before the start of the 2008 Beijing Olympics when more stringent regional emissions reductions came online. Grouping all 4 measurement periods together, we find that in 68% of the sample periods the fastest S(IV) oxidation pathway is the hydrogen peroxide pathway. The ozone pathway is fastest 21% of the time and the metal-catalyzed pathway is fastest 11% of the time. Fig. 5-4 shows the fraction of time that each oxidation pathway was fastest for the four campaigns. Given the abundant SO_2 often found in the regional atmosphere, it was somewhat surprising to see that H_2O_2 was the dominant oxidant so much of the time. In addition to the gas phase H_2O_2 observations used for the oxidation rate calculations, we can also examine the presence of H_2O_2 in the collected cloudwater. While there are many samples where H_2O_2 was low (or was depleted by reaction prior to sample retrieval and derivatization), there are also many samples, especially from the summertime, where tens to hundreds of μM of H_2O_2 remain in the cloudwater and little S(IV) remained. This residual peroxide indicates a substantial capacity during these periods for additional in-cloud sulfate production.

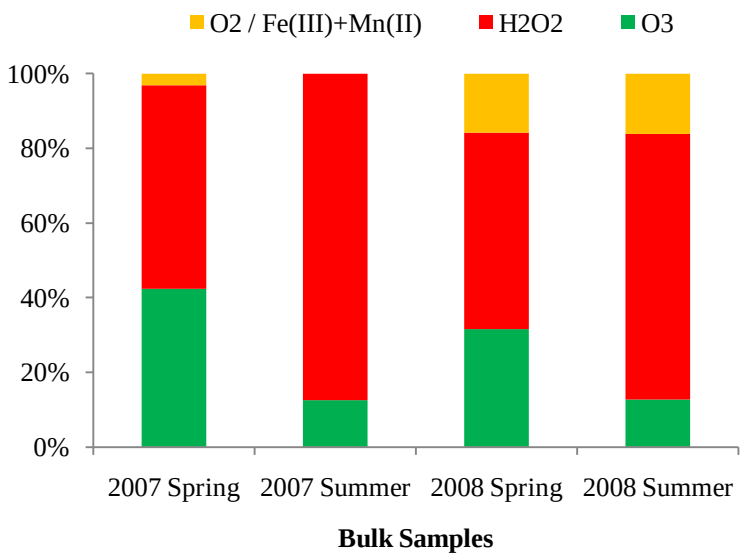

Figure 5-4. the fraction of time that each oxidation pathway was fastest for the four campaigns.

Fig. 5-1 also depicts rates of HMS formation due to reaction of dissolved S(IV) with HCHO. These rates were computed using the expression by Boyce and Hoffmann (Boyce and Hoffmann, 1984). Aqueous S(IV) concentrations and speciation were determined as outlined above for the oxidation rate concentrations. HCHO concentrations were taken from the measured HCHO concentrations in the individual cloud samples. Because these HCHO values may include some HMS already present in the cloudwater (HCHO is preserved as HMS following sample collection), these rates should be considered an upper limit to the actual HMS formation rate in Mt. Tai clouds. While HMS formation does not appear important at low pH values, the calculations suggest that it may provide an additional, important sink for dissolved SO_2 when cloud pH climbs much above 4. Future cloud composition studies in the region should include measurement of HMS to determine whether its formation is as important as suggested by the rate calculations here.

Given the fast aqueous reaction between hydrogen peroxide and S(IV), one typically expects to find only one of the two species (the one originally present in excess) remaining by the time the sample is collected and preserved. As shown in Fig. 5-5, the collected and preserved samples were typically depleted in either S(IV) or in H_2O_2. Interestingly, several samples contain both residual H_2O_2 and residual S(IV). This could reflect either the presence of S(IV) in a nonreactive form (e.g., complexed with HCHO as HMS) or continued aqueous photochemical production of H_2O_2 up until the point of sample collection and preservation.

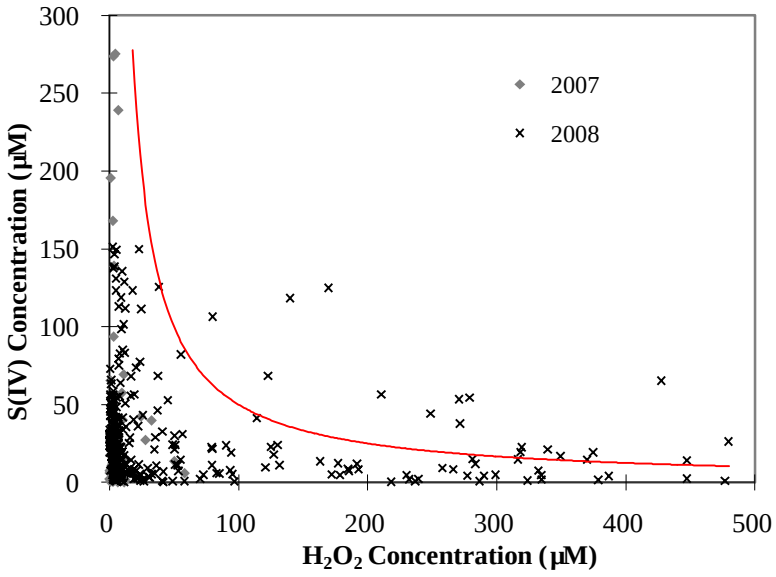

Figure 5-5. Aqueous hydrogen peroxide concentration vs. S(IV) concentration in bulk cloudwater samples collected at Mt. Tai in 2007 and 2008.

Table 5-2. Data table for samples containing both residual H_2O_2 and residual S(IV)

	pH	H_2O_2 (μM)	S(IV) (μM)	HCHO (μM)	Reaction rate (M/s)				Most important reaction way
					O_3	H_2O_2	O_2(Fe(III)/Mn(II))	HCHO	
TC070308A01	5.42	169.6	124.9	14.5	7.4E-08	1.2E-07	7.3E-07	3.2E-05	HCHO
TC070308A02	5.31	55.4	82.2	13.1	3.7E-08	3.9E-08	1.5E-07	1.7E-05	HCHO
TC070308A03	5.38	79.8	106.5	4.9	4.9E-08	2.9E-08	5.6E-08	8.8E-06	HCHO
TC070308A04	5.51	122.8	68.4	4.8	8.3E-08	3.7E-08	4.6E-08	1.5E-05	HCHO
TC070308A05	5.62	279.0	54.5	6.3	1.5E-07	4.1E-08	4.2E-08	3.4E-05	HCHO
TC070308A06	5.55	271.4	37.9	4.1	1.1E-07	4.2E-08	2.8E-08	1.7E-05	HCHO
TC070308A07	5.22	479.3	26.3	4.8	2.2E-08	5.4E-08	9.5E-08	3.9E-06	HCHO
TC070408A09	6.35	114.1	41.3	4.8	1.1E-06	7.1E-09	N/A[1]	3.4E-04	HCHO
TC070808A01	4.42	427.3	65.3	20.3	1.5E-10	1.6E-08	2.9E-09	1.2E-07	HCHO
TC070808A03	3.91	270.8	53.5	16.4	2.3E-10	1.5E-07	8.7E-10	1.1E-07	H_2O_2
TC070808A05	3.95	248.6	44.1	18.4	2.2E-10	9.7E-08	9.1E-10	9.6E-08	H_2O_2
TL070308A01	5.92	139.8	118.5	14.5	6.9E-07	9.3E-08	1.3E-06	3.2E-04	HCHO
TL070808A01	4.57	210.5	56.4	22.8	7.1E-10	3.9E-08	1.1E-08	6.3E-07	HCHO

N/A[1]: Fe(III) and Mn(II) data not available.

Table 5-2 gives a list of samples for which both S(IV) and H_2O_2 concentrations are relatively high. These samples mainly came from two cloud events, 7/3/2008 and 7/8/2008. For most of these samples, calculations suggest that complexation with HCHO to form HMS is the most important S(IV) reaction sink. This result HMS formation may be more important in these samples than S(IV) oxidation and could help explain the coexistence of S(IV) (which includes HMS) and H_2O_2 in the preserved cloudwater samples.

A comparison between oxidation rates computed for small and large cloud drop size fractions collected in 2008 with the sf-CASCC is shown in Figure 5-6. There is a tendency for oxidation rates to be higher in the large drops. This comes from the strong dependence of two of the pathways on cloud pH (faster oxidation at higher pH) and the tendency (see Fig. 3-34) for the pH to be higher in the large cloud drop size fraction. In the case of the metal-catalyzed pathway, there is an additional effect from any drop size-dependence in the Fe and Mn concentrations.

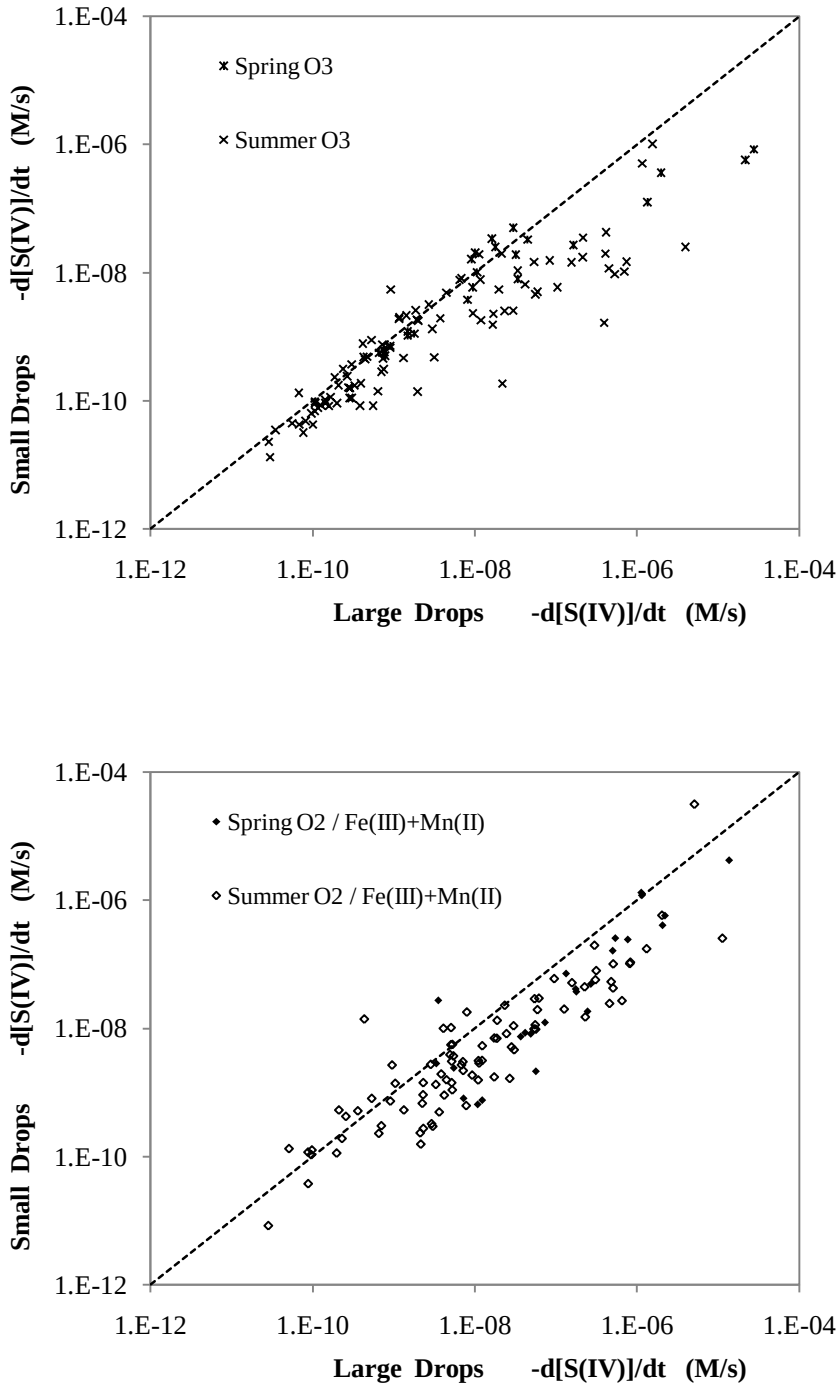

Figure 5-6. Comparison of predicted S(IV) oxidation rates in small ($4 < D < 16$ μm) and large ($D > 16$ μm) cloud drop size fraction sample pairs simultaneously collected with the sf-CASCC at Mt. Tai during the spring and summer 2008 field campaigns. Results are shown for the ozone and metal-catalyzed autooxidation pathways. (The diagonal dashed line is the 1:1 line.)

The (volume-weighted) average oxidation rate in a cloud, predicted from the oxidation rates in the large and small drop size fractions, does not necessarily equal the oxidation rate predicted from the (volume-weighted) average cloud composition. While the averaging order does not matter for the hydrogen peroxide pathway, which exhibits no dependence on drop size, it can be important for the ozone and metal-catalyzed pathways. The nonlinear dependence of these two pathways on the H^+ concentration (and the metal catalyst concentrations in the latter case) can lead to substantially different results for the two methods. We can define an oxidation enhancement ratio, resulting from chemical heterogeneity among droplet composition in a cloud, as the ratio of the volume-weighted average oxidation rate divided by the oxidation rate calculated using the volume-weighted average composition. Figure 5-7 shows the oxidation enhancement ratios for the 3 oxidation pathways, based on the sf-CASCC small and large drop composition and sample volume data.

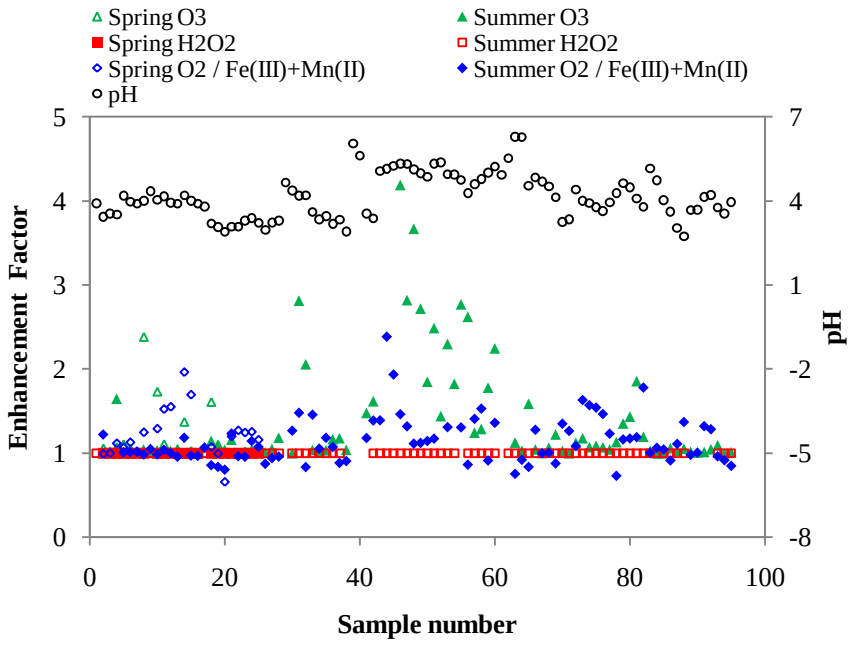

Figure 5-7. Sulfur oxidation enhancement factors determined using the 2008 sf-CASCC dataset. The enhancement factor is defined as the volume-weighted average oxidation rate divided by the oxidation rate predicted from the volume-weighted average cloud composition. See text for details.

As indicated above, no enhancement occurs for the hydrogen peroxide pathway. The ozone pathway shows a maximum oxidation enhancement factor of 4.2, with enhancement factors for several sample periods falling in the range of 1.5 to 3. The enhancement factors for the metal-catalyzed pathway range from 0.2 to 2.4. Values less than 1.0 can occur when metal catalyst concentrations are higher in the more acidic drop fraction. These results indicate the importance of considering chemical heterogeneity among the composition of droplets within Mt. Tai clouds to accurately portray rates of S(IV) oxidation by the ozone and metal-catalyzed pathways. The results here, which are based on only two independent cloud compositions, should be considered a lower bound on the true ozone and metal-catalyzed pathway oxidation enhancement present in the clouds, which likely contain a much wider variety of droplet compositions. Total S(IV)

oxidation rates (the sums of all three oxidation pathways) in Mt. Tai clouds, however, are less sensitive to chemical heterogeneity among cloud drop composition since hydrogen peroxide was observed to be the dominant oxidant in most of the cloud periods measured.

CHAPTER 6 CONCLUSIONS

6.1. CONCLUSIONS

In consideration of the huge amount of SO_2 emission in China, and the fact that aqueous phase oxidation processes are so critical to sulfate production, it is imperative to understand factors influencing cloud chemistry in China in order to accurately predict effects of increasing regional SO_2 emissions on sulfate production in that part of the world and its local, regional, and intercontinental effects. While model simulations provide valuable insight into sulfur chemistry and its sensitivity to changing emissions, *in situ* observations are needed to assess actual conditions in the region. In order to more fully investigate the cloudwater chemical composition and key species that determine the aqueous phase sulfur chemistry and to assess the ability of regional clouds to support aqueous sulfur oxidation, four field campaigns were conducted in 2007 and 2008 at Mt. Tai in eastern China. Mt. Tai is located in central Shandong province, which has the highest SO_2 emission in China. The elevation of Mt. Tai isolates the measurements from direct influence by large urban emission sources, providing a more representative picture of regional atmospheric composition. The summit is frequently in cloud during spring and summer and nearly half of the year days have fog, making Mt. Tai a reliable place to sample fog and cloudwater under the influence of regional atmospheric pollution.

Single and 2-stage Caltech Active Strand Cloudwater Collectors were used to collect bulk and drop size-resolved cloudwater samples, respectively. Key species that influence aqueous phase sulfur oxidation were analyzed, including cloudwater pH, S(IV), H_2O_2, Fe, and Mn. Gas phase SO_2, O_3, and H_2O_2 were also measured continuously during the campaigns. Other species in cloudwater including inorganic ions, total organic carbon (TOC), formaldehyde, and organic acids were also analyzed. During the 2008 campaigns, measurements of pre-cloud, interstitial, and post-cloud aerosols and trace gases were also made in order to examine the efficiency of cloud scavenging of key nitrogen- and sulfur-containing species.

Many periods of cloud interception/fog occurred during the four Mt. Tai field campaigns. During the spring 2007 campaign (03/22-04/22), there were 9 cloud events; a total of 36 bulk cloudwater samples were collected. During the summer 2007 campaign (06/20-07/20), there were 12 cloud events; a total of 66 bulk cloudwater samples were collected. During the spring 2008 campaign (03/28-04/25), there were 4 cloud events; a total of 83 cloudwater samples (including 25 bulk samples and 58 size-fractionated samples) were collected. During the summer 2008 campaign (06/14-07/16), there were 18 cloud events; a total of 333 cloudwater samples (including 117 bulk samples and 216 size-fractionating samples) were collected.

Gaseous H_2O_2 concentrations were generally lower in spring (2007 average mixing ratio of 0.17 ppbv) than in summer (2007 average mixing ratio of 0.55 ppbv). Summer 2008 H_2O_2 mixing ratios averaged 0.59 ppbv. The average concentrations of SO_2 measured

during the Mt. Tai spring campaigns were approximately double the summertime averages. Average mixing ratios of 15.4 ppbv and 14.5 ppbv were observed in spring 2007 and spring 2008, respectively, while average mixing ratios of 8.1 ppbv and 6.4 ppbv were observed in summer 2007 and summer 2008. Average O_3 concentrations were similar across all four campaigns, with mixing ratio averages of 62.1 ppbv and 66.0 ppbv in spring 2007 and spring 2008, respectively, and average mixing ratios of 72.1 ppbv and 68.0 ppbv in summer 2007 and 2008.

A wide range of cloud pH values was observed in bulk cloudwater samples collected at Mt. Tai. Cloudwater pH values ranged from 2.69 to 7.64 in 2007 and from 2.65 to 6.94 in 2008. These ranges are large enough that we should expect multiple S(IV) oxidation pathways to be important at various times. They also indicate strong variability in the relative contributions of acids and bases to regional cloud composition. TOC concentrations (volume-weighted average) in spring and summer 2008 averaged 2.6 ppmC and 15.8 ppmC, respectively. Concentrations of TOC are very high in some Mt. Tai cloudwater samples, reaching as much as 200 ppmC. SO_4^{2-}, NO_3^-, and NH_4^+ were the major inorganic species for all of the four campaigns, accounting for approximately 39.9%, 29.9% and 15.5%, by mass, of the total measured inorganic ions, respectively, during the spring 2007 campaign; accounting for about 52.8%, 15.5% and 24.8% of the total inorganic ions, respectively during the summer 2007 campaign; accounting for about 51.2%, 20.9% and 18.6% of the total inorganic ions, respectively during the spring 2008 campaign; and accounting for about 46.6%, 25.5% and 19.2% of the total inorganic ions, respectively, during the summer 2008 campaign. The average aqueous H_2O_2 values

in spring and summer 2007 were 2.8 μM and 15 μM, respectively. The average aqueous H_2O_2 values in spring and summer 2008 were 9.2 μM and 69.1 μM, respectively. The reaction between S(IV) and H_2O_2 in aqueous solution is very fast, so that measured H_2O_2 represents "residual" H_2O_2 that was not consumed by reaction between sample collection and preservation. The average aqueous S(IV) values in spring and summer 2007 were 40.4 μM and 17.7 μM, respectively. The average aqueous S(IV) values in spring and summer 2008 were 7.7 μM and 35.6 μM, respectively. As with H_2O_2, measured S(IV) represents residual S(IV) not consumed by reaction between the times of sample collection and preservation. The average bulk cloudwater Fe concentrations measured in spring and summer 2007 were 242.5 μg/L and 44.2 μg/L, respectively. Fe concentrations measured in spring and summer 2008 averaged 241.8 μg/L and 415.7 μg/L, respectively. The average Mn concentrations observed in spring and summer 2007 were 93.2 μg/L and 30.2 μg/L, respectively. Mn concentrations in spring and summer 2008 averaged 20.4 μg/L and 29.9 μg/L, respectively. The average HCHO concentrations observed in spring and summer 2007 were 21.3 μM and 25.4 μM, respectively. HCHO concentrations in spring and summer 2008 averaged 4.7 μM and 9.5 μM, respectively.

Comparison of the compositions large ($D > 16$ μm) and small ($4 < D < 16$ μm) cloud drops revealed some differences. While only a small pH difference was observed during many sample periods, fairly large pH differences, of 0.5 – 1.0 pH units or greater, were observed in some cases. Some enrichment of TOC in smaller drops was observed in some sample periods. No consistent pattern of small or large cloud drop enrichment was seen for SO_4^{2-}, NO_3^-, NH_4^+, aqueous H_2O_2, S(IV), HCHO, Fe and Mn. Higher concentrations

of Ca^{2+}, Na^{+} and Mg^{2+} were typically found in the large drops. Differences in composition among droplets can lead to differences in the rates of aqueous phase reactions.

Analysis of cloud composition and backward trajectories revealed some patterns, including high dust content in Mt. Tai clouds during periods of strong spring dust transport from northern China. Several cases of strong influence of biomass burning on Mt. Tai clouds, evidenced by high concentrations of TOC, K^{+}, and organic smoke marker species, were also observed during June. In some cases, however, no clear relationship was observed between horizontal transport patterns and cloudwater chemical composition. Mt. Tai is surrounded by regions of high pollutant emissions, giving the potential for polluted cloudwater regardless of the longer distance origins of air trajectories. Incorporating additional information about air parcel history (e.g., vertical transport and precipitation history), did provide additional insight, especially when cloud water solute content was low.

Mt. Tai clouds were found to interact strongly with $PM_{2.5}$ inorganic aerosol species. Scavenging efficiencies for sulfate aerosol were fairly high, with values ranging from 66% to 92%. Scavenging efficiencies of total sulfur showed a much broader range, from 17% to 73%, reflecting appreciable sulfur dioxide gas that remained unscavenged during some of the events. Scavenging efficiencies for ammonium particles ranged from 65% to 94%, similar to values observed for aerosol sulfate, consistent with an expected close association between ammonium and sulfate in regional aerosol particles. Scavenging

efficiencies of total N(-III) ranged from 45% to 81%. These values are considerably higher than observed for sulfur, reflecting the higher solubility of gaseous ammonia vs. sulfur dioxide. Scavenging efficiencies for aerosol nitrate ranged from 50% to 95%. Scavenging efficiencies of total N(V) were comparable or higher, ranging from 67% to 93%, consistent with the very high solubility of gaseous nitric acid. The average N(V) scavenging efficiency across studied events was 78%, while average scavenging efficiencies for N(-III) and S were 63% and 43%, respectively. These observations suggest that while most of the N(V) and nearly two-thirds of the N(-III) undergoes cloud processing in a given cloud event, more than half of the sulfur remains unprocessed.

Rates of aqueous phase S(IV) oxidation by H_2O_2, by O_3, and by O_2 with trace metal (Fe(III) and Mn(II)) catalysis were computed utilizing the cloudwater and gas phase measurements described above. Among the three S(IV) oxidation pathways, oxidation by H_2O_2 was generally found to be the fastest pathway for pH values less than approximately 5. The importance of O_3 as an oxidant increased strongly as pH values climbed above 5 to 5.3. Variations in the rate of S(IV) oxidation by ozone show little overall dependence on the ozone concentration and were governed more strongly by factors influencing cloud pH. Computed metal-catalyzed S(IV) autooxidation rates were highly variable. Overall, in 68% of the sample periods the fastest S(IV) oxidation pathway was the hydrogen peroxide pathway. The ozone pathway was fastest 21% of the time and the metal-catalyzed pathway was fastest 11% of the time. While many collected cloud samples had low concentrations of H_2O_2, there also were many samples, especially from the summertime, where tens to hundreds of μM of H_2O_2 remain in the cloudwater

and little S(IV) remained. This residual peroxide indicates a substantial capacity during these periods for additional in-cloud sulfate production.

A comparison between oxidation rates computed for small and large cloud drop size fractions revealed a general tendency for oxidation rates to be faster in the large drops for the ozone and metal-catalyzed pathways. This comes from the strong dependence of both pathways on cloud pH (faster oxidation at higher pH) and the tendency for the pH to be higher in the large cloud drop size fraction. In the case of the metal-catalyzed pathway, there is an additional effect from any drop size-dependence in the Fe and Mn concentrations. The nonlinear dependence of these two pathways on the H^+ concentration (and the metal catalyst concentrations in the latter case) can lead to biases in oxidation rates predicted from the (volume-weighted) average cloud composition. Chemical heterogeneity among cloud drop composition can enhance rates of S(IV) oxidation by ozone, vs. rates expected from average cloud composition, while it can increase or decrease rates of metal-catalyzed S(IV) autooxidation, depending on how both H^+ and metal catalyst concentrations are distributed with drop size. No enhancement occurs for the hydrogen peroxide pathway, which is essentially independent of the H^+ concentration over a relevant pH range. Enhancements up to 420% were observed for the ozone oxidation pathway and up to 240% for the metal-catalyzed pathway. While these upper limits are large, most values were smaller (suppression up to 80% was also observed for the metal-catalyzed pathway). Furthermore, total S(IV) oxidation rates (the sums of all three oxidation pathways) in Mt. Tai clouds, however, are less sensitive to chemical

heterogeneity among cloud drop composition since hydrogen peroxide was found to be the dominant oxidant in most of the cloud periods measured.

These data provide a novel and robust dataset for future evaluations of numerical simulations of the fate of SO_2 emitted in China. The importance of H_2O_2 as an aqueous phase oxidant is clear and, for the first time, observations of gas phase H_2O_2 and the presence of residual H_2O_2 in many summertime clouds has been demonstrated. In addition, measurements of the composition of clouds at Mt. Tai clearly reveal that China's air pollution has moved well beyond the point where sulfur dioxide and dust emissions are the only concerns. Abundant cloudwater ammonium, nitrate and organic matter clearly demonstrate the importance of other pollutant emissions, including NO_x from transportation, power generation, lightning, and other combustion sources, ammonia from agriculture, and organic matter from many sources, including the burning of agricultural biomass.

6.2. RECOMMENDATIONS FOR FUTURE WORK

This study represents the first extensive investigation of cloud composition and the processing of sulfur dioxide by regional clouds in eastern China. Based on the findings here, several avenues of possible future investigation are recommended:

- Future cloud composition studies in the region should include measurement of HMS to determine whether its formation is as important as suggested by the rate

calculations here. HMS measurements could also be included in aerosol chemistry studies.

- Future cloud composition studies in the region should include speciation of Fe and Mn. Mn(II) usually is the predominant oxidation state of Mn; however, the speciation of Fe is less certain. The relative abundance of the catalytically active iron form, Fe(III), and the inactive iron form, Fe(II), is important for accurately determining the metal-catalyzed S(IV) autooxidation rate. While a catalytically active fraction of 25% was assumed for this study, measurements of the actual Fe(III) abundance, and changes with cloud pH and/or actinic flux, would be especially interesting to examine.
- Additional work is needed to examine organic acids in cloudwater to better understand possible effects on cloudwater acidity. Organic acids can also act as good ligands for trace metals and may play an important role in droplet photochemistry, including Fenton-like chemistry which may be an important route for aqueous phase H_2O_2 production in these clouds.
- While the samples collected in this study were assumed to be fairly representative of cloud composition in the eastern part of China, additional measurements at other locations could help test the validity of this assumption. Other regions, such as Mt. Lu and Mt. Huang should be considered for future cloud composition studies. Continued measurements at Mt. Tai would also be extremely valuable in examining how rapidly evolving pollutant emissions in China influence cloud chemistry.

- The extremely high concentrations of TOC observed in some Mt. Tai cloud samples were unexpected and are of great interest. While the 2007/08 Mt. Tai cloud chemistry studies were not designed to examine cloud processing of carbonaceous aerosols, such a study would be well worth pursuing in the future. Interactions of regional clouds with carbonaceous aerosol particles can be studied with additional aerosol sampling techniques. For example, High-Volume Sampling of carbonaceous aerosol particles before, during and after cloud could be used to examine carbonaceous aerosol scavenging efficiencies. Faster measurements (e.g., the Aerosol Mass Spectrometer (AMS)) would provide an even better (especially faster) tool to examine scavenging efficiencies for both organic and inorganic aerosol compounds.
- It has now been more than 10 years since Mary Barth and her group modeled sulfur chemistry in the region. With the additional model input and validation data represented by this study, and many other recent studies of atmospheric chemistry in China, the time is ripe for another numerical simulation of regional cloud chemistry and its effects on China's sulfur emissions as well as other nitrogen- and carbon-containing pollutants.

REFERENCES

Abelson, P. H. (1983). "Acid rain." Science **221**(4606): 115.

Abelson, P. H. (1985). "Air pollution and acid rain." Science **230**(4726): 617.

Abelson, P. H. (1987). "Ozone and acid rain." Science **238**(4824): 141.

Adewuyi, Y. G., S. Y. Cho, et al. (1984). "Importance of formaldehyde in cloud chemistry." Atmospheric Environment **18**(11): 2413-2420.

Ahr, M., A. I. Flossmann, et al. (1989). "On the effect of the chemical composition of atmospheric aerosol particles on nucleation scavenging and the formation of a cloud interstitial aerosol." Journal of Atmospheric Chemistry **9**(4): 465-478.

Ahrens, C. D. (2000). "Meteorology Today: An Introduction to Weather, Climate, and the Environment, 6th Edition." Thomson Brooks/Cole: 172.

Alheit, R. R., A. I. Flossmann, et al. (1990). "A theoretical study of the wet removal of atmospheric pollutants. Part IV: The uptake and redistribution of aerosol particles through nucleation and impaction scavenging by growing cloud drops and ice particles." Journal of the Atmospheric Sciences **47**(7): 870-887.

Anastasio, C., B. C. Faust, et al. (1994). "Aqueous phase photochemical formation of hydrogen peroxide in authentic cloud waters." Journal of Geophysical Research-Atmospheres **99**(D4): 8231-8248.

Andreae, M. O., D. Rosenfeld, et al. (2004). "Smoking rain clouds over the Amazon." Science **303**(5662): 1337-1342.

Arends, B. G., G. P. A. Kos, et al. (1992). "Comparison of techniques for measurements of fog liquid water content." Tellus **44B**: 604-611.

Barth, M. C. and A. T. Church (1999). "Regional and global distributions and lifetimes of sulfate aerosols from Mexico city and southeast China." Journal of Geophysical Research-Atmospheres **104**(D23): 30231-30239.

Barth, M. C., P. J. Rasch, et al. (2000). "Sulfur chemistry in the National Center for Atmospheric Research Community Climate Model: Description, evaluation, features, and sensitivity to aqueous chemistry." Journal of Geophysical Research-Atmospheres **105**(D1): 1387-1415.

Bator, A. and J. L. Collett (1997). "Cloud chemistry varies with drop size." Journal of Geophysical Research-Atmospheres **102**(D23): 28071-28078.

Boyce, S. D. and M. R. Hoffmann (1984). "Kinetics and mechanism of the formation of hydroxymethanesulfonic acid at low pH." Journal of Physical Chemistry **88**(20): 4740-4746.

Bravo, H., R. Soto, et al. (2006). "Effect of acid rain on building material of the El Tajin archaeological zone in Veracruz, Mexico." Environmental Pollution **144**(2): 655-660.

Brock, C. A., P. K. Hudson, et al. (2004). "Particle characteristics following cloud-modified transport from Asia to North America." Journal of Geophysical Research-Atmospheres **109**(D23): 17.

Carter, L. J. (1979). "Uncontrolled SO_2 emissions bring acid rain." Science **204**(4398): 1179-1181.

Chan, T. W., L. Huang, et al. (2010). "Observations of OM/OC and specific attenuation coefficients (SAC) in ambient fine PM at a rural site in central Ontario, Canada." Atmospheric Chemistry and Physics **10**(5): 2393-2411.

Charlson, R. J., S. E. Schwartz, et al. (1992). "Climate forcing by anthropogenic aerosols." Science **255**(5043): 423-430.

China-MEP (2010). "2009 report on the state of the environment in China." http://jcs.mep.gov.cn/hjzl/zkgb/2009hjzkgb/201006/t20100603_190429.htm.

Chuang, P. Y., R. M. Duvall, et al. (2005). "The origin of water soluble particulate iron in the Asian atmospheric outflow." Geophysical Research Letters **32**(7): 4.

Collett, J. L., A. Bator, et al. (1994). "Acidity variations across the cloud drop size spectrum and their influence on rates of atmospheric sulfate production." Geophysical Research Letters **21**(22): 2393-2396.

Collett, J. L., A. Bator, et al. (2002). "The chemical composition of fogs and intercepted clouds in the United States." Atmospheric Research **64**(1-4): 29-40.

Collett, J. L., P. Herckes, et al. (2008). "Processing of atmospheric organic matter by California radiation fogs." Atmospheric Research **87**(3-4): 232-241.

Collett, J. L., K. J. Hoag, et al. (1999). "Spatial and temporal variations in San Joaquin Valley fog chemistry." Atmospheric Environment **33**(1): 129-140.

Collett, J. L., B. Oberholzer, et al. (1993). "Contributions of cloud processes to precipitation chemistry in mixed phase clouds." Water Air and Soil Pollution **68**(1-2): 43-57.

Dasgupta, P. K., K. Decesare, et al. (1980). "Determination of atmospheric sulfur dioxide without tetrachloromercurate(II) and the mechanism of the Schiff reaction." Analytical Chemistry **52**(12): 1912-1922.

Daube, B. C., Jr, Flagan, R.C. and Hoffmann, M.R. (1987). "Active cloudwater collector." United States Patent No. 4,697,462.

Demoz, B. B., J. L. Collett, et al. (1996). "On the Caltech Active Strand Cloudwater Collectors." Atmospheric Research **41**(1): 47-62.

Ding, X., X. Ji, et al. (1991). "Characters of cloud-fog water in Lu Shan Mountain (in Chinese)." Acta Meteorologica Sinica **49**(2): 190-197.

Dong, S. and P. K. Dasgupta (1987). "Fast fluorometric flow injection analysis of formaldehyde in atmospheric water." Environmental Science & Technology **21**(6): 581-588.

Draxier, R. R. and G. D. Hess (1997). "Description of the HYSPLIT_4 modeling system." NOAA Technical Memorandum ERL ARL-224.

Draxier, R. R. and G. D. Hess (1998). "An overview of the HYSPLIT_4 modeling system for trajectories, dispersion and deposition." Australian Meteorological Magazine **47**(4): 295-308.

Dutkiewicz, V. A. and L. Husain (1998). "Inefficient scavenging of aerosol sulfate by non-precipitating clouds in polluted air." Atmospheric Environment **32**(16): 2793-2801.

Ermakov, A. N., I. K. Larin, et al. (2006). "Size effects in the catalysis of atmospheric oxidation of SO_2 by iron ions." Kinetics and Catalysis **47**(6): 825-833.

Ervens, B., P. Herckes, et al. (2003). "On the drop-size dependence of organic acid and formaldehyde concentrations in fog." Journal of Atmospheric Chemistry **46**(3): 239-269.

Faust, B. C., C. Anastasio, et al. (1993). "Aqueous-phase photochemical formation of peroxides in authentic cloud and fog waters." Science **260**(5104): 73-75.

Fay, J. A. and D. S. Golomb (1989). "Acid rain models." Science **244**(4901): 127.

Fiedler, V., R. Nau, et al. (2009). "East Asian SO_2 pollution plume over Europe - Part 1: Airborne trace gas measurements and source identification by particle dispersion model simulations." Atmospheric Chemistry and Physics **9**(14): 4717-4728.

Fischer-Bruns, I., D. F. Banse, et al. (2009). "Future impact of anthropogenic sulfate aerosol on North Atlantic climate." Climate Dynamics **32**(4): 511-524.

Flossmann, A. I., W. D. Hall, et al. (1985). "A theoretical study of the wet removal of atmospheric pollutants. Part I: The redistribution of aerosol particles captured through nucleation and impaction scavenging by growing cloud drops." Journal of the Atmospheric Sciences **42**(6): 583-606.

Flossmann, A. I. and H. R. Pruppacher (1988). "A theoretical study of the wet removal of atmospheric pollutants. Part III: The uptake, redistribution, and deposition of $(NH_4)_2SO_4$ particles by a convective cloud using a two-dimensional cloud dynamics model." Journal of the Atmospheric Sciences **45**(13): 1857-1871.

Flossmann, A. I., H. R. Pruppacher, et al. (1987). "A theoretical study of the wet removal of atmospheric pollutants. Part II: The uptake and redistribution of $(NH_4)_2SO_4$ particles and SO_2 gas simultaneously scavenged by growing cloud drops." Journal of the Atmospheric Sciences **44**(20): 2912-2923.

Galloway, J. N., D. W. Zhao, et al. (1987). "Acid Rain: China, United States, and a remote area." Science **236**(4808): 1559-1562.

Gao, J., T. Wang, et al. (2005). "Observational study of ozone and carbon monoxide at the summit of mount Tai (1534m a.s.l.) in central-eastern China." Atmospheric Environment **39**(26): 4779-4791.

Gerber, H. (1984). "Liquid water content of fogs and hazes from visible light scattering." Journal of Climate and Applied Meteorology **23**(8): 1247-1252.

Gerber, H. (1991). "Direct measurement of suspended particulate volume concentration and far-infrared extinction coefficient with a laser-diffraction instrument." Applied Optics **30**(33): 4824-4831.

Gillani, N. V., S. E. Schwartz, et al. (1995). "Field observations in continental stratiform clouds : partitioning of cloud between droplets and unactivated interstitial aerosols." Journal of Geophysical Research-Atmospheres **100**(D9): 18687-18706.

Grgic, I., V. Hudnik, et al. (1992). "Aqueous S(IV) oxidation II. Synergistic effects of some metal ions." Atmospheric Environment Part a-General Topics **26**(4): 571-577.

Gurciullo, C. S. and S. N. Pandis (1997). "Effect of composition variations in cloud droplet populations on aqueous-phase chemistry." Journal of Geophysical Research-Atmospheres **102**(D8): 9375-9385.

Hegg, D. A. and T. V. Larson (1990). "The effects of microphysical parameterization on model predictions of sulfate production in clouds." Tellus **42B**: 272–284.

Henning, S., S. Bojinski, et al. (2004). "Aerosol partitioning in natural mixed-phase clouds." Geophysical Research Letters **31**(6): 4.

Herckes, P., M. P. Hannigan, et al. (2002). "Organic compounds in radiation fogs in Davis (California)." Atmospheric Research **64**(1-4): 99-108.

Herckes, P., T. Lee, et al. (2002). "Organic matter in Central California radiation fogs." Environmental Science & Technology **36**(22): 4777-4782.

Hitzenberger, R., A. Berner, et al. (2001). "Black carbon (BC) in alpine aerosols and cloud water - concentrations and scavenging efficiencies." Atmospheric Environment **35**(30): 5135-5141.

Hitzenberger, R., A. Berner, et al. (2000). "Black carbon and other species at a high-elevation European site (Mount Sonnblick, 3106 m, Austria): Concentrations and scavenging efficiencies." Journal of Geophysical Research-Atmospheres **105**(D20): 24637-24645.

Hoag, K. J., J. L. Collett, et al. (1999). "The influence of drop size-dependent fog chemistry on aerosol processing by San Joaquin Valley fogs." Atmospheric Environment **33**(29): 4817-4832.

Hoffmann, M. R. (1986). "On the kinetics and mechanism of oxidation of aquated sulfur dioxide by ozone." Atmospheric Environment **20**(6): 1145-1154.

Hoffmann, M. R. and J. G. Calvert (1985). "Chemical transformation modules for eulerian acid deposition models. volume II. The aqueous-phase chemistry." National Center for Atmospheric Research, Boulder, CO.

Hoose, C., U. Lohmann, et al. (2008). "Global simulations of aerosol processing in clouds." Atmospheric Chemistry and Physics **8**(23): 6939-6963.

Hoose, C., U. Lohmann, et al. (2008). "Aerosol processing in mixed-phase clouds in ECHAM5-HAM: Model description and comparison to observations." Journal of Geophysical Research-Atmospheres **113**(D7): 17.

Hoppel, W. A., G. M. Frick, et al. (1986). "Effect of nonprecipitating clouds on the aerosol size distribution in the marine boundary layer." Geophysical Research Letters **13**(2): 125-128.

Ibusuki, T. and K. Takeuchi (1987). "Sulfur dioxide oxidation by oxygen catalyzed by mixtures of manganese(II) and iron(III) in aqueous solutions at environmental reaction conditions." Atmospheric Environment **21**(7): 1555-1560.

Ivanova, I. T. and H. G. Leighton (2008). "Aerosol-cloud interactions in a mesoscale model. Part II: Sensitivity to aqueous-phase chemistry." Journal of the Atmospheric Sciences **65**(2): 309-330.

Jacob, D. J. and M. R. Hoffmann (1983). "A dynamic model for the production of H^+, NO_3^- and SO_4^{2-} in urban fog." Journal of Geophysical Research-Oceans and Atmospheres **88**: 6611-6621.

Jernelov, A. (1983). "Acid rain and sulphur dioxide emissions in China." Ambio **12**(6): 362-362.

Kanaya, Y., Y. Komazaki, et al. (2008). "Mass concentrations of black carbon measured by four instruments in the middle of Central East China in June 2006." Atmospheric Chemistry and Physics **8**(24): 7637-7649.

Kaufman, Y. J. and R. S. Fraser (1997). "The effect of smoke particles on clouds and climate forcing." Science **277**(5332): 1636-1639.

Kiehl, J. T. and B. P. Briegleb (1993). "The relative roles of sulfate aerosols and greenhouse gases in climate forcing." Science **260**(5106): 311-314.

Kim, M. G., B. K. Lee, et al. (2006). "Cloud/fog water chemistry at a high elevation site in South Korea." Journal of Atmospheric Chemistry **55**(1): 13-29.

Kim, Y. J., J. H. Woo, et al. (2009). "Chemical characteristics of long-range transport aerosol at background sites in Korea." Atmospheric Environment **43**(34): 5556-5566.

Larssen, T., E. Lydersen, et al. (2006). "Acid rain in China." Environmental Science & Technology **40**(2): 418-425.

Lazrus, A. L., G. L. Kok, et al. (1985). "Automated fluorometric method for hydrogen peroxide in atmospheric precipitation." Analytical Chemistry **57**(4): 917-922.

Lazrus, A. L., G. L. Kok, et al. (1986). "Automated fluorometric method for hydrogen peroxide in air." Analytical Chemistry **58**(3): 594-597.

Lee, T., A. P. Sullivan, et al. (2010). "Chemical Smoke Marker Emissions During Flaming and Smoldering Phases of Laboratory Open Burning of Wildland Fuels." Aerosol Science and Technology **44**(9): I-V.

Lelieveld, J. and J. Heintzenberg (1992). "Sulfate cooling effect on climate through in-cloud oxidation of anthropogenic SO_2." Science **258**(5079): 117-120.

Li, D., M. Chen, et al. (1999). "Study on air pollution and composition of fog in Shanghai (in Chinese)." Shanghai Environmental Sciences **18**(3): 117-120.

Li, J., P. Pochanart, et al. (2008). "Impact of chemical production and transport on summertime diurnal ozone behavior at a mountainous site in North China Plain." Sola **4**: 121-124.

Li, Y., G. Zhang, et al. (2008). "The chemical composition of fog water in the winter of 2006 of Nanjing (in Chinese)." China Environmental Science **28**(5): 395-400.

Li, Z. and Z. Peng (1994). "Physical and chemical characteristics of the Chongqing winter fog (in Chinese)." Acta Meteorologica Sinica **52**(4): 477-483.

Liang, J. and M. Z. Jacobson (1999). "A study of sulfur dioxide oxidation pathways over a range of liquid water contents, pH values, and temperatures." Journal of Geophysical Research **104**: 13,749-13,769.

Likens, G. E. and F. H. Bormann (1974). "Acid rain: a serious regional environmental problem." Science **184**(4142): 1171-1179.

Likens, G. E., C. T. Driscoll, et al. (1996). "Long-term effects of acid rain: Response and recovery of a forest ecosystem." Science **272**(5259): 244-246.

Likens, G. E., R. F. Wright, et al. (1979). "Acid rain." Scientific American **241**(4): 43-51.

Lu, Z., D. G. Streets, et al. (2010). "Sulfur dioxide emissions in China and sulfur trends in East Asia since 2000." Atmospheric Chemistry and Physics **10**(13): 6311-6331.

Luo, C., N. Mahowald, et al. (2008). "Combustion iron distribution and deposition." Global Biogeochemical Cycles **22**(1): 17.

Manktelow, P. T., G. W. Mann, et al. (2007). "Regional and global trends in sulfate aerosol since the 1980s." Geophysical Research Letters **34**(14): 6.

Mao, T., Y. S. Wang, et al. (2009). "A study of the atmospheric VOCs of Mount Tai in June 2006." Atmospheric Environment **43**(15): 2503-2508.

Martin, L. R. and T. W. Good (1991). "Catalyzed oxidation of sulfur dioxide in solution: the iron-manganese synergism." Atmospheric Environment Part a-General Topics **25**(10): 2395-2399.

Menon, M., S. Hermle, et al. (2007). "Effects of heavy metal soil pollution and acid rain on growth and water use efficiency of a young model forest ecosystem." Plant and Soil **297**(1-2): 171-183.

Menon, S., V. K. Saxena, et al. (2000). "Chemical heterogeneity across cloud droplet size spectra in continental and marine air masses." Journal of Applied Meteorology **39**(6): 887-903.

Moore, K. F., D. E. Sherman, et al. (2004a). "Drop size-dependent chemical composition in clouds and fogs. Part I. Observations." Atmospheric Environment **38**(10): 1389-1402.

Moore, K. F., D. E. Sherman, et al. (2004b). "Drop size-dependent chemical composition of clouds and fogs. Part II: Relevance to interpreting the aerosol/trace gas/fog system." Atmospheric Environment **38**(10): 1403-1415.

Munger, J. W., J. L. Collett, et al. (1989). "Carboxylic acids and carbonyl compounds in southern California clouds and fogs." Tellus **41**(B): 230-242.

Munger, J. W., D. J. Jacob, et al. (1995). "Formaldehyde, glyoxal, and methylglyoxal in air and cloudwater at a rural mountain site in central Virginia." Journal of Geophysical Research-Atmospheres **100**(D5): 9325-9333.

Munger, J. W., D. J. Jacob, et al. (1984). "The occurrence of bisulfite-aldehyde addition-products in fogwater and cloudwater." Journal of Atmospheric Chemistry **1**(4): 335-350.

Munger, J. W., C. Tiller, et al. (1986). "Identification of hydroxymethanesulfonate in fog water." Science **231**(4735): 247-249.

Niu, S. J., C. S. Lu, et al. (2010). "Fog Research in China: An Overview." Advances in Atmospheric Sciences **27**(3): 639-662.

Noone, K. J., R. J. Charlson, et al. (1988). "Cloud droplets: solute concentration is size dependent." Journal of Geophysical Research-Atmospheres **93**(D8): 9477-9482.

Oberholzer, B., J. L. Collett, et al. (1992). "In-cloud scavenging of gases and aerosols at a mountain site in central Switzerland." Journal of Atmospheric Chemistry **14**(1-4): 61-71.

Oberholzer, B., M. Volken, et al. (1993). "Pollutant concentrations and below-cloud scavenging of selected N(-III) species along a mountain slope." Water Air and Soil Pollution **68**(1-2): 59-73.

Ogren, J. A. and R. J. Charlson (1992). "Implications for models and measurements of chemical inhomogeneities among cloud droplets." Tellus **44B**: 208–225.

Olson, T. M. and M. R. Hoffmann (1989). "Hydroxyalkylsulfonate formation: its role as a S(IV) reservoir in atmospheric water droplets." Atmospheric Environment **23**(5): 985-997.

Pang, Y. B., N. L. Eatough, et al. (2002). "Evaluation of the performance of annular denuder samplers." Aerosol Science and Technology **36**(6): 790-798.

Parazols, M., A. Marinoni, et al. (2006). "Speciation and role of iron in cloud droplets at the puy de Dome station." Journal of Atmospheric Chemistry **54**(3): 267-281.

Park, R. J., D. J. Jacob, et al. (2004). "Natural and transboundary pollution influences on sulfate-nitrate-ammonium aerosols in the United States: Implications for policy." Journal of Geophysical Research-Atmospheres **109**(D15): 20.

Pehkonen, S. O., Y. Erel, et al. (1992). "Simultaneous spectrophotometric measurement of Fe(II) and Fe(III) in atmospheric water." Environmental Science & Technology **26**(9): 1731-1736.

Peng, Z., G. Chen, et al. (1992). "Acid mechanism of fog and its physical condition in Chongqing (in Chinese)." Chongqing Environmental Science **14**(3): 12-15.

Rao, X. and J. L. Collett (1995). "Behavior of S(IV) and formaldehyde in a chemically heterogeneous cloud." Environmental Science & Technology **29**(4): 1023-1031.

Rao, X. and J. L. Collett (1998). "The drop size-dependence of iron and manganese concentrations in clouds and fogs: Implications for sulfate production." Journal of Atmospheric Chemistry **30**(2): 273-289.

Rattigan, O. V., J. Reilly, et al. (2001). "Sulfur dioxide oxidation in clouds at Whiteface Mountain as a function of drop size." Journal of Geophysical Research-Atmospheres **106**(D15): 17347-17358.

Reilly, J. E., O. V. Rattigan, et al. (2001). "Drop size-dependent S(IV) oxidation in chemically heterogeneous radiation fogs." Atmospheric Environment **35**(33): 5717-5728.

Ren, Y., A. J. Ding, et al. (2009). "Measurement of gas-phase total peroxides at the summit of Mount Tai in China." Atmospheric Environment **43**(9): 1702-1711.

Respondek, P. S., A. I. Flossmann, et al. (1995). "A theoretical study of the wet removal of atmospheric pollutants. Part V: The uptake, redistribution, and deposition of $(NH_4)_2SO_4$ by a convective cloud containing ice." Journal of the Atmospheric Sciences **52**(11): 2121-2132.

Roelofs, G. J., P. Stier, et al. (2006). "Aerosol activation and cloud processing in the global aerosol-climate model ECHAM5-HAM." Atmospheric Chemistry and Physics **6**: 2389-2399.

Sedlak, D. L., J. Hoigne, et al. (1997). "The cloudwater chemistry of iron and copper at Great Dun Fell, UK." Atmospheric Environment **31**(16): 2515-2526.

Seidl, W. (1989). "Ionic concentrations and initial S(IV)-oxidation rates in droplets during the condensational stage of cloud." Tellus **41B**: 32–50.

Seinfeld, J. H. and S. N. Pandis (2006). "Atmospheric chemistry and physics: from air pollution to climate change." John Wiley & Sons, Inc., New York.

Shen, Z. L., Y. X. Wu, et al. (1996). "Measurement and research on cloudwater over severe acid rain areas of China." Chinese Science Bulletin **41**(20): 1726-1729.

Siefert, R. L., A. M. Johansen, et al. (1998). "Measurements of trace metal (Fe, Cu, Mn, Cr) oxidation states in fog and stratus clouds." Journal of the Air & Waste Management Association **48**(2): 128-143.

Singer, S. F. (1984). "Acid rain report." Science **226**(4676): 780.

Singh, A. and M. Agrawal (2008). "Acid rain and its ecological consequences." Journal of Environmental Biology **29**(1): 15-24.

Smith, S. J., H. Pitcher, et al. (2001). "Global and regional anthropogenic sulfur dioxide emissions." Global and Planetary Change **29**(1-2): 99-119.

Suthawaree, J., S. Kato, et al. (2010). "Measurements of volatile organic compounds in the middle of Central East China during Mount Tai Experiment 2006 (MTX2006): observation of regional background and impact of biomass burning." Atmospheric Chemistry and Physics **10**(3): 1269-1285.

Tu, F. H., D. C. Thornton, et al. (2004). "Long-range transport of sulfur dioxide in the central Pacific." Journal of Geophysical Research-Atmospheres **109**(D15): 19.

Twohy, C. H., R. J. Charlson, et al. (1989). "Chemical consequences of the initial diffusional growth of cloud droplets: a clean marine case." Tellus **41B**: 51-60.

Ulman, J. C. and V. K. Saxena (1997). "Impact of air mass histories on the chemical climate of Mount Mitchell, North Carolina." Journal of Geophysical Research-Atmospheres **102**(D21): 25451-25465.

Wai, K. M., P. A. Tanner, et al. (2005). "2-Year study of chemical composition of bulk deposition in a south China coastal city: Comparison with east Asian cities." Environmental Science & Technology **39**(17): 6542-6547.

Wang, G. H., K. Kawamura, et al. (2009). "Water-soluble organic compounds in $PM_{2.5}$ and size-segregated aerosols over Mount Tai in North China Plain." Journal of Geophysical Research-Atmospheres **114**: 10.

Wang, T., T. F. Cheung, et al. (2002). "Emission characteristics of CO, NO_x, SO_2 and indications of biomass burning observed at a rural site in eastern China." Journal of Geophysical Research-Atmospheres **107**(D12): 10.

Wang, T., V. T. F. Cheung, et al. (2001). "Ozone and related gaseous pollutants in the boundary layer of eastern China: Overview of the recent measurements at a rural site." Geophysical Research Letters **28**(12): 2373-2376.

Wang, T., A. J. Ding, et al. (2006). "Strong ozone production in urban plumes from Beijing, China." Geophysical Research Letters **33**(21): 5.

Wang, T., C. N. Poon, et al. (2003). "Characterizing the temporal variability and emission patterns of pollution plumes in the Pearl River Delta of China." Atmospheric Environment **37**(25): 3539-3550.

Wang, W. and P. Xu (2009). "Research progress in precipitation chemistry in China." Progress in Chemistry **21**: 266-281.

Wang, W. X. and T. Wang (1996). "On acid rain formation in China." Atmospheric Environment **30**(23): 4091-4093.

Wang, Y., K. M. Wai, et al. (2008). "The impacts of anthropogenic emissions on the precipitation chemistry at an elevated site in North-eastern China." Atmospheric Environment **42**(13): 2959-2970.

Wang, Z. F., J. Li, et al. (2006). "Modeling of regional high ozone episode observed at two mountain sites (Mt. Tai and Huang) in East China." Journal of Atmospheric Chemistry **55**(3): 253-272.

Warneck, P. (1989). "Sulfur dioxide in rain clouds: gas-liquid scavenging efficiencies and wet deposition rates in the presence of formaldehyde." Journal of Atmospheric Chemistry **8**(2): 99-117.

Yamaji, K., J. Li, et al. (2010). "Impact of open crop residual burning on air quality over Central Eastern China during the Mount Tai Experiment 2006 (MTX2006)." Atmospheric Chemistry and Physics **10**(15): 7353-7368.

Zhang, Q., D. G. Streets, et al. (2009). "Asian emissions in 2006 for the NASA INTEX-B mission." Atmospheric Chemistry and Physics **9**(14): 5131-5153.

Zhang, Q., D. R. Worsnop, et al. (2005). "Hydrocarbon-like and oxygenated organic aerosols in Pittsburgh: insights into sources and processes of organic aerosols." Atmospheric Chemistry and Physics **5**: 3289-3311.

Zhao, D. and B. Sun (1986). "Air pollution and acid rain in China." Ambio **15**(1): 2-5.

Zhao, Y. X. and Q. Hou (2010). "Characteristics of the acid rain variation in China during 1993-2006 and associated causes." Acta Meteorologica Sinica **24**(2): 239-250.

Zuo, Y. G. and Y. W. Deng (1999). "Evidence for the production of hydrogen peroxide in rainwater by lightning during thunderstorms." Geochimica Et Cosmochimica Acta **63**(19-20): 3451-3455.

APPENDIX A – ALIQUOTS FOR CHEMICAL MEASUREMENTS

SAMPLE PRIORITY

1. pH measurement: 2 ml sample
2. Major ion analysis by IC: 600 µl sample
3. S(IV): 1 ml sample
4. Metals: 1 ml sample
5. Formaldehyde: 1 ml sample
6. H_2O_2: 1 ml sample
7. Organic Acids: 1.4 ml sample
8. TOC: 25 ml sample

ALIQUOTS FOR CHEMICAL MEASUREMENTS

1. pH measurement

Place two 2 ml cryovials into holder
Pipette 1 ml sample into each vial
Rinse the electrode with DI water and shake to remove excess water
Place pH probe into the first vial, making sure it is in contact with sample
Remove the probe from first vial and shake off excess solution
Place the probe into the second vial, making sure it is in contact with sample
Write down the pH on the project log sheet when the reading first stabilizes (typically approximately 3 seconds)

2. Major ion analysis by IC

Pipette 600 µl sample into a polyethylene autosampler vial with Teflon-lined septum. Label vial with sample name and letters "IC."

3. S(IV)

Pipette 1.0 ml sample into a 1.5 ml glass vial with Teflon-lined cap.
Add 100 µl S(IV) preservative solution

Add 100 µl catalase solution
Close cap and mix completely
Label vial with sample name and "S(IV)."

4. Metals

Pipette 1.0 ml sample into a 2 ml cryovial
Add 100 µl 9.7% HNO_3 solution
Close cap and mix completely
Label vial with sample name and "Metals."

5. Formaldehyde

Pipette 1.0 ml sample into a 1.5 ml glass vial with Teflon-lined cap
Add 100 µl formaldehyde preservative solution
Close cap and mix completely
Label vial with sample name and "HCHO."

6. H_2O_2

Pipette 1.0 ml sample into a 1.5 ml glass vial with Teflon-lined cap.
Add 200 µl conditioning reagent
Add 200 µl fluorescent reagent
Close cap and mix completely
Label vial with sample name and "H_2O_2."

7. Organic Acids

Add 50 µl chloroform into a 1.5 ml glass autosampler vial with Teflon-lined septum
Pipette 1.4 ml sample into the vial
Close cap and label vial with sample name and "Org Acids."

8. TOC

Put 25 ml sample into a 25 ml Glass autosampler with septum
Cap and label with sample name and "TOC"

METHODS OF CHECKING ACTIVITIES OF ENZYME SOLUTIONS

1. Checking activity of peroxidase

Pipette 1.0 ml DI water into a 1.5 ml glass vial
Add 100 µl 1.0 mM H_2O_2 solution
Add 200 µl conditioning reagent
Add 200 µl fluorescent reagent
Close cap and mix completely
Label with date and "peroxidase check."

2. Checking activity of catalase

Pipette 1.0 ml DI water into a 1.5 ml glass vial
Add 100 µl 1.0 mM H_2O_2 solution
Add 100 µl catalase solution
Mix completely
Add 200 µl conditioning reagent
Add 200 µl fluorescent reagent
Close cap and mix completely
Label with date and "catalase check."

NOTES

1. Follow the aliquot procedures for blank and DI samples exactly like the procedures for fog samples

2. Make a separate DI blank for each batch of DI used at each cleaning

3. Duplicates of all aliquots should be performed for approximately 10% of the samples

APPENDIX B – 2007 CLOUDWATER DATA TABLE

Sample Name	Collection Time	Sample Weight (g)	pH	H2O2 µM	HCHO µM	S(IV) µM	Fe µg/L	Mn µg/L	SO4= µN	NO3- µN	NH4+ µN	Ca2+ µN
3.23.1	2007-3-23 04:30-05:30	150.00	3.02	5.40	53.69	29.88	1369.00	356.30	2728.88	4452.28	3775.18	2896.36
3.23.2	2007-3-23 05:30-06:30	150.00	2.86	1.89	43.18	6.31	861.20	222.40	2318.78	3197.27	3266.53	754.14
3.23.3	2007-3-23 06:30-07:30	150.00	2.69						5055.11	6265.78	6134.87	2061.98
3.23.4	2007-3-23 10:50-12:50	189.07	3.2	1.12	49.47	8.36	944.20	188.40	1629.42	2117.23	2066.69	1270.96
3.23.5	2007-3-23 12:50-13:50	342.50	3.33	2.93	21.66	2.98	511.70	97.16	1199.28	825.64	1560.13	256.05
3.23.6	2007-3-23 13:50-14:50	195.08	3.32	3.00	23.07	2.67	402.30	103.10	1463.84	561.42	1354.23	245.24
3.23.7	2007-3-23 14:50-15:50	147.57	3.27	1.90	24.61	2.16	576.80	124.80	1706.72	511.80	1407.26	203.50
3.23.8	2007-3-23 15:50-16:50	108.95	3.22	0.10	37.48	2.09	868.80	144.70	2110.72	518.06	1619.02	328.23
3.23.9	2007-3-23 16:50-17:50	123.50	3.27	0.92	29.84	1.43	641.90	111.90	1803.79	724.38	1977.75	118.59
3.23.10	2007-3-23 17:50-19:40	103.00	3.18	2.02	47.02	1.74	968.40	159.20	2206.33	940.61	1986.21	228.74
3.23.11	2007-3-23 19:40-22:40	298.90	3.04	4.32	37.51	1.27	761.40	157.40	1452.77	506.45	1206.45	72.57
3.29.1	2007-3-29 08:00-09:00	91.67	7.16	1.00	25.18	195.46	129.90	180.10	2245.63	988.68	2054.12	2184.07
3.29.2	2007-3-29 09:00-10:30	143.29	7.58	0.96	22.29	65.33	100.50	43.88	1022.01	370.23	1021.63	642.13
3.30.1	2007-3-30 16:30-17:50	141.79	5.15	0.62	19.08	17.38	285.90	272.40	2572.45	1306.42	2456.77	1321.68
3.30.2	2007-3-30 17:50-19:00	150.27	3.9	1.00	11.64	6.77	188.80	123.90	1291.21	595.70	1384.85	355.15
3.30.3	2007-3-30 19:00-19:50	148.60	3.82	0.31	10.99	5.92	96.65	47.43	1045.76	474.27	1243.86	95.18
3.30.4	2007-3-30 19:50-21:20	139.71	3.86	0.29	9.79	7.39	72.66	26.76	840.70	361.61	1102.96	53.86
4.15.1	2007-4-15 07:53-09:03	370.78	5.92	1.76	6.76	21.60	105.50	19.93	332.94	124.23	267.78	341.91
4.15.2	2007-4-15 09:03-10:10	413.78	4.52	5.23	12.67	7.54	95.15	12.55	245.79	72.85	213.33	185.99
4.15.3	2007-4-15 10:10-10:56	352.83	4.51	3.48	12.51	13.62	72.60	10.10	236.99	71.07	221.14	176.11
4.15.4	2007-4-15 10:56-12:00	322.53	4.68	3.16	13.63	13.54	103.30	14.87	403.65	101.06	280.22	270.23
4.15.5	2007-4-15 12:00-13:00	204.20	4.99	3.48	12.46	7.08	165.30	34.92	725.07	159.88	552.34	402.42
4.15.6	2007-4-15 13:00-14:00	259.80	4.69	1.78	11.95	10.72	95.83	21.14	440.72	110.54	361.11	258.79
4.15.7	2007-4-15 14:00-15:00	512.00	4.71	2.18	17.29	8.86	45.28	10.91	229.95	76.39	237.33	132.12
4.15.8	2007-4-15 15:00-16:00	130.90	6.63	3.85	22.01	31.78	39.29	7.26	223.32	82.23	235.14	252.82
4.17.1	2007-4-17 23:00-8:00	120.68	7.64	3.80	31.91	23.69	65.29	55.42	1110.63	522.97	1139.18	625.02
4.18.1	2007-4-18 17:30-18:30	230.50	7.26	4.62	36.53	275.18	118.80	93.05	2712.55	864.62	2279.58	1155.55

Sample Name	Collection Time	Sample Weight (g)	pH	H2O2 µM	HCHO µM	S(IV) µM	Fe µg/L	Mn µg/L	SO4= µN	NO3- µN	NH4+ µN	Ca2+ µN
4.18.2	2007-4-18 19:30-19:30	229.70	7.15	6.94	28.47	238.98	94.10	67.40	2002.03	602.46	1710.48	969.30
4.18.3	2007-4-18 19:30-20:30	205.83	6.95	2.78	23.40	167.92	73.98	58.01	1613.40	520.89	1598.09	709.31
4.18.4	2007-4-18 20:30-21:30	207.50	6.91	3.32	19.13	93.52	58.31	56.73	1317.42	414.18	1480.71	531.81
4.18.5	2007-4-18 21:30-22:30	423.40	6.85	2.11	17.00	31.66	77.89	48.48	1048.95	354.88	1269.90	408.99
4.18.6	2007-4-18 22:30-23:30	426.66	6.67	4.42	14.79	25.70	61.89	46.09	975.94	318.98	1197.54	330.83
4.18.7	2007-4-18 23:30-00:30	381.00	6.63	3.45	12.88	32.94	42.65	35.53	836.43	254.27	1102.40	269.16
4.18.8	2007-4-18 00:30-01:30	291.60	5.97	3.11	13.46	21.75	77.22	49.26	1197.92	408.05	1402.59	359.04
4.18.9	2007-4-18 01:30-02:30	60.00	6.5				52.27	64.92	1566.13	584.98	1566.40	633.15
4.20.1	2007-4-20 23:00-24:00	66.16	6.69				306.30	473.70	6438.68	3043.86	5271.06	3884.23
4.21.1	2007-4-21 9:00-10:00	100.00	6.53	3.17	118.67	273.64	569.00	1645.00	9733.92	7773.91	8060.42	9053.89
6.20.1	2007-6-19 19:00-0:00	238.83	5.56	3.59	21.98	139.00	310.40	197.10	2760.55	1692.78	3298.45	1626.40
6.20.2	2007-6-20 0:00-1:00	186.61	5.11	4.05	4.46	28.50	39.70	17.94	610.11	211.47	822.59	147.98
6.20.3	2007-6-20 1:00-2:00	182.61	4.93	3.82	4.34	8.65	44.75	15.86	438.84	178.30	680.49	106.71
6.20.4	2007-6-20 2:00-3:00	175.00	4.72	3.20	7.25	18.38	72.74	21.79	482.25	223.50	748.39	102.52
6.20.5	2007-6-20 7:28-8:28	95.00	5.46	6.84	3.27	4.29	4.07	7.62	183.13	36.62	220.76	65.90
6.20.6	2007-6-20 8:28-9:30	135.00	5.71	5.72	2.92	6.56	0.00	1.92	92.39	22.62	151.13	21.94
6.20.7	2007-6-20 9:30-10:30	120.00	5.47	5.34	3.34	12.09	0.00	1.82	98.90	22.54	120.79	16.56
6.20.8	2007-6-20 10:30-12:48	163.00	5.1	3.24	3.47	27.31	30.36	2.42	108.42	22.11	117.78	18.09
6.20.9	2007-6-20 12:48-14:02	160.00	5.39	4.88	4.46	18.81	0.00	1.21	93.60	23.32	117.65	31.10
6.20.10	2007-6-20 14:02-15:30	160.83	5.12	2.47	4.56	26.43	0.00	0.73	101.51	21.13	109.60	11.76
6.20.11	2007-6-20 15:30-16:30	145.33	5.23	3.12	3.18	14.54	0.00	0.62	78.46	22.29	94.48	14.40
6.20.12	2007-6-20 16:30-17:30	195.83	5.09	3.00	8.37	7.98	0.00	0.76	70.65	23.10	75.76	20.35
6.20.13	2007-6-20 17:30-18:30	88.00	5.23	3.31	3.47	21.69	0.00	1.41	100.42	22.56	117.13	24.05
6.20.14	2007-6-20 18:30-19:30	68.00	5.2				0.00	0.84	100.51	24.94	107.61	20.82
6.20.15	2007-6-20 19:30-20:30	113.83	5.24	3.22	9.41	17.91	0.00	0.80	91.35	25.73	96.94	22.01
6.20.16	2007-6-20 20:30-21:30	222.77	4.83	5.03	5.33		0.00	0.90	68.57	30.09	79.43	15.91
6.20.17	2007-6-20 21:30-22:30	229.62	4.58	4.12	5.86	5.84	0.00	1.23	79.91	39.68	91.88	19.77
6.21.1	2007-6-21 11:00-13:20	489.40	3.72	0.84	5.98	0.32	40.29	6.08	313.68	133.29	274.02	39.84
6.21.2	2007-6-21 13:20-14:50	224.26	4.08	2.82	4.21	0.29	25.84	4.61	422.79	135.46	270.11	250.45
6.21.3	2007-6-21 14:50-16:60	162.34	3.33	6.56	5.57	0.00	55.42	7.60	690.17	224.59	539.15	128.07
6.21.4	2007-6-21 16:50-17:50	187.57	3.37	2.28	9.16	11.65	37.55	9.91	856.84	192.39	558.63	155.32

Sample Name	Collection Time	Sample Weight (g)	pH	H2O2 µM	HCHO µM	S(IV) µM	Fe µg/L	Mn µg/L	SO4= µN	NO3- µN	NH4+ µN	Ca2+ µN
6.22.2	2007-6-22 20:25-21:55	255.22	3.32	5.98	16.86	32.61	330.00	25.90	1837.61	296.19	1776.69	157.86
6.22.3	2007-6-22 21:55-22:55	509.43	3.55	8.87	5.78	10.42	20.12	6.60	638.40	195.76	520.30	82.39
6.22.4	2007-6-22 22:55-23:55	440.48	3.87	8.22	7.61	3.84	0.00	1.95	205.86	50.85	185.29	79.81
6.23.1	2007-6-23 09:35-11:35	434.73	3.31	3.03	7.92	13.51	90.48	3.83	822.32	267.89	505.58	116.05
6.23.2	2007-6-23 11:35-13:35	215.69	3.04	11.46	10.24	5.82	314.30	9.38	1396.43	290.07	817.45	105.16
6.23.3	2007-6-23 13:35-16:35	242.46	3.28	1.22	20.39	31.13	499.70	30.04	3287.70	754.72	3758.22	344.46
6.23.4	2007-6-23 16:35-18:35	262.95	3.59	6.92	21.52	29.97	204.10	22.34	3421.17	873.27	4831.90	257.04
6.26.1	2007-6-26 16:25-18:55	272.02	6.86	8.18	49.39	16.99	125.30	146.40	4626.23	1644.29	6140.75	959.48
6.26.2	2007-6-26 18:55-20:55	320.72	6.86	28.01	35.63	27.12	20.23	55.44	1956.85	554.79	2789.11	290.54
6.26.3	2007-6-26 20:55-21:55	327.45	6.84	50.38	30.51	13.48	0.00	29.92	1194.29	382.06	1902.84	150.58
6.26.4	2007-6-26 21:55-22:55	309.83	6.72	58.32		5.81	0.00	26.01	969.04	339.44	1862.35	111.50
6.26.5	2007-6-26 22:55-23:55	287.61	6.5	32.70	51.49	39.68	0.00	27.53	1295.37	377.04	1821.52	152.98
6.26.6	2007-6-26 23:55-0:55	238.64	6.81	24.49	46.95	42.21	4.28	23.20	1045.83	315.34	1600.59	141.62
6.26.7	2007-6-27 00:55-01:55	236.80	6.36	9.72	56.87	57.41	0.00	28.73	1102.38	276.28	1349.13	108.59
6.26.8	2007-6-27 01:55-02:55	266.30	6.68	10.20	36.53	40.10	0.00	25.76	906.80	257.16	1426.76	105.53
7.1.1	2007-7-1 09:30-11:11	367.95	3.74	5.77	4.22	5.16	36.45	9.00	613.42	193.53	652.07	30.33
7.1.2	2007-7-1 11:11-13:41	275.63	3.72	9.17	6.64	5.16	68.32	15.11	848.75	278.37	912.20	86.92
7.1.3	2007-7-1 13:41-15:41	211.00	3.82	8.27	7.77	11.51	106.70	20.01	1246.78	331.25	1515.80	147.10
7.1.4	2007-7-1 15:41-17:41	95.00	3.71	11.48	4.99	0.00	139.60	10.89	566.22	121.78	508.00	71.97
7.1.5	2007-7-1 17:41-20:00	175.00	4.11	12.28	4.21	1.50	46.78	4.04	228.96	50.25	211.60	21.32
7.12	2007-7-12 09:30-12:30	175.00	4.54	9.70	21.29	14.60	30.03	34.54	1859.37	465.84	2443.39	263.87
7.14.1	2007-7-14 06:15-23:15	205.00	4.30				160.80	206.80	5061.76	1385.45	5847.15	678.32
7.16.1	2007-7-16 20:10-22:10	561.71	4.90	11.14	61.01	69.22	42.60	29.91	2633.17	433.59	3551.50	198.15
7.16.2	2007-7-16 22:10-23:30	503.96	3.93	6.32	17.67	35.74	48.84	15.42	1154.45	287.45	1530.13	134.08
7.16.3	2007-7-16 23:30-00:30	233.72	4.41	58.27	10.45	1.26	41.07	23.67	1088.47	220.35	1376.95	95.98
7.16.4	2007-7-17 00:30-02:00	194.07	5.96	69.60	8.79	0.11	135.00	31.41	1333.77	236.16	1469.66	129.30
7.16.5	2007-7-17 02:00-03:30	244.31	3.84	87.79	9.46	0.03	91.09	20.71	1064.37	217.96	1261.66	109.53
7.16.6	2007-7-17 03:30-06:30	513.70	3.91	71.07	10.62	0.00	60.44	19.88	1088.88	263.38	1382.18	70.61
7.17.1	2007-7-17 6:40-8:40	398.09	6.54	101.06	11.09	1.46	12.64	33.25	970.65	191.69	1390.80	208.21
7.17.2	2007-7-17 8:40-9:00	100.00	4.52						674.46	184.43	765.52	157.76

Sample Name	Collection Time	Sample Weight (g)	pH	H2O2 µM	HCHO µM	S(IV) µM	Fe µg/L	Mn µg/L	SO4= µN	NO3- µN	NH4+ µN	Ca2+ µN
7.17.3	2007-7-17 13:15-15:15	358.65	5.78	16.74	68.73	2.84	34.12	126.90	3687.32	677.15	4384.59	382.83
7.17.4	2007-7-17 15:15-17:15	295.90	6.11	15.58	63.85	0.00	169.70	89.73	3388.53	618.71	4303.60	390.28
7.17.5	2007-7-17 17:15-19:15	520.21	5.97	14.28	21.95	0.55	2.10	54.00	2342.59	380.28	2739.99	267.08
7.17.6	2007-7-17 19:15-21:15	534.00	6.04	12.30	36.28		0.00	46.39	1529.68	255.18	1893.19	187.57
7.17.7	2007-7-17 21:15-23:15	528.96	5.92	7.67	51.19		0.00	29.68	1156.64	237.70	1531.09	155.62
7.17.8	2007-7-17 23:15-0:45	512.31	5.29	4.09	19.55		0.00	15.34	1133.27	164.42	1371.83	94.51
7.18.1	2007-7-18 06:05-07:05	524.00	5.56	5.07	23.54		0.00	18.32	603.51	77.27	713.97	40.63
7.18.2	2007-7-18 07:05-08:10	520.00	5.56	7.84	34.51		0.00	19.58	751.66	74.87	812.84	37.96
7.18.3	2007-7-18 08:10-09:10	520.00	6.17	6.54	49.22		0.00	27.68	799.79	77.97	957.58	55.78
7.18.4	2007-7-18 09:10-11:10	520.00	6.26	7.11	53.99		0.00	39.42	938.92	127.59	1368.70	56.65
7.18.5	2007-7-18 11:10-12:10	436.00	6.43	6.68	65.58		0.00	37.36	1187.58	155.80	1727.36	97.89
7.18.6	2007-7-18 12:10-14:10	512.31	6.44	6.76	52.53		0.00	39.40	1257.96	185.51	1724.56	166.33
7.18.7	2007-7-18 14:10-15:20	379.15	6.60	9.60	40.50		0.00	33.70	1281.66	193.56	1682.21	214.47
7.18.8	2007-7-18 15:20-16:20	385.06	6.38	6.78	17.80		0.00	29.03	1231.57	165.50	1650.55	175.99
7.18.9	2007-7-18 16:20-17:20	433.39	6.88	5.64	29.57		0.00	24.11	980.72	153.35	1470.81	146.05
7.18.10	2007-7-18 17:20-18:30	512.31	6.55	3.51	39.46		0.00	19.68	1016.14	112.35	1350.95	130.94

APPENDIX C – 2008 CLOUDWATER DATA TABLE

Sample Name	Start Time	End Time	Sample Weight (g)	pH	TOC ppmC	H2O2 µM	HCHO µM	S(IV) µM	Fe µg/L	Mn µg/L	SO4= µN	NO3- µN	NH4+ µN	Ca2+ µN
TC032908A01	14:00	14:20	9.01	3.22		4.5965	30.938	11.73	1685.27	148.007	1188.41	1037.65	2043.90	499.71
TC032908BLK	17:00				0.044	6.0902	1.3807	1.506	50.38	1.814	3.56	1.84	0.03	4.01
TC040608A01	1:00	2:00	1.2	5.85				N						
TC040608A02	7:00	12:00						N						
TC040808A01	22:30	23:30	168.8	4.59	1.537	4.9609	5.1536	2.005	328.35	23.508	313.15	66.95	270.65	49.81
TC040808A02	23:30	1:00	156.37	5.4		26.4892	5.143	2.005	622.87	33.859	375.20	76.46	351.99	82.32
TC040908A01	1:00	3:00	60.85	6.35	3.321		5.4936	4.581	1561.74	93.161	672.89	206.62	563.27	307.88
TC040908A02	3:00	5:00	224.86	5.09	3.299	4.0008	5.4628	3.168	624.96	33.294	429.03	84.64	383.56	91.03
TC040908A03	5:00	7:00	53.06	4.4		4.3216	7.688	15.13	614.56	29.233	522.99	155.57	498.04	85.66
TC040908A04	7:00	9:00	102.37	4.05	2.67	2.9201	6.4298	18.04	395.23	17.148	338.58	77.85	278.94	36.07
TC040908A05	9:00	11:00	14.95	5.08	5.985	3.1352	6.34	16.38	447.72	18.673	272.04	51.97	267.80	46.68
TC040908A06	11:00	14:00	8.65	5		2.9978	10.648	10.81	2012.51	74.114	594.25	165.04	682.82	115.27
TC040908A07	14:00	16:00	139.93	3.69	7.321	3.5202	10.036	4.165	262.57	24.771	752.90	161.09	546.80	99.00
TC040908A08	16:00	17:30	76.68	3.57	6.582	7.4208	10.919	6.243	511.63	26.541	886.90	168.71	598.04	82.77
TC040908BLK	18:00				0.752	7.4478	1.8378	1.506	44.76	2.621	3.09	-1.64	1.57	2.48
TC041908A01	22:00	23:00	397.25	5.82	2.739	9.972	6.159	16.67	140.82	10.105	114.12	47.40	174.20	29.29
TC041908A02	23:00	0:00	449.72	5.43	1.696	15.9296	4.6051	10.52	81.78	28.648	56.25	21.02	86.41	20.60
TC042008A01	0:00	1:00	436.13	4.57	2.242	7.956	6.0166	5.268	132.61	10.369	134.96	64.46	163.80	26.02
TC042008A02	1:00	2:00	432.56	4.66	1.646	7.4828	3.9883	8.732	112.88	7.395	84.27	27.90	92.59	15.79
TC042208A01	13:00	14:00	47.61	3.53	11.74	9.0477	20.174	20.54	509.45	61.134	755.06	450.90	727.49	148.34
TC042208A02	14:00	15:00	52.57	3.42	12.71	5.1263	20.824	25.89	435.96	62.536	895.40	513.36	887.17	130.05
TC042208A03	15:00	16:00	18.99	3.51	13.67	3.1888	20.129	33.71	618.36	78.98	1150.28	620.15	1231.27	141.29
TC042208A04	16:00	17:00	0.75	N				N						
TC042208A05	17:00	18:00	2.69	3.95				N						
TC042208BLK	18:30				1.524	5.8022	1.1355	1.332	65.32	2.585	3.74	-1.18	3.63	2.93
TL032908BLK					-0.009	6.5921	1.4031	N/A	44.6	2.189	5.96	3.75	6.14	5.80
TL040608A01	1:00	2:00	7.59	6.58		9.143	36.681	99.32	1796.58	165.432	1906.87	1340.95	2657.00	648.54
TL040608A02	7:00	8:00	79.9	4.51	9.437	5.1263	22.812	5.495	1111.2	88.479	815.51	556.30	1149.60	275.61

Sample Name	Start Time	End Time	Sample Weight (g)	pH	TOC ppmC	H2O2 µM	HCHO µM	S(IV) µM	Fe µg/L	Mn µg/L	SO4= µN	NO3- µN	NH4+ µN	Ca2+ µN
TL040608A03	8:00	9:00	82.22	4.37		5.1344	18.833	9.899	1105.51	93.411	764.43	434.51	982.55	230.83
TL040608A04	9:00	10:00	102.07	4.18	8.419	4.5273	15.869	8.237	652.64	67.237	713.56	391.99	845.95	201.88
TL040608A05	10:00	11:00	50.22	4.31	9.485	5.4568	16.431	6.658	732.51	84.69	838.61	393.46	1001.93	222.96
TL040608A06	11:00	12:00	25.4	4.42	13.51	6.5982	16.598	9.982	928.82	137.259	1224.11	527.28	1348.46	391.65
TL040608BLK	18:00			5.4	0.301	3.5169	1.8717	4.83	123.75	7.489	37.68	12.50	17.94	25.53
TL040808A01	22:30	23:30	72.29	4.73	2.309	2.567	6.3201	2.753	619.71	43.1	431.16	122.36	351.31	167.48
TL040808A02	23:30	1:00	38.04	5.57	2.141	31.1252	5.466	4.082	699.63	39.786	397.16	107.37	329.68	158.18
TL040908A01	1:00	3:00	15.72	6.24	6.468		7.4239	8.237	1642	95.107	759.99	285.83	601.28	404.31
TL040908A02	3:00	5:00	75.49	5.1	3.189	3.7089	5.8266	2.503	941.52	57.055	532.51	146.57	410.72	217.39
TL040908A03	5:00	7:00	76.39	4.43		5.0703	9.1671	17.96	952.82	49.115	596.07	177.86	491.65	196.24
TL040908A04	7:00	9:00	106.71	4.09	2.289	2.3505	7.7147	18.29	267.95	19.978	406.22	96.44	305.46	85.23
TL040908A05	9:00	11:00	50.11	4.45		2.25	7.073	9.401	180.86	17.101	363.29	73.12	305.72	79.68
TL040908A06	11:00	14:00	38.21	4.71	5.181	3.5245	11.555	10.81	481.57	32.268	614.23	174.61	602.05	171.79
TL040908A07	14:00	16:00	86.49	3.71	6.38	7.0628	11.506	9.733	336.43	31.428	871.67	205.68	609.82	242.34
TL040908A08	16:00	17:30	57.21	3.6	6.851	6.3665	11.411	7.24	447.33	29.305	924.20	186.41	600.85	172.17
TL040908BLK	18:00				-0.082	9.1954	1.4935	0.841	58.2	2.494	3.82	-1.30	1.44	3.18
TL041908A01	22:00	23:00	92.28	6.2	3.708	8.406	7.5194	23.45	303.43	21.232	213.52	79.03	274.70	76.51
TL041908A02	23:00	0:00	83.73	5.73	2.177	11.2972	5.3219	18.38	155.68	9.481	101.39	35.26	140.84	27.07
TL042008A01	0:00	1:00	127.65	4.56	2.399	5.418	6.0166	3.085	163.27	10.447	144.08	67.69	178.94	27.46
TL042008A02	1:00	2:00	92.67	4.57	2.123	3.0468	5.0898	10.96	162.77	11.343	137.24	49.73	156.80	27.79
TL042208A01	13:00	14:00	56.08	3.51	10.64	5.008	21.141	17.63	631.83	76.409	879.92	530.86	789.65	232.91
TL042208A02	14:00	15:00	61.81	3.47	12.25	4.1051	22.75	22.53	563.05	83.496	1007.40	589.76	975.53	210.80
TL042208A03	15:00	16:00	29.6	3.5	13.2	1.8428	24.542	35.25	509.13	83.388	1178.59	624.57	1228.93	203.30
TL042208A04	16:00	17:00	14.09	3.63	20.181	3.7774	33.807	46.3	1097.65	158.309	1919.10	1062.97	2109.82	413.54
TL042208A05	17:00	18:00	5.49	3.81			34.197	30.59	1289.97	157.564	1820.28	1078.26	2288.46	389.92
TL042208BLK	18:30				0.833	5.8778	1.083	2.348	78.5	3.29	4.25	-1.64	0.82	2.58
TS032908BLK					-0.048	6.5122	1.8757	0.01	46.48	4.814				
TS040608A01	1:00	2:00	12.81	5.81	22.539	9.07	42.239	119	1288.29	156.342	2060.95	1459.97	3436.32	497.56
TS040608A02	7:00	8:00	73.42	4.63		7.1397	34.936	33.42	921.5	116.602	1473.36	810.85	2076.51	325.75
TS040608A03	8:00	9:00	79.92	4.45	17.86	5.4181	25.717	22.53	1160.3	89.629	1157.79	465.62	1593.55	178.00
TS040608A04	9:00	10:00	96.94	4.32	11.4	4.6171	17.27	9.65	545.11	44.041	731.88	295.64	1032.44	52.47

Sample Name	Start Time	End Time	Sample Weight (g)	pH	TOC ppmC	H2O2 µM	HCHO µM	S(IV) µM	Fe µg/L	Mn µg/L	SO4= µN	NO3- µN	NH4+ µN	Ca2+ µN
TS040608A05	10:00	11:00	69.37	4.48	12.7	5.4975	15.525	10.56	447.96	44.11	803.04	257.84	1120.47	42.05
TS040608A06	11:00	12:00	29.45	4.3	17.26	6.4155	17.799	6.409	510.14	77.947	1304.51	352.41	1607.38	75.40
TS040608BLK	18:00			5.25	1.209	4.1681	1.9495	3.75	164.19	10.368	45.69	25.76	41.62	27.61
TS040808A01	22:30	23:30	78.98	4.66	3.181	5.0542	6.248	5.079	470.01	43.15	501.90	109.11	438.68	121.90
TS040808A02	23:30	1:00	108.83	5.05		18.9756	5.6172	2.337	482.36	31.085	385.15	72.43	351.02	75.35
TS040908A01	1:00	3:00	57.29	5.48	3.771		5.665	3.5	1082	65.775	589.55	157.14	514.89	206.02
TS040908A02	3:00	5:00	165.42	4.7	2.445	4.9437	5.6911	3.833	624.24	32.308	478.16	81.85	432.64	87.00
TS040908A03	5:00	7:00	186	4.25	2.536	6.1322	6.4792	12.31	377.42	24.277	437.15	120.80	401.00	51.85
TS040908A04	7:00	9:00	179.37	4.04	2.005	2.8882	6.4992	16.55	215.21	13.03	329.55	75.27	262.44	26.56
TS040908A05	9:00	11:00	92.54	4.34	2.356	0.7028	6.3917	7.739	146.02	10.641	312.42	61.79	297.25	20.66
TS040908A06	11:00	14:00	132.09	4.38	6.304	3.2852	11.184	5.246	224.42	17.536	549.73	141.46	655.43	36.73
TS040908A07	14:00	16:00	169.65	3.61	7.389	3.1835	10.673	4.996	248.46	15.785	712.29	157.68	552.24	29.80
TS040908A08	16:00	17:30	87.64	3.55	7.282	4.8152	11.485	5.495	317.97	16.637	825.54	156.40	572.76	25.78
TS040908BLK	18:00				0.689	9.221	1.88	0.176	54.34	2.009	4.00	-1.62	1.58	2.78
TS041908A01	22:00	23:00	72.39	5.41	5.285	1.07	9.6512	25.63	153.69	17.47	129.91	39.26	348.54	35.02
TS041908A02	23:00	0:00	62.52	5.36	2.704	6.4388	6.9471	20.47	108.18	9.562	118.43	30.18	172.65	16.41
TS042008A01	0:00	1:00	84.79	4.72	2.841	4.512	6.4479	5.482	130.55	10.277	157.12	46.77	199.85	20.36
TS042008A02	1:00	2:00	100.19	4.56	1.916	4.0052	5.392	7.659	100.46	159.086	112.61	28.82	125.61	14.03
TS042208A01	13:00	14:00	76.11	3.46	14.01	2.7839	20.31	13.24	359.5	36.802	773.54	394.88	715.98	27.62
TS042208A02	14:00	15:00	85.31	3.4	14.24	2.4372	20.411	20.87	299.45	39.012	825.59	439.92	801.95	25.15
TS042208A03	15:00	16:00	52.7	3.41	17.22	3.6833	22.337	31.75	268.23	51.339	1086.11	578.23	1173.17	27.46
TS042208A04	16:00	17:00	45.28	3.5	30.29	4.7549	31.042	42.33	728.3	86.138	1748.88	981.98	2278.39	70.04
TS042208A05	17:00	18:00	10.32	3.68	23.535	4.7751	38.609	28.41	993.89	112.65	1988.05	1156.10	2860.03	146.06
TS042208BLK	18:30				0.858	9.0855	1.1862	1.589	54.76	2.318				
TC061208BLK	11:00		232.88		0.494	14.105	0.8286	0.914	36.773	2.168	3.23		1.91	3.31
TC061608A01	2:00	3:00	49.09	4.34	36.9	3.8552	48.626	139.7	2356.41	46.601	3010.69	1773.46	4443.99	556.01
TC061608A02	3:00	5:00	48.83	3.66		5.3381	30.128	150.3	4360.67	34.269	4228.25	3855.48	6424.60	702.59
TC061608A03	5:00	6:00	65.47	3.68	27.19	38.154	32.576	126.4	2722.65	151.546	2121.53	1366.85	2713.68	364.72
TC061608A04	6:00	7:30	20.88	3.8	33.47	5.0482	29.185	131.9	1164.51	40.725	3355.90	2093.41	3884.78	497.67
TC061608B01	17:00	18:00	133.52	4.22	8.02	41.025	15.642	33.62	224.936	27.571	709.13	232.55	659.04	88.41
TC061608B02	18:00	19:00	190.04	4.01	9.897	-0.0101	18.625	45.97	236.388	15.13	707.20	248.44	652.78	34.05

Sample Name	Start Time	End Time	Sample Weight (g)	pH	TOC ppmC	H2O2 µM	HCHO µM	S(IV) µM	Fe µg/L	Mn µg/L	SO4= µN	NO3- µN	NH4+ µN	Ca2+ µN
TC061608B03	19:00	20:00	204.91	4		0.9378	19.654	30.14	251.231	12.94	707.75	338.65	705.14	22.86
TC061608B04	20:00	21:00	184.79	4.13	10.97	0.4966	21.654	28.53	276.982	24.81	724.58	322.70	705.47	21.24
TC061608B05	21:00	22:00	264.76	4.48	6.977	0.0574	12.132	31.46	170.442	16.395	485.68	205.11	529.31	12.46
TC061608B06	22:00	23:00	160.96	4.07	10.32	0.2554	19.856	24.19	291.379	26.982	653.95	352.17	676.65	24.54
TC061608B07	23:00	0:00	268.14	4.34	6.373	-0.2374	15.963	16.95	205.978	19.355	448.91	217.80	471.25	21.09
TC061608B08	0:00	2:00	556.05	3.87	3.873	0.8685	5.6849	23.46	202.951	14.431	469.32	159.67	265.48	17.88
TC061608B09	2:00	3:00	259.01	3.99	2.72	3.2934	3.1657	15.72	161.712	9.406	361.73	113.29	204.61	9.80
TC061608B10	3:00	5:00	288.79	4.38	3.253	2.3903	4.1617	12.34	110.378	8.75	285.49	98.93	246.95	8.04
TC061608B11	5:00	6:00	317.78	4.07	4.212	0.5165	6.1878	26.35	111.368	8.412	292.34	159.07	231.81	4.75
TC061608B12	6:00	7:00	259.36	3.97	4.727	-0.1781	5.1535	34.81	151.683	8.813	350.54	182.66	253.50	5.35
TC061608B13	7:00	8:15	172.04	3.85	4.075	8.7369	6.7619	23.46	50.061	10.197	390.38	143.83	197.96	4.89
TC061608B14	9:00	10:30	57.25	3.1	24.65	9.8838	6.1856	20.67	4395.746	95.546	2388.88	1078.92	1270.72	52.01
TC061608B15	11:00	13:00	122.51	3.01	21.45	2.8798	9.3684	34.15	4110.52	122.919	2820.54	1302.91	1487.10	80.12
TC061608B16	13:00	15:00	146.38	2.91	25.93	1.5471	3.1874	39.74	4744.42	153.139	3806.25	1485.92	1941.06	191.19
TC061608BLK	9:00		156.68		0.665	16.396	0.7449	0.953	55.001	6.236	5.04	4.59	-0.25	6.40
TC061808A01	21:00	22:00	70.77	3.12	47.89	5.0484	35.189	36.76	2337.8	154.302	7796.60	3948.17	9118.23	483.49
TC061808A02	22:00	23:00	50.71	2.95	45.35	5.0011	39.148	34.52	3543.1	170.035	6496.45	3806.98	8119.72	418.39
TC061808A03	23:00	0:00	155.12	3.15	26.27	3.7301	25.819	25.28	1490.2	66.575	2673.19	1619.20	2946.70	225.29
TC061808A04	0:00	1:00	226.42	3.32	23.51	1.3687	21.465	30.37	975.37	37.352	1775.32	1122.08	1830.34	206.79
TC061808A05	1:00	2:00	303.66	3.38	50.04	6.3491	31.269	22.92	609.15	34.387	947.90	662.63	1217.47	124.24
TC061808A06	2:00	3:00	316.53	3.2	108.1	12.73	39.984	36.71	604.2	30.815	1076.04	751.46	1360.23	90.77
TC061808A07	3:00	4:00	277.55	2.96	196.8	16.055	58.064	29.73	1010.2	38.764	1607.84	1118.85	1864.51	93.23
TC061808A08	4:00	6:00	554.72	3.18	99.83	22.623		12.35	586.01	21.799	1034.78	705.83	1235.17	53.77
TC061808A09	6:00	8:00	155.82	3.34	48.47	232.12	31.168	3.004	616.03	19.92	1022.80	625.49	1253.66	47.23
TC061808A10BLK	17:00				1.416	19.873	1.1254	0.313	54.77	3.37	6.57	6.00	4.70	3.28
TC061808BLK	8:00		150.76		0.731	7.7615	0.3648	0.645	82.631	5.55	12.10	5.15	7.48	4.11
TC061908A01	19:00	21:00	232.03	4.95	19.01	3.0004	9.8641	59.18	824.53	61.182	2403.92	1397.76	3500.66	366.87
TC061908A02	21:00	23:00	363.6	3.92	17.45	1.2461	7.1566	66.43	710.33	45.367	1516.55	1108.78	2108.72	316.39
TC061908A03	23:00	0:30	329.56	4.51	18.97	0.5307	5.8168	73.52	596.72	36.782	1541.83	1052.91	2025.59	276.35
TC061908A04	0:30	2:00	343.74	4.33	13.94	2.934	6.1575	47.98	310.78	31.744	829.96	472.84	1196.78	161.13
TC061908A05	2:00	3:30	329.99	3.65	16.52	319.328	7.6163	23.14	387.23	23.764	763.31	339.26	846.29	90.48

Sample Name	Start Time	End Time	Sample Weight (g)	pH	TOC ppmC	H2O2 µM	HCHO µM	S(IV) µM	Fe µg/L	Mn µg/L	SO4= µN	NO3- µN	NH4+ µN	Ca2+ µN
TC061908A06	3:30	5:00	294.42	3.32	29.7	176.96	9.1318	12.95	517.86	27.967	969.38	461.61	1000.20	65.42
TC061908A07	5:00	7:00	483.77	3.48	44.73	11.473	13.167	6.988	532.52	29.492	1077.48	524.82	1465.31	78.95
TC061908A08	7:00	8:15	72.6	3.16	40.83	41.798	21.986	7.643	1063.38	63.796	1822.08	763.11	2098.21	134.41
TC061908A09BLK	12:00				1.385	13.277	0.9129	0.344	110.12	3.977	4.86	4.33	4.71	4.35
TC062008A01	16:45	17:45	82.47	3.25	22.57	25.923	6.1968	43.46	1705.03	40.633	1840.90	518.56	1730.96	39.60
TC062008A02	19:00	19:20	9.61	3.19		3.918	7.2684	27.63	1450.6	79.504	4143.15	877.01	3477.72	52.45
TC062108A01	9:00	9:40	78.41	2.86	47.1	10.282	11.684	34.29	1578.73	94.307	3861.70	1273.79	3022.23	194.19
TC062108BLK	12:00				0.822	11.8	0.8973	0.995	110.71	6.531	20.27	6.49	12.83	3.57
TC062308BLK	14:00				0.537	15.881	0.6897	0.431	53.84	2.201			-0.37	2.38
TC062508A01	23:10	0:00	117.48	6.61	20.51	6.7545	8.1684	25.97	953.29	76.138	4058.18	876.42	4304.55	465.08
TC062508A02	0:00	0:45	43.77	6.72	20.43	8.3722	7.0684	23.31	1238.49	73.452	4500.97	906.54	4883.78	482.14
TC062508A03BLK	9:00				0.999	9.9216	0.9874	0.846	104.25	5.104	73.52	16.75	57.14	26.13
TC070208A01	4:05	5:00	96.45	3.44	18.46	0.9218	6.5863	56.11	880.56	79.706	3257.37	972.17	3375.86	414.05
TC070208A02	5:00	5:50	22.53	3.42	19.2	4.5657	4.0648	24.73	684.5	65.492	4248.79	993.39	3857.14	305.39
TC070208BLK	12:00		149.56		0.723	16.563	0.8763	1.017	50.41	2.513	5.37	4.66	4.71	2.60
TC070308A01	20:00	22:00	90.1	5.42	70.92	169.584	15.417	125.9	1231.11	333.836	4939.02	1252.00	6101.87	499.19
TC070308A02	22:00	23:00	100.18	5.31	27.59	55.416	13.984	83.21	608.41	160.695	3048.56	604.74	3709.74	276.24
TC070308A03	23:00	0:00	169.25	5.38	17.54	79.785	5.8168	107.5	372.64	101.215	1811.97	342.50	2360.67	177.99
TC070308A04	0:00	1:00	174.53	5.51	12.34	122.84	5.6461	69.38	348.51	84.514	1899.41	309.18	1883.07	147.24
TC070308A05	1:00	2:00	182.25	5.62	9.594	279.008	7.1687	55.47	287.22	83.985	1008.15	226.94	1383.80	112.22
TC070308A06	2:00	3:00	176.04	5.55	8.776	271.424	4.9487	38.91	224.59	79.532	847.64	187.33	1145.43	89.92
TC070308A07	3:00	5:00	171.76	5.22	13.28	479.34	5.6345	27.34	439.71	165.052	1580.66	353.31	1929.76	165.22
TC070308A08	5:00	7:00	180.51	5.03	12.75	447.128	7.9463	15.26	279.72	167.804	1480.94	334.02	1672.65	124.04
TC070308A09	7:00	8:00	160.45	4.96	8.723	48.902	6.0501	25.32	273.12	90.307	1503.71	282.39	1633.40	105.20
TC070308A10	8:00	9:00	190.98	5.63	6.566	93.56	4.1674	8.702	186.07	52.418	1088.47	156.28	1206.57	77.05
TC070308A11	9:00	9:45	3.63	5.4				7.333			2315.92	436.21	2253.06	212.66
TC070308A12	10:00	11:00		5.31				2.145			889.72	189.77	1006.17	114.96
TC070308A13	11:00	11:40	7.24	5.21		334.432	6.1688	5.612	225.44	127.536	1193.21	280.33	1550.25	121.99
TC070408A01	15:00	15:45	227.5	4.71	6.226	12.312	3.1654	51.83	237.45	77.61	1038.41	286.35	1136.33	125.21
TC070408A02	15:45	16:45	190.49	4.33	7.734	37.467	5.4865	69.35	191.41	86.161	1134.86	319.07	1289.02	84.24
TC070408A03	16:45	17:45	185.83	4.79	9.379	11.685	3.1468	84.17	278.34	78.323	1391.45	413.92	1624.49	102.95

Sample Name	Start Time	End Time	Sample Weight (g)	pH	TOC ppmC	H2O2 µM	HCHO µM	S(IV) µM	Fe µg/L	Mn µg/L	SO4= µN	NO3- µN	NH4+ µN	Ca2+ µN
TC070408A04	17:45	19:00	195.13	4.9	11.2	24.663	5.1687	112.4	298.58	75.037	1269.11	309.47	1361.42	95.94
TC070408A05	19:00	20:00	291.94	5.17	7.897	11.495	4.3687	129.8	253.13	50.18	988.95	223.27	1085.58	109.25
TC070408A06	20:00	21:00	315.01	5.28	6.701	9.7627	5.8469	136.7	1312.158	43.319	836.10	181.92	860.17	98.76
TC070408A07	21:00	21:45	283.34	5.05	4.361	5.138	3.1548	124.3	2287.807	31.049	615.69	128.02	518.17	62.78
TC070408A08	4:30	6:30	549.86	5.5	2.793	7.051	2.3541	80.61	227.272	24.33	492.33	60.46	421.29	23.60
TC070408A09	10:00	12:00	527.15	6.35	2.903	114.056	5.692	42.34			243.88	46.18	234.72	12.05
TC070408A10	12:00	13:00	362.43	6.49	1.818	56.632	2.311	31.95	1239.939	11.805	108.76	22.80	115.07	6.64
TC070408A11	15:00	16:00	310.66	4.45	1.639	35.433	1.1654	29.88	95.53	8.031	129.15	29.74	107.16	8.40
TC070408A12	16:00	17:00	353.62	4.92	1.343	7.7446	2.1641	56.57	76.809	7.151	139.45	33.68	143.07	6.99
TC070408A13	17:00	18:00	391.64	4.74	1.725	9.4193	2.1647	15.24	709.496	6.531	202.43	63.57	199.83	8.11
TC070408A14	18:00	19:00	257.25	4.72	1.897	9.6242	2.6512	9.998	931.549	7.581	215.29	70.29	247.83	7.18
TC070408A16	19:00	20:00	180.57	4.52	2.235	16.37	2.1689	6.472	908.975	10.707	294.59	109.75	313.36	11.45
TC070408A18	20:45	22:15	143.5	4.11	4.598	17.776	2.3222	8.334	229.467	37.067	849.32	304.18	885.80	81.13
TC070608BLK	14:00		154.28		0.662	13.945	0.7546	0.649	47.262	2.192	3.52	0.82	3.27	2.96
TC070708A01	8:00	10:00	50.72	3.16	28.74	6.7747	11.333	42.35	1158.057	138.564	4668.76	2433.31	5646.51	422.90
TC070708A02	10:00	11:00	115.71	3.31	12.06	3.4314	12.817	36.79	575.658	48.342	1916.54	996.23	1855.25	176.28
TC070708A03	11:00	12:30	26.81	3.35	7.727	15.305	11.156	25.83	449.054	31.798	1130.20	650.65	1026.20	108.08
TC070708B01	15:30	16:30	17.24	3.98	22.54	3.8078	12.667	19.36	1092.25	104.057	4284.93	1996.52	5145.58	421.27
TC070808A01	14:30	15:30	105.89	4.42	8.458	427.288	21.069	65.97	459.971	47.739	1979.37	626.90	1975.13	212.54
TC070808A02	15:30	16:30	98.52	4.47	4.374	670.866	18.984	58.12	174.282	15.743	498.51	242.43	641.74	49.23
TC070808A03	16:30	17:30	178.84	3.91	3.825	270.77	17.164	54.16	172.427	13.444	472.91	201.47	511.99	38.16
TC070808A04	17:30	18:30	145.51	4.28	5.133	519.37	16.829	49.35	152.306	14.019	717.11	301.23	906.08	38.44
TC070808A05	18:30	19:30	173.45	3.95	6.867	248.62	19.165	44.77	183.787	16.629	895.24	360.15	967.65	66.30
TC070808A06	19:30	20:30	192.26	3.79	7.302	37.129	16.987	46.81	190.48	17.603	1019.11	421.34	1003.48	98.22
TC070808A07	20:30	21:30	164.57	3.64	8.939	18.701	20.165	40.99	247.274	17.463	1238.18	590.01	1222.85	116.41
TC070808A08	21:30	22:30	285.58	3.98	6.202	4.2783	18.984	34.75	178.576	14.53	696.17	352.13	790.86	63.06
TC070808A09	22:30	23:30	289.53	4.39	5.419	4.2356	17.154	23.94	163.255	13.151	696.21	309.31	841.76	60.86
TC070808A10	23:30	0:30	253.82	4.72	5.622	5.3874	16.654	21.55	179.084	14.086	841.52	359.34	1002.69	84.08
TC070808A11	0:30	1:30	227.52	4.58	6.4	29.69	21.315	9.848	206.07	17.067	884.69	375.79	1034.38	79.22
TC070808A12	1:30	3:30	142.62	4.12	10.44	79.524	25.156	22.16	367.495	32.293	1932.84	821.30	2119.96	181.22
TC070808A13	3:30	5:30	104.38	3.69	9.661	82.8	31.264	6.512	357.182	27.715	1693.92	836.31	1789.06	122.04

Sample Name	Start Time	End Time	Sample Weight (g)	pH	TOC ppmC	H2O2 µM	HCHO µM	S(IV) µM	Fe µg/L	Mn µg/L	SO4= µN	NO3- µN	NH4+ µN	Ca2+ µN
TC070808A14BLK	16:30				0.515	17.18	0.684	0.967	59.1	1.941				2.99
TC071008A01	815	915	203.99	5.19	6.035	374.656	11.234	20.32	221.5	17.109	567.41	244.62	922.07	16.12
TC071008A02	915	1015	209.05	4.72	4.505	184.632	10.236	9.564	136.05	14.055	466.74	182.15	687.15	13.60
TC071008A03	1015	1115	162.03	3.98	6.142	127.128	9.145	18.87	186.73	18.054	766.34	304.44	916.24	22.86
TC071008A04	1115	1145	28.79	3.39	12.81	35.126	12.034	6.647	440.46	51.606	1665.30	723.86	1961.21	50.74
TC071108A01	415	619	82.68	2.94	17.89	4.4728	22.813	11.93	964.06	105.056	3376.34	1902.35	3411.44	226.81
TC071108A02	619	740	46.54	2.65	40.23	16.625	34.077	15.27	2057.21	240.021	8001.93	5919.30	8926.50	755.46
TC071108BLK	1500				1.435	15.629	1.0319	0.558	188.51	10.675	71.24	20.61	55.84	8.83
TC071408A01	1800	1900	383.17	3.7	5.551	50.447	11.063	30.64	384.17	29.294	1129.31	335.75	1133.24	100.96
TC071408A02	1900	2000	440.25	3.68	4.96	2.3688	9.1564	46.91	264.96	19.102	978.88	305.57	941.61	72.77
TC071408A03	2000	2100	531.26	4.25	4.055	2.9437	8.1546	56.87	183.16	16.913	895.39	250.95	955.55	82.34
TC071408A04	2100	2200	469.42	4.19	3.221	125.06	8.8547	23.42	193.53	18.654	785.97	227.54	841.55	58.77
TC071408A05	2200	2300	434.98	3.73	3.289	316.296	9.5618	15.33	165.48	15.799	726.10	253.48	673.21	33.65
TC071408A06	2300	0	452.23	3.7	3.328	257.784	7.5211	9.746	176.42	7.935	730.42	274.22	617.25	20.88
TC071408A07	0	100	398.05	3.88	2.919	178.48	5.1546	5.314	143.62	13.64	613.39	202.68	619.50	20.70
TC071408A08	0	200	440.4	3.99	3.411	23.769	4.6158	4.622	106.24	8.254	449.80	162.38	450.33	13.04
TC071408A09	200	300	395.22	3.96	2.528	18.799	4.1546	8.891	108.04	9.788	458.35	155.62	468.11	9.29
TL061208BLK	12:00		165.61		0.583	15.551	0.9355	0.853	36.318	1.688	2.46	3.23		3.42
TL061608A01	2:00	3:00	2.37	5.14				N			3788.41	2639.87	4200.05	1750.20
TL061608A02	3:00	5:00	4.13	4.58				129.6	3987.57	23.705	5221.71	5662.68	5838.82	3119.55
TL061608A03	5:00	6:00	10.15	4.16		2.9578	31.614	138.4	5419.54	690.555	3855.18	5120.38	5010.09	405.71
TL061608A04	6:00	7:30	2.92	3.97				143.7			3931.81	4246.06	4260.05	557.08
TL061608B01	17:00	18:00	30.97	4.2	5.919	79.18	13.526	23.41	170.891	19.132	635.00	211.84	507.83	84.75
TL061608B02	18:00	19:00	36.54	3.94	9.636	0.0406	14.567	34.68	221.06	17.89	947.77	327.40	795.69	72.02
TL061608B03	19:00	20:00	48.45	3.85	11.49	0.2018	18.857	31.96	212.162	16.342	933.80	424.61	848.59	58.41
TL061608B04	20:00	21:00	43.56	3.92	11.58	1.6583	18.346	31.42	195.313	27.662	862.32	406.38	806.45	41.58
TL061608B05	21:00	22:00	79.25	4.32	7.993	-0.6615	11.958	28.79	140.449	17.93	594.32	245.56	599.90	19.36
TL061608B06	22:00	23:00	35.27	3.95	10.69	0.2594	17.598	26.63	178.165	26.945	789.02	379.18	740.40	43.11
TL061608B07	23:00	0:00	110.02	4.15	6.871	3.1231	14.354	21.57	178.592	22.947	494.95	236.92	536.87	40.68
TL061608B08	0:00	2:00	408.63	3.9	3.981	-0.1481	4.6298	24.28	127.072	15.145	461.42	165.70	288.37	22.69
TL061608B09	2:00	3:00	211.39	3.93	2.5	6.1795	2.5878	18.94	66.574	7.091	323.19	97.54	179.98	6.55

Sample Name	Start Time	End Time	Sample Weight (g)	pH	TOC ppmC	H2O2 µM	HCHO µM	S(IV) µM	Fe µg/L	Mn µg/L	SO4= µN	NO3- µN	NH4+ µN	Ca2+ µN
TL061608B10	3:00	5:00	205.23	4.2	2.758	7.1818	3.1879	23.52	80.715	6.861	245.17	95.28	185.44	4.17
TL061608B11	5:00	6:00	240.62	4	3.737	1.1235	3.1541	28.91	67.381	6.493	278.67	158.66	213.17	8.51
TL061608B12	6:00	7:00	184.75	3.9	4.268	0.2136	5.8943	29.67	67.172	6.413	329.33	182.63	219.98	6.69
TL061608B13	7:00	8:15	106.96	3.76	3.884	2.5568	5.3684	25.44	56.484	5.808	406.25	158.46	194.39	6.37
TL061608B14	9:00	10:30	17.73	3.33		1.8718	6.9618	17.18	444.828	56.723	1590.16	650.78	794.91	59.45
TL061608B15	11:00	13:00	49.4	3.17	13.45	1.7919	6.7849	19.65	485,118	61.593	2051.99	879.98	1058.24	123.44
TL061608B16	13:00	15:00	51.19	2.97	18.2	6.8014	5.1567	25.22	925.89	124.575	3108.18	1404.07	1595.01	333.15
TL061608BLK	9:00		107.09		0.642	20.25	0.9871	1.034	40.894	4.902	2.78	4.50	0.96	3.76
TL061808A01	21:00	23:00	17.88	3.3		1.3705	40.418	33.5	1990.26	236.68	6108.15	3463.29	7153.68	1172.98
TL061808A02	23:00	0:00	31.93	3.12	27.62	1.0548	30.518	31.89	1254.13	99.332	3937.72	2508.31	4392.18	483.82
TL061808A03	0:00	1:00	54.1	3.26	23.65	0.4276	33.734	32.54	878.6	56.597	2450.64	1657.29	2442.28	432.70
TL061808A04	1:00	2:00	93.26	3.41	32.38	5.3839	28.147	31.46	644.09	50.175	1324.10	855.10	1523.00	242.92
TL061808A05	2:00	3:00	94.47	3.24	79.03	9.6712	42.762	20.73	504.8	38.699	1037.95	624.51	1264.11	146.34
TL061808A06	3:00	4:00	75.17	3.02	128.9	12.286	56.849	13.35	382.24	35.179	1515.46	877.99	1703.23	139.15
TL061808A07	4:00	6:00	203.02	3.32	52.46	53.392		8.417	244.22	16.161	902.46	514.80	995.68	58.30
TL061808A08	6:00	8:00	55.34	3.45	21.57	378.464	35.846	2.663	345.79	14.598	819.47	463.96	909.44	64.95
TL061808A09BLK	17:00				1.159	18.893	1.5618	1.215	39.46	1.454			1.30	2.13
TL061808BLK	8:00		155.98		0.672	15.884	0.8626	0.981	53.8	2.582	12.83	5.51	5.51	3.11
TL061908A01	19:00	21:00	62.9	5.59	14.61	2.7169	8.4573	44.97	854.9	91.838	2168.38	1329.01	2761.59	485.75
TL061908A02	21:00	23:00	106.69	4.38	9.534	0.9039	9.1862	48.26	1009.937	68.238	1821.14	1596.54	2346.26	487.61
TL061908A03	23:00	0:30	87.37	4.64	15.75	0.791	5.3234	57.53	693.78	54.488	1831.10	1402.47	2227.02	477.53
TL061908A04	0:30	2:00	129.64	4.53	11.95	0.4946	7.9342	43.99	507.87	41.136	1026.47	576.98	1325.27	336.51
TL061908A05	2:00	3:30	105.26	3.68	15.85	283.28	7.1649	12.84	340.58	31.533	832.59	371.76	938.11	186.96
TL061908A06	3:30	5:00	89.95	3.38	27.43	192.808	8.5384	9.337	397.1	35.859	967.40	457.45	1022.56	154.46
TL061908A07	5:00	7:00	173.82	3.53	26.59	10.5	15.186	4.212	473.65	36.428	984.70	458.37	1213.15	166.51
TL061908A08	7:00	8:15	31.46	3.33	25.56	77.424	25.014	2.854	723.61	59.724	1413.75	526.83	1366.27	210.78
TL061908A09BLK	12:00				1.392	16.724	0.7816	0.878	54.48	1.821				2.64
TL062008A01	16:45	17:45	38.73	3.47	11.7	45.172	5.0748	53.62	235.48	31.986	1062.82	306.09	917.54	98.60
TL062008A02	19:00	19:20						N						
TL062108A01	9:00	9:40	29.56	2.99	23.45	22.143	12.103	36.95	692.9	86.122	2147.44	945.80	1926.29	287.28
TL062108BLK	12:00				0.922	10.762	0.6489	0.796	69.96	3.442	25.52	10.97	17.75	6.30

Sample Name	Start Time	End Time	Sample Weight (g)	pH	TOC ppmC	H2O2 µM	HCHO µM	S(IV) µM	Fe µg/L	Mn µg/L	SO4= µN	NO3- µN	NH4+ µN	Ca2+ µN
TL062308BLK	14:00				0.554	15.142	0.9813	0.953	57.95	1.801				
TL062508A01	23:10	0:00	50.49	6.8	20.25	6.5811	9.4187	31.58	1213.65	93.577	4118.95	1446.90	4173.35	422.18
TL062508A02	0:00	0:45	9.64	6.94		7.4278	6.3513	32.64	2028.46	122.696	4484.39	1313.01	4073.60	100.48
TL062508A03BLK	9:00				0.717	14.893	0.8096	1.546	77.76	2.955	29.55	14.57	15.29	19.85
TL070208A01	4:05	5:00	44.54	3.73	12.37	1.3656	4.3106	64.78	716.74	64.547	2029.80	623.46	1925.92	447.82
TL070208A02	5:00	5:50	8.18	3.67		1.1978	2.1654	53.21	686.98	54.585	2581.98	682.21	2291.54	384.59
TL070208BLK	12:00		109.02		0.67	14.995	0.6185	1.434	50.72	1.652	17.84	7.64	12.41	5.87
TL070308A01	20:00	23:00	19.05	5.92	26.08	139.84	15.167	119.9	2163.02	220.395	4079.13	1647.43	4460.97	1864.77
TL070308A02	23:00	0:00	36.32	5.9	19.05	131.672	11.812	12.54	1110.32	227.881	2628.84	729.45	2524.20	519.93
TL070308A04	0:00	1:00	48.48	5.88	10.76	185.384	5.1654	8.905	703.43	138.957	1674.80	364.17	1818.01	357.14
TL070308A05	1:00	2:00	54.49	5.83	8.377	299.096	6.3919	6.332	469.14	117.588	1173.09	299.47	1310.18	258.72
TL070308A06	2:00	3:00	63.52	5.69	7.14	229.976	5.0684	6.121	307.76	92.343	873.07	215.11	1077.35	188.44
TL070308A07	3:00	5:00	61.67	5.56	8.742	334.62	6.5461	3.257	375.98	149.5	1074.51	296.29	1310.17	282.82
TL070308A08	5:00	7:00	56.46	5.37	9.209	286.688	8.1564	2.155	324.21	178.765	1114.61	353.05	1337.72	252.03
TL070308A09	7:00	8:00	63.5	5.11	6.987	40.783	8.6043	2.489	372.52	117.136	1165.22	247.79	1326.39	187.07
TL070308A10	8:00	9:00	81.69	5.65	5.817	96.672	6.3578	1.965	223.03	67.972	934.18	150.00	1038.86	133.78
TL070308A11	9:00	9:45	1.84	5.51				N						
TL070308A12	10:00	11:00	33.42	5.31	7.771	210.944	9.2641	1.355	378.16	114.719	887.69	204.50	934.33	198.60
TL070308A13	11:00	11:40	2.3	5.23				N			1198.66	264.58	1256.77	247.48
TL070408A01	15:00	15:45	72.4	5.13	5.555	16.359	2.9022	57.02	428.88	111.984	1255.86	343.33	1095.09	222.38
TL070408A02	15:45	16:45	53.05	4.69	6.934	23.569	6.1567	78.99	351.35	131.484	1472.93	415.97	1349.12	205.14
TL070408A03	16:45	17:45	41.99	4.79	8.544	20.7	3.8161	75.15	404.92	149.73	1742.25	556.01	1642.27	255.59
TL070408A04	17:45	19:00	36.75	5.01	10.25	17.936	5.6514	124.7	491.88	146.505	1693.51	506.66	1506.73	300.69
TL070408A05	19:00	20:00	97.33	5.29	7.225	12.201	5.8343	113.2	458.79	75.162	1054.87	266.38	1100.64	198.09
TL070408A06	20:00	21:00	152.49	5.51	6.196	11.058	4.2645	102.9	1552.175	58.592	886.04	219.83	849.60	177.51
TL070408A07	21:00	21:45	56.18	5.69	5.748	7.2543	5.4789	114.5	101.092	56.279	845.31	182.40	792.24	178.22
TL070408A08	4:30	6:30	318.71	5.65	2.911	7.8985	1.9846	84.33	49.964	30.286	599.34	77.67	505.46	43.59
TL070408A09	10:00	12:00	254.91	6.37	2.857	94.368	3.388	20.61	44.547	18.617	271.27	52.22	256.62	11.62
TL070408A10	12:00	13:00	106.97	6.33	2.304	51.108	1.0098	25.49	683.008	17.202	148.97	26.68	176.40	13.50
TL070408A11	15:00	16:00	194.12	4.48	1.402	36.366	3.7865	12.38	638.061	11.434	129.07	30.06	96.83	19.86
TL070408A12	16:00	17:00	216.83	4.8	1.411	6.6934	3.0654	5.124	87.595	6.91	152.19	34.60	141.20	11.11

Sample Name	Start Time	End Time	Sample Weight (g)	pH	TOC ppmC	H2O2 µM	HCHO µM	S(IV) µM	Fe µg/L	Mn µg/L	SO4= µN	NO3- µN	NH4+ µN	Ca2+ µN
TL070408A14	17:00	19:00	413.58	4.68	1.636	9.2213	2.7564	2.527	659.246	7.425	183.91	60.47	205.00	9.59
TL070408A16	19:00	20:00	117.76	4.57	2.053	15.015	2.3056	1.196	88.822	8.933	230.45	88.40	253.17	15.44
TL070408A18	20:45	22:15	56.06	4.25	3.467	12.282	2.3564	1.225	174.094	32.332	631.08	225.80	651.42	76.75
TL070608BLK	14:00		159.03		0.54	14.413	0.8165	0.943	40.43	1.459			0.29	
TL070708A02	8:00	11:00	20.39	3.37	16.91	2.2961	12.984	38.53	876.092	116.912	2822.37	2044.73	3209.37	355.22
TL070708A03	11:00	12:30	6.64	3.36		3.0361	11.354	22.84	555.671	86.484	2246.15	1080.67	1824.21	432.39
TL070808A01	14:30	16:30	30.04	4.57	9.233	210.504	23.587	57.35	372.842	79.412	2199.16	951.39	1949.02	432.31
TL070808A04	17:30	18:30	99.18	4.17	4.834	339.37	17.985	22.16	214.125	22.667	710.09	306.23	839.08	132.37
TL070808A05	18:30	19:30	62.89	4.02	6.172	266.28	18.643	9.324	245.028	25.499	949.73	408.23	977.89	159.79
TL070808A06	19:30	20:30	73.23	3.88	6.247	30.059	18.458	4.628	239.015	22.535	1031.82	444.86	964.76	196.75
TL070808A07	20:30	21:30	55.57	3.74	7.426	6.12	22.487	13.77	295.875	24.565	1283.68	620.73	1202.03	250.94
TL070808A08	21:30	22:30	134.44	4	5.299	3.7332	19.845	23.03	225.818	17.916	721.39	383.09	802.88	125.21
TL070808A09	22:30	23:30	135.31	4.38	4.797	5.2934	18.649	16.85	211.761	15.962	675.71	317.93	795.56	101.19
TL070808A10	23:30	0:30	111.9	4.8	4.697	4.9568	17.131	15.44	220.991	17.944	841.52	365.50	963.07	140.87
TL070808A11	0:30	1:30	94.9	4.67	4.782	8.2757	23.154	8.757	228.108	19.342	884.95	383.46	1011.28	135.93
TL070808A12	1:30	3:30	39.61	4.43	6.866	2.5559	26.641	4.286	301.763	36.074	1689.70	764.16	1654.78	316.33
TL070808A13	3:30	5:30	25.61	3.98	8.243	2.294	25.219	5.864	423.332	38.823	1913.48	884.81	1949.76	323.26
TL070808A14BLK	16:30				0.584	13.703	0.937	1.328	55.69	1.329			0.82	2.53
TL071008A01	815	915	77.45	5.2	5.7	349.304	13.157	18.13	145.85	16.735	559.16	269.35	812.72	30.99
TL071008A02	915	1015	95.01	4.74	4.339		9.489	23.16	132.14	15.143	475.39	195.54	704.55	27.57
TL071008A03	1015	1115	55.98	4.02	4.995	130.2	13.651	25.42	187.92	20.556	660.38	281.07	842.33	36.87
TL071008A04	1115	1145	9.79	3.71		50.474	13.645	22.37	157.68	38.843	1059.03	472.10	1378.94	60.80
TL071108A01	415	619	15.64	3.12	0.585	7.1788	25.684	9.857	719.36	131.883	2481.52	1516.65	2056.93	393.10
TL071108A02	619	740	8.73	2.89		20.956	15.389	4.633	1928.9	306.352	5306.91	4120.27	4156.33	546.08
TL071108BLK	1500				0.839	15.83	0.6185	1.549	87.42	5.902	75.59	28.01	55.28	16.04
TL071408A01	1800	1900	200.06	3.7	5.435	90.376	11.657	25.27	234.28	25.2	1128.77	347.53	1135.02	126.68
TL071408A02	1900	2000	230.7	3.66	4.821	2.1615	8.2358	42.39	258.13	21.951	1048.09	322.53	956.34	107.21
TL071408A03	2000	2100	279.29	4.17	4.075	6.1894	7.999	31.85	282.11	20.768	965.87	278.16	1046.28	125.34
TL071408A04	2100	2200	254.92	4.17	3.252	120.788	8.0312	11.26	198.6	18.937	851.68	249.19	900.98	90.05
TL071408A05	2200	2300	208.47	3.7	3.167	386.696	8.6354	5.604	191.48	17.983	788.17	268.54	735.21	40.54
TL071408A06	2300	0	215.2	3.55	3.291	236.736	7.9874	2.338	142.12	13.001	755.32	301.93	657.65	25.12

Sample Name	Start Time	End Time	Sample Weight (g)	pH	TOC ppmC	H2O2 µM	HCHO µM	S(IV) µM	Fe µg/L	Mn µg/L	SO4= µN	NO3- µN	NH4+ µN	Ca2+ µN
TL071408A08	0	200	430.51	3.93	2.497	78.04	3.1659	1.546	126.83	8.991	538.35	191.44	556.45	22.12
TS061208BLK	12:00		220.04		0.566	13.329	0.7741	1.387	1231.74	71.716	7.42		0.33	4.11
TS061608A01	2:00	3:00	32.66	3.88	42.74	2.6486	49.379	152.6	1178.21	113.778	3191.78	1577.06	4133.38	203.54
TS061608A02	3:00	5:00	29.85	3.38	62.25	3.8444	54.321	147.9	2131.14	241.022	4079.47	2855.73	5956.51	280.36
TS061608A03	5:00	6:00	39.12	3.47	31.15	22.871	34.025	151.3	1472.74	111.41	2215.94	1296.38	2818.10	123.20
TS061608A04	6:00	7:30	13.67	3.46		191.652	28.654	13.36	1230.15	81.027	2577.14	1208.99	3039.83	131.33
TS061608B01	17:00	18:00	68.84	4.17	7.762	50.875	15.438	12.82	180.228	13.527	715.56	199.37	608.28	26.97
TS061608B02	18:00	19:00	102.6	3.98	9.834	4.0258	16.523	31.74	177.88	11.887	745.86	246.35	645.20	17.32
TS061608B03	19:00	20:00	108	3.93	11.07	0.2524	20.784	29.13	143.591	10.378	690.52	320.33	676.19	18.00
TS061608B04	20:00	21:00	100.83	4.05	10.06	0.6036	17.976	27.65	138.564	18.534	641.86	279.37	615.53	12.48
TS061608B05	21:00	22:00	151.7	4.36	6.522	-0.1295	13.759	29.44	106.275	13.541	449.48	182.97	469.13	11.42
TS061608B06	22:00	23:00	96.98	4.07	9.294	-0.0691	20.365	32.52	154.166	19.154	488.06	274.49	600.67	16.82
TS061608B07	23:00	0:00	137.11	4.17	6.78	-0.1818	14.985	37.96	125.892	16.989	450.16	220.75	468.28	17.55
TS061608B08	0:00	2:00	209.05	4	4.037	0.8283	6.4816	26.34	90.739	10.307	323.55	120.54	265.97	6.58
TS061608B09	2:00	3:00	32.08	3.74	4.293	-0.1	5.6489	22.31	116.804	10.019	551.78	172.15	303.16	4.70
TS061608B10	3:00	5:00	46.58	4.21	4.903	0.0778	5.4183	20.77	93.002	8.388	420.31	120.04	357.83	5.15
TS061608B11	5:00	6:00	43.28	4.03	4.799	-0.2845	4.9823	35.78	86.732	7.143	359.55	137.63	283.28	5.29
TS061608B12	6:00	7:00	48	3.9	5.937	-0.3523	7.1648	24.85	91.22	7.655	403.66	173.75	314.35	5.11
TS061608B13	7:00	8:15	42.3	3.92	4.616	-0.1129	5.6477	19.72	76.111	7.106	355.93	111.35	222.09	4.32
TS061608B14	9:00	10:30	15.31	3.08		1.0867	7.4894	24.66	1607.7	46.118	2419.24	1004.52	1149.02	16.90
TS061608B15	11:00	13:00	37.28	2.95	25.96	4.3473	5.1867	23.48	2420.56	69.586	3172.06	1396.67	1634.34	30.02
TS061608B16	13:00	15:00	49.33	2.82	32.16	4.798	6.5492	18.73	4730.544	98.236	4082.66	1626.23	2132.36	35.90
TS061608BLK	9:00		156.19		0.574	17.03	0.8583	0.992	36.984	4.195			-0.44	3.19
TS061808A01	21:00	23:00	43.27	3.01	49.43	5.9463	37.641	21.96	3194.23	118.005	7686.15	3784.69	9023.35	160.67
TS061808A02	23:00	0:00	82.81	3.06	33.03	1.9588	27.594	26.44	1921.83	58.842	3608.29	1843.97	4111.15	67.57
TS061808A03	0:00	1:00	116.64	3.32	24.1	1.9181	27.483	31.25	849.4	22.505	1721.07	970.24	1784.93	34.68
TS061808A04	1:00	2:00	152.17	3.38	60.96	9.0231	40.183	23.34	468.1	18.562	850.46	578.97	1205.91	35.19
TS061808A05	2:00	3:00	143.43	3.19	126	10.81	50.618	9.102	465.22	17.62	990.69	727.93	1263.08	44.37
TS061808A06	3:00	4:00	130.74	2.94	203.7	14.819	59.152	8.771	1130.25	23.666	1556.74	1130.49	1866.58	41.51
TS061808A07	4:00	6:00	249.02	3.17	124.5	13.498		6.453	745.43	18.912	1014.65	707.99	1383.62	35.48
TS061808A08	6:00	8:00	56.22	3.18	75.62	70.135	41.763	3.147	802.68	22.65	1142.93	731.73	1462.83	36.51

Sample Name	Start Time	End Time	Sample Weight (g)	pH	TOC ppmC	H2O2 µM	HCHO µM	S(IV) µM	Fe µg/L	Mn µg/L	SO4= µN	NO3- µN	NH4+ µN	Ca2+ µN
TS061808A09BLK	17:00				1.271	12.577	1.4761	1.425	42.15	1.85	4.10	2.64	2.76	2.92
TS061808BLK	8:00		139.15		0.984	11.287	0.8468	1.379	150.42	4.879	70.05	13.80	43.79	4.64
TS061908A01	19:00	21:00	107.26	4.47	21.56	0.9636	8.1968	52.28	631.6	39.653	2313.07	1200.29	3587.49	108.50
TS061908A02	21:00	23:00	176.25	4.36	11.74	1.4802	9.1648	51.34	504.13	28.488	1493.09	942.80	2080.81	69.29
TS061908A03	23:00	0:30	181.11	4.06	20.45	0.6877	8.1684	46.85	404.17	18.798	1312.68	831.60	1950.60	41.46
TS061908A04	0:30	2:00	178.88	4.06	11.24	0.9012	8.1878	44.21	487.4	35.945	776.33	437.24	1231.37	24.76
TS061908A05	2:00	3:30	151.9	3.56	18.1	318.208	6.9487	20.97	299.89	14.764	682.75	305.27	805.26	18.21
TS061908A06	3:30	5:00	145.73	3.31	31.5	171.992	11.816	6.458	492.93	23.764	890.48	415.26	1021.65	22.43
TS061908A07	5:00	7:00	231.99	3.41	57.67	9.4718	23.618	3.477	487.77	23.512	1139.89	553.17	1577.38	23.83
TS061908A08	7:00	8:15	30.78	3.06	56.52	11.281	25.558	1.603	1323.09	62.829	2383.55	777.82	2549.72	46.40
TS061908A09BLK	12:00				1.395	12.444	0.9168	0.512	60.82	2.082	3.04	2.84	4.22	1.88
TS062008A01	16:45	17:45	30.09	3.2	24.63	5.3943	6.5687	48.94	963.31	51.445	2453.30	624.50	2013.69	76.91
TS062008A02	19:00	19:20						N						
TS062108A01	9:00	9:40	32.45	2.84	60.53	7.0959	11.954	25.84	2312.22	88.349	3779.34	1315.28	3507.19	60.23
TS062108BLK	12:00				2.367	-0.1847	0.7898	1.233	238.7	8.264	157.93	26.63	139.34	5.90
TS062308BLK	14:00				0.564	15.698	0.7616	1.542	48.62	1.594			15.07	4.21
TS062508A01	23:10	0:00	15.45	5.48	28.62	4.7182	8.3169	28.41	691.99	53.003	3533.12	775.43	4556.39	151.41
TS062508A02	0:00	0:45	16.97	5.42	24.15	4.4178	7.1681	23.64	641.13	48.578	4914.07	809.45	5346.64	158.23
TS062508A03BLK	9:00				1.003	10.142	0.5416	1.207	82.25	3.92	94.13	22.63	87.23	15.89
TS070208A01	4:05	5:00	18.45	3.29	26.4	5.4678	6.3687	55.82	1035.07	130.176	5117.35	1461.25	5143.66	520.40
TS070208A02	5:00	5:50	9.89	3.22		1.7817	6.3547	49.63	983.57	73.87	4802.98	1238.09	5109.95	251.61
TS070208BLK	12:00		155.53		0.626	17.897	0.7167	1.221	48.86	1.394	6.83	4.83	2.55	3.94
TS070308A01	20:00	23:00	96.31	5	49.71	55.211	17.138	15.74	664.55	214.041	4206.03	873.70	5478.08	213.03
TS070308A02	23:00	0:00	95.04	5.02	23.98	52.904	14.735	12.33	310.28	79.503	2088.61	341.36	2723.51	57.83
TS070308A04	0:00	1:00	81.83	5.08	14.61	72.633	4.0354	6.154	226.46	65.14	1724.20	242.10	2206.56	41.36
TS070308A05	1:00	2:00	87.63	5.17	11.55	277.056	8.6943	5.485	245.66	68.382	1363.41	239.48	1654.93	37.08
TS070308A06	2:00	3:00	77.07	5.14	9.645	239.304	6.1221	3.359	180.16	58.108	970.65	171.70	1352.01	26.17
TS070308A07	3:00	5:00	69.91	4.93	16.27	447.23	10.168	3.672	362.13	160.793	2087.99	403.70	2338.35	69.29
TS070308A08	5:00	7:00	82.14	4.83	15.01	476.624	5.9783	2.317	270.18	162.002	1636.61	329.17	2011.60	40.26
TS070308A09	7:00	8:00	61.94	4.69	11.11	48.913	4.5606	1.998	229.3	96.019	1545.01	275.27	1954.89	37.22
TS070308A10	8:00	9:00	75.23	5.13	8.933	58.066	8.4186	1.957	178.4	50.441	1311.77	181.33	1612.85	27.34

Sample Name	Start Time	End Time	Sample Weight (g)	pH	TOC ppmC	H2O2 µM	HCHO µM	S(IV) µM	Fe µg/L	Mn µg/L	SO4= µN	NO3- µN	NH4+ µN	Ca2+ µN
TS070308A11	9:00	9:45	0.68	5.14				N						
TS070308A12	10:00	11:00	57.31	4.82	9.831	265.072	8.1647	0.983	166.29	81.362	1004.32	181.46	1273.78	48.86
TS070308A13	11:00	11:40	3.46	4.82				1.216			1255.92	224.29	1381.93	44.29
TS070408A01	15:00	15:45	93.56	4.58	7.508	7.2437	3.9446	76.35	212.21	78.632	1198.21	302.12	1372.61	83.22
TS070408A02	15:45	16:45	92.18	4.14	9.11	16.78	4.3548	69.43	195.6	76.15	1252.57	329.05	1500.11	33.15
TS070408A03	16:45	17:45	103.34	4.53	9.781	10.214	3.0354	42.89	176.91	57.519	1285.70	357.43	1698.44	26.29
TS070408A04	17:45	19:00	118.05	4.72	11.36	19.122	4.064	57.72	174.66	55.155	1300.71	282.75	1398.27	27.60
TS070408A05	19:00	20:00	145.85	4.89	8.577	10.255	6.0648	86.24	891.903	33.859	920.59	194.24	1100.47	20.12
TS070408A06	20:00	21:00	110.93	5.01	7.544	8.4753	6.7564	65.11	648.178	28.246	738.06	156.39	946.83	20.94
TS070408A07	21:00	21:45	176.41	4.83	4.54	4.7707	3.2464	53.68	62.238	26.445	574.99	115.43	596.28	54.62
TS070408A08	4:30	6:30	312.46	5.41	3.103	6.8483	4.168	41.57	50.853	17.884	505.97	60.55	470.87	21.75
TS070408A09	10:00	12:00	187.06	6.19		79.3432	4.0674	12.34	1000.41	13.77	291.40	41.91	281.85	9.53
TS070408A10	12:00	13:00	159.63	6.24	2.024	32.57	2.0153	6.589	1240.867	10.314	127.50	28.00	135.18	12.96
TS070408A11	15:00	16:00	54.91	4.88	2.24	21.882	2.9588	3.944	100.528	19.12	194.90	35.64	172.89	15.72
TS070408A12	16:00	17:00	84.28	4.92	1.725	5.7945	3.2548	2.581	848.896	8.555	203.01	31.52	174.68	8.25
TS070408A14	17:00	19:00	158.44	4.72	2.037	6.5113	1.5168	8.957	680.717	7.135	251.77	64.09	251.68	8.48
TS070408A16	19:00	20:00	47.37	4.42	2.692	8.3846	2.6441	12.33	96.328	10.763	355.01	113.08	391.96	11.78
TS070408A18	20:45	22:15	42.74	4	5.099	5.0434	3.0001	6.788	192.075	35.124	996.16	361.45	1049.30	46.06
TS070608BLK	14:00		137.82		0.621	12.508	0.6454	1.034	41.88	1.61	3.28		1.98	3.54
TS070708A02	8:00	11:00	83.88	3.23	17.72	2.6723	13.167	53.77	511.426	55.959	2871.21	1539.89	3158.11	168.07
TS070708A03	11:00	12:30	12.46	3.33		7.6138	13.956	37.49	307.066	28.096	1457.03	717.70	1403.07	79.56
TS070808A01	14:30	16:30	110.94	4.36	7.896	369.968	23.451	15.64	318.581	32.808	1680.34	518.76	1826.18	90.46
TS070808A04	17:30	18:30	182.8	3.94	4.574	332.19	18.667	8.518	157.51	11.067	620.85	243.14	763.89	20.15
TS070808A05	18:30	19:30	91.43	3.87	7.227	290.12	17.324	5.376	134.914	11.027	904.23	338.33	1002.12	18.03
TS070808A06	19:30	20:30	96.33	3.71	8.176	25.56	21.622	2.855	139.994	10.925	1057.20	397.33	1075.58	19.90
TS070808A07	20:30	21:30	90.36	3.58	8.864	7.1073	21.302	8.973	176.668	12.883	1248.26	553.00	1291.38	26.90
TS070808A08	21:30	22:30	115.79	3.88	6.725	2.0855	19.623	16.28	133.8	12.778	749.19	359.62	859.81	15.07
TS070808A09	22:30	23:30	119.46	4.19	5.862	1.5651	19.992	13.37	128.589	10.104	722.40	310.30	899.78	13.86
TS070808A10	23:30	0:30	111.08	4.51	5.707	1.8103	16.502	9.214	149.893	10.46	830.41	332.88	1023.05	19.92
TS070808A11	0:30	1:30	99.73	4.35	5.645	6.0404	21.846	7.586	140.855	12.654	901.29	365.60	1091.33	19.78
TS070808A12	1:30	3:30	86.48	3.98	10.7	20.571	24.897	8.622	207.018	24.715	1736.59	713.41	1952.96	49.50

Sample Name	Start Time	End Time	Sample Weight (g)	pH	TOC ppmC	H2O2 µM	HCHO µM	S(IV) µM	Fe µg/L	Mn µg/L	SO4= µN	NO3- µN	NH4+ µN	Ca2+ µN
TS070808A13	3:30	5:30	62.47	3.72	9.963	23.528	31.088	6.319	218.685	24.639	1698.46	772.82	1899.29	48.87
TS070808A14BLK	16:30				0.534	13.479	0.895	1.003	50.05	1.061			0.60	2.78
TS071008A01	815	915	87	5.11	7.053	281.2	12.899	15.96	132.7	15.634	709.11	288.36	1070.70	7.46
TS071008A02	915	1015	89.83	4.73	4.568	163.16	11.321	14.46	96.43	9.112	463.50	163.21	715.22	3.91
TS071008A03	1015	1115	78.63	4.03	5.693	95.168	11.317	6.325	139.72	12.07	588.95	214.37	827.19	7.89
TS071008A04	1115	1145	15.02	3.56		23.765	17.949	2.113	310.83	26.663	1288.02	519.72	1692.74	15.81
TS071108A01	415	619	29.52	2.99	19.98	3.2898	21.156	23.52	714.43	82.243	3513.30	1788.55	3725.55	59.09
TS071108A02	619	740	24.29	2.69	33.88	5.182	35.694	17.49	1297.09	180.249	6986.81	4091.11	7229.88	322.05
TS071108BLK	1500				1.011	8.5113	0.9874	0.951	239.03	8.878	137.70	32.41	117.94	11.66
TS071408A01	1800	1900	107.44	3.61	7.501	34.73	12.984	22.15	304.11	30.115	1430.25	381.27	1487.60	63.89
TS071408A02	1900	2000	154.71	3.72	5.511	2.6905	8.6544	20.38	173.57	15.86	989.30	289.84	970.83	29.64
TS071408A03	2000	2100	187.26	4.1	4.589	2.503	7.5482	16.57	131.69	12.62	810.59	223.99	914.39	22.99
TS071408A04	2100	2200	150.53	4.29	3.129	85.212	7.6258	6.664	105.75	10.816	698.68	195.91	799.11	14.95
TS071408A05	2200	2300	123.2	3.88	3.247	323.896	8.5483	2.125	124.49	13.593	640.67	209.86	659.76	20.07
TS071408A06	2300	0	118.59	3.55	3.409	218.096	6.6419	1.379	125.26	10.389	658.89	219.65	577.77	19.84
TS071408A08	0	200	205.18	4	2.502	41.808	2.9818	1.223	111.84	9.514	572.15	164.31	588.72	16.32

APPENDIX D – ADDITIONAL FIGURES

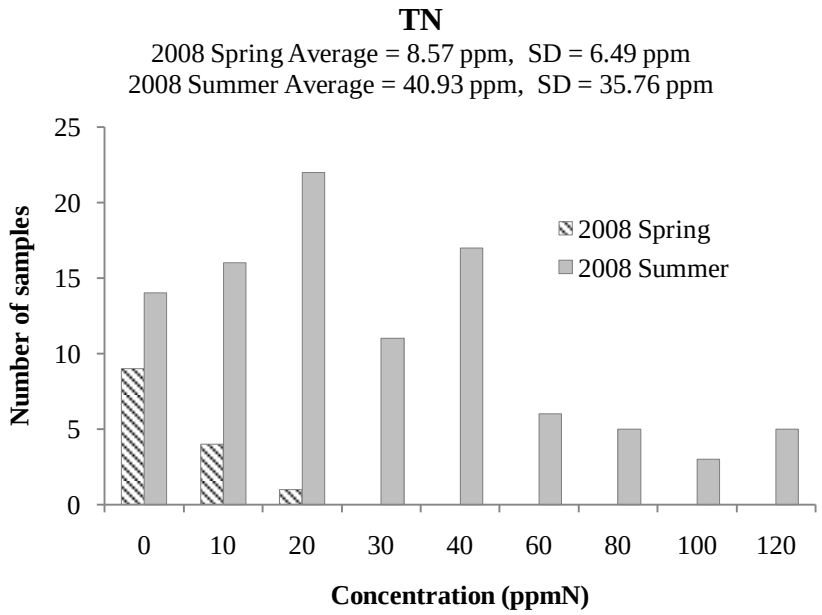

Appendix Figure 1. Frequency distributions of TN concentrations measured in bulk (CASCC) cloudwater samples collected at Mt. Tai in the 2008 sampling campaigns.

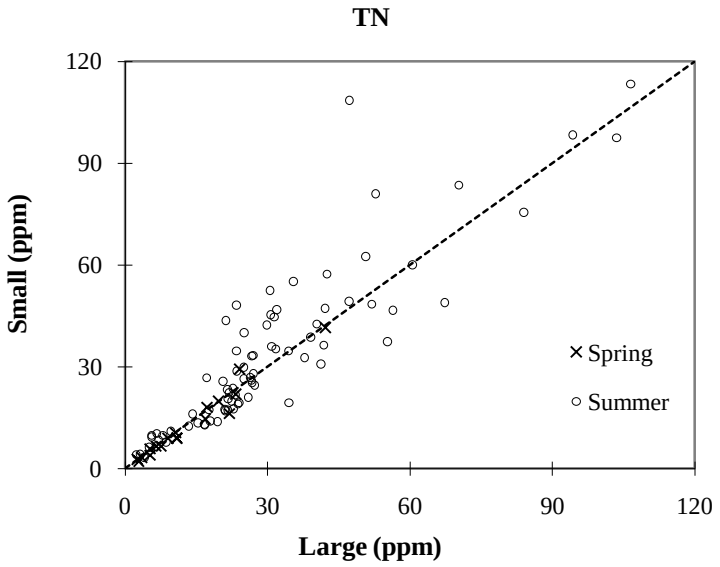

Appendix Figure 2. Comparisons of TN concentrations measured in small (4 < D < 16 μm) and large (D > 16 μm) cloud drop size fractions simultaneously collected with the sf-CASCC at Mt. Tai during the spring and summer 2008 field campaigns. (The diagonal dashed line is the 1:1 line.)

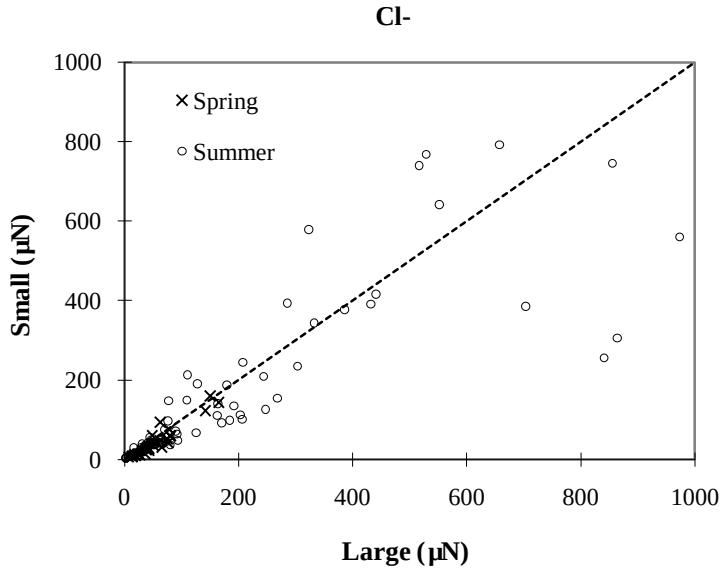

Appendix Figure 3. Comparisons of chloride ion concentrations measured in small (4 < D < 16 μm) and large (D > 16 μm) cloud drop size fractions simultaneously collected with the sf-CASCC at Mt. Tai during the spring and summer 2008 field campaigns. (The diagonal dashed line is the 1:1 line.)

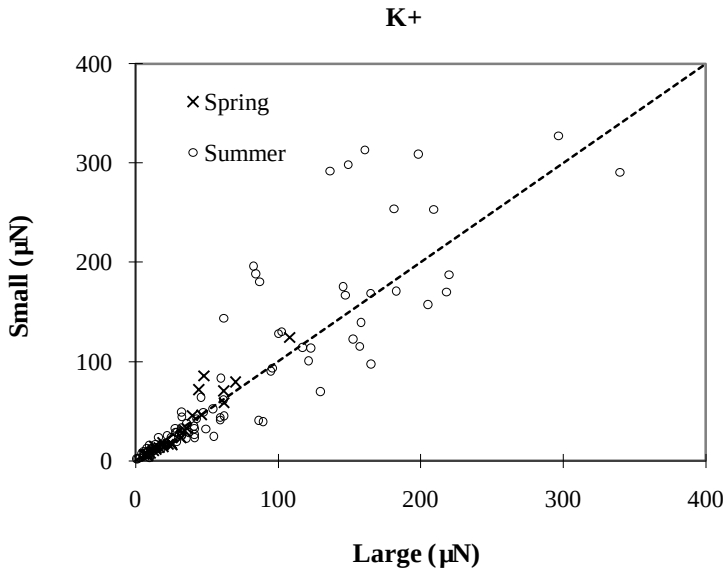

Appendix Figure 4. Comparisons of potassium ion concentrations measured in small (4 < D < 16 μm) and large (D > 16 μm) cloud drop size fractions simultaneously collected with the sf-CASCC at Mt. Tai during the spring and summer 2008 field campaigns. (The diagonal dashed line is the 1:1 line.)